Jaakko Leppänen

Development of a New Monte Carlo Reactor Physics Code

VTT

Development of a New Monte Carlo Reactor Physics Code

Jaakko Leppänen

Dissertation for the degree of Doctor of Science in Technology to be presented with due permission for public examination and debate in Auditorium F1 at Helsinki University of Technology (Espoo, Finland) on the 18th of June, 2007, at 12 o'clock noon.

Abstract

Monte Carlo neutron transport codes are widely used in various reactor physics applications, traditionally related to criticality safety analyses, radiation shielding problems, detector modelling and validation of deterministic transport codes. The main advantage of the method is the capability to model geometry and interaction physics without major approximations. The disadvantage is that the modelling of complicated systems is very computing-intensive, which restricts the applications to some extent. The importance of Monte Carlo calculation is likely to increase in the future, along with the development in computer capacities and parallel calculation.

An interesting near-future application for the Monte Carlo method is the generation of input parameters for deterministic reactor simulator codes. These codes are used in coupled LWR full-core analyses and typically based on few-group nodal diffusion methods. The input data consists of homogenised few-group constants, presently generated using deterministic lattice transport codes. The task is becoming increasingly challenging, along with the development in nuclear technology. Calculations involving high-burnup fuels, advanced MOX technology and next-generation reactor systems are likely to cause problems in the future, if code development cannot keep up with the applications. A potential solution is the use of Monte Carlo based lattice transport codes, which brings all the advantages of the calculation method.

So far there has been only a handful of studies on group constant generation using the Monte Carlo method, although the interest has clearly increased during the past few years. The homogenisation of reaction cross sections is simple and straightforward, and it can be carried out using any Monte Carlo code. Some of the parameters, however, require the use of special techniques that are usually not available in general-purpose codes. The main problem is the calculation of neutron diffusion coefficients, which have no continuous-energy counterparts in the Monte Carlo calculation.

This study is focused on the development of an entirely new Monte Carlo neutron transport code, specifically intended for reactor physics calculations at the fuel assembly level. The PSG code is developed at VTT Technical Research Centre of Finland and one of the main applications is the generation of homogenised group constants for deterministic reactor simulator codes. The theoretical background on general transport theory, nodal diffusion calculation and the Monte Carlo method are discussed. The basic methodology used in the PSG code is introduced and previous studies related to the topic are briefly reviewed. PSG is validated by comparison to reference results produced by MCNP4C and CASMO-4E in infinite two-dimensional LWR lattice calculations. Group constants generated by PSG are used in ARES reactor simulator calculations and the results compared to reference calculations using CASMO-4E data.

Tiivistelmä

Monte Carlo -neutronitransportkoodeja käytetään laajasti monissa reaktorifysiikkasovelluksissa, kuten kriittisyysturvallisuusanalyyseissä, säteilysuojelulaskuissa, detektorimallinnuksessa ja determinististen transportkoodien kelpoistamisessa. Menetelmän tärkeimpinä etuina voidaan pitää geometrian ja neutronivuorovaikutusten tarkkaa kuvaamista ilman merkittäviä approksimaatioita. Haittapuolena on laskennan hitaus, erityisesti monimutkaisia geometrioita mallinnettaessa, mikä myös jossain määrin rajoittaa menetelmän sovelluskohteita. Monte Carlo -laskennan merkitys tulee todennäköisesti kasvamaan tulevaisuudessa tietokoneiden laskentatehon ja rinnakkaislaskennan kehityksen myötä.

Kevytvesireaktoreiden lataussuunnittelu- ja turvallisuusanalyyseissä käytetään nykyisin deterministisiä reaktorisimulaattorikoodeja, joiden kytketyt neutroniikkatermohydrauliikkamallit pohjautuvat tyypillisesti nodaalidiffuusioteoreettisiin menetelmiin. Nodaalikoodien syöttöparametrit koostuvat homogenisoiduista moniryhmävakioista, jotka tuotetaan deterministisillä nippupalamaohjelmilla. Näiden ohjelmien soveltuvuus saattaa tulla kyseenalaiseksi ydintekniikan kehityksen myötä. Kasvava palama, kehittyneet sekaoksidipolttoaineet sekä uuden sukupolven ydinteknologia tulevat todennäköisesti aiheuttamaan ongelmia, erityisesti geometrian mallinnuksessa, mikäli laskentaan käytetyt ohjelmistot eivät kykene pysymään kehityksessä mukana. Eräs mielenkiintoinen lähitulevaisuuden sovelluskohde Monte Carlo -laskennalle onkin juuri homogenisoitujen ryhmävakioiden tuottaminen deterministisille reaktorisimulaattorikoodeille.

Monte Carlo -menetelmän soveltuvuutta ryhmävakioiden tuottamiseen on tutkittu yllättävän vähän, joskin kiinnostus aiheeseen on selvästi lisääntynyt kymmenen viime vuoden aikana. Homogenisoitujen ryhmävaikutusalojen laskeminen on suoraviivaista, ja se on mahdollista useimmilla Monte Carlo -neutroniikkakoodeilla. Tiettyjen parametrien laskemiseen tarvitaan kuitenkin erikoismenetelmiä, joita ei yleiskäyttöön tarkoitettujen koodien valikoimista yleensä löydy. Selvästi suurin haaste on diffuusiovakioiden laskeminen, mikä vaatii fysiikan tarkkaan mallintamiseen perustuvan Monte Carlo -laskennan ja approksimaatioon pohjautuvan diffuusioteorian yhdistämistä.

Tässä työssä käsitellään kokonaan uuden Monte Carlo -neutronitransportkoodin kehitystä. VTT:ssä kehitetty PSG-koodi on tarkoitettu reaktorifysiikkalaskuihin, erityisesti polttoainenipputasolla. PSG:n yksi tärkeimmistä sovelluskohteista on moniryhmävakioiden tuottaminen deterministisille reaktorisimulaattorikoodeille. Työssä selvitetään neutronien transport-teorian, nodaalidiffuusiomenetelmien sekä Monte Carlo -laskennan teoreettista taustaa. PSG-koodin käyttämät laskentarutiinit esitellään pääpiirteittäin, ja muita aiheeseen liittyviä tutkimuksia käydään läpi. Koodin kelpoistamiseksi kevytvesireaktorihiloille laskettuja tuloksia verrataan MCNP4C- ja CASMO-4E -ohjelmilla laskettuihin tuloksiin. PSG:n tuottamia ryhmävakioita käytetään ARES-reaktorisimulaattorilaskujen syöttöparametreina, ja tuloksia verrataan laskuihin, joissa moniryhmävakiot on tuotettu CASMO-4E -ohjelmalla.

Preface

A major part of this work deals with the on-going development of the PSG Monte Carlo reactor physics code. The work described in this thesis was started in September 2004 and carried out until the summer of 2006 at the VTT Technical Research Centre of Finland. The code development has been funded in the framework of the Finnish Research Programme on Nuclear Power Plant Safety (SAFIR) and various VTT research projects.

I wish to express my deepest gratitude to all my supervisors and seniors here at VTT, particularly our Technology Manager Dr. Timo Vanttola, Group Managers Petri Kotiluoto and Antti Daavittila and the SAFIR/EMERALD Project Manager Randolph Höglund. The development of PSG has been encouraged from the very beginning of the project, and this work would not have been possible without their full support. A special thanks goes to Markku Anttila (VTT) and Riku Mattila of the Finnish Radiation and Nuclear Safety Authority, for their expertise and consultation during the process.

There are several people outside VTT who deserve a special thanks for their useful comments and advice. I have had several useful talks with Dr. Steven van der Marck of the Nuclear Research and Consultancy Group (NRG), the Netherlands, on the calculation of effective delayed neutron parameters using the Monte Carlo method, along with other interesting research topics. In the spring of 2006 I had the opportunity to spend a period of two months at the École Polytechnique de Montréal, learning about neutron leakage models in reactor lattice calculations. I wish to thank Professors Alain Hébert and Guy Marleau for the learning experience and a pleasant stay in Montréal.

This thesis was reviewed by two distinguished reactor physics experts, Professor Emeritus Heikki Kalli, retired from Lappeenranta University of Technology, and Associate Professor Janne Wallenius from the Royal Institute of Technology, Sweden. Before completing the manuscript I received some very useful comments from Frej Wasastjerna (VTT) and Dr. Pertti Aarnio from Helsinki University of Technology.

My gratitude naturally goes to Professor Rainer Salomaa for supervising this thesis and Professor Eduard Hoogenboom from Delft University of Technology, for acting as my opponent in the defence.

The PSG code has come a log way since the first time I had the crazy idea of developing my own Monte Carlo neutron transport code. The development has been an inspiring process and a marvellous learning experience. There is still plenty of work to be done and several interesting research topics left for the future. Hopefully the completion of this thesis will only mark a milestone, rather than the final goal in PSG development.

Espoo, Finland, May 2007

Jaakko Leppänen

Contents

Chapter 1

Introduction

1.1 Nuclear Reactor Analysis

The history of nuclear power dates back to the beginning of the 20th century, when the recently discovered theories in physics suggested that the energy bound inside the atomic nucleus could exceed the energies involved in chemical reactions by a factor of one million or more. If such energy could be released, it would easily become the most significant industrial invention since the steam engine. It was also clear from the very beginning that the new form of energy could potentially be used as a weapon of war. It was foreseen as early as in the 1930s that the development of atomic weapons would completely revolutionise modern warfare and that the possession of such weapons would become a dominating factor in world politics. This prophecy became reality only a few decades later, and the tension still remains today.

Ever since its practical realisation, nuclear energy has had a major impact on the world's energy production. It turned out that the energy of the atomic nucleus could be harnessed in two fundamentally different ways: *fusion* and *fission*, although the former has not yet reached a practical scale in energy production. The released energy originates from the same source in both reaction types, but it must be pointed out how fundamentally different they are in both theory and practice.

Fusion occurs when the nuclei of two light atoms are forced to combine. The collision must occur at a high energy, which in practice implies that the temperature of the system must be raised to some 10 to 100 million degrees in order to achieve a sufficient reaction rate for a self-sustaining fusion burn. Fusion reactor theory is based on plasma physics and the main technological challenges are related to heating and confinement of the fusion plasma.

Fission reaction takes place when a heavy actinide isotope absorbs a neutron and decays by splitting in to two intermediate-mass fragments. The reaction releases up to six new neutrons, which are available to initiate new fissions. This process is called a *chain reaction* and it forms the basis of fission reactor operation. Fission can occur with or without excess energy and the possibility of attaining a self-sustaining chain reaction depends more on the neutronic properties of the reactor materials than on the physical conditions of the system[1]. Fission reactor theory is largely characterised by the transport theory of neutrons.

All nuclear reactors operating today are based on the fission chain reaction. A simplified description of a nuclear power plant does not significantly differ from conventional gas-, oil- or coal-fired plants: the reactor produces heat, which is used to generate steam, which is used to run turbines, which are connected to a generator that produces electricity. Such a description does not, however, tell the whole truth. The reactor is actually aware of everything that goes on within the system and all disturbances are inevitably reflected in the core neutronics. This is the crucial difference to conventional power plants.

Another difference is that nuclear fuel is kept inside the reactor core for a long time, usually for the duration of the entire operating cycle, which typically ranges from one to two years. The physical properties of the fuel change dramatically during the cycle and the reactor must be adjusted to cope with the changes. The boilers in conventional power plants are simply fed with a continuous stream of fuel and the reaction products are expelled at the same rate.

The complicated coupling between coolant flow and reactor power and the isotopic and mechanical changes in the fuel due to neutron irradiation are examples of phenomena that need to be modelled in nuclear reactor analysis. Nuclear engineering combines neutron transport theory and various branches of material physics and thermal hydraulics. The focus in this study is on the neutrons and their behaviour in the reactor core. Neutron transport theory is a wide topic and this study deals with one particular approach: the Monte Carlo method.

1.1.1   History of the Monte Carlo Method

The Monte Carlo method can be characterised as a brute-force calculation technique, which is particularly well-suited for complicated problems consisting of several well-defined sub-tasks. The method is simple and intuitive in its basic form and it retains

---

[1]It will be discussed later on that temperature does play a major role in fission reactor operation, but, unlike in a thermonuclear fusion reactor, a low material temperature is never a restricting factor in attaining a self-sustaining state.

a close relation to the problem it is trying to solve. Although today the method is widely used for various tasks in physics, mathematics, economics and engineering, one of its first practical applications was in the modelling of complicated particle transport problems.

The calculation technique was first called the "Monte Carlo" method by Los Alamos scientists Stanislav Ulam, John von Neumann and Nicholas Metropolis in the late 1940s, when the method was used for solving particle transport problems encountered in nuclear weapons research [1]. Although Ulam is often given the credit for its invention, the method had existed in one form or another long before its first application in transport calculation problems. The roots of the technique date back to the development of the modern theory of probability and statistics in the 19th century and similar methods have been studied even before that.

The scientists at Los Alamos, however, had access to something that had never been available before: machine-based and automated numerical computation. Indeed, even if all the theoretical aspects had been resolved, the large-scale realisation of the method would not have been possible without this capability. Even the generation of a long sequence of random numbers, which is the heart of every Monte Carlo application, is very impractical without a computer-based calculation routine.

The basic principle of the Monte Carlo calculation in particle transport problems is very simple. The life of a single neutron, photon, electron or any other particle type is simulated from its initial emission until the eventual death by absorption or escape outside the system boundaries. The frequency and outcome of the various interactions that may occur during the particle's life are randomly sampled and simulated according to interaction laws derived from particle physics. When the procedure is repeated for a large number of particles, the result is a detailed simulation of the transport process, achieved at a tremendous cost in computing time.

1.1.2 Nuclear Reactor Calculations

It was probably immediately realised by the early reactor physicists, that the Monte Carlo method would not be a practical way to solve routine neutron transport problems on a large scale. The method had certain special applications and a wonderful potential for the future, but it was simply too much for the computers of the day to handle. Deterministic methods, based on the concept of a collective density function known as the *neutron flux*, became the dominant approach in neutron transport calculation.

Deterministic neutron transport codes are still today the most widely used option in reactor physics calculations and practically the only option for solving full reactor-

scale problems involving the coupling of core neutronics and thermal hydraulics. It is not possible to approach the transport process as a single well-defined problem. The solution proceeds in steps and each level is handled by a different code, specifically designed for the task. Some of the first steps are common to both deterministic and Monte Carlo calculations.

The nuclear interaction data collected from experimental measurements and supplemented by theoretical nuclear models is gathered into large data libraries, called *evaluated nuclear data files*. The library format is designed to preserve the accuracy of the original data and it cannot be directly used for transport calculation. Monte Carlo codes are able to use neutron interaction data in a tabular point-wise form, but all deterministic codes require data pre-processing into a group-wise format. This means that the continuous energy-dependence of the reactions is condensed into a discrete energy-group representation. This *micro-group* condensation is a complicated procedure and it inevitably leads to a certain loss of generality in the applications.

The micro-group interaction data is still far too detailed to be used efficiently in reactor-scale calculations, especially since the core geometry adds more complexity to the problem. The common solution is to reduce the level of detail even further. This procedure is called *homogenisation* and it is carried out by deterministic *lattice codes*, operating at fuel pin or assembly level. The homogenised *group constants* are specific to the fuel type and the local operating conditions, and they are generated in such a way that the integral reaction rate balance is preserved in the full-scale calculation.

The final step is the application of *reactor simulator codes*, which in light water reactor (LWR) analysis are typically based on few-group *nodal diffusion methods*. The energy resolution of the original interaction data is often reduced into only two energy groups: one group for thermalised neutrons (see Section 2.2.2 of Chapter 2) and another group for all the rest. The geometry is homogenised into a mesh of macroscopic homogeneous regions, called *nodes*. The nodal calculation can handle the full-scale spatial dependence of the neutron flux and produce global power and reaction rate distributions that are coupled to a thermal hydraulics calculation. The result is either a static or a dynamic simulation of the reactor response under different operating conditions. The calculation steps in nuclear reactor analysis are summarised in Figure 1.1.

1.1.3   Monte Carlo Method in Reactor Physics

The Monte Carlo method could in principle be used directly as the neutronics solver of a reactor simulator code. The solution would be simple, straightforward and

Experimental measurements and evaluation

Level of detail: detailed physics description, no geometry

Data processing

Level of detail: paremeterised nuclear models, no geometry

2D lattice calculation

Level of detail: high-resolution nuclear data, detailed local geometry

3D reactor simulator calculation

Level of detail: homogenised description of geometry and nuclear data

Experimental measurements and nuclear models

Nuclear model codes (EMPIRE, ALICE, TALYS)

Evaluated nuclear data files

Data processing codes (NJOY, CALENDF)

Point-wise or micro-group cross section libraries

Lattice codes (WIMS, CASMO, HELIOS, PSG)

Homogenised few-group constants

Reactor simulator codes (SIMULATE, TRAB, HEXTRAN, ARES)

Static or dynamic full-core simulation

Figure 1.1: Calculation steps in nuclear reactor analysis (LWR calculations).

potentially very accurate. The reason why this is not a practical approach is very similar to the early days of reactor physics: there are simply no such computers available, neither today nor in the near future, that could handle the task within a reasonable calculation time.

The Monte Carlo method has come a long way since the late 1940s and computer capacities have evolved more than anyone could have imagined. Typical modern applications are related to criticality safety analyses, validation of deterministic reactor physics codes and various dosimetry calculations, ranging from radiation shielding problems to detector modelling and medical applications. The common factor is the need to model the geometry and the interaction physics to within maximum accuracy.

The simplicity and the potential to produce very accurate results are indeed amongst the most attractive features of the Monte Carlo method. The neutron transport process is handled at the lowest possible level and the best available knowledge on neutron interactions with matter is available for the calculation. The evaluated nuclear data files can be accessed without major modifications and the same data can be used for any type of application. The reason why the method is so well-suited to reactor physics problems is the linearity of the transport process: neutrons, which act as the carriers of the fission chain reaction, interact only with the surrounding medium and not with each other. The linearity of the problem also makes it very suitable for parallel calculation, which increases the efficiency quite significantly.

An interesting near-future application for the Monte Carlo method is group constant generation for deterministic reactor simulator codes. The task is currently handled by second-generation lattice codes, and it is becoming increasingly challenging along with the development of nuclear technology. High-burnup fuels, complicated assembly designs, advanced MOX technology and next-generation reactor systems may cause problems for the deterministic codes, originally developed for conventional LWR calculations. A Monte Carlo based lattice code brings the advantages of the calculation method and may open up new possibilities in reactor simulation.

Some studies have been carried out on the subject and the interest has clearly increased over the last few years. It is likely that group constant generation and other new applications[2] will become standard Monte Carlo problems with the development in computer capacity. Group constant generation is also one of the main topics in this study.

---

[2]Another relatively new application for the Monte Carlo method is burnup calculation, which is usually realised by coupling a Monte Carlo neutron transport code and a deterministic fuel depletion code. This type of calculation is very computing-intensive, since the time-consuming transport calculation has to be repeated for a large number of depletion steps. Monte Carlo burnup calculation would not have been practical with table-top computers available ten years ago.

1.2   Scope of the Study

This study has been built around the development of a new Monte Carlo neutron transport code, developed at the Technical Research Centre of Finland (VTT). The project has been given the working title "Probabilistic Scattering Game", or PSG. The topics covered in this text serve the purpose of this development, and both theoretical and practical aspects of transport theory and Monte Carlo calculation are discussed.

1.2.1   Status of the PSG Project

The development of PSG started in September 2004. The first comparable results were obtained in early 2005 and the project was included in a VTT research programme a few months later. Code capabilities and some preliminary results were introduced in two reactor physics conferences in 2005 [2, 3] and later in 2006 [4] and 2007 [5].

In technical terms, the PSG code can be characterised as a three-dimensional, continuous-energy Monte Carlo neutron transport code. The code is specifically intended for reactor physics calculations, particularly at the fuel assembly level. PSG uses an analog Monte Carlo game and the so-called k-eigenvalue criticality source method for simulating a self-sustaining fission chain reaction.

It must be pointed out that this thesis is not a description of a complete code. It describes the state of the project in the summer of 2006, when the code development was frozen and the main focus turned to the writing of this text. PSG has not yet been made available through commonly used public channels, such as the OECD/NEA Data Bank [6]. The code has been used at VTT and mainly as a research tool in parallel with other Monte Carlo and deterministic transport codes. Only the most essential calculation methods and code capabilities are fully covered in this text. Certain features that have been developed, but not sufficiently tested, are referred to without discussing the underlying theory or the practical implementation of the methods. New features are constantly being developed, studied, planned and envisioned.

1.2.2   Structure of the Thesis

This thesis is divided in two parts. Part I, comprising Chapters 2–7, provides a solid theoretical background on the topics essential to this work. Chapter 2 is an introduction to the physics of neutron interactions and the general operating principles of nuclear fission reactors. Deterministic calculation methods are covered in

Chapters 3 and 4, with an emphasis on the few-group nodal diffusion method. A separate derivation for Fick's law, which is the foundation of diffusion theory, is provided in Appendix A. The theoretical background is mainly collected from various reactor physics textbooks [7–11] and a reader who is familiar with the basics may want to skip the first few chapters.

Deterministic transport theory is intentionally kept at a distance from the Monte Carlo method, which is further divided into the simulation of the particle histories in Chapter 5 and the collection of results in Chapter 6. The approach taken throughout this text is that the Monte Carlo method is a *simulation technique*, rather than a sophisticated mathematical theory[3]. Owing to the stochastic nature of the transport process, the method can be applied to its solution while retaining a close relation to the underlying physics. This approach differs to some extent from the presentations in most textbooks [11, 12]. It is the author's opinion that the Monte Carlo method is too often seen as merely another technique used for solving the Boltzmann transport equation. Such an approach is considered both complicated and misleading.

The final chapter in the first part deals with more practical issues: the fundamental nuclear interaction data used by all neutron transport codes and the processing of the data into different code-specific formats. Although this topic is easily disconnected from the other topics in this text, the origin of the interaction data is considered essential for all neutron transport applications and the quality of the data is reflected in the entire calculation process.

The scientific value of this thesis and the practical work related to PSG development are mainly contained in Part II, which comprises Chapters 8–10. PSG methodology, discussed in Chapter 8, follows the basic theory of Monte Carlo neutron transport calculation, introduced earlier in Chapter 5. Group constant generation in PSG is the topic of Chapter 9, in which several cross-references are made to results derived in the first part of the text. PSG is put into practice in Chapter 10, which introduces some example results calculated for the purpose of code validation. The emphasis is on LWR calculations and on the statistical validity of the result estimates. Chapter 11 is left for conclusions, and some plans for future development are briefly discussed.

1.2.3 Scientific Value of This Work

The single most important contribution of this work is that the development of a new transport calculation code has been started. Instead of modifying or writing a

---

[3]The calculations in this study involve mainly analog Monte Carlo methods, which are quite consistent with the underlying physical processes. It should be noted, however, that there are several non-analog techniques, in which the relation between the physics and the simulation is less obvious.

customised version of an existing code, PSG is completely written from scratch. The code uses standardised ENDF format [13] reaction data, read from ACE format data libraries. This library format was originally developed for the Los Alamos MCNP Monte Carlo code [14]. Since the data format is shared with MCNP, some of the interaction physics is handled in a similar manner as well. It must be pointed out, however, that PSG is an entirely independent project and it does not include any parts taken from the MCNP source code.

The characteristic feature of PSG is that it specialises in reactor physics calculations, particularly at the fuel assembly level. This specialisation removes some requirements necessary for general-purpose codes, but it also poses additional challenges and demands for the calculated output parameters. Some of the important and less traditional features of PSG are briefly introduced below.

Delta-tracking Method

Monte Carlo particle transport methods are conventionally based on a ray-tracing algorithm, which requires the use of complicated geometry routines. PSG relies on a slightly different approach, originally developed by E. R. Woodcock in the 1960s [15]. The Woodcock delta-tracking method is not widely used in Monte Carlo neutron transport codes[4], probably because it places certain limitations on the capability to calculate integral reaction rates inside regions of small volume or low collision rate. These limitations become significant in detector-type calculations, but the method is seen to be well-suited to the typical applications of PSG in particular.

The main advantage of the delta-tracking method is that it considerably simplifies the geometry routines and may speed-up the calculation in complicated geometries. The basic delta-tracking algorithm is introduced in Section 5.3.3 of Chapter 5. This method was extended in the PSG code to overcome certain efficiency problems encountered in lattice geometries containing localised heavy absorbers, such as control rods or burnable absorber pins. The practical implementation of the method in PSG is described in Section 8.3.1 of Chapter 8.

Uniform Energy Grid for Cross Section Data

The development of a completely new Monte Carlo code has allowed the full utilisation of presently available computer resources. Some procedures used in PSG would

---

[4]Delta-tracking (Woodcock-tracking, delta-scattering, pseudo-scattering) is used as an optional tracking method in the RCP01 [16], RACER [17], MCU [18] and VMONT [19] Monte Carlo codes and in the HOLE geometry package available for MONK and MCBEND [20].

not have been feasible ten years ago. One significant improvement is the substantial increase in computer memory. This has enabled the algorithms to be designed in such a way that the available memory is not considered a limiting factor. It is possible to attain a significant speed-up in certain calculation routines, if memory is allowed to be used wastefully during the process.

An example of such design is the methodology used for storing and accessing the interaction data. The procedures are designed in such a way that time-consuming iteration is cut to a minimum by using a uniform energy grid for all reaction cross sections. The price of the efficiency is that a large number of redundant data points needs to be stored, which considerably increases the required amount of computer memory. The details of the procedure are discussed in Section 8.2.2 of Chapter 8.

The uniform energy grid and the use of delta-tracking are the main reasons why the PSG code runs significantly faster compared to the main reference code, MCNP. Code performance is discussed in Section 10.6 of Chapter 10.

Parallelisation

Parallel calculation is becoming increasingly important in scientific computation. Computer clusters composed of PC workstations have become affordable and easy to set up. Parallelisation is a viable option in computing-intensive calculation tasks and it enables the treatment of many problems, otherwise too impractical to approach.

The Monte Carlo method is particularly well-suited for parallel calculation and the efficiency increases almost linearly as the number of parallel tasks is increased. Most of the state-of-the-art Monte Carlo codes are capable of running parallel calculations, and this aspect has been taken into consideration already from the beginning of PSG development. The efficiency gain achieved by using multiple computers simultaneously for the same task is demonstrated in Section 10.6.2 of Chapter 10.

Generation of Homogenised Group Constants

Group constant generation for deterministic reactor simulator codes was listed earlier as one of the interesting near-future applications of the Monte Carlo method. This task requires a certain level of specialisation and most of the widely-used general-purpose transport codes are not capable of performing this task without extensive modifications. Group constant generation is also one of the main themes in this study and PSG is probably one of the first attempts to develop an entirely new Monte Carlo neutron transport code specifically for this task.

The main difficulty in the generation of homogenised group constants is the calculation of the neutron diffusion coefficient. This constant is based on a heuristic approximation and it is essentially the only parameter without any continuous-energy counterpart in Monte Carlo calculation. A survey of previous studies [21–25] on group constant generation using the Monte Carlo method is given in Section 9.2 of Chapter 9. The studies introduce various methods for calculating the diffusion coefficient. PSG uses yet another approach, introduced in Section 9.3.3. The method is based on certain physical implications derived from few-group diffusion theory in Section 4.1.3 of Chapter 4.

Homogenisation and infinite lattice calculations are closely related to neutron leakage models, which are artificial corrections needed to account for the radial and axial streaming of neutrons across the non-physical geometry boundaries. This topic is briefly discussed in Chapters 4 and 9, but basically is left beyond the scope of this study. Another important element of group constant generation is fuel depletion calculation, which is the topic of Section 4.4. The present version of PSG is not capable of performing burnup calculation and more detailed studies are left for the future.

1.3   Example of a Monte Carlo Calculation

Before proceeding any further, it is considered illustrative to give a simple example of how the Monte Carlo method actually works. The calculation is based on the generation of a sequence of random numbers, which are used together with statistical laws to simulate the desired process. This type of calculation method is called stochastic, since the exact outcome of the simulation is always slightly different, if the procedure is repeated with a difference sequence of random numbers. The results are randomly distributed and characterised by a statistical mean value and an associated standard deviation. This is what differentiates the method from deterministic calculation, in which the outcome is always the same for the same set of input parameters.

The problem in this example case is the calculation of a decimal value for π. It is known that this constant is defined as the ratio of the circumference to the diameter of a circle and approximately equal to 3.141592653589793... It is also known that the area of a circle is given by:

$$A = \pi r^2 \,, \tag{1.1}$$

where r is the radius of the circle. This result can be used in the calculation as described in the following.

Consider a unit circle, i.e. a circle with radius $r = 1$. The area of such circle is simply $A_c = \pi \times 1^2 = \pi$. Imagine that the circle is confined within a square with
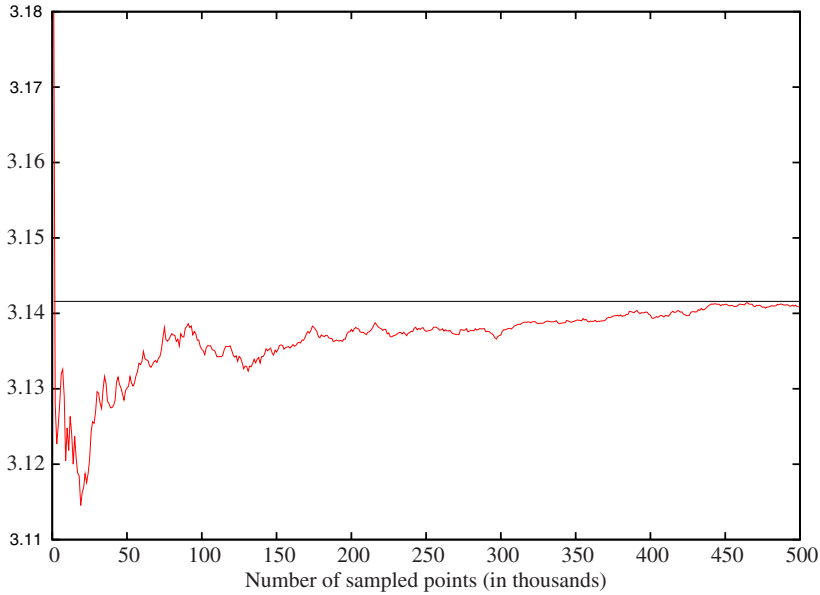
Figure 1.2: The Monte Carlo estimate of π as function of the number of selected random points.

side-to-side diameter $a = 2$. The area of the square is $A_s = a \times a = 4$. Imagine next that random points are selected uniformly inside the square. The probability that a point inside the square is also inside the circle is given by the ratio of the two areas:

$$P = \frac{A_c}{A_s} = \frac{\pi}{4}. \tag{1.2}$$

The value of π can hence be written using this probability as:

$$\pi = 4P. \tag{1.3}$$

A Monte Carlo estimate of P is easy to calculate. First, select a large number of points inside the square by setting their co-ordinates x and y randomly between -1 and 1. Second, calculate the number of points falling inside the circle, i.e. the points at which condition:

$$x^2 + y^2 < 1 \tag{1.4}$$

is fulfilled. According to Eq. (1.3), this number, multiplied by four and divided by the total number of points, should approach π. The result of one such simulation is plotted in Figure 1.2. It is seen that the estimate is, in fact, close to the correct value, as the number of simulated points increases. This procedure is not the most efficient

way to estimate the value of π using the Monte Carlo method, but it is probably the simplest one, and it clearly demonstrates the idea and the flow of the calculation process.

The simulation in this example case is called *implicit*, which is always the case when the simulation is not directly related to a stochastic process. The calculations discussed in this study are mainly *analog*, which implies that the numerical simulation and the underlying physical process are closely related. Neutron transport problems are probably among the most straightforward applications of the Monte Carlo method. Each neutron is simulated separately by tracking its path from one interaction to the next. The probability distributions characterising the interactions can be quite complicated, but they are directly related to physical measurable quantities. The collection of the final results is very similar to making experimental measurements.

Part I

Theoretical Background

Chapter 2

Physical Background

2.1   Neutron Interactions with Matter

Nuclear fission reactors are based on a self-sustaining chain reaction, carried on by neutrons in a fissile material. Neutrons carry no electric charge and they can easily penetrate through the electron cloud and the Coulomb potential barrier of the atomic nucleus. Neutron interactions are mediated by the strong nuclear force, which has a very limited range of about 10^{-15} m, about the same order of magnitude as the diameter of the nucleus. Neutrons interact very easily with any type of nuclei, even at low energy. Neutrons do not generally interact with each other[1], which results in the linearity of neutron transport theory, discussed in Chapter 3. This chapter deals with the basic physics of neutron interactions and the fundamental operating principles of nuclear fission reactors. The physical background is necessary for understanding the Monte Carlo simulation, in which individual neutrons are tracked from one interaction to the next.

The physics of neutron interaction are described by classical kinematics together with complex nuclear physics based on quantum mechanics. The classical nature is most clearly seen in elastic scattering reactions, which at sufficiently low energies are very similar to simple billiard ball like collisions. The quantum mechanical origin becomes apparent in events where the neutron penetrates deep inside the target nucleus and interacts with the constituent nucleons. Some complicated wave phenomena, such as neutron diffraction, are encountered when low-energy neutrons interact with a crystalline material structure.

---

[1]Neutron-neutron interactions are insignificant simply because the atomic density in a medium always exceeds the density of neutrons by several orders of magnitude. There are some exceptions involving extremely high neutron densities, such as neutrons stars.

It must be pointed out that apart from elastic *potential scattering* (see Section 2.1.3), the various neutron interactions encountered in fission reactor applications are not too different from each other. They all involve the formation of an excited short-lived *compound nucleus*, which rapidly decays into its ground state. The decay mode determines the reaction type, which in transport calculation are conveniently divided into capture, fission and scattering. The mere binding energy is not sufficient to induce all possible reaction modes. In such a case there is a certain limit for the kinetic energy of the incident neutron, below which the reaction may not occur[2]. Such *threshold reactions* are found in all three reaction categories.

The probability of an interaction between the incident neutron and the target nucleus is characterised by the *microscopic cross section*, which depends on the target nucleus, the interaction type and the energy of the incident neutron. At low energy, the probabilities of all compound reactions are directly proportional to the time the neutron spends within the reach of the strong nuclear force. This induces a characteristic $1/v$-dependence (inverse of neutron speed) on the cross sections.

The dependence becomes more complicated as the energy increases and the quantum-mechanical level-structure gives rise to a complex variation in the reaction cross sections. If the total neutron energy is close to the energy of a compound excited state, the interaction probability can suddenly rise by several orders of magnitude. This can be seen in the cross section curves as sharp peaks, or *resonances*. The resonances become narrower and more closely spaced with increasing energy. After some point, individual peaks can no longer be distinguished from each other. This is called the *unresolved resonance region*. At still higher energies, the resonances become overlapping and form a smooth continuum.

The following subsections introduce the characteristic features of the main reaction modes. The practical treatment of the collision physics in the Monte Carlo simulation is discussed in Section 5.4 of Chapter 5.

2.1.1 Capture

It is quite common that terms "capture" and "absorption" are used synonymously. In this text, a clear difference is made between the two concepts. Capture refers to all

---

[2]Interactions are possible below the threshold energy as well, but the cross sections are low and other reaction modes dominate the reaction probabilities. Two reaction modes available to all isotopes at all energies are elastic potential scattering and radiative neutron capture. The (n,γ) reaction probabilities of some isotopes, such as ^{3}H and ^{4}He, are low enough to be ignored completely. The low interaction probability for these isotopes results from the high instability of the product nucleus, which tends to decay by neutron emission immediately after relaxation into ground state. It should be noted, however, that (n,γ) is never a threshold reaction.

reactions in which no secondary neutrons are emitted. Absorption includes fission and all capture reactions, i.e. reactions in which the incident neutron is lost.

The simplest capture mode is the *radiative neutron capture*, or the (n,γ)-reaction. The incident neutron is bound in the target nucleus and the excess energy discharged in high-energy photon emission. An example of such a reaction is the radiative neutron capture of ^{238}U[3]:

$$^{238}\text{U} + \text{n} \longrightarrow {}^{239}\text{U}^* \longrightarrow {}^{239}\text{U} + \gamma \,. \tag{2.1}$$

The (n,γ)-reaction is practically the only capture mode available to neutron-rich actinide isotopes. Fission and multiplying scattering reactions become predominant at higher energies.

Other important capture reactions include (n,p), (n,α) and (n,^{3}He). These are typically threshold reactions, although there are some exceptions among the lighter isotopes. One example is the (n,α)-reaction of ^{10}B, which is written as:

$$^{10}\text{B} + \text{n} \longrightarrow {}^{11}\text{B}^* \longrightarrow {}^{7}\text{Li} + {}^{4}\text{He} \,. \tag{2.2}$$
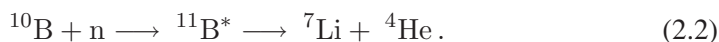
The (n,γ) cross section of ^{238}U is plotted in Figure 2.1. Uranium and other actinides are heavy isotopes with over 90 protons and 140–160 neutrons in the nucleus. The compound reactions are complicated and all actinide cross sections are characterised by a large number of resonances. The first resonance peaks are clearly distinguished at a relatively low energy. The unresolved resonance range begins at about 10 keV. This and the continuum region are seen in the figure as a smooth continuous curve.

2.1.2 Fission

Fission is an interaction in which the compound excited state formed after neutron absorption decays by energetically splitting the nucleus in two fragments:

$$^{235}\text{U} + \text{n} \longrightarrow {}^{236}\text{U}^* \longrightarrow {}^{135}\text{Xe} + {}^{98}\text{Sr} + 3\text{n} \,. \tag{2.3}$$
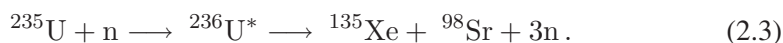
This is not the only reaction by which the intermediate ^{236}U nucleus can be split. It is typical, however, that two, instead of three or more, intermediate mass isotopes are produced, one slightly heavier than the other. The fission products are excessively rich in neutrons and undergo multiple β^--decays to reach more stable configurations.

Fission reaction is possible for all actinides[4] and it becomes predominant at high-energy absorptions in the MeV-range. The reaction actually requires some 6 MeV

---

[3]The emission of beta-particles and neutrinos is omitted in all reactions for the sake of clarity.

[4]High-energy fission is possible for some lighter isotopes as well, such as lead and tungsten. The reaction probabilities are low but measurable.
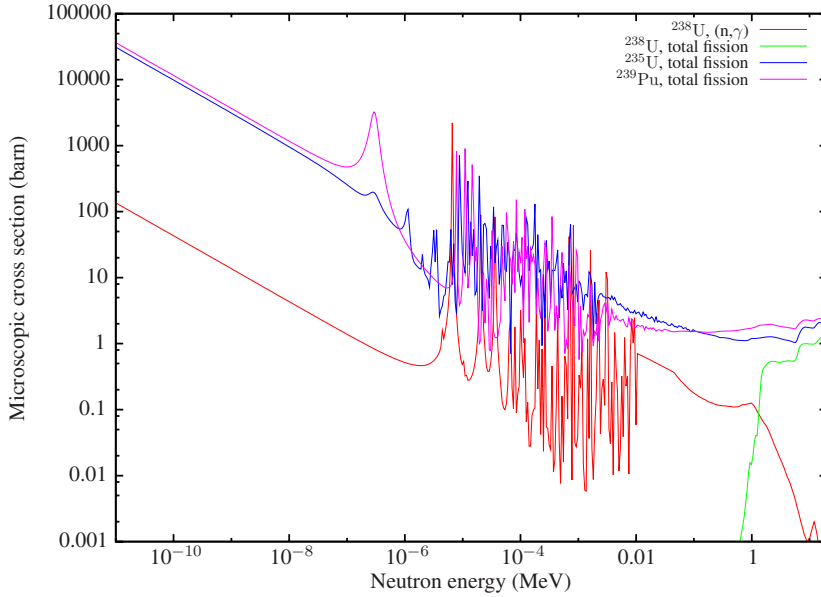
Figure 2.1: The (n,γ) cross section of ^{238}U *and the fission cross sections of* ^{235}U, ^{238}U, *and* ^{239}Pu *(ENDF/B-VI, 300 K data).*

of energy to occur. The energy released in the compound nucleus formation is of the order of 5 MeV. The missing energy gap is what makes the reaction so strongly dependent on the so-called parity effect: the changing of the neutron number from an odd to an even value releases another few MeV, which is enough to raise the energy above the fission threshold. Isotopes with an odd number of neutrons (^{235}U, ^{239}Pu, ^{241}Pu, ^{242}Am, etc.) are *fissile*, i.e. they can undergo fission by absorbing low-energy neutrons. *Fissionable* even-N isotopes (^{238}U, ^{237}Np, ^{240}Pu, ^{241}Am, etc.), on the other hand, have fission thresholds of the order of 1 MeV. The fission cross sections of ^{235}U, ^{238}U and ^{239}Pu are plotted in Figure 2.1.

The fission reaction produces one to six new neutrons. The average yields are linear functions of the incident neutron energy, and the number also depends on the isotope mass. In addition to the *prompt* neutrons emitted at the fission event, more neutrons are produced in the decay chains of fission product isotopes with a high excess number of neutrons. The radioactive neutron emission reaction is practically instantaneous, but it can follow the decay of another radioactive isotope with a longer lifetime. An example of such reaction chain is the decay of fission product ^{87}Br:

$$^{87}\text{Br} \longrightarrow {}^{87}\text{Kr}^* \longrightarrow {}^{86}\text{Kr} + \text{n} \,. \tag{2.4}$$
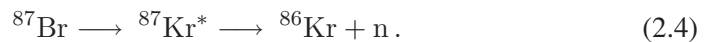
The lifetime of the decay chain is dominated by the first reaction, which has the half-

life of 56 s. This reaction determines the time it takes for the neutron to be emitted after the fission event. Such *delayed neutrons* have a significant impact on the reactor time constants, as will be seen in Section 4.3.2 of Chapter 4.

The average prompt fission neutron yields of ^{235}U, ^{238}U, ^{239}Pu and ^{241}Am are plotted in Figure 2.2. It can be seen how the number of emitted neutrons increases as function of isotope mass and incident neutron energy. The delayed neutron yields of the same isotopes range from 0.0043 for ^{241}Am to 0.0440 for ^{238}U. The values are practically independent of energy up to about 4 MeV, after which there is a clear drop in the yield. A more interesting factor from reactor physics point of view is the *fraction* of fission neutrons emitted as delayed, which for the four isotopes is plotted in Figure 2.3. The high delayed neutron fractions of the uranium isotopes is a safety feature that makes uranium-based fuels superior to other fuel types in many respects.

Fission neutrons are emitted isotropically, which results from the fact that multiple particles are produced in the reaction and the conservation laws of energy and momentum cannot dictate the coupling between the incident and emitted directions of motion. Further, the lifetime of the intermediate state is long enough for the incident neutron to "forget" its original direction.

The prompt fission neutron energy distribution is the shape of a Maxwellian function, peaked at around 1 MeV. The tails of the distribution extend to just below 10 MeV at the high end and to about 100 eV at the low end. The prompt fission spectra of ^{235}U, ^{238}U, ^{239}Pu and ^{241}Am are plotted in Figure 2.4. The distributions are slightly different for different isotopes, but practically independent of the incident neutron energy. Delayed neutrons are born at considerably lower energies, which has to be taken into account in reactor calculations (see Section 4.3.2 of Chapter 4).

The total energy released in fission (Q-value) is of the order of 200 MeV and it depends slightly on the target isotope. The components of energy release in ^{235}U fission are given in Table 2.1[5]. Most of the energy, around 80%, is released as the kinetic energy of the fission fragments. This energy is deposited instantly at the fission site. The entire 200 MeV of fission energy, however, is not recoverable. Some fraction is carried away by neutrons and photons that end up leaking outside the reactor core. About 4% of the energy is completely lost to neutrinos, which practically do not interact with matter. Not all the energy is released instantly either. The radioactive decay of fission products accounts for about 6% of the total fission Q-value. The time constants of the decay vary from milliseconds to thousands of years.

The description of the fission reaction given above mainly applies to the so-called *first-chance fission*. This means that the excited state decays directly by splitting

---

[5]Energy is also released in (n,γ)-reactions, which have a noticeable contribution in the total reactor heat production (see Section 9.4 of Chapter 9).
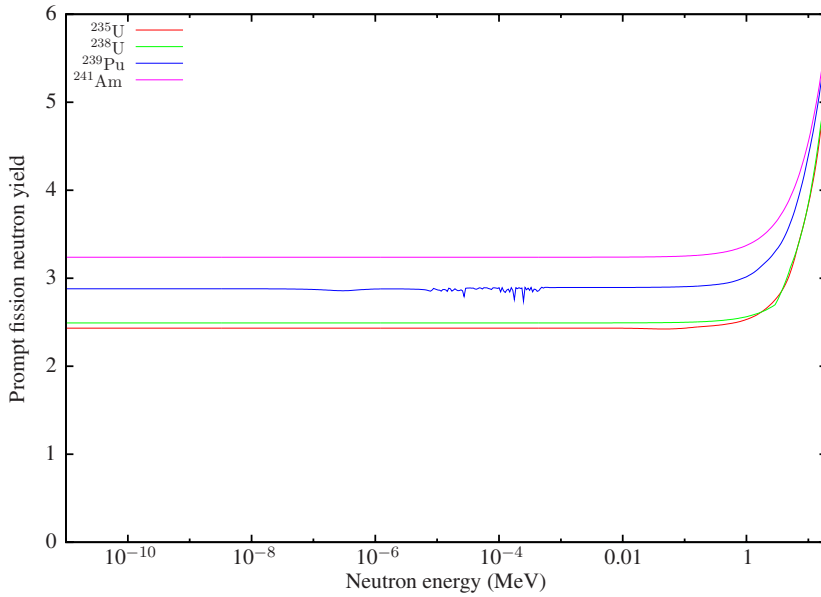
Figure 2.2: Average prompt fission neutron yields of ^{235}U, ^{238}U, ^{239}Pu and ^{241}Am (ENDF/B-VI). It should be noted that the energy-dependence is linear, which is not completely clear on the logarithmic scale.
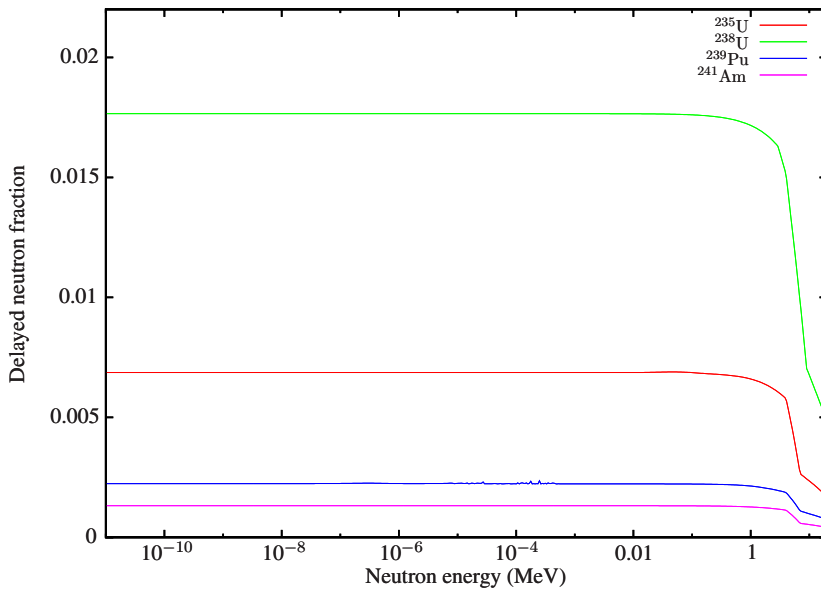
Figure 2.3: Total delayed neutron fractions of ^{235}U, ^{238}U, ^{239}Pu and ^{241}Am.
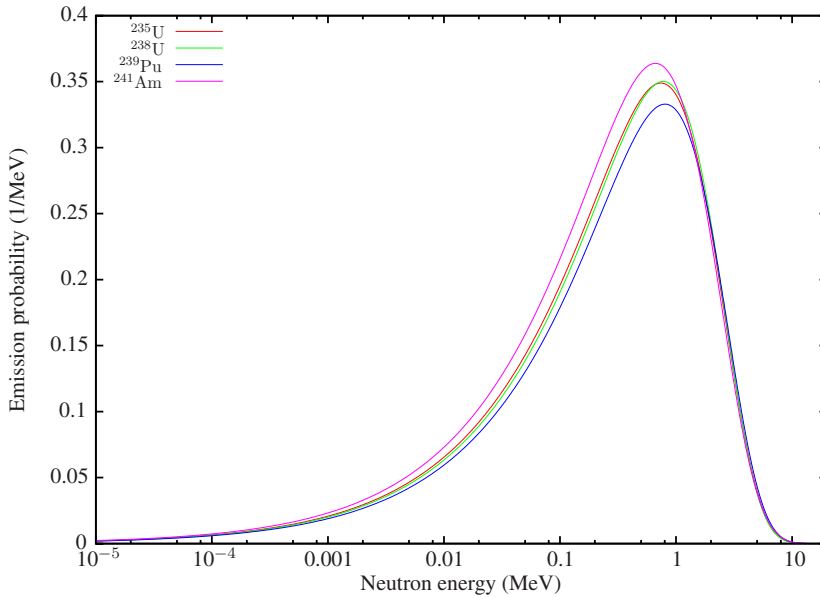
Figure 2.4: Prompt fission spectra of ^{235}U, ^{238}U, ^{239}Pu *and* ^{241}Am *(ENDF/B-V).*

the nucleus in two fragments. At higher incident energies, some of the compound energy can be released by neutron emission before the nucleus is split. Such reactions are called second-, third- and fourth-chance fissions and so on, depending on the number of neutrons emitted before the final decay. The physics of the fission reaction becomes increasingly complicated as the incident neutron energy increases to tens or hundreds of MeV. The complicated physics has to be consistently modelled in the Monte Carlo calculation, but in fission reactor applications it is sufficient to consider only the lowest few fission channels[6].

2.1.3 Scattering

Scattering collisions can be divided into elastic and inelastic reactions, in which one or more secondary neutrons are emitted. The difference is that elastic reactions preserve the total kinetic energy of the reacting particles. A direct result is that the energy loss suffered by the neutron is directly coupled to the angle between the incident and the scattered direction. This simplifies the collision kinematics quite significantly, as

---

[6]All fission reactions are often represented by a single total fission channel. The total is mainly composed of the first-chance fission, which for fissile odd-N isotopes spans the entire energy range. The second- and third-chance fission channels contribute above about 5 and 10 MeV, respectively.

Table 2.1: Components of the average energy release in the fission of ^{235}U *(from ENDF/B-VI.5).*

Component	Energy (MeV)	Fraction
Kinetic energy of fission fragments	169.1	83.5 %
Kinetic energy of prompt neutrons	4.8	2.4 %
Kinetic energy of delayed neutrons	0.007	0.004 %
Kinetic energy of prompt gammas	7.0	3.4 %
Kinetic energy of delayed gammas	6.3	3.1 %
Total energy released by delayed betas	6.5	3.2 %
Energy carried away by neutrinos	8.8	4.3 %
Total energy release per fission (sum)	202.5	100.0 %
Maximum recoverable energy	193.7	95.7 %

will be seen in Section 5.4.3 of Chapter 5.

In the simplest case of potential scattering, the neutron interacts with the target nucleus without penetrating inside. This type of elastic reaction is typical for low-energy neutrons, and it is available to all isotopes. Elastic potential scattering cross sections are practically constant at low energy and zero absolute temperature. The thermal motion of the target atoms increases the collision frequency, which results in a similar $1/v$-dependence as observed for the compound reaction cross sections. Scattering reactions become resonant at higher energies. The neutron starts to interact more with the constituent nucleons and the interaction becomes a compound reaction. The compound excited state can decay directly into the ground state by neutron emission, in which case the reaction is elastic.

In the inelastic case, some of the absorbed energy is released via γ-emission. The reactions are further divided into *level scattering* and *continuum inelastic scattering*. The decay of each discrete energy level is treated as a separate reaction channel. The continuum reaction includes scattering from all higher energy levels, which cannot be resolved from each other. The difference between the two is that level scattering can be associated with a discrete reaction Q-value, which couples the change in the neutron energy directly to the scattering angle, similar to the elastic case. The Q-value of the continuum reaction is given by a distribution and the simple relation between the energy loss and the scattering angle does not apply.

If the incident neutron energy is sufficiently high (typically in the MeV-range), the inelastic reaction can result in the emission of multiple neutrons, or a neutron and another particle, such as proton, α or ^{3}He. There are several such inelastic reaction
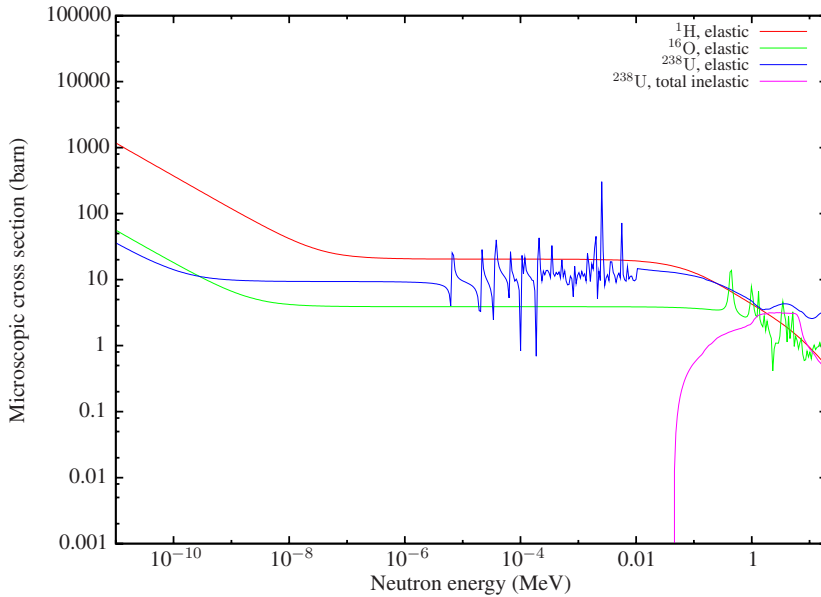
Figure 2.5: The elastic scattering cross sections of ^{1}H, ^{16}O and ^{238}U and the total inelastic scattering cross section of ^{238}U (ENDF/B-VI, 300 K data).

types, especially at neutron energies exceeding about 10 MeV. In fission reactor applications, however, it is practically sufficient to consider only two-body inelastic scattering and (n,2n)-reactions.

Elastic scattering cross sections of ^{1}H, ^{16}O and ^{238}U and the total inelastic scattering cross section of ^{238}U are plotted in Figure 2.5. The elastic potential scattering range of ^{16}O extends to about 0.5 MeV, after which the cross section becomes resonant. The resonance region of ^{238}U begins at a much lower energy and for ^{1}H the only scattering mode is potential scattering. The threshold energies of the inelastic reactions are in the high keV-range. Comparison to the other reaction cross sections of the same isotopes in Figure 2.1 shows a clear resemblance in the resonance structure. This is exactly what is to be expected, since all the compound reactions result from the decay of the same intermediate states.

Elastic potential scattering reactions are practically isotropic in the centre-of-mass frame-of-reference at low energy[7]. Considerable anisotropies are observed at higher energies, especially near resonances. Inelastic reactions are typically isotropic near the threshold energy, but the anisotropy increases with incident neutron energy.

---

[7]The so-called s-wave scattering mode is isotropic, and dominates at low energy. Higher scattering modes are anisotropic and start to contribute as the incident neutron energy increases.

2.2 Temperature Effects on Interactions

In practice, the only effect that can influence the fundamental interaction laws between neutrons and the target nuclei at the microscopic level, is the thermal motion of the atoms. It was mentioned earlier that elastic potential scattering cross sections are nearly constant at zero temperature, but the thermal motion induces an $1/v$-dependence on the cross sections. The increase results from the fact that the average velocity of the target atom becomes comparable to, or even exceeds the velocity of the neutron. This effectively increases the reaction rate as more collisions occur compared to scattering from stationary nuclei.

2.2.1 The Doppler-effect

Another significant temperature effect is the *Doppler-broadening* of resonance peaks, which is caused by increasing material temperature. This increases parasitic neutron absorption in the fuel, which has a profound meaning for reactor stability.

The interpretation of the Doppler-effect depends on the point of view. In reactor theory, the increased parasitic absorption is interpreted to result from the weakening of resonance self-shielding (see Section 2.3.5). Self-shielding, however, is a macroscopic effect, which does not present itself to individual neutrons. From the viewpoint of a single neutron, it is the random variation in the relative velocity between the neutron and the target nucleus that causes an increase in the interaction probability. When the neutron energy is close to a high resonance peak, the energy-dependence is strong, and the thermal motion of the target atom occasionally shifts the energy closer to the peak value.

Figure 2.6 shows the Doppler-broadening of a low-energy capture resonance peak of ^{240}Pu. It should be noted that the interaction probability is not affected at the microscopic level. The broadening is an artificial modification performed on the interaction data that takes into account the thermal motion of the atoms.

2.2.2 Temperature Effects on Collision Dynamics

The thermal motion of the target atoms also affects the dynamics of scattering reactions and target motion has to be taken into account in the collision equations (see Section 5.4.3 of Chapter 5). A low-energy collision with a moving target often leads to an increase in the neutron energy. The result is that neutrons are collected in the low-energy region. The kinetic energy of the target atoms follows the Maxwell-
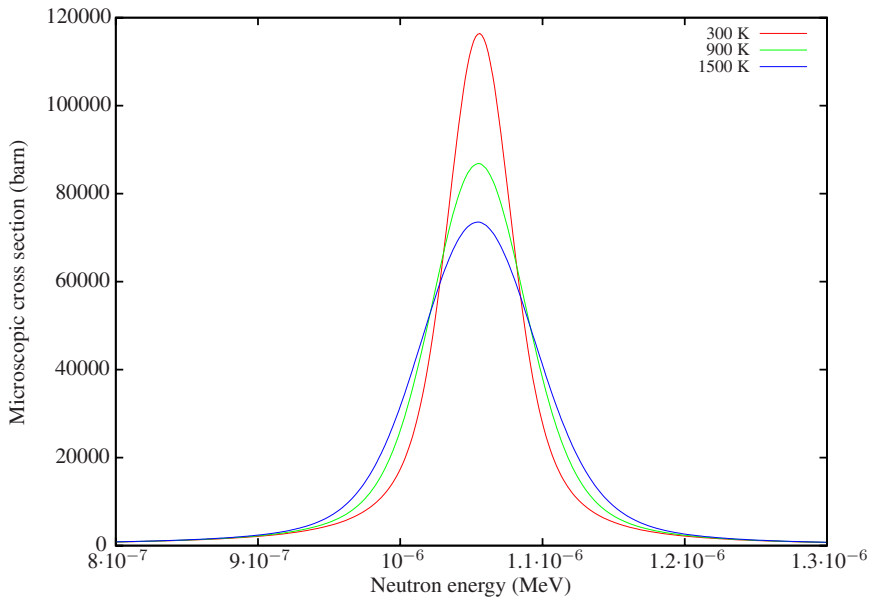
Figure 2.6: The Doppler-broadening of a low-energy radiative capture resonance of ^{240}Pu *(ENDF/B-VI.8).*

Boltzmann distribution and the average energy ranges from about 0.03 to 0.10 eV, depending on material temperature. The distribution of thermalised neutrons is not exactly Maxwellian, since the $1/v$-absorption shifts the peak towards higher energies.

2.2.3 Reactions with Bound Nuclei

It has been assumed so far that the interactions take place between neutrons and free target atoms. This is a good approximation when the neutron energy is well above the energy that binds the atom in a molecule or a crystalline lattice. Such binding energies are of the order of a few eV. Below this limit, scattering from certain bound atoms cannot be treated as a collision with a free particle without inflicting large errors in the calculation. Common examples are a hydrogen atom bound in the water molecule and a carbon atom bound in graphite.

The molecular and lattice bindings have an impact on both elastic scattering cross sections and the collision dynamics. The reaction is strongly dependent on material temperature and usually treated as a special type of inelastic collision. In the case of a crystalline lattice, the neutron may interact with the entire macroscopic lattice structure, giving rise to complicated diffraction effects. The free and bound elastic
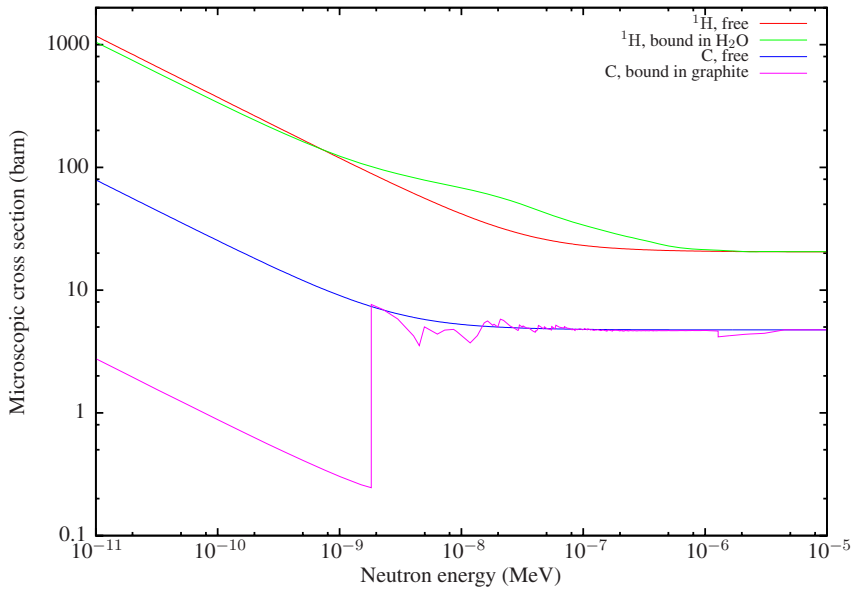
Figure 2.7: The free and bound elastic scattering cross sections of ^{1}H and natural carbon (ENDF/B-VI, 300 K data).

scattering cross sections of ^{1}H in water and natural carbon in graphite are plotted in Figure 2.7. The hydrogen cross section smoothly increases below 1 eV. The changes in the graphite cross section are more dramatic and they result from various lattice effects. The bound and the free atom cross sections coincide above a few eV.

2.3 Nuclear Reactors

This section gives a general description of the operating principles of nuclear fission reactors. The emphasis is on the design of thermal light water reactors, to which the deterministic calculation methods introduced in the following chapters mainly apply. The common feature to all reactor designs is that their physics is based on a self-sustaining chain reaction, carried on by fission neutrons in a multiplying medium.

2.3.1 Fission Chain Reaction

Since a large fraction of fission neutrons are born below the fission threshold of even-N isotopes (see Figures 2.4 and 2.1), the majority of fissions always occur in

fissile nuclides, typically ^{235}U or ^{239}Pu. A self-sustaining chain reaction means that the average number of neutrons emitted in fission reactions is sufficiently large to induce at least an equal number of new fissions. If reactor power is to be kept constant, the number of emitted neutrons must exactly match the number of neutrons in the previous "generation".

It is seen in Figure 2.2 that the average fission neutron yields range from about 2 to 6. In order to maintain the steady-state operating condition, excess neutrons need to be removed from the reaction chain before inducing new fissions. A fraction of neutrons escape the reactor core. Some are absorbed in the coolant and structural materials, or in the fuel without causing new fissions. The remaining excess part is left for reactor control. Some reactivity reserve is needed for reactor start-up and power adjustment, and for the compensation of various negative reactivity effects that emerge during the operation.

2.3.2   Thermal and Fast Reactors

As seen in Figure 2.4, fission neutrons are born at a high energy, around 1 MeV. Figure 2.1 shows that the fission cross section of ^{235}U is about one barn at that energy range. It is also seen that the low-energy cross sections are about 100 to 1000 times higher. A high cross section means high interaction probability, which in turn implies that less fissile material is needed to attain a self-sustaining chain reaction. Therefore, it would be beneficial to have more neutrons in the low-energy region.

This is the operating principle of thermal reactors. Fast fission neutrons are slowed down by elastic scattering collisions in the *moderator*, which is simply a material consisting of light isotopes. The most commonly used moderator materials are light and heavy water and graphite. As was discussed in Section 2.2.2, the slowing-down process is terminated in the thermal energy region, where neutrons accumulate in balance with the moderator atoms.

It is important to realise the significance of elastic scattering for the life of a single neutron in a thermal reactor. The average neutron lifetime in a typical LWR core is of the order of 0.1 ms [7]. The slowing-down process takes about 0.01 ms and the rest of the time is spent scattering around in the moderator. According to computer simulations, over 90% of reactions consist of elastic scattering with hydrogen atoms in water. Of that fraction, over 30% occurs below 1 ev energy. About 80% of fissions are caused by thermalised neutrons.

Fast reactors operate on a different principle. Figure 2.1 shows that between the high-energy range where the neutrons are born and the low-energy region where they end up after thermalisation, there is a resonance region where the radiative capture cross

section of ^{238}U is high. A significant fraction of neutrons in thermal reactors are lost in these capture resonances. Neutrons in fast reactors are intentionally kept at a high energy, simply by avoiding the use of good moderator materials. The coolant of choice in present fast reactors is liquid sodium, but also lead, lead-bismuth and helium gas-cooled reactor designs have been proposed. The fast energy spectrum increases the fission probability of all actinides, including ^{238}U, as more neutrons are available above the threshold energy. The average fission neutron yields are increased as well (see Figure 2.2), which makes it possible to attain a much better neutron economy compared to thermal reactors.

The historical idea behind the improved neutron economy is the so-called *breeder* reactor, which produces more fissile material (plutonium from ^{238}U) than it consumes. The idea can also be reversed and the reactor used as a *burner*, for the incineration of hazardous and long-lived plutonium and minor actinide isotopes in spent nuclear fuel. Despite all the attractive features, fast reactor technology has so far been shadowed by the economic success of the common light water reactor[8].

2.3.3   Reactor Geometries

Nuclear energy has 60 years of history, during which any experimental configuration that can be made critical has probably been attempted. The design of power reactors, however, has well converged into a handful of basic concepts. The most common reactor types in use today are the light water-cooled pressurised (PWR) and boiling water reactor (BWR).

A typical reactor fuel consists of ceramic fuel pellets of about 1 cm in diameter, encapsulated inside gas-tight metallic cladding. These fuel pins are arranged in a regular lattice and collected in small bundles, or assemblies. BWR fuel assemblies contain about 100 fuel pins and PWR assemblies two to three times that. The height and number of fuel assemblies dictates the core size, which depends on reactor power. The typical number of fuel assemblies ranges from 150 to 900 and the total number of pins from 40,000 to 150,000. The number of fuel pellets is counted in millions.

The fuel assemblies are loaded in the reactor core, which in PWRs and BWRs is enclosed inside a thick pressure vessel. The difference between the two designs is that the coolant is re-circulated inside the pressure vessel of a BWR. The water boils

---

[8]The list of currently operational fast reactors includes the FBTR (India), JOYO (Japan) and BOR-60 (Russia) experimental reactors and the Phenix (France) and BN-600 (Russia) demonstration reactors. Some major fast reactor programmes, such as the French Super Phenix and the Japanese Monju, have been cancelled during the past decade, although the Monju-programme is planned to be restarted in 2008. Three fast reactors are currently under construction: BN-800 in Russia, PFBR in India and CEFR in China [26].

in the reactor core and leaves the vessel as high-temperature, high-pressure steam. The coolant flow in a PWR is simply forced through the reactor core by the main circulation pumps and kept in the liquid phase by high pressure. Steam is produced in a secondary water loop using separate steam generators.

The geometries of the various reactor types differ quite significantly at the core level, which affects the modelling aspects as well. A BWR core has more detail and heterogeneity than a typical PWR core. The two-phase coolant flow adds a whole new dimension to the problem. BWR fuel assemblies are typically equipped with additional water channels to provide for better moderation, which complicates the assembly design. BWR control rods are cruciform in shape and they are inserted in water channels between the assemblies. PWR control rods are usually the size of a single fuel pin and they are inserted in guide tubes located inside the assembly[9].

The above description applies to the typical LWR cores, which cover about 80% of the world's nuclear reactors. Another popular design for water-cooled reactors is the channel-type core, in which the fuel assemblies are loaded in separate pressure tubes. This design is used in the Canadian CANDU heavy water reactors and the Russian graphite-moderated RBMK. A promising reactor concept for the future is the high-temperature gas-cooled reactor (HTR or HTGR). The core is basically built from graphite, either using stacked hexagonal blocks or as a pile of spherical fuel pebbles. The fissile material is packed in microscopic multi-layer fuel particles, which are randomly dispersed in graphite matrix. Sodium-cooled fast reactors are sometimes built in a pool-type configuration. The reactor core and the main circulation pumps are located in a large pool of liquid metal, which acts as the primary coolant loop.

2.3.4   Reactor Fuels and Materials

LWR fuels are made of uranium oxide (UOX, UO_2), i.e. low-enriched uranium and natural oxygen in a 1:2 atomic ratio[10]. The enrichment varies from about 2 to 5% ^{235}U. Some heavy water and graphite-moderated reactors may operate on natural uranium (0.72% ^{235}U). Fast reactor fuels are typically more enriched. Natural uranium contains some trace amounts of ^{234}U, which is also present in the reactor fuel. The oxygen content in UOX fuel is high. Natural oxygen is mainly composed of isotope ^{16}O, which is not a significant neutron absorber.

---

[9]The design of Russian VVER-440 pressurised water reactors differs quite significantly from their western counterparts. The fuel pins are arranged in a hexagonal, rather than square lattice and surrounded by a hexagonal channel box. The reactor uses so-called flux-trap control rods, which are the size of a normal fuel assembly. The absorber part is attached to a full-length follower fuel assembly, which is inserted in the core from below as the absorber is lifted.

[10]In addition to oxide fuels, metallic, nitride and carbide fuels are used in more unconventional reactor designs and concepts.

As a nuclear fuel is burnt, the isotopic composition changes as a result of fission and various neutron capture reactions. At the end of the LWR operating cycle, approximately 2% of the original ^{238}U has been transmuted into plutonium and minor actinides. Most of the initial ^{235}U and about half of the produced fissile plutonium has been fissioned into several hundred intermediate-mass isotopes. The isotopic changes in the fuel have to be taken into account in reactor analysis, as will be discussed in Section 4.4 of Chapter 4.

The most significant trans-uranium isotopes in the irradiated fuel are the three plutonium isotopes, ^{239}Pu, ^{240}Pu and ^{241}Pu. The fissile ^{239}Pu is produced from ^{238}U by the neutron capture reaction in (2.1) followed by two β^--decays with relatively short half-lives. The higher plutonium isotopes are produced from ^{239}Pu by successive neutron capture reactions. The rest of the actinide content consists of ^{237}Np, minor plutonium isotopes (^{238}Pu and ^{242}Pu) and the higher actinides, namely americium and curium. In addition, a significant fraction of ^{235}U is converted into ^{236}U by radiative capture.

The build-up of fission product isotopes affects reactor operation in several ways. The single most important isotope is ^{135}Xe, which has an exceptionally high thermal neutron capture cross section, about a million times larger compared to ^{238}U. Xenon-135 is produced both directly in fission and in the decay of another fission product isotope, ^{135}I:

$$^{135}\text{I} \longrightarrow {}^{135}\text{Xe} \,. \tag{2.5}$$

The half-lives of the two isotopes are 6.57 and 9.14 hours, respectively. The build-up of ^{135}Xe is a delayed effect that may lead to the so-called *xenon poisoning*. This is a phenomenon that may prevent reactor operation for several hours or, in certain unfavourable conditions, induce spatial power oscillations in the reactor core.

Over 99% of fissions in a fresh LWR UOX fuel occur in the fissile ^{235}U. Fissile plutonium isotopes begin to contribute after the fuel has been irradiated in the reactor for some time. At the end of the operating cycle, about 50% of fissions occur in ^{239}Pu, which is actually an appreciable contributor in the overall energy output. Recycled plutonium, either from reprocessed reactor fuel or from disposed nuclear weapons, can be used as the fissile material in so-called *mixed oxide* fuels (MOX). MOX fuels are presently used in several reactors in countries like France, Belgium and Switzerland, and their use is likely to increase in the future[11].

Other materials in the reactor core include moderator, absorbers and various structural and support materials. Good moderators are composed of light isotopes and are

---

[11]MOX technology aims at higher fuel utilisation and lower production of long-lived plutonium isotopes. Some advanced fuel concepts promise a zero net-production of plutonium in LWRs fully loaded with MOX fuel [27–30]. The modelling of such systems may require the use of advanced transport methods.

characterised by low capture and high scattering cross sections. Viable moderators include light and heavy water, graphite and beryllium.

Movable control rods, typically made of boron steel or carbide, are used for reactor start-up and shut-down, power adjustment and reactivity compensation. *Burnable absorbers* are high-absorbing materials mixed in the fuel. The absorber is slowly depleted by neutron irradiation, which compensates for the reactivity loss caused by increasing burnup. Boric acid (H_3BO_3) is used in PWRs as a *soluble absorber*. Boron is dissolved in the coolant water and the concentration slowly reduced as the fuel is burnt. There is a clear difference between homogeneously distributed soluble absorber and localised absorbers rods. Dissolved boron absorbs neutrons throughout the reactor core, as soon as they are thermalised in the moderator. Burnable absorber pins and control rods create a very localised depression in the thermal neutron density, which mainly affects the reaction rates in the nearby fuel pins.

Various support structures are needed to maintain the geometry of the reactor core. Zirconium alloys are the most commonly used cladding materials in LWR fuels, and they are also used in spacer grids, assembly flow channel walls and other support structures. The neutron capture cross section of natural zirconium is low and the alloys are corrosion resistant and mechanically durable in the reactor conditions.

2.3.5 LWR Neutron Spectrum

All thermal reactors share the same characteristic features in their neutron energy spectra. Neutrons are born at a high energy and collected in the thermal region after being slowed down by elastic collisions in the moderator. The spectrum is composed of two Maxwellian energy peaks. The high-energy peak results from the energy distribution of prompt fission neutrons (see Fig 2.4), and the low-energy peak is formed by neutrons thermalised in the moderator. This basic shape is clearly seen in Figure 2.8, which shows three flux distributions[12] in a PWR core at different moderator temperatures

It can be seen that there are several deep gaps in the spectra at discrete energy points. These gaps are caused by the high reaction probabilities near the resonance peaks. The distributions clearly show the effects of the low-energy capture reso-

---

[12]Neutron flux is defined in the following chapter as the neutron density multiplied by velocity and it basically characterises the rate at which neutrons encounter surrounding atoms while streaming through the medium. This rate increases substantially with energy, which clearly emphasises the role of fast neutrons. The *number* of neutrons in the thermal energy region at a given time clearly exceeds the number of fast neutrons. If the reactor core is frozen in time, almost 90% of neutrons lie below 0.625 eV, which is commonly defined as the upper boundary of the thermal energy region in LWR analysis. In terms of neutron flux, the thermal fraction is of the order of 15%.
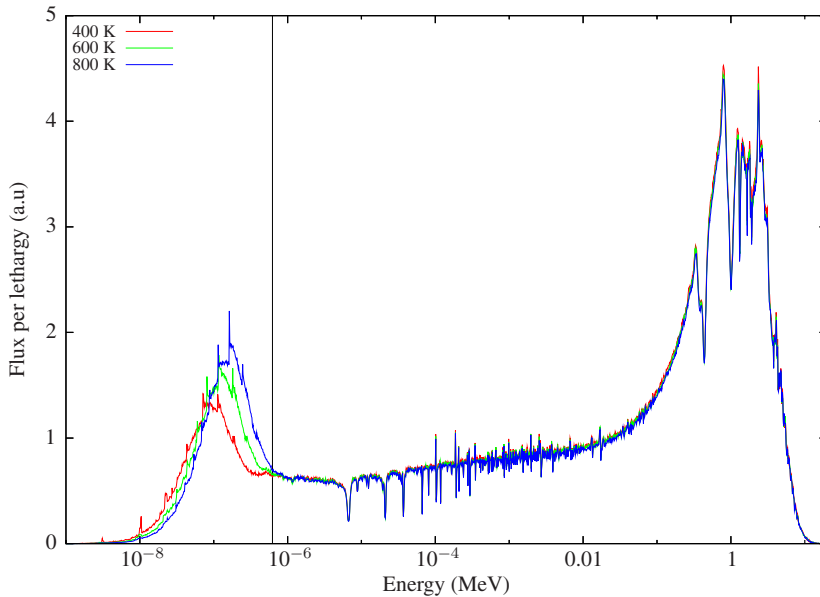
Figure 2.8: Typical LWR flux spectra at different moderator temperatures (PWR pin-cell model, calculated by PSG).

nances of ^{238}U (see Fig. 2.1). The impact of ^{16}O elastic scattering resonance at about 0.4 MeV (see Fig. 2.5) is clearly visible as well. It is also seen that an increase in the moderator temperature shifts the thermal peak up on the energy scale.

The resolution in the spectra and the logarithmic scales used in the cross section plots do not quite do justice for the high reaction probabilities at resonance energies. The low-energy capture resonances of ^{238}U, for example, are so high, that it is practically impossible for a neutron with energy corresponding to the exact peak value to pass through a fuel pin without being captured[13]. The flux depression and *resonance self-shielding* are important factors in deterministic transport theory, and need to be taken into account when cross sections are condensed into discrete energy groups. This topic will be discussed in the following chapters.

The high absorption rate in the fuel also induces a spatial self-shielding effect and a localised depression in neutron density. Thermal neutrons streaming from the moderator are absorbed in a thin surface layer of the fuel pellet, causing a peak in fission rate distribution. Fissile isotopes and burnable absorber are depleted more efficiently near the surface and the isotope concentrations become non-uniform as the fuel is burnt. This *rim-effect* has to be taken into account in fuel depletion calculations.

---

[13]This probability is of the order of 10^{-69}.

Chapter 3

Neutron Transport Theory

3.1 Basic Concepts

The objective of neutron transport calculation is to solve the nuclear reaction rate distribution within the boundary conditions of the physical system, such as the core of a nuclear reactor. All deterministic solution methods are derived from *transport theory*. The general principle of the theory is not complicated, since it is based on simple conservation laws and a few mathematical definitions. In many respects, the transport theory of neutrons is very similar to the other transport problems encountered in various fields of physics, such as the motion of molecules in a fluid or the drifting of ions and electrons in a plasma.

There are, however, some crucial differences as well. One of the characteristic features of neutron transport calculation is the complicated energy-dependence of the interaction probabilities between neutrons and the nuclei in the medium. This results from the strong quantum-mechanical nature of the compound-nuclear reactions, as was discussed in the previous chapter. Another significant property is that neutrons do not experience the Coulomb potentials of the surrounding atoms. The forces acting in the collisions have very limited range and the neutron paths between scattering collisions are described by straight lines. Further, neutron interactions with each other can be ignored, which results in the linearity of the collision term in the transport equation.

The description of neutron transport theory given in this text is not complete in detail, since there are literally hundreds of textbooks written on the subject[1]. The general

---

[1]See e.g. the classic reactor physics coursebooks by Duderstadt & Hamilton [7], Lamarsh [9] and Bell & Glasstone [8].

form of the transport equation is introduced and some related topics discussed. The basic principles of the solution methods are briefly reviewed, but the practical implementation is left for the following chapter, which deals with nodal diffusion methods, commonly used in reactor simulator codes.

An understanding of the fundamental theory is important, not so much for the understanding of the Monte Carlo simulation, but for the derivation of the result estimates. Perhaps even more important in this respect is to understand what the basic concepts imply in practice. The Monte Carlo method is put aside for the remainder of this chapter and the main focus is turned from the life of a single neutron to a mathematical density function known as the *neutron flux*.

3.1.1 Physical Interpretation of the Cross Section

As was mentioned in Chapter 2, the probability of a single neutron interacting with a target nucleus is characterised by the microscopic cross section. This interpretation is best understood by considering a beam of neutrons hitting a thin sample perpendicular to the direction of motion. Let the intensity of the neutron beam be I (in neutrons/cm^{2}s) and all neutrons have the same speed and direction. For simplicity, the target sample is assumed to be only one atomic layer thick and that the neutrons have only one chance of interacting while passing through it. The target has cross-sectional area A and it is made of a homogeneous material with surface atomic density N_A (in atoms/cm^2).

The total reaction rate in the sample is proportional to the beam intensity, the atomic density of the material and the cross-sectional area of the target [7]:

$$R = \sigma_{\mathrm{t}} I A N_A \, . \tag{3.1}$$

The proportionality coefficient σ_{t} is the microscopic total cross section of the target material. The rate at which neutrons hit the sample is IA. Since N_A is the number of atoms per unit area, it can be seen that σ_{t} is essentially the interaction probability with a single nucleus, characterised by a parameter that can be interpreted as the effective cross sectional area of the nucleus.

The average reaction probabilities on a macroscopic scale are characterised by *macroscopic cross sections*, which are defined as the microscopic cross section multiplied by the nuclear density:

$$\Sigma_i(\mathbf{r}, E) = N(\mathbf{r}) \sigma_i(E) \, . \tag{3.2}$$

The physical interpretation of the macroscopic cross section is that it describes the interaction probability per path length travelled by the neutron [7].

Combined cross sections, such as total, total fission and total absorption can be calculated simply by summing over the corresponding reaction channels:

$$\sigma(E) = \sum_i \sigma_i(E) \, . \tag{3.3}$$

If the medium consists of several isotopes, the macroscopic cross section of the material is calculated as the sum over all the constituents:

$$\Sigma_i(\mathbf{r}, E) = \sum_m N_m(\mathbf{r})\sigma_{m,i}(E) \, . \tag{3.4}$$

In summary: $\sigma_i(E)$ describes the neutron interaction probability with a single nucleus and $\Sigma_i(\mathbf{r}, E)$ is related to the interaction properties of a medium consisting of several nuclei. The former is a quantity characteristic of the isotope species, while the latter is effectively a material property that depends on the isotopic composition.

3.1.2   Reaction Rate and Neutron Flux

The state of a neutron in the six-dimensional phase space can be described using six independent co-ordinates: three co-ordinates for the position and three co-ordinates for the velocity. It is more convenient for the dynamics of scattering collisions to write the equations using momentum instead of velocity, in which case the Cartesian co-ordinate system is written as (x, y, z, p_x, p_y, p_z), or as $(\mathbf{r}, \mathbf{p})$, using the vector notations.

The momentum vector is typically replaced by a two-component unit direction vector $\hat{\mathbf{\Omega}}$ and the energy E of the particle. The co-ordinate system then becomes $(\mathbf{r}, \hat{\mathbf{\Omega}}, E)$. The direction vector $\hat{\mathbf{\Omega}}$ depends on two angular variables, η and ϑ, and it can be written using the three Cartesian direction vectors as:

$$\begin{aligned}
\Omega_x &= \sin\eta\cos\vartheta \\
\Omega_y &= \sin\eta\sin\vartheta \\
\Omega_z &= \cos\eta
\end{aligned} \tag{3.5}$$

Figure 3.1 illustrates the definitions.

Angular Neutron Density and Flux

The density function describing a neutron population in the six-dimensional phase-space is the *angular neutron density*, $n(\mathbf{r}, \hat{\mathbf{\Omega}}, E)$. When this function is multiplied
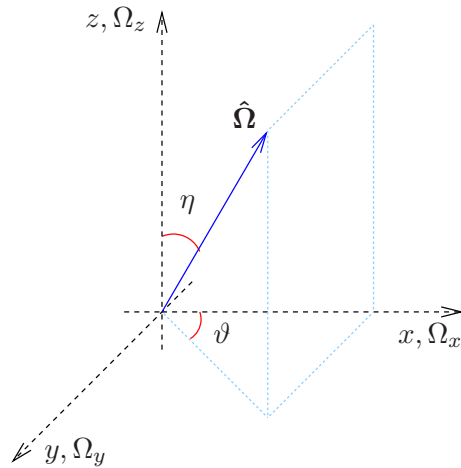
Figure 3.1: The definition of the angular variables in the Cartesian co-ordinate system.

by the speed (the absolute value of the velocity vector: $v = \sqrt{\mathbf{v} \cdot \mathbf{v}}$) corresponding to the energy variable E, the result is another density function, known as the *angular neutron flux*:

$$\psi(\mathbf{r}, \hat{\mathbf{\Omega}}, E) = v n(\mathbf{r}, \hat{\mathbf{\Omega}}, E) . \tag{3.6}$$

The angular flux has no physical significance on its own, but it is related to the rate at which neutrons with energy E stream through space in direction $\hat{\mathbf{\Omega}}$. The time-dependence of the two density functions is omitted for simplicity.

The significance of the angular flux is in that it relates the neutron interaction rate to the physical properties of the medium. The interaction rate basically depends on four variables: the density of neutrons and target nuclei in the medium, the neutron velocity, which determines the rate at which neutrons encounter the surrounding atoms, and the probability of a single neutron-nucleus interaction. The rate-density of reaction i can be written using the macroscopic cross section and the neutron flux as:

$$r_i(\mathbf{r}, \hat{\mathbf{\Omega}}, E) = \Sigma_i(\mathbf{r}, E) \psi(\mathbf{r}, \hat{\mathbf{\Omega}}, E) . \tag{3.7}$$

To be precise, this definition gives the average total number of interactions of type i per unit time, inflicted by neutrons streaming through an infinitesimal element of the six-dimensional phase about $(\mathbf{r}, \hat{\mathbf{\Omega}}, E)$.

For scattering reactions, it is also necessary to define the *differential* reaction rate density, i.e. the average rate at which neutrons scatter from energy E to E' and from

direction $\hat{\mathbf{\Omega}}$ to $\hat{\mathbf{\Omega}}'$:

$$r_\mathrm{s}(\mathbf{r}, \hat{\mathbf{\Omega}} \to \hat{\mathbf{\Omega}}', E \to E') = \Sigma_\mathrm{s}(\mathbf{r}, \hat{\mathbf{\Omega}} \to \hat{\mathbf{\Omega}}', E \to E')\psi(\mathbf{r}, \hat{\mathbf{\Omega}}, E). \qquad (3.8)$$

The differential scattering rate does not usually depend on the absolute direction of the incident and the scattered neutron, but rather on the angle between the directions. The change in the neutron direction is often written using the *scattering cosine*, $\mu = \cos\theta = \hat{\mathbf{\Omega}} \cdot \hat{\mathbf{\Omega}}'$, or the cosine of the angle θ between the direction vectors before and after the collision. The differential scattering rate density is then written as:

$$r_\mathrm{s}(\mathbf{r}, \mu, E \to E') = \Sigma_\mathrm{s}(\mathbf{r}, \mu, E \to E')\psi(\mathbf{r}, \hat{\mathbf{\Omega}}, E). \qquad (3.9)$$

The *double-differential scattering cross section*, $\Sigma_\mathrm{s}(\mathbf{r}, \hat{\mathbf{\Omega}} \to \hat{\mathbf{\Omega}}', E \to E')$ is not a similar parameter to the other macroscopic cross sections. It is a distribution that characterises the probability of a particular scattering reaction when integrated over an energy interval and angular space. The integration over the full space-angle yields the single-differential scattering cross section that is a distribution of the energy variable only:

$$\int_{4\pi} \Sigma_\mathrm{s}(\mathbf{r}, \hat{\mathbf{\Omega}} \to \hat{\mathbf{\Omega}}', E \to E')d\hat{\mathbf{\Omega}}' = \int_{-1}^{1} \Sigma_\mathrm{s}(\mathbf{r}, \mu, E \to E')d\mu = \Sigma_\mathrm{s}(\mathbf{r}, E \to E').$$
$$(3.10)$$

This parameter gives the scattering probability from energy E to E' per unit path length travelled by the neutron. The *total* scattering cross section is obtained by integration over all final energies:

$$\Sigma_\mathrm{s}(\mathbf{r}, E) = \int_0^\infty \Sigma_\mathrm{s}(\mathbf{r}, E \to E')dE' = \int_{-1}^{1}\int_0^\infty \Sigma_\mathrm{s}(\mathbf{r}, \mu, E \to E')d\mu dE'. \quad (3.11)$$

This variable can be treated similar to the other reaction cross sections.

Scalar Neutron Density and Flux

The angular dependence is irrelevant in capture reactions and in reactions in which the secondary neutrons are emitted isotropically, such as fission. For such cases, it is convenient to define the concept of a *scalar flux*, which is given by the angular neutron flux integrated over the full space-angle:

$$\phi(\mathbf{r}, E) = \int_{4\pi} \psi(\mathbf{r}, \hat{\mathbf{\Omega}}, E)d\hat{\mathbf{\Omega}} = v \int_{4\pi} n(\mathbf{r}, \hat{\mathbf{\Omega}}, E)d\hat{\mathbf{\Omega}} = vn(\mathbf{r}, E), \qquad (3.12)$$

where $n(\mathbf{r}, E)$ is the scalar (or total) neutron density. The reaction rate density (3.7) can then be written in the form of:

$$r_i(\mathbf{r}, E) = \Sigma_i(\mathbf{r}, E)\phi(\mathbf{r}, E), \qquad (3.13)$$

53

from which the total rate of reaction i (inflicted by neutrons with energy E) in volume V is obtained by integration:

$$R_i(E) = \int_V r_i(\mathbf{r}, E)d^3r = \int_V \Sigma_i(\mathbf{r}, E)\phi(\mathbf{r}, E)d^3r .$$ (3.14)

The scalar flux can be interpreted as the average total rate at which neutrons (with a given energy) travel through an infinitesimal volume element d^3r about $\mathbf{r}$. Integration of (3.12) over volume and time yields another interpretation:

$$\int_V \int_t \phi(\mathbf{r}, E)d^3r dt = \int_V \int_t vn(\mathbf{r}, E)d^3r dt = \int_V \int_s n(\mathbf{r}, E)d^3r ds ,$$ (3.15)

where the last identity results from changing the integration variable from time to distance ($ds = vdt$). The integrated scalar flux is hence equivalent to the total path length travelled by all neutrons within volume V in time t. The connection to reaction rate (3.14) is seen by remembering that the macroscopic cross section gives the interaction probability per path length travelled by a single neutron.

3.1.3 Neutron Current

In addition to the concept of a neutron flux, which is essentially a six-dimensional density function describing the state of the neutron population, it is useful to define concepts related to the directional flow of neutrons. The *angular current density* is defined as [7]:

$$\mathbf{j}(\mathbf{r}, \hat{\boldsymbol{\Omega}}, E) = \mathbf{v}n(\mathbf{r}, \hat{\boldsymbol{\Omega}}, E)$$ (3.16)

and it is related to the angular flux by:

$$\mathbf{j}(\mathbf{r}, \hat{\boldsymbol{\Omega}}, E) = \hat{\boldsymbol{\Omega}}\psi(\mathbf{r}, \hat{\boldsymbol{\Omega}}, E) .$$ (3.17)

The angular current density gives the rate at which neutrons with energy E and direction $\hat{\boldsymbol{\Omega}}$ pass through a specifically oriented surface at $\mathbf{r}$.

Although the angular neutron flux and the angular current density have the same absolute value, their interpretations are significantly different. The angular dependence of ψ is simply related to the neutron density in the six-dimensional phase-space and the angular variable gives two of the six co-ordinates. For the angular current density, the angular variable also explicitly defines the orientation of the neutron flow with respect to the surrounding geometry.

When the angular current density is integrated over the full space-angle, the result is another vector quantity called *neutron current density*:

$$\mathbf{J}(\mathbf{r}, E) = \int_{4\pi} \mathbf{j}(\mathbf{r}, \hat{\boldsymbol{\Omega}}, E)d\hat{\boldsymbol{\Omega}} .$$ (3.18)

To be precise, this is actually equivalent to the mathematical concept of flux density [31], widely used in electromagnetic field theory [32].

One of the crucial differences between the flux and the current quantities is seen by comparing Eqs. (3.12) and (3.18). If the neutron density is completely isotropic with respect to the angular co-ordinates, the latter yields a zero and the former a non-zero result.

What is exactly meant by "neutron current" may slightly differ from author to author. In this text, the concept refers to the integral rate at which neutrons pass through a defined surface:

$$ J = \int_{\hat{\mathbf{\Omega}}} \int_S \int_E \left[\mathbf{j}(\mathbf{r}, \hat{\mathbf{\Omega}}, E) \cdot \hat{\mathbf{u}} \right] d\hat{\mathbf{\Omega}} d^2 r dE \,, \tag{3.19} $$

where the integration is carried over solid angle $\hat{\mathbf{\Omega}}$, surface S with normal $\hat{\mathbf{u}}$ and energy interval E. This parameter is equivalent to the electric or magnetic flux in electromagnetic field theory.

3.2 General Transport Theory

General neutron transport theory forms the basis of all deterministic calculation methods, including diffusion theory, which is the topic of Chapter 4. The fundamental assumptions in neutron transport calculation are that neutrons can be treated as point-like particles travelling in straight lines between the points of collision, and that all neutron-neutron interactions can be ignored. Additional assumptions of isotropic and time-independent material compositions are often made to further simply the calculation. The time-dependent neutron transport equation is formulated in the following. Delayed neutrons and multiplying scattering reactions are omitted in the equations for the sake of simplicity.

3.2.1 Time-dependent Transport Equation

The basis of transport theory can be derived from the particle density balance inside an infinitesimal element of the six-dimensional phase-space. In the Cartesian geometry space, the particles are initially located inside an infinitesimal volume element $d^3r = dxdydz$ about position $\mathbf{r}$. The infinitesimal element in the angular space is the differential solid angle $d\hat{\mathbf{\Omega}}$ about the direction of motion $\hat{\mathbf{\Omega}}$. The energies of the particles are simply distributed within interval dE about E. An illustration is given in Figure 3.2.
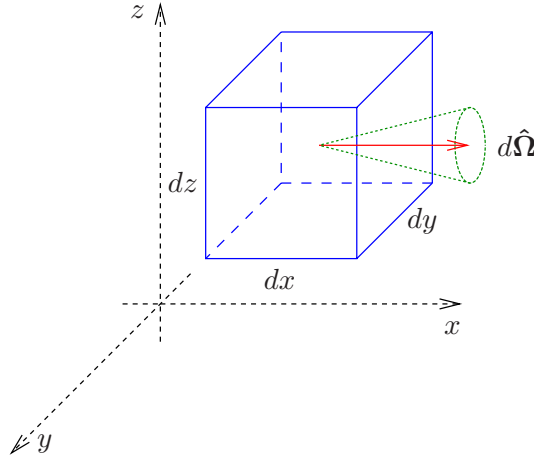
Figure 3.2: A particle located inside an infinitesimal volume element d^3r and moving in the direction of the positive x-axis. The energy of the particle lies within interval dE about a given value E.

The neutron balance inside the six-dimensional phase-space element is described by the transport equation[2] [7]:

$$\frac{1}{v}\frac{\partial}{\partial t}\psi(\mathbf{r}, \hat{\boldsymbol{\Omega}}, E, t) + \hat{\boldsymbol{\Omega}} \cdot \nabla\psi(\mathbf{r}, \hat{\boldsymbol{\Omega}}, E, t) + \Sigma_\text{t}(\mathbf{r}, E)\psi(\mathbf{r}, \hat{\boldsymbol{\Omega}}, E, t) = q(\mathbf{r}, \hat{\boldsymbol{\Omega}}, E, t),$$
(3.20)

where $\Sigma_\text{t}(\mathbf{r}, E)$ is the macroscopic total cross section of the medium and $q(\mathbf{r}, \hat{\boldsymbol{\Omega}}, E, t)$ is a generalised source term. The first term on the left-hand side is the time-rate of change in the angular neutron density. The second term describes neutron stream-ing, or the rate at which neutrons travelling in the direction of motion $\hat{\boldsymbol{\Omega}}$ leave and enter the differential volume element d^3r. The third term consists of all interactions removing neutrons from the flux either by absorption or scattering away from the differential angular and energy space. If the source and loss terms are in balance, the time-dependence disappears, and the result is the steady-state transport equation discussed in Section 3.2.3.

The source term $q(\mathbf{r}, \hat{\boldsymbol{\Omega}}, E, t)$ on the right-hand side of (3.20) can be written as the sum of three parts:

$$q(\mathbf{r}, \hat{\boldsymbol{\Omega}}, E, t) = q_\text{ex}(\mathbf{r}, \hat{\boldsymbol{\Omega}}, E, t) + q_\text{s}(\mathbf{r}, \hat{\boldsymbol{\Omega}}, E, t) + q_\text{f}(\mathbf{r}, E, t),$$
(3.21)

where $q_\text{ex}(\mathbf{r}, \hat{\boldsymbol{\Omega}}, E, t)$, $q_\text{s}(\mathbf{r}, \hat{\boldsymbol{\Omega}}, E, t)$ and $q_\text{f}(\mathbf{r}, E, t)$ are the external, scattering and fission sources, respectively. The external source term is independent of flux and it

---

[2]The neutron transport equation is the linear form of the more general Boltzmann equation, although the terms "transport equation" and "Boltzmann equation" are often used synonymously.

gives the rate at which neutrons are emitted into the phase-space element by external sources. The other two terms depend intrinsically on the reaction rates inflicted by the neutron flux.

The probability that a neutron with energy E' and moving in direction $\hat{\mathbf{\Omega}}'$ will scatter into energy interval dE about E and differential solid angle $d\hat{\mathbf{\Omega}}$ about $\hat{\mathbf{\Omega}}$ at position $\mathbf{r}$ is characterised by the macroscopic double-differential scattering cross section. The scattering source can be written by integrating the differential scattering rate density (3.8) over all incident energies and directions:

$$q_{\mathrm{s}}(\mathbf{r}, \hat{\mathbf{\Omega}}, E, t) = \int_{4\pi} \int_0^\infty \Sigma_{\mathrm{s}}(\mathbf{r}, \hat{\mathbf{\Omega}}' \to \hat{\mathbf{\Omega}}, E' \to E)\psi(\mathbf{r}, \hat{\mathbf{\Omega}}', E', t)d\hat{\mathbf{\Omega}}'dE' . \quad (3.22)$$

It should be noted that the medium typically consists of more than one isotope species and that several different scattering modes can be associated with each isotope. Since all the available scattering reactions need to be included within the source term, Eq. (3.22) should, in fact, be written as a sum over several terms. The summation is omitted here for the sake of clarity and the same practice is applied to all similar cases from here on.

Since fission neutrons are emitted isotropically, the fission source term is independent of the angular variables. Hence, instead of using the angular flux, it is more convenient to write the fission source term using the scalar flux as:

$$q_{\mathrm{f}}(\mathbf{r}, E, t) = \frac{1}{4\pi} \int_0^\infty \chi(E)\nu\Sigma_{\mathrm{f}}(\mathbf{r}, E')\phi(\mathbf{r}, E', t)dE' , \quad (3.23)$$

where $\chi(E)$ is the fission spectrum[3], i.e. the probability that the energy of the emitted neutron falls on interval dE about E. For the sake of convenience, the fission neutron production term, $\nu\Sigma_{\mathrm{f}}(\mathbf{r}, E)$, is treated as a single quantity and the average number of emitted fission neutrons is written without energy-dependence.

3.2.2 Neutron Continuity Equation

The transport equation describes accurately the balance in the angular neutron density. For physical interpretation it would be more convenient, however, to derive a balance equation for the scalar neutron density, which is closer to the intuitive concept of a particle density. This equation is attained by simply integrating (3.20) over the full space-angle.

---

[3]It is a common practice to assume that the prompt fission spectrum is independent of the incident neutron energy. This is a good approximation in the energy range of typical fission reactor applications. (see Section 2.1.2 of Chapter 2).

The integration of the time-derivative term and the removal term is straightforward:

$$\int_{4\pi} \frac{1}{v} \frac{\partial}{\partial t} \psi(\mathbf{r}, \hat{\mathbf{\Omega}}, E, t) d\hat{\mathbf{\Omega}} = \frac{1}{v} \frac{\partial}{\partial t} \int_{4\pi} \psi(\mathbf{r}, \hat{\mathbf{\Omega}}, E, t) d\hat{\mathbf{\Omega}} = \frac{1}{v} \frac{\partial}{\partial t} \phi(\mathbf{r}, E, t) \quad (3.24)$$

and

$$\int_{4\pi} \Sigma_{\mathrm{t}}(\mathbf{r}, E) \psi(\mathbf{r}, \hat{\mathbf{\Omega}}, E, t) d\hat{\mathbf{\Omega}} = \Sigma_{\mathrm{t}}(\mathbf{r}, E) \int_{4\pi} \psi(\mathbf{r}, \hat{\mathbf{\Omega}}, E, t) d\hat{\mathbf{\Omega}}$$
$$= \Sigma_{\mathrm{t}}(\mathbf{r}, E) \phi(\mathbf{r}, E, t) \,. \tag{3.25}$$

The angular neutron flux is simply replaced by the scalar flux. The fission source term (3.23) was already written without the angular dependence. The external source is independent of the flux and the angular dependence depends on the source type. The integration of the two remaining terms is less straightforward.

The integration of the scattering source (3.23) is written as:

$$\int_{4\pi} \left[\int_{4\pi} \int_0^\infty \Sigma_{\mathrm{s}}(\mathbf{r}, \hat{\mathbf{\Omega}}' \to \hat{\mathbf{\Omega}}, E' \to E) \psi(\mathbf{r}, \hat{\mathbf{\Omega}}', E', t) d\hat{\mathbf{\Omega}}' dE' \right] d\hat{\mathbf{\Omega}} \,. \tag{3.26}$$

It should be noted, however, that since the integration is carried over the full space-angle, and because the double-differential scattering cross section depends only on the *angle* between directions $\hat{\mathbf{\Omega}}'$ and $\hat{\mathbf{\Omega}}$, it does not make any difference whether the reaction is written as $(\hat{\mathbf{\Omega}}' \to \hat{\mathbf{\Omega}})$ or $(\hat{\mathbf{\Omega}} \to \hat{\mathbf{\Omega}}')$. By interchanging the variables and re-organising some terms, Eq. (3.26) can be written as:

$$\int_{4\pi} \int_0^\infty \left[\int_{4\pi} \Sigma_{\mathrm{s}}(\mathbf{r}, \hat{\mathbf{\Omega}} \to \hat{\mathbf{\Omega}}', E' \to E) d\hat{\mathbf{\Omega}} \right] \psi(\mathbf{r}, \hat{\mathbf{\Omega}}', E', t) d\hat{\mathbf{\Omega}}' dE'$$
$$= \int_{4\pi} \int_0^\infty \Sigma_{\mathrm{s}}(\mathbf{r}, E' \to E) \psi(\mathbf{r}, \hat{\mathbf{\Omega}}', E', t) d\hat{\mathbf{\Omega}}' dE'$$
$$= \int_0^\infty \Sigma_{\mathrm{s}}(\mathbf{r}, E' \to E) \left[\int_{4\pi} \psi(\mathbf{r}, \hat{\mathbf{\Omega}}', E', t) d\hat{\mathbf{\Omega}}' \right] dE'$$
$$= \int_0^\infty \Sigma_{\mathrm{s}}(\mathbf{r}, E' \to E) \phi(\mathbf{r}, E', t) dE' \,. \tag{3.27}$$

The final term in (3.20) left to be integrated is the streaming term, which can also be written using the angular current density (3.17):

$$\hat{\mathbf{\Omega}} \cdot \nabla \psi(\mathbf{r}, \hat{\mathbf{\Omega}}, E) = \nabla \cdot \hat{\mathbf{\Omega}} \psi(\mathbf{r}, \hat{\mathbf{\Omega}}, E) = \nabla \cdot \mathbf{j}(\mathbf{r}, \hat{\mathbf{\Omega}}, E) \,. \tag{3.28}$$

Using the divergence theorem, the integration over the full space-angle yields [7]:

$$\int_{4\pi} \nabla \cdot \mathbf{j}(\mathbf{r}, \hat{\mathbf{\Omega}}, E) d\hat{\mathbf{\Omega}} = \nabla \cdot \mathbf{J}(\mathbf{r}, E), \qquad (3.29)$$

where $\mathbf{J}(\mathbf{r}, E)$ is the neutron current density (3.18).

When the results of Eqs. (3.24)–(3.29) are collected and external sources omitted for convenience, the *neutron continuity equation* can be written as:

$$\frac{1}{v}\frac{\partial}{\partial t}\phi(\mathbf{r}, E, t) + \nabla \cdot \mathbf{J}(\mathbf{r}, E) + \Sigma_t(\mathbf{r}, E)\phi(\mathbf{r}, E, t)$$

$$= \int_0^\infty \left[\Sigma_s(\mathbf{r}, E' \to E)\phi(\mathbf{r}, E', t) + \frac{1}{4\pi}\chi(E)\nu\Sigma_f(\mathbf{r}, E')\phi(\mathbf{r}, E', t) \right] dE'.$$
$$(3.30)$$

This equation is also known as the *neutron balance equation* and it forms the starting point for the derivation of diffusion theory, discussed in the following chapter. It should be noted that no approximations were made in the derivation of (3.30) from (3.20).

3.2.3 Equilibrium State and Criticality

The time-rate of change of neutron flux determines whether the flux level, and hence the fission power, is increasing or decreasing. In the first case the system is said to be *super-critical* and in the second case *sub-critical*. A steady-state system is called *critical*[4], and in such a case, the time-dependence can be omitted. The transport equation (3.20) becomes:

$$\hat{\mathbf{\Omega}} \cdot \nabla\psi(\mathbf{r}, \hat{\mathbf{\Omega}}, E) + \Sigma_t(\mathbf{r}, E)\psi(\mathbf{r}, \hat{\mathbf{\Omega}}, E) = q(\mathbf{r}, \hat{\mathbf{\Omega}}, E). \qquad (3.31)$$

The equilibrium state in a macroscopic system without external sources always implies criticality and vice versa. In such a case, there is an exact balance between the fission (and multiplying scattering) source rate and the rate of neutron loss by absorption and leakage. The chain reaction in the system is stationary and self-sustaining. Criticality also implies that there exists a positive solution to the steady-state transport equation (3.31).

If, however, external sources are present, the equilibrium state simply corresponds to a balance between the total rates of neutron source and loss. Since a fraction of

---

[4]The use of the term "critical" is not necessarily the best choice of words in this context. A reactor operating at a constant power level is basically said to be in a "critical condition", which may sound a bit disturbing, especially to someone thinking in medical terms.

neutrons is being introduced in the system from external sources, the chain reaction is not self-sustaining and the system is in a sub-critical equilibrium state. In fact, equilibrium in the presence of external sources may exist only in a non-self-sustaining state.

The system in which the transport equation is to be solved is usually a simplified description of the physical reality. Transport methods are often applied in some partial volume of the full-scale system, in which the geometry is described in great detail, but the presence of the surrounding world is modelled using artificial *boundary conditions*. In reactor lattice calculations, for example, the geometry may consist of a single fuel assembly, often infinite in the axial direction, which is surrounded by *reflective* or *periodic* boundary conditions[5]. This means that the solution corresponds to a repeated lattice of identical fuel assemblies, infinite in all spatial directions.

Even though such geometry is modelled as a steady-state system, the given set of parameters does not, in general, lead to an equilibrium state, and hence to the existence of a solution to (3.31). The existence of the solution must then be forced by allowing some variation in the system parameters. The problem then practically becomes the finding of a system that *does* satisfy the equilibrium condition.

The usual approach is to formulate the task as a *criticality eigenvalue problem*. The fission source term is divided by a constant k_{eff}, which becomes the eigenvalue that yields the eigenflux solution to (3.31). By writing out the source terms, the transport equation becomes:

$$\hat{\mathbf{\Omega}} \cdot \nabla \psi(\mathbf{r}, \hat{\mathbf{\Omega}}, E) + \Sigma_{\text{t}}(\mathbf{r}, E)\psi(\mathbf{r}, \hat{\mathbf{\Omega}}, E)$$

$$= \int_{4\pi} \int_0^\infty \Sigma_{\text{s}}(\mathbf{r}, \hat{\mathbf{\Omega}}' \to \hat{\mathbf{\Omega}}, E' \to E)\psi(\mathbf{r}, \hat{\mathbf{\Omega}}', E')d\hat{\mathbf{\Omega}}'dE' \qquad (3.32)$$

$$+ \frac{1}{k_{\text{eff}}}\frac{1}{4\pi}\int_0^\infty \chi(E)\nu\Sigma_{\text{f}}(\mathbf{r}, E')dE'\,.$$

A similar eigenvalue form can be written for the neutron continuity equation (3.30) and the same approach will be used for the neutron diffusion equation in the following chapter. The physical interpretation of k_{eff}, also known as the *effective multiplication factor*, is that it determines the criticality state of the system:

$$k_{\text{eff}} \begin{cases} < 1 & \implies \text{system is sub-critical} \\ = 1 & \implies \text{system is critical} \\ > 1 & \implies \text{system is super-critical} \end{cases} \,. \qquad (3.33)$$

---

[5]Also called specular and translational boundary conditions, respectively.

It must be pointed out and understood that the solution of the eigenvalue problem, (3.32), is not equivalent to the solution of the physical problem, (3.31), except in the very special case that the system is critical and k_{eff} is exactly unity. It is instead the solution of a similar problem, in which the average fission neutron yields are artificially modified in order to meet the balance between the rates of neutron source and loss.

The result is that the eigenflux solution becomes distorted, both in space and energy, as the importance of fission neutrons is either over- ($k_{\text{eff}} < 1$) or under-estimated ($k_{\text{eff}} > 1$). Since the flux solution is used for calculating reaction rates, the distortion can have a significant impact on the results of the calculation. This problem will be revisited several times throughout this text.

An alternative approach is to assume that the time-dependence of the flux can be fully separated from the rest of the variables. It will be shown in Section 4.3 of Chapter 4 that the time-dependence takes an exponential form and the separation of variables can be written as:

$$\psi(\mathbf{r}, \hat{\mathbf{\Omega}}, E, t) = \psi(\mathbf{r}, \hat{\mathbf{\Omega}}, E)e^{\alpha t}. \tag{3.34}$$

The substitution of this into the time-dependent transport equation (3.20), yields for the time-derivative term:

$$\frac{1}{v}\frac{\partial}{\partial t}\psi(\mathbf{r}, \hat{\mathbf{\Omega}}, E)e^{\alpha t} = \frac{\alpha}{v}\psi(\mathbf{r}, \hat{\mathbf{\Omega}}, E)e^{\alpha t} \tag{3.35}$$

and the exponential multiplier is cancelled in all terms. The transport equation is then written as:

$$\frac{\alpha}{v}\psi(\mathbf{r}, \hat{\mathbf{\Omega}}, E) + \hat{\mathbf{\Omega}} \cdot \nabla\psi(\mathbf{r}, \hat{\mathbf{\Omega}}, E) + \Sigma_{\text{t}}(\mathbf{r}, E)\psi(\mathbf{r}, \hat{\mathbf{\Omega}}, E)$$

$$= \int_{4\pi}\int_0^\infty \Sigma_{\text{s}}(\mathbf{r}, \hat{\mathbf{\Omega}}' \to \hat{\mathbf{\Omega}}, E' \to E)\psi(\mathbf{r}, \hat{\mathbf{\Omega}}', E')d\hat{\mathbf{\Omega}}'dE' \tag{3.36}$$

$$+\frac{1}{4\pi}\int_0^\infty \chi(E)\nu\Sigma_{\text{f}}(\mathbf{r}, E')dE'.$$

It is seen that there is now an additional reaction rate term, with an effective cross section α/v, that can be adjusted to attain balance between the source and loss terms. Parameter α is the eigenvalue of the problem and the criticality condition can be written correspondingly as:

$$\alpha \begin{cases} < 0 & \Longrightarrow \text{system is sub-critical} \\ = 0 & \Longrightarrow \text{system is critical} \\ > 0 & \Longrightarrow \text{system is super-critical} \end{cases}. \tag{3.37}$$

It is important to understand the physical interpretation of the additional term. Even in some textbooks (see e.g. Ref. [11]), the negative α-value is incorrectly interpreted as non-physical *negative* absorption. However, in the case of a sub-critical system, the term must be written on the right-hand side of the equation, in which case it becomes positive, and is interpreted as *time-production* of neutrons. Similarly, the positive α-value in a super-critical system yields a new loss term, which is interpreted as neutron *time-absorption*.

The α-eigenvalue method and the time-production and -absorption reactions are thoroughly discussed in Reference [33]. It is shown that the method is equivalent to performing a full time-dependent transport calculation. The topic is revisited in Section 5.5.2 of Chapter 5, which deals with criticality calculations in the Monte Carlo method.

It must be noted that, even though the α-eigenvalue method may yield physically more consistent results compared to the previous k-eigenvalue method, it is not necessarily superior in lattice calculations. The reason is that the modelled system is, in fact, in a steady-state condition, and the time-dependence is induced in the transport equation by the approximations made on the boundary conditions. A better approach to the problem using *leakage corrections* is taken in Section 4.2.3 of the following chapter.

3.3 Solution Methods

All deterministic transport methods aim at finding a flux solution to the neutron transport equation, either (3.20) or (3.31). The main challenge in the solution is not the mathematical formulation of the equations, but rather the complex angular and energy-dependence of the coefficients and source terms. These problems are discussed in the following.

3.3.1 Discretisation of the Energy Variable

The common feature to all deterministic solution methods is that approximations are needed to deal with the continuous energy-dependence of flux and cross sections. The energy spectrum is divided into discrete groups, which are indexed in descending order, starting from the highest group ($g = 1$) with upper energy boundary E_0. The *angular group flux* in group g is defined as:

$$\Psi_g(\mathbf{r}, \hat{\mathbf{\Omega}}) = \int_{E_g}^{E_{g-1}} \psi(\mathbf{r}, \hat{\mathbf{\Omega}}, E)dE \,, \tag{3.38}$$

the corresponding *scalar group flux* as:

$$\Phi_g(\mathbf{r}) = \int_{E_g}^{E_{g-1}} \phi(\mathbf{r}, E)dE \,, \tag{3.39}$$

and the *group current density* as:

$$\mathbf{J}_g(\mathbf{r}) = \int_{E_g}^{E_{g-1}} \mathbf{J}(\mathbf{r}, E)dE \,. \tag{3.40}$$

Reaction cross sections are averaged over the same energy intervals in such a way that the integral reaction rate densities are preserved. The integration of (3.13) over the energy variable yields:

$$\int_{E_g}^{E_{g-1}} r_i(\mathbf{r}, E)dE = \int_{E_g}^{E_{g-1}} \Sigma_i(\mathbf{r}, E)\phi(\mathbf{r}, E)dE = \Sigma_{i,g}(\mathbf{r})\Phi_g(\mathbf{r}) \,, \tag{3.41}$$

where $\Sigma_{i,g}(\mathbf{r})$ is the group-wise cross section of reaction i in energy group g. From the balance requirement and the definition of the group flux in (3.39), it follows that the group-wise cross section must be calculated as:

$$\Sigma_{i,g}(\mathbf{r}) = \frac{\displaystyle\int_{E_g}^{E_{g-1}} \Sigma_i(\mathbf{r}, E)\phi(\mathbf{r}, E)dE}{\displaystyle\int_{E_g}^{E_{g-1}} \phi(\mathbf{r}, E)dE} \,, \tag{3.42}$$

or in other words, as the flux-weighted average of the energy-dependent macroscopic cross section $\Sigma_i(\mathbf{r}, E)$. The time-dependence of the neutron flux was omitted in the above equations, since the flux is used only as the weighting function for the cross section condensation.

Definition (3.42) is only a formal example, but the energy group condensation of any interaction parameter is carried out in a very similar way. It will be discussed in Chapter 7 that the same procedure is applied on the fundamental microscopic cross section data in the generation of fine-group cross section libraries for deterministic transport codes. The following chapter deals with the generation of homogenised few-group constants using very similar means.

The energy group condensation also reveals a very fundamental problem in deterministic transport calculation: the flux solution is used for calculating the group-wise cross sections, which in turn are needed for the solution of the transport equation. In principle, the solution of the problem should be known before applying the solution method.

3.3.2 Treatment of Angular Dependence

The energy-dependence is not the only problem in solving the transport equation. Another problem lies in the angular dependence. The integration over the angular variable yields the neutron continuity equation (3.30), which is independent of $\hat{\mathbf{\Omega}}$. The problem with this equation, however, is that there is another function to be solved, namely the current density $\mathbf{J}(\mathbf{r}, E, t)$. The connection of the two unknown functions necessarily demands the reinstatement of the angular dependence.

The exact treatment of the angular variable is simply not possible and approximate methods and additional assumptions are needed to attain a solution. There are practically four main categories of deterministic solution methods:

   I. The method of characteristics

  II. The collision probability method

 III. The discrete ordinates method

 IV. The method of spherical harmonics

The latter two are also called the S_n and the P_n method, respectively. The description of all the above methods is not reasonable within the scope of this text. Instead, the following chapter describes the use of *diffusion theory*, which is one of the simplest means to approach neutron transport problems. The theory has its limitations, but it is widely and successfully used in various reactor-scale LWR calculations. The diffusion theory is basically equivalent to the first-order spherical harmonics method (P_1), but it can also be derived directly, as will be done in the following.

Chapter 4

Diffusion Theory and Nodal Methods

4.1   Diffusion Theory

Diffusion processes are encountered in various fields of physics and they are related to the collective movement of a large number of particles through a permeable medium. The phenomenon is stochastic at the microscopic level, as each particle undergoes an individual random walk process while colliding with its surroundings. A typical example is the mixing of gases or liquids initially separated from each other. The common feature to all diffusion processes is that the motion takes place without a net external force, from a higher to a lower concentration.

The diffusion model can also be used for describing the flow of neutrons through the reactor core. Neutron diffusion theory is based on general transport theory, and as was stated in the previous chapter, it is one of the simplest means to solve neutron transport problems. A good starting point for the derivation of diffusion theory is the neutron continuity equation (3.30)[1], which is integrated over the energy variable to remove the continuous energy-dependence.

Each term in (3.30) is integrated over some energy interval corresponding to energy group g (see Section 3.3.1 of Chapter 3 for the energy discretisation). The integration of most of the terms in the left-hand side of (3.30) is simple, and it is sufficient to replace the scalar flux $\phi(\mathbf{r}, E, t)$ by the scalar group flux $\Phi_g(\mathbf{r}, t)$, the total cross section $\Sigma_\text{t}(\mathbf{r}, E)$ by the group-wise total cross section $\Sigma_{\text{t},g}(\mathbf{r})$ and the neutron current

---

[1]The neutron continuity equation depends on three spatial variables, energy and time. It is important to realise that this equation is not an approximate form of the Boltzmann transport equation (3.20). The penalty of removing the angular dependence of the neutron flux is the introduction of a new unknown function, namely the neutron current density.

density $\mathbf{J}(\mathbf{r}, E, t)$ by the group current density $\mathbf{J}_g(\mathbf{r}, t)$. The integration of the time-derivative term yields:

$$\int_{E_g}^{E_{g-1}} \frac{1}{v} \frac{\partial}{\partial t} \phi(\mathbf{r}, E, t) dE = \frac{\partial}{\partial t} \int_{E_g}^{E_{g-1}} \frac{1}{v} \phi(\mathbf{r}, E, t) dE = \frac{1}{v_g} \frac{\partial}{\partial t} \Phi_g(\mathbf{r}, t), \quad (4.1)$$

where:

$$\frac{1}{v_g} = \frac{\int_{E_g}^{E_{g-1}} \frac{1}{v} \phi(\mathbf{r}, E) dE}{\int_{E_g}^{E_{g-1}} \phi(\mathbf{r}, E) dE} = \frac{\int_{E_g}^{E_{g-1}} n(\mathbf{r}, E) dE}{\int_{E_g}^{E_{g-1}} \phi(\mathbf{r}, E) dE}. \quad (4.2)$$

The integration of the source terms is a bit more complicated. The group-wise form of the fission source (3.23) is written as:

$$\int_{E_g}^{E_{g-1}} \left[\int_0^\infty \chi(E) \nu \Sigma_f(\mathbf{r}, E') \phi(\mathbf{r}, E', t) dE' \right] dE$$

$$= \int_0^\infty \left[\int_{E_g}^{E_{g-1}} \chi(E) dE \right] \nu \Sigma_f(\mathbf{r}, E') \phi(\mathbf{r}, E', t) dE' \quad (4.3)$$

$$= \chi_g \sum_{g'=1}^G \left[\nu \Sigma_{f,g'}(\mathbf{r}) \Phi_{g'}(\mathbf{r}, t) \right],$$

where the summation is carried over all G energy groups. The group-wise fission spectrum χ_g is assumed to be independent of the incident neutron energy and it gives the fraction of neutrons emitted in group g:

$$\chi_g = \int_{E_g}^{E_{g-1}} \chi(E) dE. \quad (4.4)$$

The integration of the scattering source (3.22) proceeds very similarly:

$$\int_{E_g}^{E_{g-1}} \left[\int_0^\infty \Sigma_s(\mathbf{r}, E' \to E) \phi(\mathbf{r}, E', t) dE' \right] dE$$

$$= \int_0^\infty \left[\int_{E_g}^{E_{g-1}} \Sigma_s(\mathbf{r}, E' \to E) dE \right] \phi(\mathbf{r}, E', t) dE' \quad (4.5)$$

$$= \sum_{g'=1}^G \left[\Sigma_{s,g' \to g}(\mathbf{r}) \Phi_{g'}(\mathbf{r}, t) \right],$$

where the summation is carried over all G energy groups. The *group-transfer cross section* is given by:

$$\Sigma_{s,g'\to g}(\mathbf{r}) = \frac{\int_{E_g}^{E_{g-1}} \int_{E_{g'}}^{E_{g'-1}} \Sigma_s(\mathbf{r}, E' \to E)\phi(\mathbf{r}, E')dE dE'}{\int_{E_{g'}}^{E_{g'-1}} \phi(\mathbf{r}, E')dE'} . \quad (4.6)$$

The collection of the above results yields for the group-wise continuity equation:

$$\frac{1}{v_g}\frac{\partial}{\partial t}\Phi_g(\mathbf{r}, t) + \nabla \cdot \mathbf{J}_g(\mathbf{r}, t) + \Sigma_{t,g}(\mathbf{r})\Phi_g(\mathbf{r}, t) = \sum_{g'=1}^{G}\left[\Sigma_{s,g'\to g}(\mathbf{r})\Phi_{g'}(\mathbf{r}, t)\right]$$

$$+\chi_g \sum_{g'=1}^{G}\left[\nu\Sigma_{f,g'}(\mathbf{r})\Phi_{g'}(\mathbf{r}, t)\right] \quad (4.7)$$

The scattering source in the above equation also includes reactions within the group boundaries. The theory derived so far does not contain any additional approximations, as long as the group-wise cross sections are consistently defined.

4.1.1 Fick's Law

This is where the actual diffusion theory begins. The *diffusion approximation* suggests that the neutron current density is proportional to the flux gradient:

$$\mathbf{J}_g(\mathbf{r}, t) = -D_g(\mathbf{r})\nabla\Phi_g(\mathbf{r}, t) , \quad (4.8)$$

where the proportionality factor $D_g(\mathbf{r})$ is known as the *diffusion coefficient*. The diffusion approximation is also known as *Fick's law* and it was originally developed for the diffusion theory of gases. For the purpose of this study, it is best to view the diffusion coefficient merely as a proportionality factor that links the neutron current to the gradient of the neutron flux. The validity of (4.8) relies on four approximations [7]:

   I. The angular flux is only weakly dependent on the angular variables.

   II. The fission source is isotropic.

   III. The time derivative of neutron current density is small compared to flux gradient.

   IV. The anisotropic energy-transfer contribution can be ignored in group-to-group scattering.

The weak dependence in item I is more specifically assumed to be linear, which yields the equivalence with one-group first-order spherical harmonics method.

The derivation of Fick's law is given in Appendix A. Based on the above assumptions, the diffusion coefficient is shown to take the form of:

$$D_g(\mathbf{r}) = \frac{1}{3\Sigma_{\text{tr},g}(\mathbf{r})} \, , \tag{4.9}$$

where $\Sigma_{\text{tr},g}(\mathbf{r})$ is the transport-corrected total cross section, or simply the *transport cross section*, given by:

$$\Sigma_{\text{tr},g}(\mathbf{r}) = \Sigma_{\text{t},g}(\mathbf{r}) - \overline{\mu}_g \Sigma_{\text{s},g}(\mathbf{r}) \, . \tag{4.10}$$

Parameter $\overline{\mu}_g$ is the cosine of the average scattering angle. In a sense, the angular dependence of the double-differential scattering cross section is contained within the transport cross section (4.10), while the group-transfer cross section (4.6) holds the energy-dependence. The separation of the energy-transfer from the angular-transfer is one of the approximations in diffusion theory, as discussed in Appendix A.

The group-diffusion equation can be written after (4.8) is substituted into (4.7) yielding:

$$\frac{1}{v_g}\frac{\partial}{\partial t}\Phi_g(\mathbf{r},t) - \nabla D_g(\mathbf{r}) \cdot \nabla\Phi_g(\mathbf{r},t) + \Sigma_{\text{t},g}(\mathbf{r})\Phi_g(\mathbf{r},t)$$
$$= \sum_{g'=1}^{G}\left[\Sigma_{\text{s},g'\rightarrow g}(\mathbf{r})\Phi_{g'}(\mathbf{r},t)\right] + \chi_g\sum_{g'=1}^{G}\left[\nu\Sigma_{\text{f},g'}(\mathbf{r})\Phi_{g'}(\mathbf{r},t)\right] \tag{4.11}$$

When all energy groups are included, the number of equations is equal to the number of unknown functions and the problem can be solved, at least in principle. Geometries encountered in practice are usually composed of discrete homogeneous material regions[2]. In such a case, it is convenient to remove the continuous spatial dependence of the cross sections, and the streaming term is reduced to:

$$-\nabla D_g \cdot \nabla\Phi_g(\mathbf{r},t) = -D_g\nabla \cdot \nabla\Phi_g(\mathbf{r},t) = -D_g\nabla^2\Phi_g(\mathbf{r},t) \, . \tag{4.12}$$

---

[2]It should be noted that this is an approximation, and not entirely valid due to the inhomogeneities introduced by variation in temperature and fuel burnup.

Equation (4.11) is then written as:

$$\frac{1}{v_g}\frac{\partial}{\partial t}\Phi_g(\mathbf{r},t) - D_g\nabla^2\Phi_g(\mathbf{r},t) + \Sigma_{\mathrm{t},g}\Phi_g(\mathbf{r},t) = \sum_{g'=1}^{G}\left[\Sigma_{\mathrm{s},g'\to g}\Phi_{g'}(\mathbf{r},t)\right]$$

$$+\chi_g\sum_{g'=1}^{G}\left[\nu\Sigma_{\mathrm{f},g'}\Phi_{g'}(\mathbf{r},t)\right]$$

$$(4.13)$$

The group-transfer cross sections are often combined with the absorption cross section to form the *group removal cross section*:

$$\Sigma_{\mathrm{r},g} = \Sigma_{\mathrm{a},g} + \sum_{g'\neq g}\Sigma_{\mathrm{s},g\to g'} = \Sigma_{\mathrm{t},g} - \Sigma_{\mathrm{s},g\to g}, \qquad (4.14)$$

where the absorption cross section includes fission, and the summation is carried over all group-transfer reactions out of group g. This definition may simplify the above set of equations to some extent.

The validity of diffusion theory depends on several factors. The first item in the list of approximations on page 67 is basically translated into a requirement that scattering is the dominant interaction process, and not highly anisotropic. Diffusion calculations give good results in large, nearly homogeneous regions, where the spatial dependence of the neutron flux is not too strong, i.e. where the flux gradient is small. Problems may arise in the following cases:

I. Near vacuum boundaries and low-density material regions.

II. Near high-absorbing materials, such as control rods or burnable absorber pins.

III. In large material regions with highly anisotropic scattering properties, such as moderator channels filled with water.

Unfortunately, all the above cases are commonly encountered in reactor analysis.

4.1.2 Two-group Diffusion Method

A typical approach in light water reactor diffusion calculation is to divide the energy spectrum into only two energy groups. Group 1, or the *fast group* consists of neutrons above 0.625 eV. Neutrons below this energy belong to group 2, or the *thermal group*. The group boundary is chosen in such a way that the energy peak formed by fully thermalised neutrons (see Fig. 2.8 on page 48) is completely enclosed within the

thermal group. Up-scattering, i.e. the scattering of neutrons from group 2 to group 1 is almost negligible.

The two-group diffusion equations are derived from the general few-group diffusion equation 4.13 by making a few simplifications. The steady-state equations in the criticality eigenvalue form can be written as:

$$-D_1 \nabla^2 \Phi_1(\mathbf{r}) + \Sigma_{r,1} \Phi_1(\mathbf{r}) = \frac{1}{k_{\text{eff}}} \left[\nu \Sigma_{f,1} \Phi_1(\mathbf{r}) + \nu \Sigma_{f,2} \Phi_2(\mathbf{r}) \right]$$

$$-D_2 \nabla^2 \Phi_2(\mathbf{r}) + \Sigma_{a,2} \Phi_2(\mathbf{r}) = \Sigma_{s,1 \to 2} \Phi_1(\mathbf{r})$$

(4.15)

The two-group fission spectrum is simply $\chi_1 = 1$ for the fast group and $\chi_2 = 0$ for the thermal group, since the minimum emission energy of fission neutrons is of the order of 100 eV, well above the group boundary. The fast removal cross section $\Sigma_{r,1}$ gives the rate at which neutrons are removed from the fast group either by absorption or down-scattering to group 2:

$$\Sigma_{r,1} = \Sigma_{a,1} + \Sigma_{s,1 \to 2} \,.$$

(4.16)

The removal cross section in group 2 is practically reduced to $\Sigma_{a,2}$, due to the lack of up-scattering.

An alternative approach is to write the removal cross section only for the fast energy group, and without absorption:

$$\Sigma_{\text{rem}} = \Sigma_{s,1 \to 2} - \Sigma_{s,2 \to 1} \frac{\Phi_2}{\Phi_1} \,.$$

(4.17)

The two-group diffusion equations are then written as:

$$-D_1 \nabla^2 \Phi_1(\mathbf{r}) + \left(\Sigma_{a,1} + \Sigma_{\text{rem}} \right) \Phi_1(\mathbf{r}) = \frac{1}{k_{\text{eff}}} \left[\nu \Sigma_{f,1} \Phi_1(\mathbf{r}) + \nu \Sigma_{f,2} \Phi_2(\mathbf{r}) \right]$$

$$-D_2 \nabla^2 \Phi_2(\mathbf{r}) + \Sigma_{a,2} \Phi_2(\mathbf{r}) = \Sigma_{\text{rem}} \Phi_1(\mathbf{r})$$

(4.18)

This formulation also takes into account the up-scattering to group 1.

4.1.3 Physical Implications of Diffusion Theory

Diffusion coefficient is a parameter based on an approximation, and it has no continuous-energy counterpart in general transport theory. This is one of the problems encountered in group constant generation (see Sec. 4.2.1), especially using the Monte Carlo method. Diffusion theory itself, however, can be used to relate certain results to

physical quantities that can be easily simulated in the Monte Carlo calculation. The problems related to the calculation of the diffusion coefficient and the method used in the PSG code are thoroughly discussed in Chapter 9. The theoretical basis is derived in the following. The applicability of these results is naturally limited to problems where the diffusion theory can be used with good accuracy.

Consider an infinite homogeneous medium and a point source emitting neutrons at a constant rate S into energy group g. Let $\Phi_g^0(\mathbf{r})$ be the group flux consisting only of neutrons emitted at the source point. All neutrons emitted into group g in fission or scattering reactions outside the source are excluded from $\Phi_g^0(\mathbf{r})$, so that the problem is essentially reduced to neutron diffusion in a non-multiplying infinite homogeneous medium. The group-diffusion equation (4.13) can now be written without time-dependence as:

$$-\nabla^2\Phi_g^0(\mathbf{r}) + \frac{\Phi_g^0(\mathbf{r})}{L_g^2} = 0\,, \qquad (4.19)$$

where

$$L_g^2 = \frac{D_g}{\Sigma_{\mathrm{t},g} - \Sigma_{\mathrm{s},g\to g}} = \frac{D_g}{\Sigma_{\mathrm{r},g}}\,. \qquad (4.20)$$

This differential equation is easily solved, and the solution in a spherical co-ordinate system is written as [7]:

$$\Phi_g^0(r) = \frac{S}{4\pi D_g}\frac{1}{r}e^{-r/L_g}\,, \qquad (4.21)$$

where variable r is the distance from the point source.

The attention is now turned to parameter L_g and the physical interpretation of the diffusion process. The removal rate in a small spherical shell located between r and $r + dr$ is given by:

$$dR = \Sigma_{\mathrm{r},g}\Phi_g^0(\mathbf{r})d^3r = \Sigma_{\mathrm{r},g}\Phi_g^0(r)4\pi r^2 dr \;=\; \Sigma_{\mathrm{r},g}\frac{S}{D_g}re^{-r/L_g}dr$$
$$\;=\; \frac{S}{L_g^2}re^{-r/L_g}dr \qquad (4.22)$$

The probability that a source neutron is removed from the flux between r and $r + dr$ is simply the removal rate divided by the source strength:

$$p(r)dr = \frac{dR}{S} = \frac{r}{L_g^2}e^{-r/L_g}dr\,. \qquad (4.23)$$

This probability can be used for calculating the mean distance at which the neutrons are removed from the flux. A more common practice in reactor physics is to calculate

the mean of the square distance:

$$\overline{r_g^2} = \int_0^\infty r^2 p(r) dr = \int_0^\infty \frac{r^3}{L_g^2} e^{-r/L_g} dr = \cdots = 6L_g^2. \tag{4.24}$$

The details of the integration are cumbersome but trivial and hence omitted.

The main result is that parameter L_g, which depends on the diffusion coefficient according to (4.20), can be related to a physical property, namely the mean square-distance the neutrons travel from the emission site before being removed from the flux by scattering or absorption.

In two-group diffusion theory, the thermal group value, L_2, is called the *thermal diffusion length* and L_2^2 the *thermal diffusion area*. The fast group value, L_1, is called the *fast diffusion length* or the *slowing-down length*. Owing to historical reasons, the square of L_1 is also known as the *neutron age* or *Fermi-age*, since it essentially depends on how long it takes a fission neutron to slow down to the thermal energy region. The sum of the group-wise diffusion areas is known as the *migration area*:

$$M^2 = L_1^2 + L_2^2, \tag{4.25}$$

which is a measure of the total distance the neutrons cover while diffusing through the medium.

4.1.4   Solution of the Multi-group Diffusion Equations

The neutron diffusion problem is characterised by a coupled set of partial differential equations, dependent on three spatial variables and time. The solution methods are not that different from the methods used for other similar mathematical problems. The exact procedure largely depends on geometry. Basically the set of diffusion equations must be solved separately for each energy group in each material region and the solutions coupled together using appropriate boundary conditions. It is not reasonable to go into details within the scope of this text, since the topic is extensively covered even in introductory textbooks on nuclear engineering [34]. A formal solution is derived for the steady-state problem and the procedure demonstrated by a simple example. Time-dependence is discussed separately in Section 4.3.

The solution is based on the assumption that inside a homogeneous material region, the spatial and energy-dependence of the neutron flux can be separated from each other [7][3]. All group fluxes are then characterised by the same spatial shape function

---

[3]This approximation is clearly broken if the region consists of several materials, since the interaction properties are strongly dependent on neutron energy.

$\mathcal{R}(\mathbf{r})$ and the separation of variables can be written as:

$$\Phi_g(\mathbf{r}) = \Phi_g \mathcal{R}(\mathbf{r}) . \qquad (4.26)$$

The substitution of (4.26) into (4.13) yields:

$$\frac{1}{\mathcal{R}(\mathbf{r})} \nabla^2 \mathcal{R}(\mathbf{r}) = \frac{1}{D_g \Phi_g} \left[\Sigma_{\mathrm{t},g} \Phi_g - \sum_{g'=1}^{G} \left[\Sigma_{\mathrm{s},g' \to g} \Phi_{g'} + \chi_g \nu \Sigma_{\mathrm{f},g'} \Phi_{g'} \right] \right] . \qquad (4.27)$$

Since the LHS of the equation depends only on the spatial co-ordinates and the RHS on energy, both sides must be equal to a constant, independent of all variables. The result is that all group-fluxes must satisfy:

$$\nabla^2 \Phi_g(\mathbf{r}) + B^2 \Phi_g(\mathbf{r}) = 0 . \qquad (4.28)$$

This equation is known as the *Helmholtz equation* and it is encountered in various problems in physics and engineering [35].

The solution of the Helmholtz equation depends on the boundary conditions and the form of the Laplacian differential operator ∇^2, which is fixed by the co-ordinate system. In a simple one-dimensional multiplying slab geometry, the equation is written as:

$$\frac{d^2}{dx^2} \Phi_g(x) + B^2 \Phi_g(x) = 0 . \qquad (4.29)$$

Assuming that $B^2 > 0$, a general solution can be written in the form of:

$$\Phi_g(x) = \sum_{n=1}^{\infty} \left[C_{1,n,g} \sin(B_n x) + C_{2,n,g} \cos(B_n x) \right] = \sum_{n=1}^{\infty} \left[\Phi_{n,g}(x) \right] , \qquad (4.30)$$

where constants $C_{1,n,g}$ and $C_{2,n,g}$ are different for each energy group. This solution is essentially a Fourier series expansion with a number of unknown coefficients. The terms $\Phi_{n,g}(x)$ in Eq. (4.30) are the eigenfunctions of the Helmholtz equation and also called the *normal modes* of the neutron flux. Each normal mode corresponds to an eigenvalue B_n.

It can be shown that, when the time-dependence of the flux is included, all normal modes except the one corresponding to the first eigenvalue B_1 die out very rapidly [7] (see also Sec. 4.3.1). In a steady-state system, the $\Phi_{1,g}(x)$ flux is the only solution left, and it is called the *fundamental mode* of the neutron flux. Consequently, the higher normal modes with $n > 1$ are called *transient modes*. The square of the lowest eigenvalue B_1 is called the *geometry buckling* of the reactor and denoted by B_g^2 from here on. Eigenmode flux solutions similar to (4.30) can be derived for a variety of one-, two-, and three-dimensional geometries.

The unknown coefficients in the solution must be fixed by the boundary conditions. To demonstrate the procedure, it is next assumed that the width of the slab is h and that the flux falls to zero at each boundary. If the origin is fixed at the centre of the slab, the asymmetric sine-function must be dropped by setting $C_{1,1,g} = 0$. By applying the boundary conditions, the solution can be written as:

$$\Phi_g(-\frac{h}{2}) = \Phi_g(\frac{h}{2}) = 0 \implies \Phi_g(x) = \Phi_g^0 \cos(Bx),\tag{4.31}$$

where $B = \pi/h$ and Φ_g^0 is the peak value to which the flux is normalised.

The eigenvalues can be related to the physical parameters of the system by substituting (4.28) into (4.13). If only a single energy group is used in the calculation, the substitution yields for the fundamental mode solution:

$$-DB_g^2\Phi + \Sigma_a\Phi = \frac{1}{k_{\text{eff}}}\nu\Sigma_f\Phi,\tag{4.32}$$

from which:

$$k_{\text{eff}} = \frac{\nu\Sigma_f/\Sigma_a}{1 + L^2B_g^2} = \frac{k_\infty}{1 + L^2B_g^2},\tag{4.33}$$

where $L^2 = D/\Sigma_a$ is the diffusion area, defined as in (4.20), and $k_\infty = \nu\Sigma_f/\Sigma_a$ is the *infinite multiplication factor*, i.e. the multiplication factor of the system in the absence of neutron leakage. For a critical system $k_{\text{eff}} = 1$ and it is convenient to define the *material buckling* as:

$$B_m^2 = \frac{k_\infty - 1}{L^2}.\tag{4.34}$$

The criticality condition can then be written as:

$$B_m^2 = B_g^2.\tag{4.35}$$

This equation effectively relates a material parameter B_m^2 to the geometrical flux shape characterised by B_g^2.

The above equations become somewhat more complicated when more energy groups are included. For the two-group structure discussed in Section 4.1.2, the substitution of (4.28) into (4.13) yields:

$$
\begin{aligned}
-D_1B_g^2\Phi_1 + \Sigma_{r,1}\Phi_1 &= \frac{1}{k_{\text{eff}}}\left[\nu\Sigma_{f,1}\Phi_1 + \nu\Sigma_{f,2}\Phi_2\right] \\
-D_2B_g^2\Phi_2 + \Sigma_{a,2}\Phi_2 &= \Sigma_{s,1\to2}\Phi_1
\end{aligned}
\tag{4.36}
$$

from which k_{eff} can be solved as:

$$k_{\text{eff}} = \frac{1}{\Sigma_{\text{r},1}} \left[\frac{\nu\Sigma_{\text{f},1}}{1 - L_1^2 B_{\text{g}}^2} + \frac{\nu\Sigma_{\text{f},2}\Sigma_{\text{s},1\to2}}{\Sigma_{\text{a},2}(1 - L_1^2 B_{\text{g}}^2)(1 - L_2^2 B_{\text{g}}^2)} \right], \qquad (4.37)$$

where the diffusion areas are given by:

$$
\begin{aligned}
L_1^2 &= \frac{D_1}{\Sigma_{\text{r},1}} = \frac{D_1}{\Sigma_{\text{a},1} + \Sigma_{\text{s},1\to2}} \\
L_2^2 &= \frac{D_2}{\Sigma_{\text{a},2}}
\end{aligned}
\qquad (4.38)
$$

The infinite multiplication factor is written as:

$$k_\infty = \frac{\nu\Sigma_{\text{f},1}}{\Sigma_{\text{r},1}} + \frac{\nu\Sigma_{\text{f},2}\Sigma_{\text{s},1\to2}}{\Sigma_{\text{a},2}\Sigma_{\text{r},1}} \qquad (4.39)$$

and the material buckling as:

$$B_{\text{m}}^2 = \frac{k_\infty - 1}{L_1^2 + L_2^2} = \frac{k_\infty - 1}{M^2}, \qquad (4.40)$$

where $M^2 = L_1^2 + L_2^2$ is the migration area (4.25).

The above results are closely related to nodal diffusion calculations, discussed in the following section. The flux solution is written as the sum of analytical form functions corresponding to the flux modes, similar to (4.30). Some of the related parameters are calculated by the PSG code, as will be discussed in Section 9.3 of Chapter 9.

4.2 Nodal Diffusion Methods

The diffusion theory is best applied in geometries consisting of large[4] homogeneous material regions without sharp spatial changes in the neutronic properties of the medium. This is generally not the case for typical light water reactors. The active core region is extremely complicated in detail, as there are hundreds of fuel assemblies, each consisting of tens to hundreds of fuel pins. The assemblies can also be internally very complicated, especially in BWRs.

---

[4]The geometrical scale of a system must be compared to the neutron mean free path between the collisions. In light water reactors, this is typically less that one centimetre for thermal neutrons and 5–10 centimetres for fast fission neutrons.

The neutron flux in such a complicated system is not a smoothly varying function of the spatial co-ordinates, especially at low energy. The high absorption rate of low-energy neutrons in the fuel causes the thermal flux to drop near the fuel pins. This effect is especially pronounced near MOX pins, pins containing burnable absorber and pins with high fuel burnup. A similar effect is observed near (partially inserted) control rods, which also bring additional variation in the axial direction. The thermal flux is peaked inside water channels and near reflector regions at the core periphery.

The above difficulties make it impossible to use diffusion theory for detailed full-core calculations. Other deterministic methods based on a more accurate description of transport theory are not practical either, simply because of the enormous size of the computing task. The same restriction applies to the Monte Carlo method.

A widely used practical solution to the problem is to reduce the spatial detail of the geometry to a level where diffusion theory is applicable. The reduction has to be carried out in such a way that the diffusion calculation gives consistent results with the detailed transport theory calculation (if such could have been performed). This procedure is known as *homogenisation* [10].

The basic principle of the calculation method is simple. The reactor core is described as a three-dimensional array of homogeneous macro-regions, or *nodes*. In the radial direction, it is natural to set the node boundaries around a single fuel assembly, although other divisions are used as well. The axial direction is typically divided into 10–20 segments, depending on the active core height.

The solution proceeds by writing the few-group diffusion equations locally for each node, coupling the adjacent nodes together to obtain a global flux description and solving the system of equations by iteration. The calculation does not necessarily have to rely on diffusion theory, but it is the simplest approach and considered sufficient for most LWR applications[5].

4.2.1 Homogenisation

The first part of the nodal calculation is the generation of homogenised group constants for each node. The procedure largely relies on the fact that the local physical properties within each nodal region are more dependent on the physical properties and thermal-hydraulic conditions inside the assembly, than on the global position of the assembly in the reactor core [36][6]. This makes it possible to perform the ho-

---

[5]Higher-order spherical harmonics methods (P_N-methods) can be used as well.

[6]There are some cases where this assumption becomes questionable. One example is a mixed MOX/UOX core loading, in which each MOX assembly is surrounded by four UOX assemblies with significantly different reactor physical properties.

mogenisation by running a detailed two-dimensional transport calculation in a geometry composed of a single fuel assembly, surrounded by reflective or periodic boundary conditions. The procedure is performed by *lattice transport codes* and it has to be repeated for each assembly type at different burnup and thermal hydraulic conditions, in order to cover every node in the full-core geometry.

The homogenised group constants are generated in such a way that the integral reaction rate balance is preserved within the lattice cell. The procedure is very similar to the energy group condensation, discussed in Section 3.3.1 of Chapter 3. The difference is that the integration is also carried over the volume of the lattice cell. The homogenised flux is written as:

$$\Phi_g = \int_V \int_{E_g}^{E_{g-1}} \phi(\mathbf{r}, E) d^3 r dE \qquad (4.41)$$

and the homogenised cross section of reaction i as:

$$\Sigma_{i,g} = \frac{\int_V \int_{E_g}^{E_{g-1}} \Sigma_i(\mathbf{r}, E) \phi(\mathbf{r}, E) d^3 r dE}{\int_V \int_{E_g}^{E_{g-1}} \phi(\mathbf{r}, E) d^3 r dE} \; . \qquad (4.42)$$

Similar equations can be written for the homogenisation of the other interaction parameters as well.

Deterministic lattice codes calculate the neutron flux using *micro-group* transport methods. The number of energy groups typically ranges from 40 to 70. Because of the limitations posed by the calculation methods, it is not possible to obtain a spatially continuous flux solution needed for the calculation of integrals (4.41) and (4.42). The geometry is instead divided into discrete *micro-regions*, each consisting of a single material. The flux solutions are calculated for each region and the results combined afterwards. For a simple reaction cross section this procedure can be written as:

$$\Sigma_{i,g} = \frac{\sum_j \left[V_j \sum_h \left[\Sigma_{i,j,h} \Phi_{j,h} \right] \right]}{\sum_j \left[V_j \sum_h \Phi_{j,h} \right]} \; , \qquad (4.43)$$

where V_j is the volume of micro-region j. The outer summation is carried over all micro regions in the homogenised cell and the inner summation over all micro groups h, contained within group g.

The homogenisation of the diffusion coefficient differs from the other parameters to some extent. Fick's law (4.8) defines this parameter as the ratio of neutron current

density to the flux gradient. The diffusion coefficient is *always* defined as an energy-integrated value, and the homogenisation basically implies the integration of $D_g(\mathbf{r})$ over the cell volume in such a way that the group currents over the boundary surfaces are preserved [10].

In practice, the homogenised diffusion coefficient is often calculated using the transport cross section, as in (4.9). It is discussed in Appendix A that the energy condensation of $\Sigma_{\text{tr},g}(\mathbf{r})$ must be carried out using the current spectrum, not the flux spectrum as the weighting function. It is often the case, however, that the transport cross section is homogenised similar to any other reaction cross section:

$$
\Sigma_{\text{tr},g} = \frac{\int_V \int_{E_g}^{E_{g-1}} \left[\Sigma_{\text{t}}(\mathbf{r}, E) - \overline{\mu} \Sigma_{\text{s}}(\mathbf{r}, E) \right] \phi(\mathbf{r}, E) d^3 r dE}{\int_V \int_{E_g}^{E_{g-1}} \phi(\mathbf{r}, E) d^3 r dE} \, . \tag{4.44}
$$

The flux spectrum is generally softer than the current spectrum, which leads to the over-estimation of $\Sigma_{\text{tr},g}$ and hence to the under-estimation of the diffusion coefficient.

4.2.2 Nodal Calculations

It was discussed in Section 4.1.4 that the solution of the few-group diffusion equation inside a homogeneous material region can be written using a set of analytical form functions, each corresponding to a different flux mode. The same approach is taken in the nodal calculations. The local flux solutions are coupled to each other by a set of boundary conditions.

The problem is, however, that there are not enough degrees of freedom to enable a very accurate description of the flux shape over the node boundaries. The solution applied in advanced nodal methods is to actually allow the flux to be discontinuous at each boundary, which makes it possible to preserve the volume-integrated reaction rates and surface-averaged fluxes and currents. This is achieved by adding more degrees of freedom in the system by introducing so-called *assembly discontinuity factors* [37], which are defined for each boundary surface as the ratio of the surface-averaged to the volume-averaged flux:

$$
F_{i,g}^{\text{s}} = \frac{\frac{1}{A} \int_{S_i} \int_{E_g}^{E_{g-1}} \phi(\mathbf{r}, E) d^2 r dE}{\frac{1}{V} \int_V \int_{E_g}^{E_{g-1}} \phi(\mathbf{r}, E) d^3 r dE} \, , \tag{4.45}
$$

where A is the area of surface i and V is the volume of the assembly cell. It is also possible to define the discontinuity factors for cell corners as:

$$F_{j,g}^{\text{c}} = \frac{\displaystyle\int_{E_g}^{E_{g-1}} \phi(\mathbf{r}, E)dE}{\displaystyle\frac{1}{V}\int_V \int_{E_g}^{E_{g-1}} \phi(\mathbf{r}, E)d^3rdE} \; , \qquad (4.46)$$

where the integral in the numerator is evaluated at corner j.

It is not considered necessary to go into the details of advanced nodal methods in this text. The calculation of assembly discontinuity factors is revisited in Section 9.3.5 of Chapter 9, which deals with group constant generation in the PSG code. It is worth mentioning, however, that the role of the diffusion coefficient as an independent parameter becomes less important when the discontinuity factors are applied in the calculation.

4.2.3   Leakage Corrections in the Infinite-lattice Calculation

It was discussed in Section 3.2.3 of Chapter 3 that the modelling of a sub- or super-critical geometry as a steady-state system introduces distortion in the spatial and energy-dependence of the neutron flux. The distortion results from the fact that the fission source terms in the transport equation are divided by the effective multiplication factor, k_{eff}, and the flux contribution of fast fission neutrons becomes either over- ($k_{\text{eff}} < 1$) or under-estimated ($k_{\text{eff}} > 1$).

This problem is inevitable when homogenised group constants are generated in lattice calculation. The geometry consists of a two-dimensional fuel assembly model, surrounded by reflective or periodic boundary conditions. The system is effectively an infinite lattice of identical assembly cells. The net current over the cell boundaries is zero and there is no neutron leakage in or out of the system. It is clear that the geometry is not critical by default, which leads to a distorted flux solution. Since the flux is used for generating the homogenised group constants, the resulting parameters are distorted as well.

The solution is to balance the source and sink terms by adding some artificial neutron leakage in the system using so-called *leakage models*. A correction term, $\mathcal{L}(\mathbf{r}, \hat{\boldsymbol{\Omega}}, E)$, is introduced in the transport equation. This term is either positive or negative, corresponding to inward and outward net current, respectively. The sign depends on the criticality state of the system. Since all deterministic transport methods are based on the discretisation of the energy variable, the leakage term can be written for each

micro-group as $\mathcal{L}_h(\mathbf{r}, \hat{\mathbf{\Omega}})$. The treatment of the angular variable depends on the solution method.

The simplest leakage model is the homogeneous B_1 fundamental mode approximation. It is assumed that the correction term can be derived from the fundamental mode flux solution, satisfying the Helmholtz equation (4.28). The term is independent of spatial and angular variables and written as:

$$\mathcal{L}_h = -D_h \nabla^2 \Phi_h = D_h B_g^2 \Phi_h \,, \tag{4.47}$$

where D_h is the diffusion coefficient and Φ_h the homogeneous group flux in micro-group h. The geometry buckling B_g^2 is iterated to attain $k_{\text{eff}} = 1$ for the final solution. The leakage reaction is essentially modelled as homogeneous neutron production ($B_g^2 < 0$) or absorption ($B_g^2 > 0$) and the model has a certain analogy with the α-eigenvalue method, discussed in Section 3.2.3 of Chapter 3.

This simple model is applied in various deterministic lattice codes [38] and a similar procedure for the Monte Carlo method is derived in Section 9.5 of Chapter 9. Other, more elaborate leakage models do exist [39], but are not considered essential for the present study and hence not discussed here.

4.3 Time-dependent Diffusion Problems

The spatial, angular and energy-dependence of the neutron flux have been discussed throughout this chapter. The time-dependence of the Boltzmann transport equation (3.20) was kept when the basic form of the group-diffusion equation (4.13) was derived, but not much has yet been said about the time behaviour of the neutron population. The topic was briefly discussed with the α-eigenvalue method in Section 3.2.3 of the previous chapter and the approach taken here is very similar.

4.3.1 Point Reactor Kinetics Model

It was assumed in Section 4.1.4 that the spatial and energy-dependence of the flux can be separated from each other, when the diffusion equation is written in a homogeneous medium without time-dependence. The resulting Helmholtz equation (4.28) yields a flux solution that for each energy group can be written as a linear combination of spatial modes, each corresponding to an eigenvalue B_n^2. It is next assumed that the time-dependence is also separable, in which case the flux can be written as:

$$\Phi_g(\mathbf{r}, t) = \sum_{n=1}^{\infty} \left[\Phi_{n,g}(\mathbf{r}, t) \right] = \sum_{n=1}^{\infty} \left[\Phi_{n,g}(\mathbf{r}) \mathcal{T}_n(t) \right]. \tag{4.48}$$

Each normal mode $\Phi_{n,g}(\mathbf{r})$ has its own characteristic time behaviour that corresponds to a separable time-dependent amplitude function $\mathcal{T}_n(t)$.

Most textbooks (see e.g. [7, 40]) deal with reactor kinetics problems using one-group diffusion theory. This simple representation leads to the so-called *point reactor kinetics model* and it basically implies that the shape of the neutron flux remains constant and only its amplitude is allowed to change. The same approach is taken here. The substitution of (4.48) into (4.13) yields for mode n of the one-group flux:

$$\Phi_n(\mathbf{r})\frac{1}{v}\frac{\partial}{\partial t}\mathcal{T}_n(t) + \left[-D\nabla^2\Phi_n(\mathbf{r}) + \Sigma_a\Phi_n(\mathbf{r})\right]\mathcal{T}_n(t) = \nu\Sigma_f\Phi_n(\mathbf{r})\mathcal{T}_n(t). \quad (4.49)$$

The spatial dependence can be dropped by using (4.28) for the streaming term and Eq. (4.49) can be written in the form of:

$$\frac{1}{v}\frac{\partial}{\partial t}\mathcal{T}_n(t) + \left[DB_n^2 + \Sigma_a - \nu\Sigma_f\right]\mathcal{T}_n(t) = 0. \quad (4.50)$$

The solution of this simple first-order differential equation is written as:

$$\mathcal{T}_n(t) = \mathcal{T}_n(0)e^{-\lambda_n t}, \quad (4.51)$$

where

$$\lambda_n = v\left[DB_n^2 + \Sigma_a - \nu\Sigma_f\right]. \quad (4.52)$$

Since for the eigenvalues B_n^2 of the spatial mode:

$$B_1^2 < B_2^2 < \cdots < B_{n-1}^2 < B_n^2 < \dots, \quad (4.53)$$

it is easy to see that:

$$-\lambda_1 > -\lambda_2 > \cdots > -\lambda_{n-1} > -\lambda_n > \dots, \quad (4.54)$$

which implies that the higher normal modes die out when $t \to \infty$ and the fundamental mode ($n = 1$) dominates the asymptotic behaviour.

It is common practice to write the time eigenvalues in (4.52) as:

$$\lambda_n = -\frac{k_n - 1}{l_n}, \quad (4.55)$$

where

$$k_n = \frac{\nu\Sigma_f}{\Sigma_a + DB_n^2} = \frac{\nu\Sigma_f/\Sigma_a}{1 + L^2B_n^2} = \frac{k_\infty}{1 + L^2B_n^2} \quad (4.56)$$

and

$$l_n = \frac{1}{v(\Sigma_a + DB_n^2)} = \frac{1}{v\Sigma_a(1 + L^2B_n^2)}. \quad (4.57)$$

It is seen that for the fundamental mode solution, $B_n^2 = B_1^2 = B_g^2$, and Eq. (4.56) becomes equivalent to (4.33), implying that $k_1 = k_{\text{eff}}$. It should also be noted that the negative of λ_1 is basically equivalent to the α-eigenvalue discussed in Section 3.2.3 of Chapter 3.

Parameter l_n in (4.57) characterises the average time the neutrons spend diffusing through the reactor core before their eventual absorption or escape. The fundamental mode value l_1 is called the *prompt neutron lifetime* and denoted by l_p in this text. An associated quantity is the *neutron generation time*[7], given by:

$$\Lambda = \frac{1}{v\nu\Sigma_\text{f}} = \frac{l_\text{p}}{k_{\text{eff}}} \ .\tag{4.58}$$

This parameter can be interpreted as the average time between neutron emission and its subsequent absorption leading to a new fission [7].

Typical values for l_p in thermal and fast reactors are 0.1 ms and 0.1 μs, respectively [7]. According to (4.51), this would imply that for a k_{eff} only 0.01% above criticality, the neutron flux, and hence the power level, would double in about 0.7 s in the thermal reactor and in 0.7 ms in the fast reactor. Such time constants clearly point out the importance of delayed neutrons, as discussed in the following.

4.3.2 Impact of Delayed Neutrons

It was discussed in Section 2.1.2 of Chapter 2 that some small fraction of fission neutrons, typically 0.1–1.7%, is not emitted instantly, but after the radioactive decay of certain precursor fission product isotopes. Despite their small flux contribution, the impact of delayed neutrons on reactor kinetics is essential. This is because critical reactors actually operate in a slightly sub-critical state, made critical by the emission of delayed neutrons.

There are several fission product isotopes with neutron emission reactions in their radioactive decay chains. It is not possible in practice to treat each chain separately. The reactions are instead divided into equivalent *precursor groups*, each having a representative lifetime and neutron yield. The conventional representation uses six groups, with half-lives ranging from about 0.02 to 55 seconds. The group-wise half-lives are not the same for all isotopes, which complicates the treatment to some extent[8].

---

[7]The terminology related to the reactor time constants varies to some extent. The prompt neutron lifetime is also known as the *prompt removal time*. It has been suggested that the neutron generation time should be renamed as the *neutron reproduction time* [41].

[8]Some recent data evaluations have started to use an eight-group representation with standardised decay parameters.

Table 4.1: Half-lives (in seconds), decay constants and relative yields of delayed neutron precursor groups in ^{235}U, ^{238}U and ^{239}Pu fission [7].

	^{235}U(n,f)			^{238}U(n,f)			^{239}Pu(n,f)		
j	$T_{1/2}$	λ_j	$\overline{\nu}_j/\overline{\nu}_d$	$T_{1/2}$	λ_j	$\overline{\nu}_j/\overline{\nu}_d$	$T_{1/2}$	λ_j	$\overline{\nu}_j/\overline{\nu}_d$
1	54.51	0.013	0.038	52.38	0.013	0.013	53.75	0.013	0.038
2	21.84	0.032	0.213	21.58	0.032	0.137	22.29	0.032	0.280
3	6.00	0.116	0.188	5.00	0.139	0.162	5.19	0.134	0.216
4	2.23	0.311	0.407	1.93	0.359	0.388	2.09	0.332	0.328
5	0.50	1.398	0.128	0.49	1.406	0.225	0.55	1.263	0.103
6	0.18	3.872	0.026	0.17	4.030	0.075	0.22	3.209	0.035

The delayed neutron constants of three important actinides are listed in Table 4.1. The total delayed neutron yields $\overline{\nu}_d$ of the three isotopes are 0.0167, 0.0440 and 0.0065, respectively, and the values are practically constant up to about 5 MeV. All the associated parameters are hence usually given without energy-dependence. The *physical delayed neutron fraction*[9] is defined for each precursor group j as:

$$\beta_j(E) = \frac{\overline{\nu}_j}{\overline{\nu}_p(E) + \overline{\nu}_d} , \qquad (4.59)$$

where $\overline{\nu}_p(E)$ is the prompt neutron yield. The total fraction is given by:

$$\beta(E) = \frac{\overline{\nu}_d}{\overline{\nu}_p(E) + \overline{\nu}_d} = \sum_{j}^{J_d} \left[\beta_j(E) \right] , \qquad (4.60)$$

where J_d is the total number of precursor groups. Although the delayed neutron *yields* are practically independent of energy, it is clear that the corresponding *fractions* are not, as is also seen in Figure 2.3 on page 36. This implies that these variables should basically be condensed into energy group-wise values, similar to all the other parameters in a multi-group model. It is common practice, however, to average the values over the entire flux spectrum:

$$\beta_{0,j} = \frac{\int_V \int_0^\infty \beta_j(E)\Sigma_f(\mathbf{r}, E)\phi(\mathbf{r}, E)d^3rdE}{\int_V \int_0^\infty \Sigma_f(\mathbf{r}, E)\phi(\mathbf{r}, E)d^3rdE} , \qquad (4.61)$$

even if there are more groups in the diffusion calculation. The homogenised physical delayed neutron fraction ("beta-zero") is denoted by β_0 in this text.

---

[9]The physical delayed neutron fraction is often called simply the "delayed neutron fraction".

If the neutron flux is assumed to be in a steady-state condition, the impact of delayed neutron emission can be covered by slight modifications in the fission spectra. Time-dependent problems, however, require the explicit treatment of delayed neutron emission times. The one-group time-dependent fission source term with delayed neutrons takes the form of:

$$q_f(\mathbf{r}, t) = (1 - \beta_0)\nu\Sigma_f\Phi(\mathbf{r}, t) + \sum_{j}^{J_d} \left[\lambda_j C_j(\mathbf{r}, t)\right]. \tag{4.62}$$

The concentrations of the precursor isotopes are coupled to the fission rate, which depends on the neutron flux. The isotope balance can be written as[10]:

$$\frac{\partial}{\partial t}C_j = \beta_{0,j}\nu\Sigma_f\phi(\mathbf{r}, t) - \lambda_j C_j(\mathbf{r}, t). \tag{4.63}$$

Since the flux, the fission rate and hence the precursor concentrations all share the same spatial dependence, the time-dependence of the fundamental flux mode is characterised by:

$$\frac{1}{v}\frac{\partial}{\partial t}\mathcal{T}(t) + \left[DB_g^2 + \Sigma_a - (1 - \beta_0)\nu\Sigma_f\right]\mathcal{T}(t) - \sum_{j}^{J_d} \left[\lambda_j C_j(t)\right] = 0. \tag{4.64}$$

This leads to the point kinetics equations, which are often written using the neutron density as [40]:

$$\frac{\partial}{\partial t}n(t) - \left[\frac{\rho - \beta_0}{\Lambda}\right]n(t) - \sum_{j}^{J_d} \left[\lambda_j C_j(t)\right] = 0$$

$$\frac{\partial}{\partial t}C_j(t) = \frac{\beta_{0,j}}{\Lambda}n(t) - \lambda_j C_j(t), \quad j = 1, \ldots, J_d \tag{4.65}$$

where the *reactivity* is defined by:

$$\rho = \frac{k_{eff} - 1}{k_{eff}}. \tag{4.66}$$

It is clear that the system becomes far more complicated when delayed neutron emission is considered. Instead of solving a single differential equation, a set of $J_d + 1$ coupled equations need to be solved. It is next assumed that the time-dependence of the flux and the precursor concentrations takes the form of:

$$\mathcal{T}(t) \sim e^{\omega t}, \tag{4.67}$$

---

[10]It should be noted that the depletion of the precursor isotopes due to neutron absorption is not taken into account. It is usually assumed that this is not a serious flaw in the model, since the lifetimes of the isotopes are short.
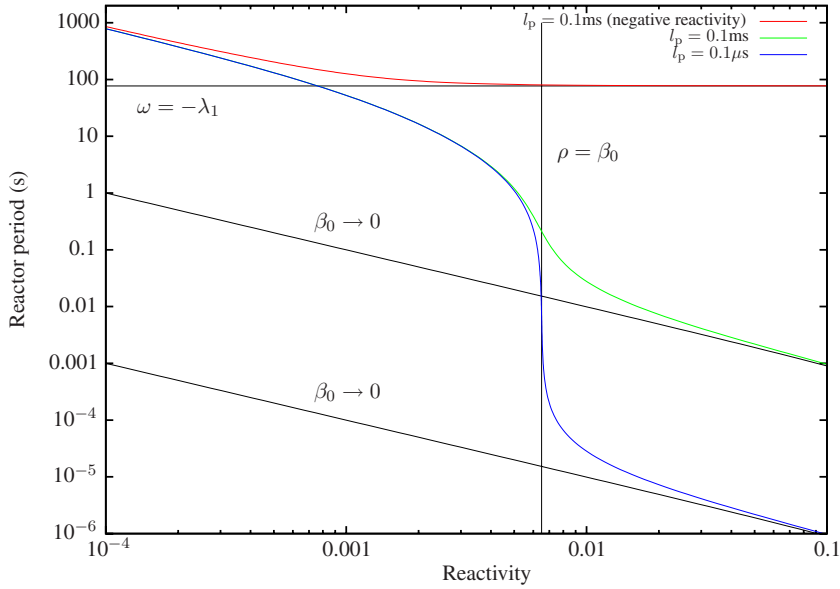
Figure 4.1: Stable reactor period as a function of reactivity. The top curve gives the negative of reactor period (decaying flux amplitude) as a function of negative of reactivity.

which substituted into (4.65) yields a relation between time constant ω and ρ:

$$\rho = \frac{\omega l_p}{1 + \omega l_p} + \frac{\omega}{1 + \omega l_p} \sum_{j=1}^{J_d} \left[\frac{\beta_{0j}}{\omega + \lambda_j} \right]. \tag{4.68}$$

This is known as the *inhour equation*. The reciprocal of ω is known as the *reactor period* and it is plotted as a function of reactivity Figure 4.1[11].

The top curve shows the negative of reactor period as a function of negative of reactivity and it corresponds to an exponentially decaying flux amplitude. It can be seen that the period approaches a constant value as the reactivity becomes more negative. This level is determined by the decay of the most long-lived delayed neutron precursor group:

$$\lim_{\rho \to -\infty} \omega(\rho) = -\lambda_1 \tag{4.69}$$

---

[11]Equation (4.68) actually has $J_d + 1$ roots and Figure 4.1 shows the period corresponding to the largest value. This is known as the *stable reactor period*. It can be shown that all the other solutions are negative. The corresponding terms are hence exponentially decaying and the stable period characterises the asymptotic time behaviour of the reactor as $t \to \infty$.

and it gives the maximum rate at which the fission power of the reactor is possible to be brought down.

The other two curves show the reactor period as a function of positive reactivity in two cases corresponding to the prompt neutron lifetimes typical of thermal and fast reactors. The dynamics of the system changes dramatically when reactivity exceeds the delayed neutron fraction, which is also seen in the plot. In such a condition, the chain reaction becomes self-sustaining by the emission of prompt neutrons. The more the prompt neutrons dominate the neutron multiplication, the closer the reactor time constant becomes to the value determined only by the prompt neutron lifetime, as in Eq. (4.55):

$$\rho \gg \beta_0 \implies \omega(\rho) \approx \frac{\rho}{l_{\mathrm{p}}(1 - \rho)} \; . \tag{4.70}$$

Such a system is said to be in a *prompt super-critical state*.

4.3.3 Reactor Dynamics

The point reactor kinetics model, as discussed above, contains several crude approximations. The model breaks down in large thermal reactor cores. The reason is that the time it takes for a spatial perturbation to spread over the entire core may be long compared to reactor period. In such a case, the assumption of a constant flux shape is clearly not applicable, as the flux may even be subject to spatial oscillations.

Another problem is the treatment of energy-dependence, which does not take into account the delayed neutron emission spectra. Delayed neutrons are born well below the fission threshold of ^{238}U, and they are slowed down past the capture resonances more easily than prompt neutrons. Delayed neutron emission can hence be considered less valuable for the fission chain reaction in fast reactors and more valuable in thermal reactors.

Some of the restrictions to the applicability of the point kinetics model can be lifted without changing the basic form of the equations by defining the associated parameters in a more general manner. One such improvement is to replace the physical delayed neutron fraction by the *effective delayed neutron fraction*, which takes into account the importance of the emitted neutrons to the continuation of the chain reaction. The effective fraction of delayed neutrons belonging to precursor group j is given by:

$$\beta_{\mathrm{eff},j} = \frac{\int_V \int_0^\infty \phi^\dagger(\mathbf{r}, E)\beta_j(E)\Sigma_{\mathrm{f}}(\mathbf{r}, E)\phi(\mathbf{r}, E)d^3rdE}{\int_V \int_0^\infty \phi^\dagger(\mathbf{r}, E)\Sigma_{\mathrm{f}}(\mathbf{r}, E)\phi(\mathbf{r}, E)d^3rdE} \; , \tag{4.71}$$

where $\phi^\dagger(\mathbf{r}, E)$ is the *adjoint neutron flux*. A very similar adjoint flux-weighting must be applied for the neutron generation time. Adjoint calculations are related to a more general topic of *perturbation theory*. The topic is discussed in various reactor physics textbooks [7, 8], but left beyond the scope of this study[12].

The point kinetics model does not take into account the possible time-dependence of reactivity. Such dependence can be induced by reactivity control, or by the various temperature effects in the reactor materials, such as the Doppler-broadening of capture resonances in fuel isotopes or the boiling of coolant water. The result is a complex physical system, involving coupling between reactivity, reactor power and the rate of heat removal from the core.

The branch of nuclear engineering that deals with such coupled phenomena is known as *reactor dynamics*. It is clear that the point reactor kinetics model is insufficient for such calculations. The heat removal alone is a complicated thermal-hydraulics problem, which may require the modelling of two-phase coolant flow and the consideration of secondary systems coupled to the primary loop by heat exchangers.

The neutronics models in reactor dynamics codes are typically based on time-dependent one or three-dimensional nodal diffusion methods. The homogenised group constant data is generated using lattice codes, which have to be capable of calculating the various kinetic and delayed neutron parameters needed in the calculation. The methods used in the PSG code are discussed in Section 9.3.4 of Chapter 9.

4.4   Fuel Depletion

It was mentioned earlier that one of the local parameters in the infinite-lattice calculation is fuel burnup. As in the homogenisation, the changes in the fuel composition can be assumed to be more dependent on the type of the fuel assembly and the local operating conditions, than on the global position of the assembly in the reactor core. Fuel depletion calculations are hence performed at the assembly level, and often by the same computer codes that generate the homogenised group constants. Such codes are typically referred to as *assembly burnup codes*. Since the changes in the fuel composition are slow compared to reactor time constants, the transport calculation is performed without time-dependence.

---

[12]As an intuitive description it can be said that the adjoint calculation implies exchanging the source and detector regions and performing the transport calculation backwards. The adjoint flux-weighted delayed neutron fraction is basically equivalent to the fraction of fission reactions caused by delayed neutrons. This interpretation forms the basis of the methods used for calculating β_{eff} in a forward Monte Carlo simulation.

Isotope balance in a material subject to neutron irradiation is characterised by the set of *Bateman equations* [10]:

$$\frac{dN_j}{dt} = \sum_{i \neq j} \left[(\gamma_{i \to j}\sigma_{\mathrm{f},i}\Phi + \lambda_{i \to j} + \sigma_{i \to j}\Phi)\, N_i \right] - (\lambda_j + \sigma_j \Phi)\, N_j \,, \qquad (4.72)$$

where N_j is the atomic density of isotope j.
  $\gamma_{i \to j}$ is the fractional fission product yield of j in the fission of isotope i.
  $\sigma_{\mathrm{f},i}$ is the microscopic fission cross section of isotope i.
  Φ is the spectrum-averaged scalar flux in the fuel region.
  $\lambda_{i \to j}$ is the decay constant of decay $i \to j$.
  $\sigma_{i \to j}$ is the microscopic transmutation cross section of reaction $i \to j$.
  N_i is the atomic density of isotope i.
  λ_j is the decay constant of isotope j.
  σ_j is the microscopic total transmutation cross section of isotope j.

The two terms on the right-hand side of (4.72) describe the production and depletion rates of isotope j. The production term is written as the sum over all other isotopes and it is further divided into fission, decay and transmutation source terms. The decay constant $\lambda_{i \to j}$ takes into account the branching ratio of each decay event. The depletion term consists of all radioactive decay and neutron-induced transmutation events, in which isotope j is transformed into other species. The total transmutation cross section σ_j includes all reactions excluding elastic scattering and inelastic two-body scattering. All parameters are homogenised one-group values and the neutron flux is normalised to a specific power density.

The Bateman equations written for different isotopes are coupled to each other by the production and depletion terms. The time-dependent nuclide concentrations must be solved from a system of linear first-order differential equations. The problem can be written in matrix form as:

$$\dot{\mathbf{n}} = \mathbf{A}\mathbf{n} \,, \qquad (4.73)$$

where vector $\mathbf{n} = (N_1 \ N_2 \ \dots \ N_J)^T$ contains the concentrations of the isotopes and matrix $\mathbf{A}$ all the coefficients of N_j.

The general solution of matrix equation (4.73) is analogous to the solution of a similar first-order scalar differential equation, and may be written as:

$$\mathbf{n}(t) = e^{\mathbf{A}(t-t_0)}\mathbf{n}(t_0) \,. \qquad (4.74)$$

The problem of finding the solution to the nuclide concentrations is then practically reduced to the calculation of the matrix exponential function $e^{\mathbf{A}}$. There are various

numerical methods for performing this task [42], as well as alternative methods for solving the set of Bateman equations. Detailed descriptions can be found in various textbooks [10] and in the manuals of several computer codes performing fuel depletion calculation [43, 44].

The input data needed for burnup calculation includes isotopic decay constants and fission product yields read from a nuclear data library, together with homogenised fission and transmutation cross sections provided by the transport calculation. Fuel pins are often divided into several annular regions to account for the rim-effect caused by the spatial self-shielding of the fuel isotopes (see Section 2.3.5 of Chapter 2). This is especially important for high-absorbing burnable absorber pins.

The burnup calculation proceeds in discrete time steps, assuming time-independent material compositions throughout the interval. The length of each step can vary and shorter steps are required at the beginning of the cycle to allow the saturation of fission product poisons. The transmutation cross sections are given by a steady-state neutron transport calculation at the beginning of each step. After the burnup step has been completed, a new set of cross sections is calculated for the changed material composition and the procedure is repeated for the next time step.

Chapter 5

Monte Carlo Simulation

5.1 Monte Carlo Method in Neutron Transport Calculation

It is often stated that Monte Carlo codes *solve* the neutron transport equation (3.20) using stochastic methods. This statement is misleading to some extent, since the spatial, angular, and energy-dependent flux (the solution of the transport equation) is never resolved during the calculation. In fact, the transport equation, or even the concept of a neutron flux, is not necessary for understanding the basics of the Monte Carlo simulation[1]. The problem of reviewing the simulation merely as another solution method for the Boltzmann transport equation is that the nature of the underlying process is easily forgotten.

The strength of the Monte Carlo method lies in the capability to calculate statistical estimates for integral reaction rates without explicitly solving for the flux distribution. The capability to deal with complex variation in spatial and energy variables is what makes Monte Carlo calculation such an attractive alternative to the deterministic transport methods.

The calculation of the output parameters can be separated from the actual simulation, which is carried out one neutron at a time. Rather than dealing with equations of continuous variables, the collection of results is based on discrete *events*. This approach also has its downsides: various important transport parameters are based on differential quantities, which are not easy to calculate using Monte Carlo. Another problem is related to adjoint calculation, which basically implies running the simulation in reverse. This is possible in theory, but very difficult in practice if the probability

---

[1]It should be reminded that the neutron flux is essentially a mathematical density function, rather than a physical, measurable quantity.

distributions describing neutron interactions are continuous functions of the energy variable. Adjoint calculations are discussed in various textbooks (see e.g. Ref [12]). The theory introduced in this study, however, is based on the forward method and an analog Monte Carlo game.

The approach taken in this chapter is that the actual parameters of interest can be resolved by simulating the random walk of individual neutrons. Comprehensive knowledge of neutron transport theory is not necessary for understanding the basic principles of the simulation. The physics is practically restricted to the modelling of neutron interactions. Transport theory will be revisited in the following chapter, where the simulated results are related to the concepts introduced in Chapters 3 and 4, but for now the main attention is turned back to the individual neutron.

5.2   Mathematical Basis

The general Monte Carlo method has profound mathematical roots starting from the Markovian chains in the theory of probabilistics. Particle transport calculation, however, is one of the most analog and straightforward applications of the method and a thorough mathematical approach to the problem would not serve its purpose in this context. Instead, it is considered sufficient to introduce the most essential concepts needed for carrying out the simulation. The rest of the process is treated as if the results were collected from actual physical measurements.

5.2.1   Probability Distribution Functions

Each stochastic process related to a random variable x is characterised by a probability distribution $f(x)$, which is defined in such a way that the probability of the event occurring between x and $x + dx$ is given by:

$$dP = f(x)dx \, . \tag{5.1}$$

The distribution function $f(x)$ is also called the *probability density function*, or PDF. Consequently, the probability of the event occurring on interval $[a, b]$ of the variable is:

$$P(a < x < b) = \int_a^b dP = \int_a^b f(x)dx \, . \tag{5.2}$$

A natural requirement for the PDF is that the integration yields non-negative and finite values.

The probability that the event occurs before the variable reaches a certain value is given by the *cumulative distribution function*, or CDF, which is calculated from (5.1) by direct integration:

$$F(x) = P(x' < x) = \int_{-\infty}^{x} f(x')dx' \,.$$ (5.3)

The PDFs are assumed to be properly normalised, i.e. the integration of $f(x)$ over all value space must yield $P = 1$ and hence:

$$\lim_{x \to \infty} F(x) = 1 \,.$$ (5.4)

In the simplest case, the random variable is uniformly distributed between two values, a and b. The PDF is then:

$$f(x) = \begin{cases} \dfrac{1}{b-a} & \text{when } a \le x \le b \\ 0 & \text{when } x < a \text{ or } x > b \end{cases}$$ (5.5)

and the CDF given by integration:

$$F(x) = \begin{cases} 0 & \text{when } x < a \\ \dfrac{x-a}{b-a} & \text{when } a \le x \le b \\ 1 & \text{when } x > b \end{cases}$$ (5.6)

A special case of the uniform distribution is when $a = 0$ and $b = 1$. The random variable is then uniformly distributed on the unit interval. Such a variable is denoted by ξ from here on. Values for ξ can be calculated using numerical pseudo-random number generators[2] and all the other random numbers are derived from these values. The selection of random values from probability distributions is called *sampling*. This is carried out using one or several uniformly distributed random variables, together with the appropriate distribution functions. Some of the methods are introduced below.

5.2.2   The Inversion Method

The simplest of the sampling procedures is the *inversion method* [12, 45], in which the sampling of variable x from distribution $f(x)$ is carried out using the cumulative

---

[2]It should be noted that the generation of uniformly distributed (pseudo-) random numbers is by no means a trivial topic. It is assumed, however, that the distribution of variable ξ is random enough to serve its purpose in this context.

distribution function, $F(x)$. At first, a uniformly distributed variable, ξ, is selected on the unit interval. The value of ξ is then set equal to the cumulative probability of the event, so that the corresponding value of x can be calculated from the inverse function of the CDF:

$$F(x) = \xi \iff x = F^{-1}(\xi)\,. \tag{5.7}$$

Values of x sampled in this way are distributed according to $f(x)$.

The process is best understood by considering an example. Figure 5.1 illustrates the sampling of a random variable from an exponential probability distribution. First, a value for the uniformly distributed random variable, ξ, is sampled on the unit interval. Let the value be $\xi = 0.8979$ in this case. The value of the corresponding exponentially distributed variable, x, is then calculated from the inverse function of the CDF. In this case, the value becomes $x = F^{-1}(\xi) = 7.1552$. The figure shows the PDF and the CDF of the exponential distribution together with the sampled values of ξ and x. The figure also shows a simulated distribution of values sampled using the inversion method.

5.2.3 Rejection Techniques

In many cases, either the cumulative distribution function (5.3) or its inverse is expensive to calculate, or even worse, cannot be solved at all in closed form. Examples of such cases are the normal distribution and the Maxwell-Boltzmann distribution. There are several numerical variations to the inversion method that can be used to sample values from any type of distribution [45], but it is often more efficient to take a completely different approach.

The so-called *rejection techniques* [12, 45] have the advantage that the sampling procedure can be out carried using only the PDF of the random variable. In the simplest form, a constant $c \geq 1$ and another density function $g(x)$ are assigned to $f(x)$ in such a way that:

$$f(x) \leq cg(x) \tag{5.8}$$

for all values of x. First, a value for x is sampled from distribution $g(x)$. Another random variable, ξ, is then sampled on the unit interval and the value of x is accepted as a sample from $f(x)$ if:

$$\xi < \frac{f(x)}{cg(x)}\,. \tag{5.9}$$

If the inequality does not hold, the value is discarded and the procedure is repeated from the beginning. It can be shown that the distribution of the accepted values follows exactly $f(x)$.
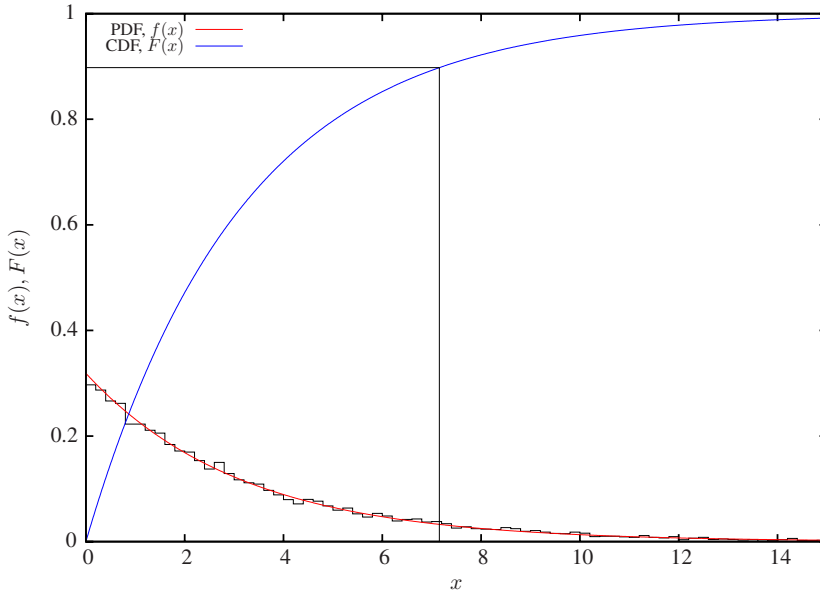
Figure 5.1: Sampling of a random variable x from an exponential probability distribution. The histogram curve on the background shows the distribution of 10,000 randomly sampled values.

There are certain properties that are desired for function $g(x)$. It is obvious that the function should be chosen in such a way that the sampling can be performed using the inversion method (or some other efficient technique). Another important aspect is that the difference between functions $cg(x)$ and $f(x)$ should be small, or more precisely, the ratio of the integrals:

$$E = \frac{\displaystyle\int_{-\infty}^{\infty} f(x)dx}{\displaystyle\int_{-\infty}^{\infty} cg(x)dx} \tag{5.10}$$

as close to unity as possible. This ratio is known as the *efficiency* of the algorithm. If the efficiency is low, computing time is wasted as the re-sampling loop has to be repeated over and over again before finding an acceptable value for the variable.

5.2.4   Sampling from Tabular Distributions

The probability distributions in practical applications are often given, not as parametrised functions, but rather as tabulated PDF and CDF distributions. Examples of

such a case are some energy and angular distributions of neutrons emitted in nuclear reactions. The sampling method that is to be used depends on the format in which the probability data is given and the interpolation scheme used for values between the tabulated data points.

One commonly used method, especially for describing the angular distributions of two-body scattering collisions, is the sampling of equi-probable intervals [12, 14]. The CDF of the probability distribution is divided into N intervals. The $N + 1$ tabulated values are chosen in such a way that the cumulative probability is the same for each interval $x_n < x < x_{n+1}$:

$$\int_{x_n}^{x_{n+1}} f(x)dx = \frac{1}{N} .$$ (5.11)

The value simply results from the fact that all the interval probabilities must be summed up to unity.

The sampling algorithm proceeds as follows. First, the interval is sampled by taking the integer part of:

$$n = N\xi + 1 .$$ (5.12)

The value of the random variable x is then interpolated between the two tabulated values, x_n and x_{n+1}:

$$x = x_n + (N\xi - n)(x_{n+1} - x_n) .$$ (5.13)

The accuracy of the method depends on the number of intervals and the type of the distribution function. For angular distributions, a typical number of equi-probable scattering cosine intervals is 32, which is considered sufficient for most scattering reactions.

The described method applies to angular distributions only when either the emission energy is directly coupled to the value of the scattering angle, or when there is no correlation at all between the two distributions and the emission energy can be sampled independently. This is not the case for all reaction modes. In many cases, the values need to be sampled from combined distributions. Further, the distribution functions are not necessarily two-dimensional, in that the shape of the distribution depends on the energy of the incident neutron. The detailed description of the techniques used for sampling values from the ENDF[3] probability distributions is not given here. A complete description can be found in references [13] and [14].

---

[3]The ENDF data format is introduced in Section 7.2 of Chapter 7.

5.3 Neutron Tracking

Neutron tracking refers to the process of simulating the movement of a single neutron through the different material regions of the geometry. The shortest length of path that the neutron makes between the points of interaction is called a *track*. The track can also be cut short by a material boundary surface located between the two points. The entire set of tracks made from the initial emission to the final absorption or escape is called a *neutron history*. The number of neutron histories is hence equal to the total number of emitted source neutrons.

The basis of the simulation process is the sampling of the free path length between two collision points. In most textbooks [7, 12], the corresponding probability distribution is derived from the attenuation of a uniform one-speed neutron beam (see also Section 3.1.1 of Chapter 3). Since the approach taken in this chapter is to look at things from the viewpoint of a single neutron, the distribution is derived in a slightly different, although completely analogous manner.

5.3.1 Sampling the Free Path Length

It was stated earlier that the microscopic total cross section describes the neutron interaction probability with a single nucleus and that the macroscopic total cross section is the interaction probability per path length travelled by the neutron. Consider a neutron travelling through an infinite homogeneous medium with constant interaction probability, described by the macroscopic total cross section, Σ_t[4]. According to the definition of Σ_t, the probability that the neutron will undergo an interaction while moving distance dx in the medium is simply:

$$dP = \Sigma_t dx \, . \tag{5.14}$$

Assume that the neutron is located within distance x from an arbitrary zero position. Let $P_0(x)$ be the probability that the neutron has reached x without any interaction. When the neutron moves forward by distance dx from x, the reduction in $P_0(x)$ is equal to the conditional probability that the neutron will interact within the interval:

$$dP_0 = -P_0(x)dP = -P_0(x)\Sigma_t dx \, . \tag{5.15}$$

The solution of this differential equation yields for the *non-interaction probability*:

$$P_0(x) = e^{-x\Sigma_t} \, . \tag{5.16}$$

---

[4]The energy-dependence of Σ_t is omitted because the neutron can change its energy only in interactions.

The probability that the neutron first moves distance x without interactions and then has its first interaction within the next dx is simply:

$$P_0(x)dP = P_0(x)\Sigma_t dx = \Sigma_t e^{-x\Sigma_t} dx . \tag{5.17}$$

The PDF of the free path length is then:

$$f(x) = \Sigma_t e^{-x\Sigma_t} \tag{5.18}$$

and the CDF:

$$F(x) = \int_0^x \Sigma_t e^{-x'\Sigma_t} dx' = 1 - e^{-x\Sigma_t} . \tag{5.19}$$

The probability distribution is exponential and the neutron distance to the next collision site can be sampled using the inversion method. From (5.19) and (5.7) it follows that:

$$x = -\frac{1}{\Sigma_t} \ln(1 - \xi) = -\frac{1}{\Sigma_t} \ln \xi , \tag{5.20}$$

where the last identity results from the fact that $1 - \xi$ and ξ are similarly distributed. An example of sampling from the exponential distribution was already given in Figure 5.1. The cross section in that case was $\Sigma_t = 0.3188 \text{ cm}^{-1}$.

The average path length travelled by the neutron without interactions, or the *mean free path*, ℓ, can be calculated from the non-interaction probability (5.16):

$$\ell = \int_0^\infty x e^{-x\Sigma_t} dx = \frac{1}{\Sigma_t} . \tag{5.21}$$

In the example case, $\ell = 3.1364$ cm, which is easily seen in Figure 5.1.

5.3.2 Tracking in Finite Geometry Regions

The prerequisite of calculating the probability distributions of the neutron path length is that the material is homogeneous, i.e. that the macroscopic total cross section does not depend on the spatial neutron co-ordinates. The calculation of the integrals becomes more complicated in the case of an inhomogeneous medium and it is possible that the probability functions cannot be resolved at all in closed form.

In most cases of interest, the geometry consists of not one, but of several homogeneous material regions, or *cells*. Since the material properties are different in each region, the collision probability changes each time the neutron crosses a cell boundary. The problem is that the free path length sampled in one material is not statistically valid in the next. The solution is to stop the neutron at the boundary surface and

adjust or re-sample the remaining distance to the next collision site. The result is a ray-tracing algorithm that follows the neutron from one surface to the next.

Consider a situation in which the neutron is initially in a material characterised by macroscopic total cross section Σ_{t1}. The distance to the nearest material boundary within the line-of-sight is denoted by d and beyond that lies another material, with total cross section Σ_{t2}. The free path length, x_1 in material 1 has been sampled in such a way that $x_1 > d$. The path length x_2 in material 2 must then be adjusted from the remaining part, $x_1 - d$. The adjustment has to be made without compromising the statistical validity of the sample, which is assured by preserving the non-interaction probability (5.16):

$$e^{-x_2\Sigma_{t2}} = e^{-(x_1-d)\Sigma_{t1}} \quad \Longrightarrow \quad -\Sigma_{t2}x_2 = -(x_1 - d)\Sigma_{t1}$$

$$\Longrightarrow \quad x_2 = (x_1 - d)\frac{\Sigma_{t1}}{\Sigma_{t2}} \,. \tag{5.22}$$

The total path length from the starting position is then:

$$x = d + x_2 = d + (x_1 - d)\frac{\Sigma_{t1}}{\Sigma_{t2}} \,. \tag{5.23}$$

A statistically equivalent result is attained if x_2 is sampled independently, using cross section Σ_{t2} and a new random number ξ. The equivalence results from the fact that neutrons "forget" their past history and the intersection point at the boundary surface can be treated as any other starting point of a neutron track. The re-sampling technique is clearly simpler and it can also be more efficient than the adjustment of the path length, especially if multiple boundary surfaces are crossed between the collision points.

Both of the above methods require the information about the distance to the nearest boundary surface. In order to calculate the surface distances, the geometry has to be set up using simple geometrical objects, such as planes, spheres, cylinders and other surfaces that can be written in closed form. The equations that need to be solved may become complicated as the solution depends on the surface parameters as well as the initial position and flight direction of the neutron.

Consider, for example, an infinite circular cylinder of radius r parallel to z-axis and centred at (x_0, y_0). The equation describing the surface is:

$$\mathcal{F}(x, y) = (x - x_0)^2 + (y - y_0)^2 - r^2 = 0 \,. \tag{5.24}$$

The initial neutron position and direction are given by three Cartesian co-ordinates, (x, y, z) and three direction vectors $(\Omega_x, \Omega_y, \Omega_z)$. The equation from which the distance d must be resolved becomes:

$$(x + \Omega_x d - x_0)^2 + (y + \Omega_y d - y_0)^2 - r^2 = 0 \,. \tag{5.25}$$

The solution can be written as:

$$d = \frac{-\Omega_x(x - x_0) - \Omega_y(y - y_0)}{\Omega_x^2 + \Omega_y^2}$$

$$\pm \frac{\sqrt{(\Omega_x^2 + \Omega_y^2)r^2 - \left[\Omega_x(y - y_0) - \Omega_y(x - x_0)\right]^2}}{\Omega_x^2 + \Omega_y^2}, \quad (5.26)$$

which is relatively simple to calculate within the transport code. It is often the case, however, that the cells in reactor geometries are composed of several elementary surfaces. The only way to calculate the distance to the *nearest* surface, is to calculate the distances to all cell boundaries within the line-of-sight[5], and then pick the shortest value. This task may become complicated and time-consuming, especially if the neutron mean free path is long compared to the characteristic dimensions of the system. In such a case, the neutron may have to cross several material boundaries before reaching the final collision point.

5.3.3 Delta-tracking Method

The conventional ray-tracing algorithm can be replaced by an alternative method, known as *delta-tracking*, which samples the next collision point without handling the surface crossings. The procedure was initially proposed by Woodcock [15] in the 1960s and it is briefly introduced in the textbook by Lux and Koblinger [12]. Delta-tracking is used in the HOLE geometry package [20] available for Monte Carlo codes MONK and MCBEND. The technique is also used as an optional tracking method in the RCP01 [16], RACER [17], MCU [18] and VMONT [19] codes.

This section introduces the main principle of the basic Woodcock delta-tracking method, together with an intuitive explanation for the statistical validity of the procedure. A purely mathematical verification is given in Ref. [46]. The PSG code uses an extended delta-tracking method, which is described in detail in Section 8.3.1 of Chapter 8.

Consider an interaction in which the neutron is not absorbed and both the incident energy and the direction of flight are preserved. Such interaction is denoted from here on as a *virtual collision*[6], characterised by cross section $\Sigma_0(\mathbf{r}, E)$. It is obvious

---

[5]Even determining which surfaces are located within the line-of-sight may become quite complicated, since some surfaces are only partially included in the cell definition.

[6]Virtual collisions are sometimes called *pseudo-scattering* reactions and delta-tracking is also known as the pseudo-scattering method. The name "delta-tracking" apparently originates from the fact that virtual collisions are essentially scattering reactions, in which the angular and energy distributions are characterised by δ-functions and the state of the particle is completely preserved.

that an arbitrary number of virtual collisions may occur during the neutron lifetime, without affecting the statistics or the outcome of the simulation in any way.

The key idea in the delta-tracking method is to add an appropriate virtual collision cross section to each material total in such a way that the modified total cross section has the same value in all materials. The result is that the total interaction probability, in this case the sum of real and virtual collision probabilities, is the same in all materials. This eliminates the need to adjust the free path length each time the neutron enters a new material, and eventually, the need to calculate the surface distances.

The value of the virtual collision cross section is given by:

$$\Sigma_0(\mathbf{r}, E) = \Sigma_{\mathrm{m}}(E) - \Sigma_{\mathrm{t}}(\mathbf{r}, E), \qquad (5.27)$$

where $\Sigma_{\mathrm{t}}(\mathbf{r}, E)$ is the physical total cross section of the material and $\Sigma_{\mathrm{m}}(E)$ is the maximum of all total cross sections in the system, also known as the *majorant*. The value of $\Sigma_{\mathrm{m}}(E)$ is the same for all materials and hence independent of the spatial co-ordinates.

The tracking procedure begins by sampling the free path length from (5.20), using the majorant cross section. The neutron is then moved to the tentative collision site, where the type of the collision, either real or virtual, is sampled. It does not matter if the neutron crosses one or several material boundaries, as long as the physical total cross section at the end point of the track is available for the calculation.

The probability of sampling a virtual collision is simply the ratio of the virtual collision cross section to the majorant cross section:

$$P = \frac{\Sigma_0}{\Sigma_{\mathrm{m}}} = \frac{\Sigma_{\mathrm{m}} - \Sigma_{\mathrm{t}}}{\Sigma_{\mathrm{m}}} = 1 - \frac{\Sigma_{\mathrm{t}}}{\Sigma_{\mathrm{m}}}, \qquad (5.28)$$

where the spatial and energy-dependence are omitted for convenience. Since virtual collisions do not affect the state of the neutron in any way, the procedure is simply repeated until a real collision is sampled with probability $1 - P$. It should be noted that the numerical value of Σ_0 is not needed at all and it was defined only to simplify the procedure.

The following example illustrates the problem. Consider a neutron passing through three material layers. The boundary surfaces are located at x_1 and x_2 and all three materials are associated with different total cross sections. The PDF of the free path length is a piece-wise continuous function:

$$f(x) = \begin{cases} \Sigma_{\mathrm{t}1}e^{-\Sigma_{\mathrm{t}1}x} & \text{when } x \leq x_1 \\ \Sigma_{\mathrm{t}2}e^{-\Sigma_{\mathrm{t}1}x_1 - \Sigma_{\mathrm{t}2}(x-x_1)} & \text{when } x_1 < x \leq x_2 \\ \Sigma_{\mathrm{t}3}e^{-\Sigma_{\mathrm{t}1}x_1 - \Sigma_{\mathrm{t}2}(x_2-x_1) - \Sigma_{\mathrm{t}3}(x-x_2)} & \text{when } x > x_2 \end{cases} , \qquad (5.29)$$

where the additional terms in the second and third interval result from the conditional non-interaction probabilities. The CDF can be calculated from (5.29) by integration. The majorant cross section in this case is equal to Σ_{t2}, which is defined to have the largest value. Both distribution functions and a simulated PDF distribution calculated using the delta-tracking method are plotted in Figure 5.2.

The example implies that the delta-tracking method is essentially a rejection technique that is used for sampling values from a piece-wise continuous exponential distribution. The difficulty is not in the functional form of the partial distributions, but in that the discontinuity points are not known without calculating the surface distances.

The main advantage of the delta-tracking method is the simplified geometry treatment, which may also speed-up the calculation to some extent. The problem of calculating the shortest optical surface distance is reduced to the calculation of the sign of the surface function at each tentative collision point. Consider the circular cylinder case as an example. If the value of the surface function:

$$\mathcal{F}(x, y) = (x - x_0)^2 + (y - y_0)^2 - r^2 \tag{5.30}$$

is positive, the neutron lies outside the surface and if it is negative, the neutron is inside it. The neutron flight direction plays no role and the maximum number of free variables is reduced from six to three.

An interesting observation is that the material total cross sections are needed only to sample between real and virtual collisions, or more specifically, that they are not used for sampling the collision distances. The spatial dependence hence plays no role in the procedure, as long as the value of Σ_t is available at the tentative collision sites. This enables the modelling of inhomogeneous material regions, which may have various applications inside and outside the scope of reactor physics [47, 48][7].

The main disadvantage of the delta-tracking method is that surface crossings are not recorded at all. The resulting penalty is that the track-length estimate of neutron flux[8] is not available and reaction rates have to be calculated using the (potentially less efficient) collision estimator. Further, surface flux and current estimates can be easily calculated only at the outer geometry boundary.

Another problem arises when there are localised heavy absorbers, such as control rods or burnable absorber pins, in the geometry. In such a case, the majorant cross section is dominated by the high absorption cross sections of the absorber isotopes.

---

[7]Continuously varying material properties are traditionally encountered in astrophysics, atmospheric radiation transport and inertial confinement fusion studies. Applications in reactor physics could include the modelling of axial void distribution in a BWR flow channel or continuous temperature (or burnup) distributions inside fuel pellets.

[8]The flux and reaction rate estimates will be discussed in the following chapter.
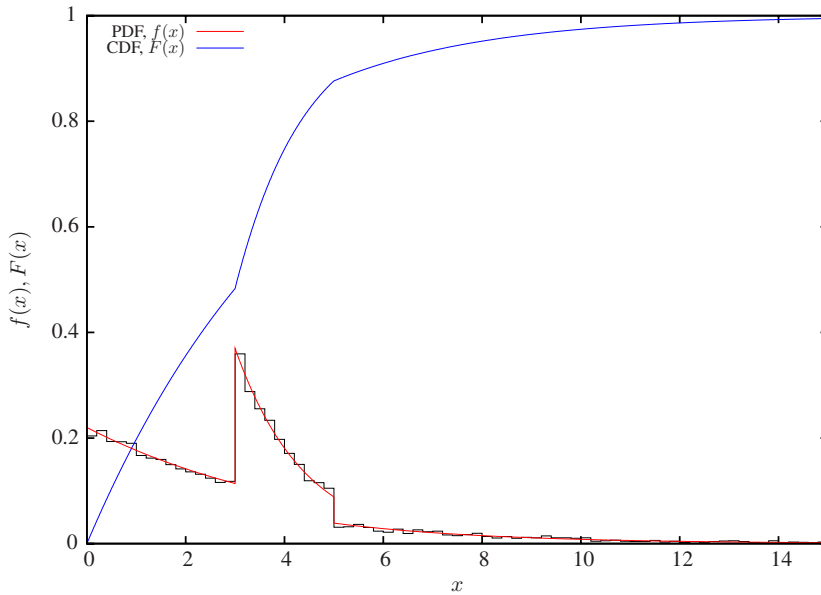
Figure 5.2: The free path length probability distributions of a neutron passing through three different materials. The histogram curve on the background shows the distribution of 10000 random values sampled using the delta-tracking method.

The probability of a neutron actually entering such a region can be relatively low, since the absorber pins typically cover only a small fraction of the total volume. The result is that the virtual collision frequency is significantly increased and computing time is wasted in the re-sampling of the collision site. A simple means to avoid this problem in lattice geometries is discussed Section 8.3.1 of Chapter 8, which introduces the method used in PSG.

5.4 Interactions

The exact manner in which neutron interactions are handled by the Monte Carlo codes may vary. This section gives a generalised description of how to sample the interaction type and how each reaction can be simulated. The topic will be revisited in Chapter 8, where the procedures used in the PSG code are introduced in more detail.

Once the collision site has been sampled using either of the two methods described above, the simulation proceeds by sampling the interaction. The probability of se-

lecting isotope m from all the constituent isotopes of a material with macroscopic total cross section Σ_{t} is:

$$P_m = \frac{\Sigma_{\text{t},m}}{\Sigma_{\text{t}}} . \tag{5.31}$$

The probability of selecting reaction i from all the available reaction channels of isotope m is:

$$P_i = \frac{\sigma_{i,m}}{\sigma_{\text{t},m}} = \frac{\Sigma_{i,m}}{\Sigma_{\text{t},m}} . \tag{5.32}$$

The conditional probability of selecting reaction i of isotope m is then:

$$P_{i,m} = P_i P_m = \frac{\Sigma_{i,m}}{\Sigma_{\text{t},m}} \frac{\Sigma_{\text{t},m}}{\Sigma_{\text{t}}} = \frac{\Sigma_{i,m}}{\Sigma_{\text{t}}} . \tag{5.33}$$

The sampling can be carried out by first selecting the target nucleus and then the reaction from the available reaction channels of the isotope. The alternative method is to sample the reaction directly from a pre-determined list of channels generated for each material. It is easy to see from (5.33) that these two methods are equivalent. The reaction types can be roughly divided into capture, fission and scattering. Each type is introduced in the following. The underlying physics was already discussed in Chapter 2. The description given here is more related to their treatment in the simulation process.

5.4.1 Capture

Since the emission of non-neutron secondary particles is insignificant in neutron transport problems, all (n,0n)-reactions, such as (n,γ), (n,α) and (n,p), can be treated in a similar manner. Such reactions are commonly denoted here as "capture", although neutron capture in some contexts refers specifically to the (n,γ)-reaction. The reason to use this nomenclature is to differentiate the (n,0n)-reactions from neutron absorption, which also includes fission.

Neutron capture in an *analog* Monte Carlo game simply leads to the termination of the neutron history. The alternative method is to treat the capture reactions *implicitly*. Each neutron is assigned with a statistical weight, which basically determines the importance of the particle, or the number of neutrons the simulated history actually represents. Instead of terminating the neutron history at the capture site, the weight is reduced according to the capture probability. The implicit capture treatment belongs to the large variety of *variance reduction techniques*, which will be discussed in Section 6.4 of Chapter 6.

5.4.2 Fission

Fission reaction leads to the termination of the original neutron history and the generation of new source neutrons. The number of emitted neutrons is determined by the fission nubar, $\bar{\nu}$, which depends on the target nucleus and the energy of the incident neutron. The usual practice used for sampling the number of emitted neutrons is to take the truncated integer value N of $\bar{\nu}$ and add one neutron with the probability determined by the remaining decimal fraction [12, 14][9]:

$$\text{number of emitted neutrons} = \begin{cases} N+1 & \text{if } \xi \leq \bar{\nu} - N \\ N & \text{if } \xi > \bar{\nu} - N \end{cases}. \qquad (5.34)$$

If delayed neutron parameters are available in the interaction data, the type of each emitted neutron is sampled. The probability of emitting a delayed neutron is simply:

$$P_{\text{d}} = \frac{\bar{\nu}_{\text{d}}}{\bar{\nu}_{\text{t}}} = \frac{\bar{\nu}_{\text{d}}}{\bar{\nu}_{\text{p}} + \bar{\nu}_{\text{d}}} \qquad (5.35)$$

and the probability of a prompt neutron $P_{\text{p}} = 1 - P_{\text{d}}$. The delayed neutron data must include the prompt (or total) and delayed nubars and the delayed neutron precursor abundances and decay constants, usually given in six or eight precursor groups. The group in which a delayed neutron belongs is sampled according to the corresponding relative abundances. The emission times depend on the decay of the precursor isotopes (see Section 4.3.2 of Chapter 4). The time of emission is exponentially distributed and it can be sampled similar to the neutron free path length (5.20):

$$t = -\frac{1}{\lambda_j} \ln \xi, \qquad (5.36)$$

where λ_j is the decay constant of the corresponding delayed neutron precursor group.

The energy of each fission neutron is sampled independently and prompt and delayed neutron energies are sampled from different distributions. The energy distributions in the ENDF format nuclear data are typically given as parametrised Maxwell, Watt or evaporation spectra, or as arbitrary tabulated functions of emission energy.

5.4.3 Scattering

Scattering reactions are by far the most complicated of the three interaction types in Monte Carlo calculation. Unlike in capture and fission reactions, the neutron history

---

[9]An alternative method is discussed in Ref. [49].

is not terminated, but new energy and direction are sampled for the incident neutron. Scattering collisions can be divided into elastic and inelastic reactions. Inelastic scattering can also be multiplicative, in that more than one neutron is emitted in the reaction.

Collision Kinematics of Elastic Scattering and Inelastic Level Scattering

Elastic scattering collisions are two-body interactions that preserve the total kinetic energy of the constituent particles. This implies that the emission energy and the scattering angle are directly coupled to each other. Inelastic level scattering can be treated in a similar manner. The difference is that some constant discrete amount of the initial kinetic energy (the reaction Q-value) is bound in the target nucleus during the process.

The treatment of scattering reactions requires the solution of the kinetic collision equations, based on the conservation laws of energy and momentum. The equations can be written directly for a two-body system, but the procedure is considerably simplified if a transformation is first made from the laboratory frame (L-frame) to the centre-of-mass frame (C-frame). The frames of reference have been mentioned a few times before, but at this point it is necessary to explain what is exactly meant by the terminology.

The L-frame is fixed to the reactor geometry and it is the co-ordinate system where the neutron tracking takes place. The target nuclei may either be assumed stationary or they may have some velocity component due to thermal motion. It is common that the target motion is taken into account using the so-called *free-gas model*. The terminology is a bit misleading, however, since the only thing that the free-gas treatment does for the collision kinematics, is that it takes into account the thermal motion of the target nucleus by sampling the velocity from a Maxwellian distribution.

The C-frame is used only for the collision kinematics. The origin is fixed to the common centre-of-mass of the two-body system. Both the neutron and the target are always moving with respect to the origin and to each other[10]. The initial L-frame target velocity presents itself only in the co-ordinate transformation and it does not make any difference in the C-frame equations. What makes the collision treatment so simple in the C-frame system, is that the total momentum is always zero. The kinetic energies of the particles remain constant in elastic reactions and inelastic Q-values are the same in both frames of reference. The two co-ordinate systems are illustrated in Figure 5.3.

---

[10]Assuming that the mass of the target nucleus is finite.
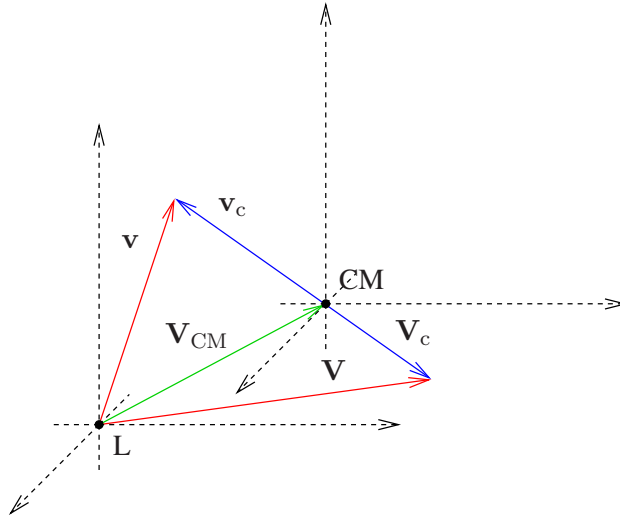
Figure 5.3: Neutron and target velocities in C- and L-frame. The origin of the C-frame is moving with velocity $\mathbf{V}_{\mathrm{CM}}$ relative to the origin of the L-frame.

The co-ordinate transformation from L- to C-frame is made by subtracting the relative velocity between the systems from the L-frame velocities. If the initial neutron and target velocities in the L-frame are $\mathbf{v}$ and $\mathbf{V}$, the velocity of the centre-of-mass system in the L-frame is given by:

$$\mathbf{V}_{\mathrm{CM}} = \frac{m\mathbf{v} + M\mathbf{V}}{m + M} = \frac{\mathbf{v} + A\mathbf{V}}{1 + A}, \tag{5.37}$$

where m and M are the neutron and the target mass, respectively, and A is the atomic weight ratio:

$$A = \frac{M}{m}. \tag{5.38}$$

The initial C-frame velocities of the neutron and the target are then given by:

$$
\begin{aligned}
\mathbf{v}_{\mathrm{c}} &= \mathbf{v} - \mathbf{V}_{\mathrm{CM}} = \frac{A(\mathbf{v} - \mathbf{V})}{1 + A} \\[2mm]
\mathbf{V}_{\mathrm{c}} &= \mathbf{V} - \mathbf{V}_{\mathrm{CM}} = -\frac{\mathbf{v} - \mathbf{V}}{1 + A}
\end{aligned}
. \tag{5.39}
$$

The collision kinematics is dictated by the conservation laws of energy and momen-

tum, which in the C-frame are written as:

$$\frac{1}{2}mv_c'^2 + \frac{1}{2}MV_c'^2 = \frac{1}{2}mv_c^2 + \frac{1}{2}MV_c^2 + Q \quad , \tag{5.40}$$

$$m\mathbf{v}_c' + M\mathbf{V}_c' = m\mathbf{v}_c + M\mathbf{V}_c = 0$$

where Q is the reaction Q-value in the case of inelastic scattering ($Q < 0$) and $\mathbf{v}_c'$ and $\mathbf{V}_c'$ are the velocities after the collision. The equations can be simplified to:

$$v_c'^2 + AV_c'^2 = v_c^2 + AV_c^2 + \frac{2Q}{m} \quad . \tag{5.41}$$

$$\mathbf{v}_c' + A\mathbf{V}_c' = \mathbf{v}_c + A\mathbf{V}_c = 0$$

Since the total momentum vanishes, the neutron and the target must be moving in opposite directions.

From the momentum equation in (5.41) it follows that:

$$\mathbf{v}_c' = -A\mathbf{V}_c' \implies v_c'^2 = A^2 V_c'^2 \tag{5.42}$$

$$\mathbf{v}_c = -A\mathbf{V}_c \implies v_c^2 = A^2 V_c^2$$

The substitution of the square speeds in the energy conservation equation in (5.41) yields for the neutron and the target:

$$v_c'^2 + \frac{1}{A}v_c'^2 = v_c^2 + \frac{1}{A}v_c^2 + \frac{2Q}{m} \quad , \tag{5.43}$$

$$A^2 V_c'^2 + AV_c'^2 = A^2 V_c^2 + AV_c^2 + \frac{2Q}{m}$$

from which the final speeds can be solved as:

$$v_c' = \sqrt{v_c^2 + \frac{2AQ}{(A+1)m}} \quad . \tag{5.44}$$

$$V_c' = \sqrt{V_c^2 + \frac{2Q}{A(A+1)m}}$$

It is immediately seen that the final speeds, and hence the energies, are independent of the change in the directions of motion. This would not be the case if the equations were written in L-frame. The procedure is even more simplified in the case of elastic scattering, where $Q = 0$. In such a case, there is no change in the neutron and target speeds and energies at all.
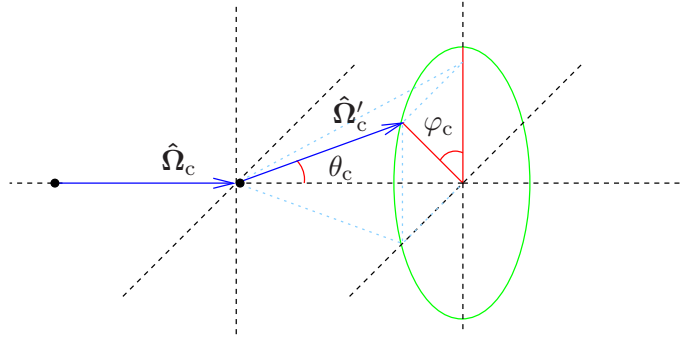
Figure 5.4: The incident ($\hat{\Omega}_c$) and collided ($\hat{\Omega}'_c$) neutron directions and the polar (θ_c) and the azimuthal (φ_c) scattering angles.

The change in the neutron direction ($\hat{\Omega}_c \rightarrow \hat{\Omega}'_c$) can be divided into two components and described using two independent scattering angles: the polar angle θ_c between the incident and collided direction and the azimuthal angle φ_c determining the rotation of the collided direction vector over the incident direction of motion. Figure 5.4 illustrates the definitions.

Since the target nuclei are treated as symmetric point-like particles, the azimuthal angle is always isotropic in the centre-of-mass system. The polar angle can be either isotropic or anisotropic, depending on the reaction. Low-energy collisions with light nuclei are typically s-wave potential scattering reactions, which are isotropic in the C-frame. The anisotropy increases with neutron energy and target mass number.

In principle, the collision treatment is very simple. After the initial velocities have been transformed into the C-frame using (5.37) and (5.39) and the scattered neutron and target speeds calculated from (5.44), the polar scattering angle is sampled from the appropriate distribution. The neutron direction vector is rotated over the sampled θ_c and a uniformly distributed φ_c to make the transformation $\hat{\Omega}_c \rightarrow \hat{\Omega}'_c$. The new velocities are then given by:

$$
\begin{aligned}
\mathbf{v}'_c &= \hat{\Omega}'_c v'_c \\
\mathbf{V}'_c &= -\hat{\Omega}'_c V'_c
\end{aligned}
\tag{5.45}
$$

The direction of the target velocity must be opposite to the neutron velocity in order to preserve the zero total momentum condition. These velocities are then converted back to the L-frame using (5.39), which completes the procedure.

The method has three non-trivial steps: 1) the sampling of the initial L-frame target velocity (free-gas treatment); 2) the sampling of the scattering angles in the C-frame,

109

and 3) the azimuthal rotation of the direction vectors.

As was mentioned in Section 5.2.3, the Maxwell-Boltzmann distribution of the target velocity cannot be sampled using the inversion method. There are various rejection techniques [12, 45] that can be used for sampling the target energy, from which the speed can be easily calculated. The direction of motion is sampled from an isotropic distribution[11]. The alternative technique is to sample each velocity component independently. It can be shown that, in the Cartesian co-ordinate system, the x-, y- and z-components of the Maxwellian velocity distribution are in fact normally distributed. Unfortunately, the normal distribution cannot be sampled directly either, but both efficient rejection techniques [12] and other methods [50] exist for the task.

The sampling of the scattering angles depends on the anisotropy of the reaction. If the polar angle is isotropic in the C-frame, there is absolutely no correlation between the incident and the scattered directions and vector $\hat{\mathbf{\Omega}}'_{\mathrm{c}}$ can be sampled isotropically. In the opposite case, the cosine of the polar angle, $\mu_{\mathrm{c}} = \cos\theta_{\mathrm{c}}$, is sampled from the distribution given in the nuclear data library[12]. The initial direction vector $\hat{\mathbf{\Omega}}_{\mathrm{c}}$ is then tilted and rotated over the uniformly distributed azimuthal angle. There are several procedures for accomplishing this task, based on both rejection techniques and the direct conversion of the angles [12, 14, 51, 52]. A simple method given in Ref. [12] is written as:

$$
\begin{aligned}
\Omega'_z &= \Omega_z \cos\theta + \alpha\cos\varphi \\[2mm]
\Omega'_y &= \frac{1}{1 - \Omega_z^2}\left(\Omega_y\beta + \Omega_x\alpha\sin\varphi\right) \quad, \\[2mm]
\Omega'_x &= \frac{1}{1 - \Omega_z^2}\left(\Omega_x\beta - \Omega_y\alpha\sin\varphi\right)
\end{aligned} \tag{5.46}
$$

where $(\Omega_x, \Omega_y, \Omega_z)$ and $(\Omega'_x, \Omega'_y, \Omega'_z)$ are the Cartesian components of the direction vectors before and after the rotation,

$$
\begin{aligned}
\alpha &= \sqrt{1 - \Omega_z^2} \\[2mm]
\beta &= \cos\theta - \Omega_z\Omega'_z
\end{aligned} \tag{5.47}
$$

and the azimuthal angle φ is sampled uniformly between 0 and 2π.

Some physical restrictions arise in the case of inelastic level scattering, when the reaction Q-value is negative. In particular, the functions under the square roots in (5.44)

---

[11]Methods for sampling uniformly distributed two- and three-dimensional direction vectors are given in Ref. [12]

[12]It is common practice to write the angular distributions in terms of the scattering cosine instead of the polar angle itself.

must be positive[13]. The conditions can be written in the form of:

$$Q \;>\; -\left(\frac{A+1}{A}\right)\frac{1}{2}mv_c^2$$

$$Q \;>\; -(A+1)\frac{1}{2}MV_c^2 \tag{5.48}$$

If the square speeds are converted to the L-frame using (5.39), it is easy to see that both conditions reduce to a single restriction:

$$Q > -\left(\frac{A}{A+1}\right)\frac{1}{2}m(\mathbf{v} - \mathbf{V})^2 \,. \tag{5.49}$$

Since inelastic scattering occurs well above the range of thermal energies, $\mathbf{v} \gg \mathbf{V}$, and the condition can be written using the L-frame neutron energy as:

$$Q > -\left(\frac{A}{A+1}\right)E \,. \tag{5.50}$$

Other Inelastic Reactions

The above description of Maxwellian target motion (the "free-gas model") is able to produce the thermal peak in the neutron spectrum. Unfortunately, the model is unable to sufficiently reproduce the most important scattering reaction in light water reactors, namely the scattering of neutrons from hydrogen atoms bound in water. The reason is that the recoil energy of the target nucleus is comparable to the molecular binding energy of the atom, which cannot be treated as a free particle. Elastic scattering reactions with bound nuclei are hence treated effectively as special types of inelastic scattering. The manner by which the bound elastic scattering is handled depends on the application and the discussion is deferred until Section 8.4 of Chapter 8.

Continuum inelastic reactions differ from inelastic level scattering in that the reaction Q-value is given by a distribution, rather than a discrete number. The common practice is to sample both the energy and the scattering angle directly in the L-frame from the distributions given in the interaction data. Energy and momentum are not necessarily conserved in individual reactions, but the probability distributions are constructed in such a way that the conservation laws hold on average for a large number of collisions.

When more than two particles are emitted in a scattering collision, the coupling between energy and scattering angle no longer holds. The reason is that there are simply more free variables than there are restrictions set by the physical conservation

---

[13]Zero values are not acceptable since it would yield zero final velocities, which would violate the conservation laws.

laws. The emission energies and scattering angles of secondary neutrons must then be sampled from separate probability distributions, as in the case of continuum inelastic scattering. Examples of such reactions include multiplying scattering collisions and collisions in which other particles are emitted with the secondary neutron, such as (n,np), (n,nα) and (n,n^{3}He). The emission of all non-neutron secondary particles is irrelevant in neutron transport problems and only the emitted neutrons need to be considered.

5.5 Simulating the Neutron Chain Reaction

It was stated in Section 3.2.3 of Chapter 3 that the solution of the steady-state transport equation depends on the criticality state of the system and the presence of external sources. The Monte Carlo game behaves in a similar manner when a population of neutrons is simulated. The calculation methods can be correspondingly divided into external and criticality source simulations.

5.5.1 External Source Method

All neutron histories in the external source method are started from a user-defined source distribution. Fission reactions are not treated as terminating events, but rather as points where the histories are split into two or more new paths. The neutrons are tracked until they are either captured or escape the system.

This type of simulation corresponds to solving the transport equation with external sources. The requirement for the calculation to converge is that the system is subcritical, which corresponds to the existence of a finite solution to the transport equation. If the multiplication factor is above unity, a single source neutron may in theory generate an infinite number of neutron histories.

The external source simulation is physically consistent, in that no artificial modifications are needed to complete the calculation. The results are unbiased in energy, space and time. The average total number of histories generated from N_0 source neutrons is given by:

$$N = N_0 \left(1 + k + k^2 + \dots\right) = \frac{N_0}{1 - k} , \qquad (5.51)$$

where k is the multiplication factor of the sub-critical system. It can be seen that when k approaches unity, N approaches infinity and the system becomes self-sustaining.

Simulations of this type are necessary in radiation shielding problems, dose-rate calculations and various engineering tasks involving neutron sources used for diagnostic purposes. The medium does not have to be multiplying, in which case the calculation closely resembles the Monte Carlo simulation of photon transport. The simulation may also include time-dependence, which is useful for calculating detector responses to pulsed neutron sources.

External source calculations can be used for simulating the reactor physics of sub-critical accelerator-driven systems (ADS), but the method is not practical in reactor physics calculations of conventional critical reactors. The simulation of a self-sustaining chain reaction corresponds to solving the transport equation without external sources.

5.5.2   Criticality Source Method

The alternative to the external source method is the criticality source method, in which case the simulation proceeds in *cycles*, or *generations*. The source distribution in each cycle is given by the fission reaction distribution calculated in the previous cycle. This procedure differs from the external source simulation in that the neutron histories are also terminated by fission. All histories in one cycle are completed before beginning the next, and the results in each cycle are treated independently.

In order to start-up the simulation, an initial guess for the source distribution is either provided by the user or generated automatically by the code itself. The initial guess may be far from the saturated distribution, and a number of cycles must be discarded at the beginning of the simulation before starting to record the result estimates. This is to ensure that the results are not influenced by a poor initial guess[14]. The saturated source distribution directly corresponds to the fundamental flux mode, discussed in Section 4.1.4 of Chapter 4.

The number of new source neutrons generated by the end of each cycle is generally not equal to the number of histories started at the beginning of the cycle. The ratio

---

[14]Fission source convergence is an important research topic and subject to both theoretical and practical considerations [53–55]. One of the main problems is that the multiplication factor tends to converge before the fission source, and there are no simple indicators that would ensure that the source distribution has reached its equilibrium state. The OECD/NEA has established an expert group for addressing this issue [56, 57]. The latest version of the MCNP5 code has the capability to assess source convergence in criticality problems using so-called *Shannon entropy* [58]. Similar features are planned for the future versions of PSG as well, but at this time the topic is considered far too extensive to be included in this text.

defines the multiplication factor in cycle n:

$$k_n = \frac{\text{number of source neutrons in cycle } n+1}{\text{number of simulated histories in cycle } n} \ . \qquad (5.52)$$

Since the value usually differs from unity either systematically or due to random variation, the source size is constantly changing, which results in problems with the simulation. The solution is to artificially add or remove neutrons from the population to maintain a constant source size. Two criticality source methods are introduced in the following.

The k-eigenvalue Method

The k-eigenvalue method is used for simulating a stationary self-sustaining chain reaction and it is equivalent to solving the eigenvalue form of the neutron transport equation. The population size is maintained by adjusting the number of source neutrons at the beginning of each cycle, which is equivalent to dividing the fission source term in transport equation (3.32) by the k_{eff}-eigenvalue.

If $k_n > 1$, the number of source neutrons in generation $n + 1$ exceeding the user-given population size have to be discarded before starting the transport cycle. In the opposite case, $k_n < 1$, and a number of source neutrons have to be duplicated to attain the desired population size. The neutrons involved in the procedure are selected randomly, in an effort to preserve the distribution of the population.

The modification of the source population gives rise to the same problem that was discussed in Section 3.2.3 of Chapter 3, namely the over- or under-estimation of the fission source importance when the system is far from criticality. As in the deterministic case, this results in a distortion of the neutron spectrum, which has an impact on all the results of the calculation. It must again be pointed out that this is not a flaw in the calculation method or even in transport theory, but rather the result of forcing a non-equilibrium system into a steady-state condition. The solution is basically equivalent to finding an answer to an impossible problem by adjusting the problem itself.

It is important to understand both the reasons and the consequences of these physical inconsistencies. The source of the problem is not in that neutrons are added to, or removed from, the population. Such modification is completely acceptable due to the linearity of the transport process, provided that the population size is sufficiently large and the neutrons are selected randomly. The problem is that the neutrons are not, in fact, selected in a completely random manner and the population is biased in energy, space and time.

The biasing is best understood by considering the population control in a super-critical system as a procedure that selects only a part of the total population to continue the simulation. Imagine then a sample of neutrons taken from a reactor core that has been frozen in time. It is obvious that the sample contains neutrons at all energies, not only those recently born in fission (bias in energy). The neutrons are distributed more or less homogeneously throughout the geometry, not only in fissile materials (bias in space). The bias in time is best understood by noting that the simulation actually proceeds in generations, not in time. The lifetime of two neutrons in the same generation may differ by several orders of magnitude, especially in thermal systems where the diffusion times are long, but many neutrons are lost in capture resonances before thermalisation.

The k-eigenvalue method is the most widely used method in Monte Carlo reactor physics calculations and most of the time it produces reliable results. Problems may arise in systems far from criticality, especially in highly heterogeneous geometries with large moderator regions. In such cases, the kinetic parameters may be off by several orders of magnitude and the flux spectrum seriously distorted [33].

An extreme example case is a reactor core surrounded by a thick water reflector. It is assumed that the system is highly reactive and remains in a prompt super-critical state even without the extra reactivity provided by the reflector. Since the k-eigenvalue method operates in terms on neutron generations, instead of time, interactions in all regions are equally important for core neutronics. The result is that the reflector contribution is grossly over-estimated. In reality, the neutrons thermalised in the reflector play no role in reactor operation. The time constants may well be so short that the system is blown apart before the first neutron has reached the thermal energy region in the reflector.

The α-eigenvalue Method

The α-eigenvalue method in transport theory was introduced in Section 3.2.3 of Chapter 3. The method takes advantage of the fact that the neutron flux, after being relaxed into its fundamental mode, can be written as the product of a static shape function and a time-dependent amplitude function:

$$\psi(\mathbf{r}, \hat{\mathbf{\Omega}}, E, t) = \psi(\mathbf{r}, \hat{\mathbf{\Omega}}, E)e^{\alpha t} \,. \tag{5.53}$$

The substitution of this into the time-dependent transport equation yields for the time derivative term:

$$\frac{1}{v}\frac{\partial \psi}{\partial t} = \frac{\alpha}{v}\psi(\mathbf{r}, \hat{\mathbf{\Omega}}, E)e^{\alpha t} \,. \tag{5.54}$$

The amplitude function is cancelled in all terms and the result is a steady-state equation for $\psi(\mathbf{r}, \hat{\mathbf{\Omega}}, E)$. Depending on the sign of the α-eigenvalue, the additional term

is placed on the left- or right-hand side of the equation and interpreted respectively as time-absorption or time-production of neutrons.

The same idea is applied in the Monte Carlo calculation. The difference to the k-eigenvalue method is that the neutron population is balanced by adding or removing neutrons throughout the cycle, not at the event of fission. The "cross section" for the time-production or time-absorption reaction is just α/v and the value of α is iterated to yield $k_n = 1$ in (5.52).

The method is unbiased and it can be shown to be equivalent to performing a fully time-dependent calculation [33]. The procedure is a bit more complicated to implement in the Monte Carlo code, compared to the basic k-eigenvalue method, and convergence problems may arise in some cases, especially if $k_n \ll 1$.

It must be noted that even though the α-eigenvalue method is physically consistent, it does not necessarily yield better results. The reason is the same as in the deterministic case. Reactor calculations are often performed at pin or assembly level, in which case the geometry is approximated by an infinite lattice of identical cells. It is actually the formulation of the problem, not the solution method that differs from the physical reality. Better results in lattice calculations would be obtained by using leakage models (see Section 4.2.3 of Chapter 4) for adjusting the population size. Such models are not available for the widely used general-purpose Monte Carlo codes, but a simple leakage model based on the B_1 fundamental mode approximation has been developed for PSG. The methodology is introduced in Section 9.5 of Chapter 9.

Chapter 6

Result Estimates in Monte Carlo

6.1 Scoring

So far, the discussion of the Monte Carlo method has been limited to the simulation of neutron histories consisting of tracks between sampled collision points. The other half of the Monte Carlo game is the collection of results from the simulated events. The simulation proceeds in a stochastic manner and all results are, in fact, random variables. The methodology introduced here applies mainly to the procedures used in the PSG code. The realisation differs from the conventional approach [12, 14] to some extent.

The estimation of results can be treated separately from the transport simulation. As was mentioned earlier, the Monte Carlo method does not yield a flux solution to the neutron transport equation. Instead, everything is based on discrete events. This differentiates the method from deterministic calculation, which deals with equations of continuous variables. In fact, the collection of the results has a certain analogy to making experimental physical measurements.

One of the most essential capabilities of the Monte Carlo method is the evaluation of flux integrals of type:

$$R = \int_t \int_V \int_E f(\mathbf{r}, E)\phi(\mathbf{r}, E)dt d^3 r dE \,, \tag{6.1}$$

where the integration is carried over time, some spatial volume and the desired energy interval. The response function $f(\mathbf{r}, E)$ may represent any physical parameter and the only restriction is that its value must be known for all points within the integration domain. The response function is usually either unity or a reaction cross section, in which case the result is the corresponding reaction rate.

It is important to notice that the integration is always carried over time. To be precise, the result of Eq. (6.1) is the *number of responses*, not the response rate, or where $f = 1$, the *fluence*, not the flux. It is common practice, however, to talk about response or reaction rates and flux integrals, since time-integrated and time-averaged quantities are basically equivalent because the results are normalised afterwards. Here is a clear analogy to experimental measurements: reaction rates are often determined by counting the number of observed interactions within a specified time window [59].

The time integration in criticality source calculations is basically extended to infinity. The absolute initial time is not fixed and the simulation proceeds in generations, which means that the lifetimes of the neutrons are not restricted. The whole procedure is somewhat different for time-dependent external source simulations, which are not discussed here.

The simulated events that are recorded for calculating the results are called *scores*[1]. Such events include absorptions, scattering collisions, surface crossings, track lengths and other events that occur during the neutron lifetime. The scores can be combined in various ways to form statistical *estimates*[2] of the physical quantities.

6.1.1 Analog and Implicit Estimators

The simplest way to estimate the results is to score the physical interactions (fission, capture, scattering, etc.) or event sequences that are simulated during the calculation. This type of estimate is called *analog*, since it is directly related to the simulation process. In order to understand what exactly is meant by the analog estimate, consider the following three examples.

The integral reaction rate of a specific interaction is calculated by using the corresponding macroscopic reaction cross section as the response function in (6.1). An analog Monte Carlo estimate can be made by simply counting the number of sampled interactions of the specified type. Another example is the prompt neutron lifetime (see Section 4.3.1 of Chapter 4), which is the average time between prompt neutron emission and eventual loss by absorption or escape. An analog estimate is easily made by scoring the lifetimes of simulated neutrons and taking the average over all histories. The third example is the *generation estimate* of the multiplication factor, which is given by the ratio of population sizes in two consequent neutron cycles (see Eq. (5.52) in Section 5.5.2 of Chapter 5).

---

[1]The terminology may slightly differ from author to author.

[2]Terms "estimate" and "estimator" are used interchangeably in this text.

The analog estimate is practical in cases where the parameter of interest is derived from a complicated process that occurs as a part of the simulation. In most cases, however, there are other, more efficient *implicit* (non-analog) estimators available. This is particularly the case for the calculation of integral reaction rates. The implicit Monte Carlo equivalent of calculating an integral of type (6.1) is to take the appropriate *flux estimator* and multiply it by the value of the response function. The integration is carried out by summing over the scored values [12]:

$$R = \sum_{i=1}^{I} s^i = \sum_{i=1}^{I} f^i \phi^i \,. \tag{6.2}$$

The values may naturally depend on neutron energy and spatial co-ordinates.

If the integration is not extended to cover the entire spatial and energy space, only scores made within the desired sub-space are included in the sum. The integral reaction rate inside a single geometry cell, for example, is estimated by recording scores in that particular cell only. Reaction rates integrated over an energy interval are calculated by including scores made by neutrons with energy within the limiting values.

The integral reaction rates calculated this way do not correspond to any physical results. This is because the values depend on the source size. The more neutron histories are run, the more scores are included in the sum and hence the larger the value of the integral. The results are coupled to physical parameters by appropriate *normalisation*. This topic is discussed in Section 9.4 of Chapter 9.

Some of the most important implicit flux estimators are introduced in the following. All estimators integrate the flux either over a volume or a surface area. Point-wise estimators of the flux integrals exist [12], but are considered insignificant for lattice calculations and hence not discussed here.

6.1.2   Collision Estimate of Neutron Flux

The *collision estimator* [12] is probably the simplest and the most intuitive way to calculate flux integrals. The estimate is based on the fact that the *total* interaction rate can be evaluated by counting the number of collisions[3]. Similarly, the *expected* rate of an arbitrary reaction can be estimated by summing over the fractional reaction probabilities, given by Eq. (5.33). When generalised to an arbitrary response function, the scored value can be written as:

$$\phi^i = \frac{1}{\Sigma_{\mathrm{t}}^i} \implies s^i = \frac{f^i}{\Sigma_{\mathrm{t}}^i} \,, \tag{6.3}$$

---

[3]This is actually an analog estimate of the total reaction rate.

where Σ_t^i is the macroscopic total cross section of the material filling the cell at the collision site.

If the total cross section is used as the response function, $s^i = 1$, and the sum over the scored values yields the total number of interactions. If the response function is set to unity, the summation is carried over the reciprocals of the total cross section, which according to (5.21) is equivalent to the neutron mean free path. The result is the total average path length covered by the neutrons. It can be seen from (3.15) that this is equivalent to the integrated flux.

The reason why the collision estimator is more efficient than the analog reaction rate estimate (i.e. counting the number of sampled interactions) is that the score is recorded even if the particular interaction does not occur.

6.1.3   Track Length Estimate of Neutron Flux

The most efficient method for calculating flux integrals in homogeneous material regions is called the *track length estimator* [12]. Each time a neutron makes a track inside the region, the track length is recorded. The starting and end points of the track can be either reaction sites or intersections with the boundary surfaces. The recorded score is:

$$\phi^i = l^i \implies s^i = f^i l^i \,, \tag{6.4}$$

where l^i is the length of the track. It may not be obvious that the flux estimates are related to the track lengths. The relation can be seen by remembering that the integrated flux is essentially the total track length made by neutrons passing through the region.

The advantage of the track length estimator over the collision estimator is its better efficiency in small geometry regions. Instead of having to collide within the region, it is sufficient that neutrons pass through it. The difference is emphasised in optically thin volumes and in materials with low interaction probability. The extreme case is a void region, in which the neutrons do not collide at all.

The track length flux estimator cannot be used with delta-tracking, simply because the surface crossings are not recorded. Tracks are made between interactions and cells and materials may change between the collision points. The value of the response function may not remain constant, and even if it does, the number of tracks equals the number of interactions. The method would hence not yield better statistics compared to the collision estimator. It should also be noted that it is very difficult to use the track length estimator with inhomogeneous material regions. This restriction does not apply to the collision estimator

6.1.4 Surface Flux and Current Estimators

An analog estimate of neutron current integrated over a surface region is given by the number of neutrons crossing the surface (see the definition of neutron current in Section 3.1.3 of Chapter 3). The quantity has angular dependence and the integration can be carried over a limited range of angles by restricting the angle between the incident neutron direction and the surface normal.

The angular current density is related to angular flux by (3.17). The *surface flux estimator* can hence be derived from the analog current estimator. The scored value is [14]:

$$\phi^i = \frac{1}{|\mu^i|} \implies s^i = \frac{f^i}{|\mu^i|} \, ,$$
(6.5)

where μ^i is the cosine of the angle between the incident neutron direction and the surface normal. The scores are made each time the neutron crosses the surface. Estimate (6.5) can also be derived as the limiting case of the track length estimator in an infinitely thin volume region.

The surface flux and current estimators cannot be scored when the delta-tracking method is used. The topic is hence not discussed any further.

6.2 Collecting the Results

Integral reaction rates are collected by summing over the scored values, as in (6.2). Other types of estimates are calculated in a similar manner. For reasons that will become apparent later, it is sometimes useful not to carry the summation over all scores, but rather a *batch* of I_n values. This means that the scores are divided into N batches and the total number of scores is given by:

$$I = \sum_{n=1}^{N} I_n \, .$$
(6.6)

In criticality source calculations, it is natural to include all scores made within one generation into a single batch. The number of batches N is then equal to the number of active neutron generations. The estimate of integral reaction rate R in generation n is given by:

$$R_n = \sum_{i=1}^{I_n} f^i \phi^i \, .$$
(6.7)

It should be noted that the batch size I_n depends on random events and it does not generally remain constant throughout the simulation.

In many cases, the parameter of interest is not the absolute value of an integral reaction rate, but a new parameter formed by combining two or more existing estimates. An example of such a case is the generation-wise estimate of a homogenised cross section Σ:

$$\Sigma_n = \frac{\displaystyle\sum_{i=1}^{I_n} \Sigma^i \phi^i}{\displaystyle\sum_{i=1}^{I_n} \phi^i} \,. \tag{6.8}$$

From here on, all batch- or generation-wise estimates are denoted by variable X_n, regardless of the way in which they are formed.

The generation-wise estimates are not so interesting *per se*. The parameters are random variables and their values differ from one generation to the next. They become interesting when statistical methods are applied to the sequence of batch values. Each parameter is associated with the statistical sample mean (or simply "mean"), accompanied by the corresponding standard deviation [50]. The mean value is referred to as the result of the simulation and the standard deviation is a measure of *statistical accuracy*, or *precision*. The mean value of estimate X is given by the arithmetic mean taken over the batch values:

$$\overline{X} = \frac{1}{N} \sum_{n=1}^{N} X_n \,. \tag{6.9}$$

The standard deviation is given by:

$$\sigma(X) = \sqrt{\frac{1}{N(N-1)} \sum_{n=1}^{N} (X_n - \overline{X})^2} \,. \tag{6.10}$$

This formulation is not very practical, however, since all batch values need to be stored in order to get the final estimate. A more convenient form can be written as:

$$\sigma(X) = \sqrt{\frac{1}{N(N-1)} \left[\sum_{n=1}^{N} X_n^2 - \frac{1}{N} \left(\sum_{n=1}^{N} X_n \right)^2 \right]} \,. \tag{6.11}$$

Using this definition, it is sufficient to accumulate only the sums of the batch values and their squares. Frequently used quantities related to the standard deviation are the variance $\sigma(X)^2$ and the relative statistical error, which in this text is denoted by:

$$E(X) = \frac{\sigma(X)}{\overline{X}} \,. \tag{6.12}$$

Before proceeding any further, it is necessary to explain what is meant by the statistical accuracy of the simulation. Basically the standard deviation is a measure of how much the mean value is likely to deviate from the true result, which is the value that would be attained if the simulation could be carried on forever. A more useful qualitative interpretation is that the standard deviation is a measure of how much the results of two identical but independent simulations are likely to differ from each other. Either way, the statistical accuracy has very little to do with the *physical* accuracy of the simulation, if the simulation itself is subject to approximations.

6.3 Estimation of Precision

The standard deviation (6.10) does not provide very much quantitative information about the statistical accuracy of estimate X, if the probability distribution is not known. Luckily, there is a very fundamental law in statistics, which determines the type of the distribution. The *central limit theorem* [50] states that the sum of a large number of arbitrarily distributed random variables is itself a random variable following the *normal distribution*[4]. The assumptions are that the distribution is the same for each term in the sum, that the values are independent and that both the mean and the standard deviation of the unknown distribution exist and are finite. The probability density function of the normal distribution is written as:

$$f(x) = \frac{1}{\sigma\sqrt{2\pi}} e^{-\frac{(x-\bar{x})^2}{2\sigma^2}} .$$
(6.13)

The CDF cannot be solved in closed form, but it can be written using the error function as:

$$F(x) = \frac{1}{2}\left[1 + \mathrm{erf}\left(\frac{x - \bar{x}}{\sigma\sqrt{2}}\right)\right] .$$
(6.14)

Another useful law in statistics is the *law of large numbers* [50], which implies stochastic convergence, i.e. that the standard deviation (6.10) of an estimate approaches zero as the number of terms N approaches infinity. So in theory, the result estimate X should be normally distributed, provided that the above assumptions hold. Further, the statistical accuracy of the result should always improve if the number of simulated histories is increased.

---

[4]The normal distribution is also known as the Gaussian distribution.
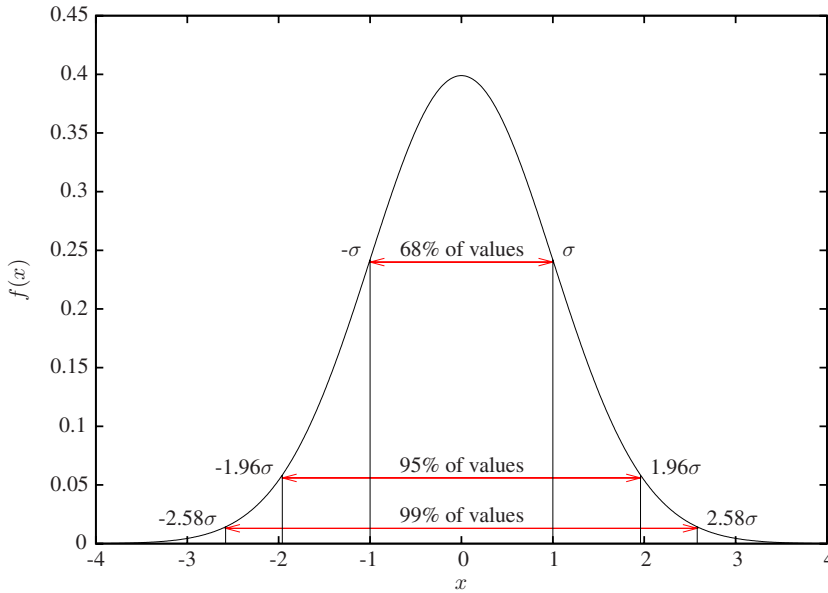
Figure 6.1: The ($\overline{x} = 0, \sigma = 1$) normal distribution and the 68%, 95% and 99% confidence intervals.

6.3.1 Confidence Intervals

The fact that the results of the simulation follow a well-known probability distribution allows the standard deviation to be related to a more easily interpreted measure of statistical accuracy, namely the *confidence interval*. The confidence interval determines the probability at which the result lies within a certain distance from the true mean value of the distribution. The confidence interval of a normally distributed random variable can be written as [50]:

$$P(\overline{x} - z_{\alpha/2}\sigma < x < \overline{x} + z_{\alpha/2}\sigma) = \int_{\overline{x}-z_{\alpha/2}\sigma}^{\overline{x}+z_{\alpha/2}\sigma} f(x)dx = 2F(\overline{x} + z_{\alpha/2}\sigma), \quad (6.15)$$

where the last identity results from the symmetry of the normal distribution. The value of the cumulative distribution function must be calculated numerically.

The most commonly used confidence intervals are the ($z_{\alpha/2} = 1$, $P = 0.68$) "one-sigma" interval and the ($z_{\alpha/2} = 1.96$, $P = 0.95$) 95% interval[5]. The one-sigma value is also called the *standard error* or the *statistical error* and the results are often given in the form of $\overline{X} \pm \sigma(X)$. Figure 6.1 illustrates the definitions.

---

[5]The term "95% confidence interval" is sometimes used for the two-sigma interval, for which the probability is actually 0.955.

The 95% confidence interval is often used for assessing the statistical significance of differences observed between two sets of results. This type of comparison is typical in code validation. The calculated results are compared to experimental values, or to the results given by another computer code. If the mean values lie within 1.96σ from each other, it can be assumed that the variation is simply due to statistical noise. If the discrepancies are larger or clearly systematic, it can be an indication of an error in the calculation routines. Two examples are given in Figures 6.2 and 6.3. The plotted curves are PDF distributions corresponding to homogenised fission cross sections in one of the MCNP-PSG comparison calculations in Section 10.2.1 of Chapter 10 (VVER-440 calculation case). The differences are clearly significant in the first plot, while the overlapping distributions in the second comparison suggest that the differences may well result from random statistical variation.

It must be pointed out that this type of comparison should never be made without understanding how to interpret the outcome. There is a good chance that two generally well consistent results suddenly differ by more that 1.96σ in one simulation. It is also possible that two results which usually differ significantly from each other suddenly yield consistent results. The stochastic nature of the process should always be kept in mind.

6.3.2 Validity of the Central Limit Theorem

It is important to realise that the above confidence intervals are applicable only if the central limit theorem holds and the results are normally distributed. The possibility of incorrectly interpreting statistically invalid results can be demonstrated by a crude example. Consider a random variable, uniformly distributed between -1 and 1. The mean value and the associated standard deviation are 0 and $1/\sqrt{3}$, respectively. If it is assumed that the confidence intervals of the normal distribution are applicable in this case, 95% of the values should fall between -1.1316 and 1.1316, which is obviously not the case with this distribution since the values are restricted between -1 and 1.

There are two practical concerns related to the summation over the scored values and the validity of the central limit theorem:

   I. Are the values truly independent?

  II. Is the number of terms sufficiently large?

The first condition is relatively easy to fulfil. The independence of the values depends on how they are formed. The estimate of a simple reaction rate integral (6.7) is calculated by summing over the scored values. The flux estimates, ϕ^i, are calculated from independent tracks or collisions.
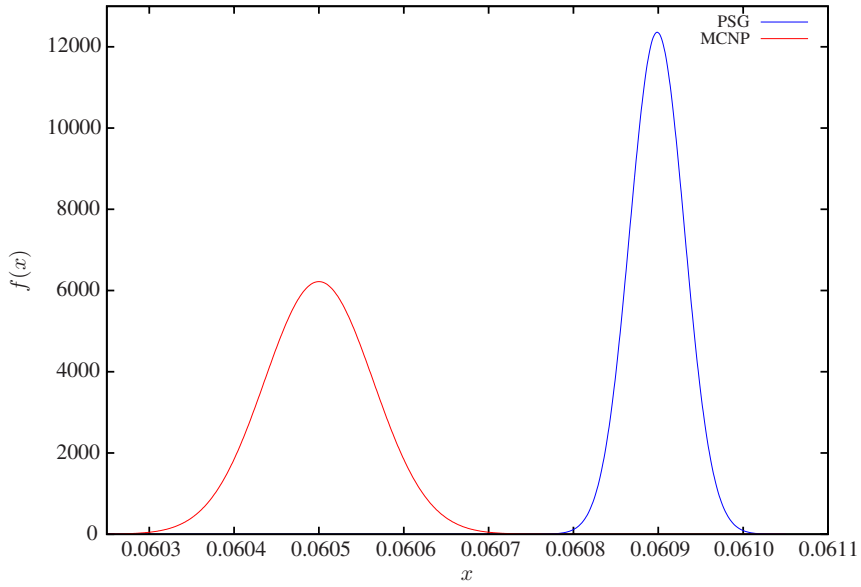
Figure 6.2: Statistically significant differences between thermal-group fission cross sections calculated by MCNP and PSG (VVER-440 calculation case).
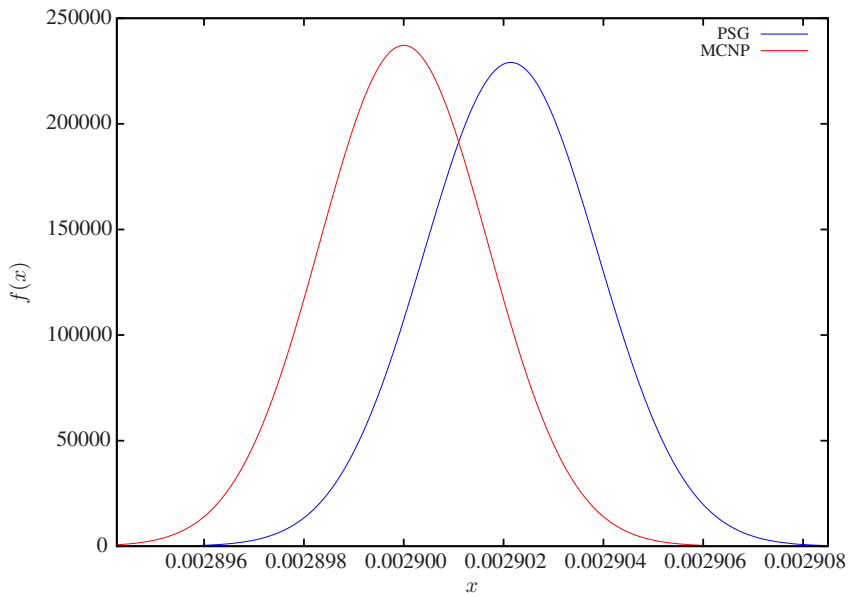
Figure 6.3: Statistically insignificant differences between fast-group fission cross sections calculated by MCNP and PSG (VVER-440 calculation case).

Problems may arise, however, if the generation-wise estimate is formed by combining two or several existing estimates, as in (6.8). Values scored at the same event may be included in several terms of the sum, which basically violates the independence criterion. In most cases, the distribution is probably sufficiently close to the normal distribution for the confidence intervals to apply, but there may be some additional uncertainty in the results.

The second question is more difficult to answer. There is no theoretical limit that would determine the minimum required number of terms. In practice, however, it can be shown that this number is usually not very large [50]. The number of scores can be increased simply by running a larger number of neutron histories. In some cases, the parameters need to be evaluated in a small region of the geometry, where the scoring events are scarce. In such cases, the mere increasing of the number of neutron histories may not be an effective means to improve the statistics. There are various *implicit* methods to overcome this problem. Such methods are briefly discussed in the following section.

The use of the confidence intervals is an important part of interpreting the results. It is hence vital that the above assumptions truly hold. Statistical methods for testing the normality of the output parameters are often included in the routines of Monte Carlo codes. There are various statistical tests, such as the χ^2-test and the *Kolmogorov-Smirnov test* [60], which can be used for the purpose. The present version of the PSG code does not offer the capability to perform this type of statistical analysis, but similar methods applied on the final results are discussed in Section 10.5 of Chapter 10.

6.4   Non-analog Monte Carlo

It was discussed earlier that better statistics on integral reaction rate estimates can be attained by using flux estimators based on non-analog methods, rather than the simple counting of the sampled interactions. Similar implicit methods can be used for the actual simulation, which has so far been described as a process completely analogous with physical reality.

Non-analog (implicit) Monte Carlo methods and *variance reduction techniques* cover a wide range of statistical trickery. The aim is to modify the random walk process in such a way that the neutron histories having the largest contributions on the results are scored more frequently than the rest. The statistical validity of the simulation is preserved by appropriate biasing of the scores.

Variance reduction techniques are most useful in deep penetration problems and other calculations in which the detector region lies far or isolated from the neutron source.

Criticality source calculations, especially lattice calculations in an infinite geometry, do not greatly benefit from the use of such methods. The simplest implicit modifications to the analog Monte Carlo game are described in the following, but the topic is not discussed in detail. The use of variance reduction techniques is thoroughly covered in References [12] and [14].

Each simulated neutron history in an analog Monte Carlo game represents the transport of a single particle. It is easy to imagine that by assigning each neutron with a *statistical weight* larger than unity, the neutron may actually represent the contribution of several particles. If the weight is below unity, the contribution is less significant than in the case of the analog simulation. Each time the neutron makes a score, the scored value is multiplied by the weight. In order to maintain the average importance of the scores from one cycle to the next, the total weight of the source population is normalised to a fixed value at the beginning of each cycle.

One reason to use the statistical weights is that absorption reactions can be treated implicitly, rather than by terminating the neutron history. This way, more scores can be made in regions that would normally be less accessible to neutrons. The implicit absorption means that the statistical weight is reduced by the fractional absorption probability:

$$W' = W \left(1 - \frac{\Sigma_\mathrm{a}}{\Sigma_\mathrm{t}} \right) , \tag{6.16}$$

where W and W' are the neutron weights before and after the collision and Σ_a and Σ_t are the absorption and the total cross section, respectively. The reduction of the neutron weight is statistically equivalent to the termination of the neutron history [12].

Eventually, after several collisions, the statistical weight is reduced to such a low value that the contribution to the overall results becomes practically negligible and the tracking of the neutron a waste of computing time. The solution is to assign a cut-off value and terminate neutrons after their weight has fallen below the limit with certain probability. This procedure is called *Russian roulette* and it can be implemented in various ways. The simplest way is to write the termination probability as:

$$P = 1 - \frac{W}{W_0} , \tag{6.17}$$

where W_0 is the neutron weight at the beginning of the history. If the neutron survives the test, its weight is restored to W_0.

Similar implicit methods can be used for fission and multiplying scattering reactions [12]. In such cases, the neutron weight is multiplied by the number of emitted particles and a single neutron chosen to continue the simulation.

Chapter 7

Nuclear Data

7.1 Evaluated Nuclear Data

The results of any reactor physics code are significantly influenced by the nuclear interaction data used in the calculations. All code-specific data is derived from certain master files, known as *evaluated nuclear data libraries*. The data in these libraries represents the best available knowledge of the interactions between neutrons and the target nuclei, based on experimental measurements and theoretical nuclear models.

Due to the complexity of the interaction physics, there are always gaps and uncertainties in the measured data and flaws in the theoretical models. The data is not perfect and there are some significant discrepancies between different evaluations, even for the most well known isotopes. These differences are inevitably reflected in the results of all reactor physics calculations as an additional source of uncertainty.

The uncertainties may become pronounced in continuous-energy Monte Carlo calculations, as the cross section data is used without energy group condensation and other modifications that may actually even out some of the differences. Comparison studies [61–65] have shown that the cross section library based discrepancies in criticality calculations can exceed the differences between two codes or the uncertainties resulting from geometry or material compositions. This is an important aspect to be considered and it is hence important to understand the procedures underlying the generation of the interaction data. This chapter follows the path of the data from experimental measurements to the code-specific libraries used in the transport calculation. The current world standard for storing and distributing the fundamental interaction data is the ENDF data format [13], described in Section 7.2.

The ENDF format data is not directly usable in any transport code. The production of code-specific libraries using the NJOY nuclear data processing system [66] is the topic of Section 7.3. The remainder of this first section introduces some of the experimental and theoretical methods used for assembling the evaluated data libraries, as well as some procedures used for data validation.

7.1.1 Measurements

The experimental arrangement for nuclear reaction data measurement basically consists of a neutron source, target and detector. The energy spectrum of the source has to be well determined, and in some cases it is important that the distribution is as narrow as possible. Thin targets are used, so that the neutron mean free path in the material is long compared to sample thickness and the contributions of scattered and secondary neutrons can be ignored. Thick samples and broad spectra are used in integral tests to verify the results of thin sample measurements and cross section evaluations.

The total cross section can be determined simply by measuring the fraction of the neutron beam that traverses from the source through the target without interaction. Partial cross sections, such as fission or radiative capture, are measured by recording the photons or secondary particles emitted from the irradiated sample. The angular distributions of differential scattering cross sections are determined by measuring the scattering contribution as a function of the angle between the beam line and the detector.

Neutron sources are usually driven by particle accelerators. Charged particles, electrons or ions, are collided in a suitable target material, in which neutrons are emitted in various direct or indirect nuclear interactions. The energy distribution of the source depends on the energy of the collided particle, the target material and the interaction type. The source spectrum can be modified using moderator and absorber materials.

A commonly used measurement technique, in which the energy spectrum of the neutron source is immediately resolved, is the time-of-flight method (TOF). The emission time is fixed and the beam is guided to the target through a long tube. Fast neutrons reach the target earlier than slow ones and the energy spectrum can be resolved from the neutron flight time. The TOF method is an efficient technique, in that a wide energy range can be covered in a single measurement.

There are several factors, such as sample impurities and source and detector deficiencies, that hinder the measurements. In addition, background noise due to scattering from shielding and structural materials may cause systematic error in the results. Some isotopes may be particularly difficult to measure because of poor availability

or short half-life in the case of radioactive isotopes. The conditions of the experiment need to be recorded, and thoroughly known when the data is used for cross section evaluation.

Experimental measurements are carried out in several locations throughout the world. In Europe, one such location is the GELINA time-of-flight facility in the Institute for Reference Materials and Measurements (IRMM), located in Geel, Belgium [67]. New high-resolution, high-energy measurements are being planned in many research laboratories such as the n_TOF facility at CERN [68], and the Spallation Neutron Source at Oak Ridge National Laboratory [69].

Experimental data on neutron, charged particle and photo-nuclear interactions is stored in a standardised, computer-readable format, known as EXFOR [70]. The EXFOR data is maintained and distributed by the core data centres of the IAEA Nuclear Reaction Data Centres Network (NRDC) [71][1]. A closely related database is the Computer Index to Neutron Data, or CINDA [72], which is a bibliographic file that acts as an index to EXFOR. The CINDA file contains detailed information and references to experimental and theoretical work related to the recorded measurements.

7.1.2 Evaluation

The evaluation process combines experimental measurements and theoretical nuclear models, and produces uniform and complete data sets in a standardised, computer-readable form. The evaluation work begins with choosing the experimental data. The quality of the data is assessed, and unreliable or erroneous measurements are eliminated. This preparatory phase is essential, since the available data is usually scattered, and originates from measurements made under different experimental conditions. The EXFOR and CINDA databases serve as the sources of raw data and information on the details of each measurement.

Theoretical cross sections are calculated according to nuclear models that are estimated to be the most suitable for the particular case. Model parameters are then adjusted to reproduce the experimental data, which may not be complete for all isotopes. This is especially the case for short-lived nuclides or isotopes that for some other reason are difficult to measure[2]. Since the final evaluation covers the entire energy range, gaps in the data need to be filled, which emphasises the quality of the theoretical models.

---

[1]The core data centres of the NRDC are the National Nuclear Data Center (NNDC) at Brookhaven National Laboratory, the OECD/NEA Data Bank, the Nuclear Data Section of IAEA and the Russia Nuclear Data Center (CJD).

[2]The EXFOR data of ^{135}Xe, for example, consists of less than 80 measured data points, all in the thermal energy region.

The evaluated cross section curves are stored as a combination of tabular point-wise data, parametrised resonance functions and statistical probability tables in the unresolved resonance region. The point-wise representation applies to regions where the cross sections behave smoothly: the low-energy region below the first resonances and the high-energy continuum.

One of the simplest descriptions of discrete resonance peaks in a functional form is the single-level Breit-Wigner resonance formula (SLBW), which for radiative capture is written as [7]:

$$\sigma_\gamma(E) = \sigma_0 \frac{\Gamma_\gamma}{\Gamma} \sqrt{\frac{E_0}{E}} \left(\frac{1}{1+y^2} \right), \qquad y = \frac{2}{\Gamma}(E - E_0), \qquad (7.1)$$

where E_0 is the peak energy. Parameters Γ and Γ_γ are the total and the radiative line widths that characterise the probabilities of compound nucleus formation and decay via radiative capture, respectively. Physically more accurate representations include the multi-level Breit-Wigner, the Reich-Moore and the Adler-Adler approximations, which all belong to the more general R-matrix resonance theory [73].

Discrete peaks cannot be distinguished in the unresolved resonance region and probabilistic representations must be used instead. One such representation is the level-statistical Hauser-Feshbach resonance theory [73], which is also used in the ENDF file format. In this theory, individual peaks are not separated, but the resonance parameters, such as level spacings and partial widths, are described by probability distributions that statistically yield the same average behaviour as the experimental data.

Figure 7.1 shows an example of evaluated resonance data together with experimental measurements. The solid curves represent thermal fission cross sections of ^{241}Pu taken from the ENDF/B-VI.8 and the JEF-2.2 evaluated nuclear data files. The measured data is from the EXFOR database and it was originally collected from a series of experiments carried out at the Institute for Reference Materials and Measurements in 1991. It should be noted that the experimental data is included for comparison only, and neither of the evaluations is based on this particular set of data.

7.1.3 Validation

There are several methods for testing the evaluated nuclear data. Purely mathematical methods, based on statistical distribution laws, can be used for verifying theoretical models and spotting clear errors in the data. Physical inconsistencies are eliminated, and the validity of the evaluation tested against experimental integral and thin-sample measurements. The data is also tested in various application environments, using well-defined benchmark experiments.
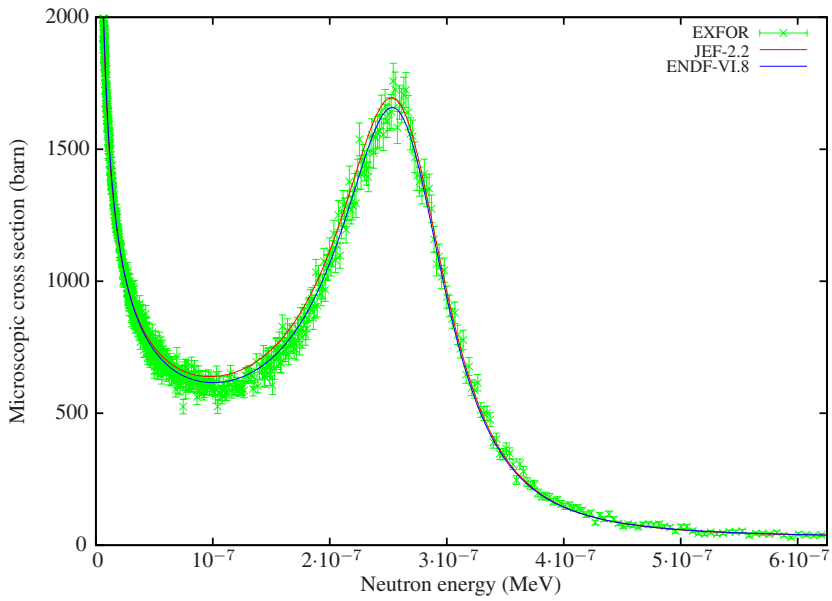
Figure 7.1: Measured and evaluated fission cross sections of ^{241}Pu in the thermal energy region.
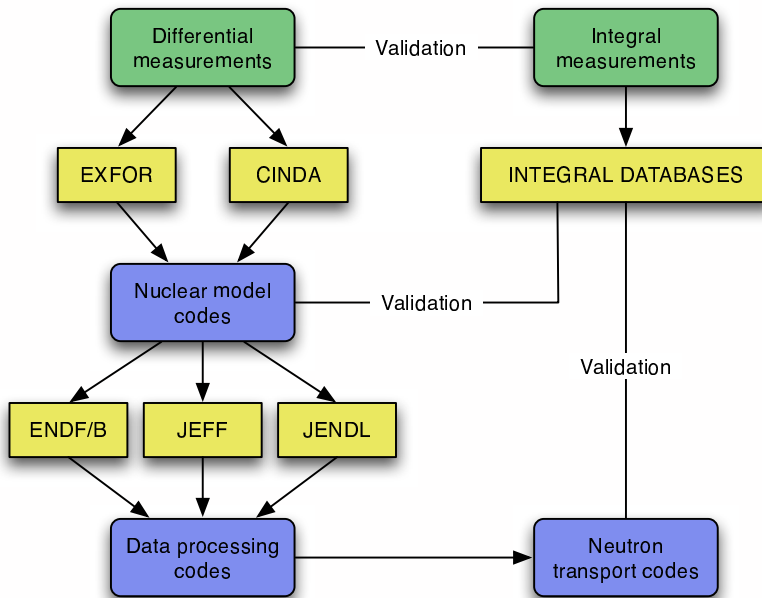
Figure 7.2: The generation and validation of evaluated nuclear data.

Essential tools for code and data validation in reactor physics applications are the CD/DVD-ROM handbooks of the International Criticality Safety Benchmark Evaluation Project (ICSBEP) [74, 75] and the International Reactor Physics Experiment Evaluation Project (IRPhEP) [76, 77]. The ICSBEP handbook is a large collection of detailed data on critical experiments that have been carried out in research laboratories throughout the world since the early 1950s. The experiments cover a wide range of applications ranging from fast-spectrum uranium and plutonium systems to thermal LWR configurations. While the ICSBEP project is focused on criticality calculations, the IRPhEP handbook covers a wider range of reactor physics parameters.

Once the evaluation work has been completed, the data is converted into a standardised format for distribution. The current world standard is the American ENDF data format, which has replaced several national formats used in the past, such as the British UKNDL and the German KEDAK. The time span from the beginning of the evaluation to the final release of the validated data typically ranges from 5 to 10 years. The data generation and validation process is summarised in Figure 7.2.

7.2   ENDF File Format

The history of the ENDF file format [13] goes back to the development of the first ENDF/B evaluated nuclear data libraries compiled at Brookhaven National Laboratory (BNL) in the United States[3]. The current version of the standard, ENDF-6, however, is completely detached from the data itself, and it is used in several evaluation projects around the world. The ENDF file format is maintained by the US Cross Section Evaluation Working Group (CSEWG) [78], co-ordinated by the National Nuclear Data Center at BNL.

The ENDF format libraries contain various data on nuclear interactions and radioactive decay. Owing to historical reasons, the data is divided hierarchically into "tapes", "materials" and "files". Each file contains certain type of data, such as reaction cross sections, resonance parameters, angular and energy distributions, thermal scattering data, radioactive decay data, and so on.

Reaction cross sections in the resolved energy range are given using the parametrised resonance formulae, together with tabular point-wise data. The unresolved resonance region is represented using energy-dependent statistical average values and probability distributions for resonance widths, level spacings and other parameters according to the Hauser-Feschbach resonance theory. For many isotopes, there is not enough

---

[3]The ENDF (Evaluated Nuclear Data File) file format should not be confused with the American ENDF/B (Evaluation of Neutron Data File/Brookhaven) evaluated data files.

experimental data for detailed evaluation, and constant average resonance parameters are assumed over the unresolved range. The processing of such data yields smooth averaged cross sections over the unresolved range.

Angular distributions of scattering reactions are given as 32 equi-probable cosine bin distributions, tabular probability distribution functions, or as the coefficients of Legendre polynomials. The emission energy is coupled to the scattering angle in the simplest two-body collisions (see Section 5.4.3 of Chapter 5). Continuum inelastic scattering and reactions involving more than two particles require the use of combined distributions, in which the emission energy and the scattering angle are either independent or coupled.

Fission reaction data relevant to transport calculation includes the yields and energy distributions of prompt and delayed fission neutrons. The fission nubar data are given using a polynomial representation or as point-wise tabulated data. Fission neutrons are emitted isotropically in the laboratory frame-of-reference and angular distributions are not needed. The energy distributions are given in the form of parametrised Maxwell, Watt or evaporation spectra, or as arbitrary tabulated data. Delayed neutrons are divided into 6 or 8 groups, characterised by different yields, decay constants and energy distributions.

There are three major evaluation projects in the world: the American ENDF/B [78], the Western European JEFF [79] and the Japanese JENDL [80]. The projects are not completely independent and both collaboration and exchange of data occur over the project boundaries. The collaboration has many forms and one example is the Working Party on International Evaluation Co-operation (WPEC) [81], organised by the OECD/NEA[4]. The main goals of the working party are to develop the quality and completeness of the libraries and to promote convergence of the data by eliminating the most important discrepancies.

7.3   Data Processing

The ENDF file format is designed in such a way that the data files remain relatively compact, and yet preserve the accuracy of the original evaluation. The data format is not directly accessible to transport calculation codes, which use the cross sections in group- or point-wise form. The most widely used processing code that can be used for producing data libraries to a large variety of transport codes is the NJOY nuclear data processing system, introduced below.

---

[4]In addition to the three major projects, the Chinese CENDL, the Russian BROND, and the FENDL project of the IAEA are included in the WPEC group.

7.3.1 The NJOY Code

The NJOY code [66] is a modular nuclear data-processing system, developed at the Los Alamos National Laboratory. The system consists of a main program that drives independent functional modules, each designed for a specific task. The data flow in the generation of continuous-energy cross section libraries for Monte Carlo codes MCNP and PSG is illustrated in Figure 7.3. A short description of each module is given below.

RECONR: The RECONR module constructs point-wise continuous-energy cross sections from the resonance parameters and interpolation schemes of the ENDF format data. Average resonance widths and level spacings in the unresolved resonance range are converted into cross sections by taking the weighted averages from the probability distributions.

The energy grid is generated in such a way that linear interpolation may be used between the data points. The grid generation is an iterative procedure, in which new points are added between exiting ones, until each energy interval of each cross section represents the original data to within the desired accuracy, determined by the user-defined fractional reconstruction tolerance.

BROADR: Cross sections in the ENDF files are evaluated at a specific temperature. The BROADR module takes the point-wise ENDF file (PENDF) generated by RECONR and converts it to any desired temperature applying Doppler-broadening on the cross sections. The procedure leaves the energy and angular distributions untouched. A new optimal energy grid is generated for the data, similar to the RECONR module.

PURR: The PURR module generates probability tables from the unresolved resonance parameters in the ENDF files. These tables can be used by Monte Carlo codes instead of the averaged cross sections constructed by RECONR.

ACER: The ACER module converts all data into the ACE data format used by the MCNP code and generates an entry for the "xsdir" directory file. Some error and consistency checking is performed on the data before the finalisation.

7.3.2 Library Formats

The above description of point-wise data generation is an example only. The NJOY code also has various optional modules, which can be used for calculating effective heat and gas production cross sections, etc. The generation of thermal bound atom
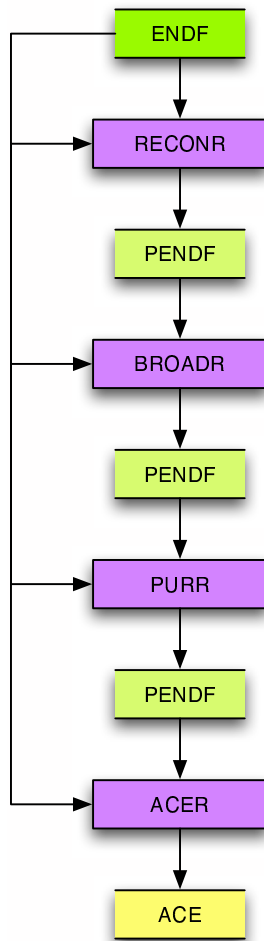
Figure 7.3: The NJOY data flow in the generation of continuous-energy cross section libraries for MCNP/PSG.

scattering data differs from the given description. If the ENDF data contains no probabilistic unresolved resonance parameters, the execution of the PURR module is omitted. It should be noted that the current version of the PSG code does not handle unresolved resonances in this format.

The last module in the chain makes the actual conversion of the PENDF data into the ACE format, which was originally developed for the MCNP code. The reason why the ACE format was chosen to be used with PSG, was to get the actual code development started as soon as possible. The advantage is that exactly the same libraries can be used for code validation against MCNP calculations. This eliminates

137

the uncertainties originating from the interaction data and reveals more clearly all the flaws and programming errors in the code.

The generation of group-wise cross section data has a few additional steps in the process. Group-wise data is used by all deterministic codes and some Monte Carlo codes, such as KENO [52] and GMVP [82]. The number of energy groups typically ranges from 50 to 300.

The most obvious difference to the point-wise data format is that cross sections are condensed over discrete energy intervals. The condensation of the reaction cross section of reaction i over energy group g is written as:

$$\sigma_{i,g} = \frac{\displaystyle\int_{E_g}^{E_{g-1}} \sigma_i(E)f(E)dE}{\displaystyle\int_{E_g}^{E_{g-1}} f(E)dE} \,, \tag{7.2}$$

where $f(E)$ is an energy-dependent weighting function. The group condensation is carried out in the GROUPR module of the NJOY code. The cross sections are generated taking into account resonance self-shielding effects (see Section 2.3.5 of Chapter 2). This module also produces group-wise fission spectra and group-to-group scattering matrices from the continuous energy and angular distributions.

It is obvious that the group condensation results in a loss of information. In order to preserve the physical consistency, the cross sections should be weighted by the space and energy-dependent flux spectrum (see Eq. (3.42) in Chapter 3). Since the flux solution is not known before the transport calculation, an analytical weight function has to be used instead. Another approximation has to be made when calculating the resonance self-shielding effects. The flux depression depends on the concentration of the isotope, which may be different in the applications where the data is used.

These problems point out some of the advantages of continuous-energy Monte Carlo calculation. The point-wise data format is simpler, more accurate and much closer to the original evaluation. The format is general and it can be used in any type of application. It should also be noted that resonance self-shielding is a phenomenon that does not present itself to individual neutrons. The collective flux depression effect is consistently taken into account in the simulation without additional procedures.

Part II

Practical Implementation in the PSG Code

Chapter 8

Methodology in the PSG Code

8.1 Overview

The PSG code can be described as a three-dimensional, continuous-energy Monte Carlo neutron transport code. The code has certain characteristic features, which make it specifically suited for reactor physics calculations at the fuel assembly level. The same features restrict the generality of the applications to some extent, but there is no reason why any problem in reactor physics could not be approached with PSG.

The development of PSG is still at an early stage. The program code is written from scratch using standard ANSI-C language. The code is mainly developed in the Linux operating system, but it has also been compiled and tested in OS/X and some UNIX machines. The main processes of PSG are illustrated in Figure 8.1. Basically the program flow consists of a few pre-processing steps for the user input and the interaction data, the main transport calculation cycle and the final collection of the output parameters.

If the program is run in a parallel calculation mode, the transport cycle is executed simultaneously in multiple hosts. The parallel tasks do not interact or exchange data until the termination of the main cycle. This type of parallelisation is possible due to the linearity of the Monte Carlo method. It is both efficient and easy to implement. The downside is that the system cannot cope with run-time errors in any of the hosts. Since there is no dynamic load sharing, the calculation time depends on the slowest task and efficiency problems may arise if the code is run in a very asymmetric parallel environment. The parallelisation is implemented using the Message Passing Interface (MPI) [83], which is a library standard that offers high-level access to parallel calculation and communication and data sharing between the tasks.
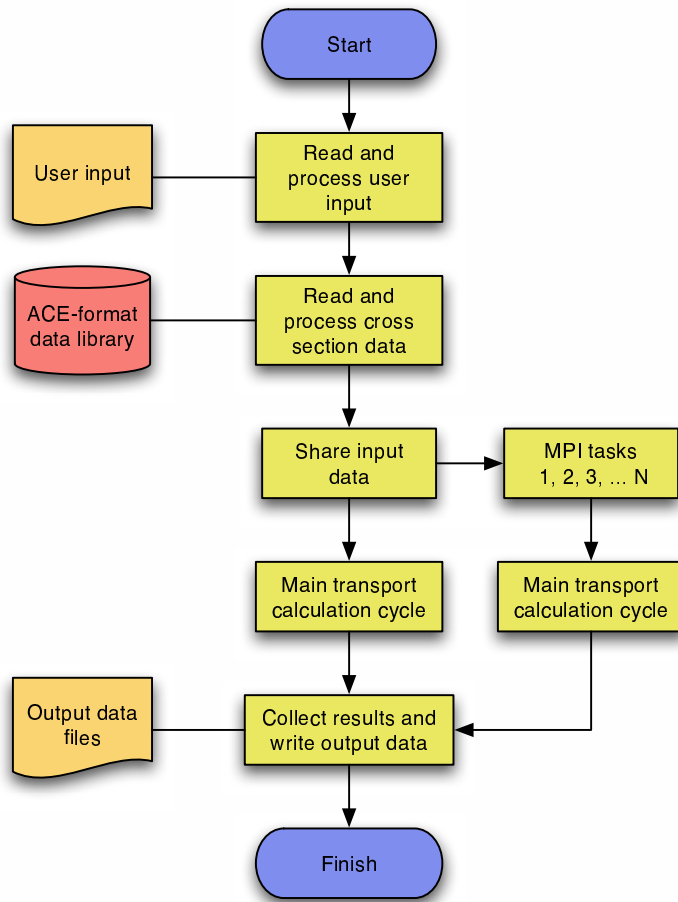
Figure 8.1: Data flow and main processes in the PSG code.

The single most important special feature of PSG is the capability to generate few-group constants and diffusion parameters for reactor simulator codes. Neutron leakage models for fundamental mode calculation are under development and burnup calculation is being planned. Since homogenised group constants are traditionally produced by deterministic lattice transport codes, PSG can be labelled as one of the first codes, if not the very first code, in an entirely new lattice code generation.

The calculation of the output parameters is fully described in the following chapter. This chapter introduces the methodology used for the actual transport calculation[1].

---

[1]This thesis is not intended to give a complete description of the calculation methods used in PSG. A separate user manual with a detailed methodology description is being planned, but at the time of writing, this text is unfortunately the best available description of the code methodology.

Neutron tracking in PSG is based on the Woodcock delta-tracking algorithm, which was described in Section 5.3.3 of Chapter 5. The practical implementation, including a modification in the basic technique, is described in Section 8.3. The physical background and the general Monte Carlo treatment of neutron interactions have been discussed in Chapters 2 and 5. The PSG methods are briefly reviewed in Section 8.4. The methodology description begins with the introduction of the point-wise cross section data format.

8.2   Cross Section Data

The generation of homogenised group constants requires the lattice calculation to be repeated for all fuel types and it needs to cover all operating conditions within the reactor core. It is hence essential that the running time of a single case is cut to a minimum. Delta-tracking gives some advantage in complicated geometries, but an equally or even more significant reduction in calculation time is gained from a special treatment used for the cross section data in PSG.

8.2.1   The General Point-wise Data Format

The name of the format implies that the cross section data is given as tables of energy-cross section pairs. The tables are generated directly from the ENDF format files, without any energ group condensation. The values between the data points are calculated using linear interpolation. If the incident energy, E, lies between two tabulated energy points, E_j and E_{j+1}, the value of the cross section is given by [13]:

$$\sigma(E) = \frac{E - E_j}{E_{j+1} - E_j}(\sigma_{j+1} - \sigma_j) + \sigma_j \,, \tag{8.1}$$

where σ_j and σ_{j+1} are the tabulated cross section values corresponding to the two energy points.

The energy grid in an ACE format data library is constructed by the NJOY code in such a way that the original ENDF data is reproduced with maximum accuracy (see Section 7.3 of Chapter 7). The number of points in the energy grid is determined by the complexity of the reaction data and the reconstruction tolerance used in the generation. The typical number of energy points for actinide cross sections ranges from about 20,000 to 70,000. Lighter isotopes contain less detail.

The energy grids are arbitrary in the sense that there are no analytical means to determine the grid interval in which a specific energy value falls. Instead, the energy grid

index j, which satisfies the condition:

$$E_j < E < E_{j+1} \qquad (8.2)$$

has to be found by iteration. This procedure is repeated so frequently that its contribution in the overall calculation time can become quite significant.

Each isotope uses the same energy grid for all reaction channels, although threshold reaction cross sections are given only for the points above the threshold energy. The energy grids are not the same for two different isotopes, and a material consisting of several isotopes is associated with an equal number of energy grids.

The sampling of the free neutron path length uses either the material total cross section, or in case of delta-tracking, the majorant cross section (see Section 5.3 of Chapter 5). The calculation of the material total cross section requires the summation over all isotope totals, which means that the interpolation procedure has to be carried out for each isotope in the material, every time the path length is sampled. The calculation of the majorant cross section is even more complicated, and delta-tracking also uses the material totals for sampling the reaction type.

8.2.2   Cross Section Data in the PSG Code

In order to speed-up the calculation, it was decided to derive a slightly modified data format for the PSG code. The idea is to use the same energy grid for all the isotopes of all materials in the system. The advantage of this approach is that the energy grid index has to be determined only each time the neutron changes its energy. Another significant improvement is that the majorant cross section can easily be generated at the pre-processing stage, before the actual transport calculation

The philosophy in using the same energy grid for all isotopes is that computer memory is allowed to be used wastefully, in order to gain efficiency in the calculation. This is not a serious problem for today's computers, as the amount of memory is usually not a limiting factor. PSG has three different data formats and each of them requires some substantial pre-processing. The first step is the generation of the uniform energy grid, after which the cross sections are reconstructed for each new energy point. Values not coinciding with a point in the original data are calculated from the neighbouring points by linear interpolation, as in (8.1).

Method I: Re-formulation of the Energy Grid

The first option is to use a fixed-size energy grid, which has to be set up in such a way that all reaction channels are reproduced with sufficient accuracy. It was decided
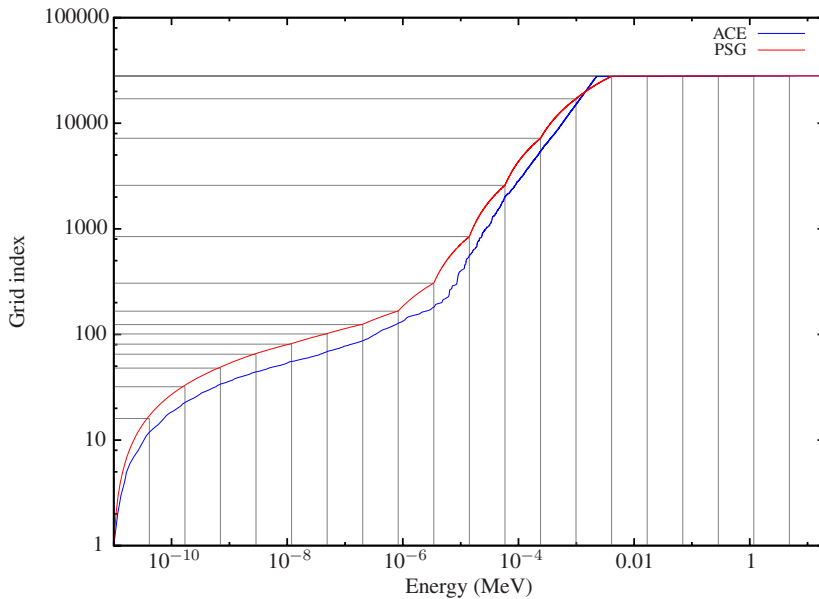
Figure 8.2: The energy grid index as function of energy for ^{235}U. The PSG data is generated using 20 main energy intervals and the same total number of energy points as the original ACE format data.

to construct this grid in such a way that the correct interval could always be found without iteration, and it was hoped that this would speed-up the calculation even more. The energy points in the ACE libraries are not uniformly distributed throughout the spectrum. The resolution is highest at the region of closely-spaced resonances. Clearly, the energy points in the modified grid should have a similar distribution to produce an accurate representation of the original data.

It turned out that the best way to replicate such a distribution is to use two nested energy grid structures[2]. The full energy scale is first divided into N main intervals, all with the same lethargy width. The fraction of total energy points assigned for each main interval is then set equal to the same fraction calculated from the original ACE data. The energy points are distributed within each interval in such a way that the lethargy width between two points is the same throughout the interval. This confusing procedure is best illustrated by the example in Figure 8.2, which shows the cumulative number of energy points as a function of energy for the original ACE format data and the grid generated by PSG.

---

[2]In theory, it might be better to use even more levels in the representation, but two nested structures were considered sufficient for the present format.

It is obvious that the points in the modified grid differ from the exact locations of the points in the original grid. The result is that resonance peaks and other sharp changes in the data may become "smeared", since there are no energy points corresponding to the peak values as in the original format. There is no other solution to the problem than to simply increase the total number of energy points, which in turn increases the resolution.

A typical PC workstation with 1 Gb memory can easily handle a PSG lattice calculation with 500,000 energy points, which is about 10 times the typical maximum number of energy points in the ACE format data. The memory requirement increases linearly as new isotopes are added to the system[3].

Method II: Accurate Representation of the Original ACE Data

The second approach is to include all energy points of all isotopes in the original ACE data, which preserves all the information available in the cross section library. Even though the energy grid interval has to be iterated only each time the neutron changes its energy, this procedure may become time-consuming if the number of grid points is large. To overcome this problem, another energy grid structure is used. The full energy scale is divided into a smaller number of sub-intervals, each interval holding pointers to the main grid. The procedure of finding the correct grid index is carried out in two parts. First, the correct sub-interval is located analytically. The final grid index is then found by iteration from the set of points within this interval.

The result of using this grid format is that all cross sections contain a large fraction of redundant data points, i.e. points that lay on a straight line between two original values. This is the price of efficiency. The memory requirement is strongly dependent on the number of isotopes in the problem. As more nuclides are included, not only the amount of useful information, but also the size of the energy grid and hence the amount of redundant data are substantially increased. Memory problems may occur in large calculation tasks, and alternative data formats are probably necessary in burnup calculation planned for the future versions of PSG.

Method III: Re-formulation of the Energy Grid and Histogram Data

The third cross section data format uses the same procedure for generating the energy grid as the first method. The difference is that instead of interpolating the values between two data points, the cross section is simply set equal to the value at the lower

---

[3]To be precise, the increase is not exactly linear, as the required amount of memory also depends on the number of available reaction channels, which is different for each isotope.

boundary. The result is a histogram representation. Even though the cross sections are constant between the energy grid points, the representation is not equivalent to the micro-group data format. The difference is that the values are taken directly from the original data, without energy-group condensation. Although the motivation for developing the histogram data format was the reduction of calculation time by eliminating the interpolation step during the transport cycle, it turned out not offer a major improvement over the linear interpolation.

The three data formats are illustrated in Figure 8.3. The selection of the format to be used in the calculations depends on several factors. The second method offers an accurate representation of the original data, but is potentially less efficient and may require an excessive amount of computer memory if the number of isotopes is large. The re-formulation of the energy grid produces more compact data, but it also adds more uncertainty in the problem.

So far, no significant differences compared to the accurate representation have been observed in the results, if more than about 100,000 energy points are used in either of the formats based on the re-formulated energy grid. In most cases, about half of that has been considered sufficient. No significant discrepancies have been encountered between the histogram and the linear data format either, even if the number of grid points is low. These observations may indicate that the calculation is not very sensitive to the resolution of the cross section data, which is an important finding, considering the development of burnup calculation in the future. It is important, however, that the inevitable loss of information is not completely ignored. There is no way to be sure that a resolution found to be sufficient in most cases is sufficient in all cases imaginable.

8.2.3   Additional Pre-processing

After the energy grid is generated and all the cross sections reconstructed using the new grid, bound atom data (see Figure 2.7 on page 42) is added in the free-atom cross sections. The original elastic scattering cross sections are set to zero for the energy points where the bound isotope data is defined. The bound scattering reactions are then simply added in the list of reaction channels. New isotope totals are calculated from the modified cross sections.

PSG also has an interpolation method for producing effective intermediate temperature cross sections from two libraries generated at different temperatures. The procedure is based on mixing the isotopes in the appropriate ratio. It can be shown that the Doppler-broadening of the cross sections induces a dependence proportional to the square root of the absolute temperature [7]. The atomic fraction of the low
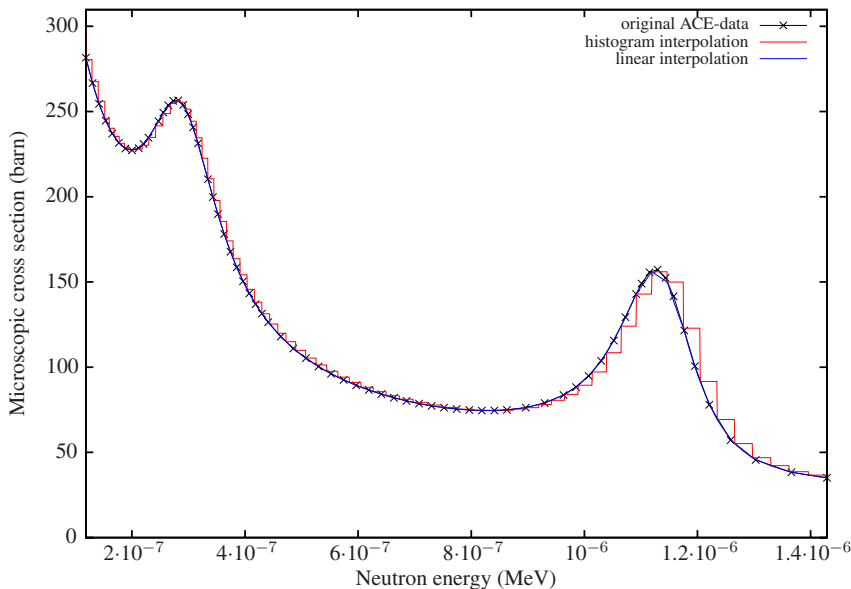
Figure 8.3: The linear-interpolated and histogram data formats used in PSG, together with the original ACE data (total cross section of ^{235}U from ENDF/B-VI). The number of energy grid points is set low to emphasise the differences.

temperature isotope is calculated from:

$$f_1(T) = \frac{\sqrt{T_2} - \sqrt{T}}{\sqrt{T_2} - \sqrt{T_1}} \; , \tag{8.3}$$

where T is the interpolation temperature and T_1 and T_2 are the temperatures of the low- and high-temperature cross section libraries, respectively. The fraction of the high temperature isotope is simply $f_2(T) = 1 - f_1(T)$.

A similar method has been used in a special VTT version of the MCNP4B code. Such a procedure has also been studied at the Nuclear Research and Consultancy Group (NRG) [84] and planned for the future version of MCNP5[4]. The method is not yet fully tested in PSG and it is hence not discussed here in detail. The extensive pre-processing of data in PSG offers the possibility to perform the interpolation directly on the cross sections, instead of mixing two isotopes at different temperatures. Such a methodology is considered for future code versions.

---

[4]An external processing code called "Doppler" has been developed at Los Alamos National Laboratory [85, 86]. The methodology is included in an in-house version of the MCNP5 code, but the code is not publicly available at the time of writing.

8.3 Neutron Transport

The neutron tracking procedure in PSG does not significantly differ from the general description given in Section 5.3 of Chapter 5. The code uses an extended delta-tracking method for sampling the free path lengths between collisions. The practical implementation of the tracking procedure is given in the following. The geometry description in PSG is briefly introduced in Section 8.3.2.

A simplified overview of the transport cycle in the k-eigenvalue criticality source mode is given in Figure 8.4. The flow chart describes the calculation steps during the simulation of one neutron generation. The source distribution in each cycle is given by the fission neutron distribution recorded during the previous cycle. The main loop is carried over all source neutrons. In order to maintain the size of the population, the source size is modified as described in Section 5.5.2 of Chapter 5.

The result estimates are scored after the final neutron collision site has been sampled. An alternative solution is to score during the delta-tracking process, after each real or virtual collision. This approach leads to a larger number of scores, especially in regions where the real collision probability is low. Comparisons have shown that there is no large reduction in the statistical uncertainty of parameters integrated over the entire geometry. The calculation time, however, is significantly increased.

8.3.1 The Extended Delta-tracking Method

As was described in Section 5.3.3 of Chapter 5, the delta-tracking method is based on introducing virtual collisions in the tracking process in such a way that the effective total cross section, denoted as the majorant, can be set equal in all material regions. This has the advantage that the free path length does not have to be adjusted or re-sampled each time the neutron crosses a material boundary, which simplifies the geometry routines.

The majorant cross section used for sampling the collision distances is generated from the cross section data at the pre-processing stage, before starting the transport calculation. This cross section is simply the maximum of all material totals at each energy point.

The basic delta-tracking method leads to efficiency problems when high-absorbing materials occupy small and localised portions of the geometry[5]. A typical example of

---

[5]In theory, the problem is not specifically related to high absorption cross sections, but to high reaction probabilities in general. In practice, however, such conditions usually arise from the use of localised heavy absorbers.
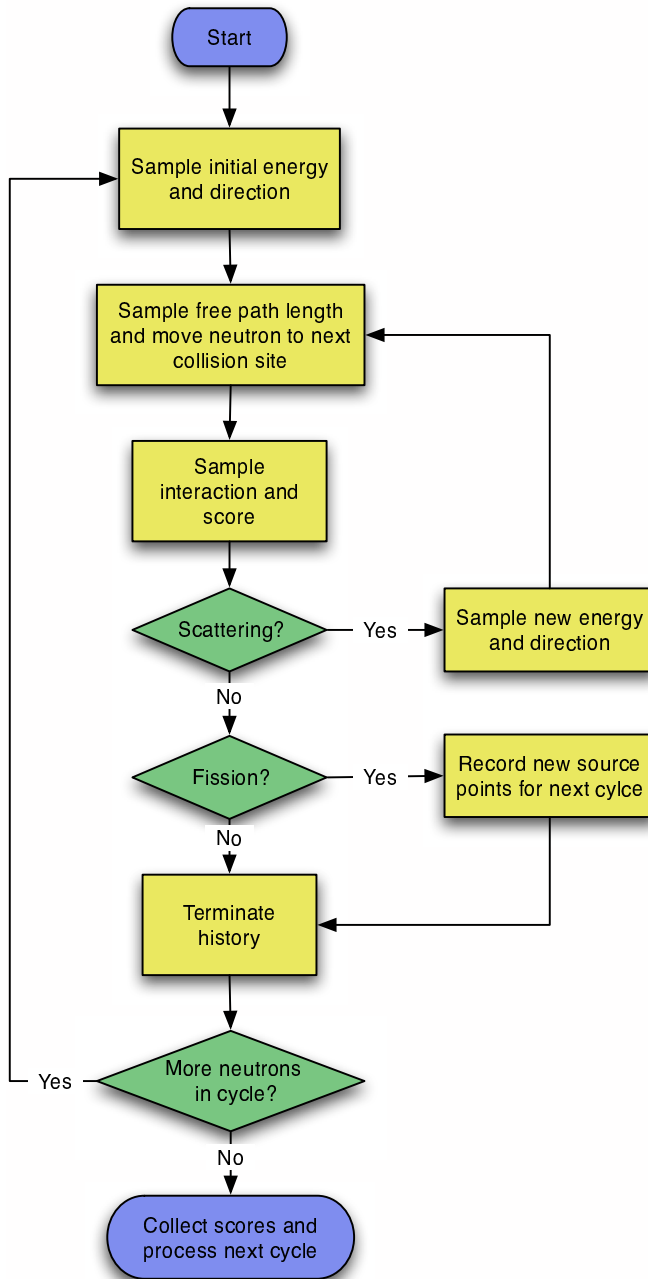
Figure 8.4: The transport cycle in PSG (k-eigenvalue criticality source mode).

such conditions is a fuel assembly partially loaded with burnable absorber pins. The thermal capture cross sections of gadolinium isotopes, ^{155}Gd and ^{157}Gd in particular, dominate the majorant cross section at low energy. The probability of a neutron actually finding one of such pins in the geometry is relatively low, which results in a dramatic increase in the virtual collision rate, and computing time is wasted in the re-sampling loop.

The efficiency problems of delta-tracking are well known, and most of the codes applying this method use it as an optional tracking routine in combination with the conventional ray-tracing algorithm. One example is the HOLE geometry package [20], which can be used in Monte Carlo codes MONK and MCBEND. The model enables the use of delta-tracking in certain special geometry types enclosed within specified sub-regions, or "holes".

Another popular approach is to use delta-tracking and switch to the conventional method when the majorant cross section becomes excessively high compared to the material total. This solution is general and very effective, but since the application of such a method requires advanced geometry routines that are able to calculate the flight distances to complicated surface types, it was decided to take yet another approach with PSG.

The solution takes advantage of the fact that PSG is mainly intended to be used for lattice calculations, or at least they are the applications in which code performance becomes an issue. The common feature in most fuel assembly-level geometries is that localised heavy absorbers are contained within cylindrical material regions and located in a systematic lattice structure. This generalisation applies to burnable absorber pins, PWR control rods (excluding VVER-440 control elements) and absorber pins inside BWR control blades.

The method developed for PSG takes advantage of two majorant cross sections. The *high majorant* $\Sigma_{m,1}(E)$ is constructed from the maximum values of all material total cross sections, similar to the majorant in the basic delta-tracking method. The second, *low majorant* $\Sigma_{m,2}(E)$, is constructed in a similar manner, only excluding the materials labelled by the user as heavy absorbers.

If the difference between the two values is significant at some energy point, the collision distance is first sampled using the low majorant, which produces longer path lengths. The sampled distance is then compared to the *minimum safe distance*, or the shortest optical distance to regions containing the heavy absorber. If the material boundary is not crossed, the sampled distance is accepted. In the opposite case, the neutron is moved to the surface of the heavy absorber and the remaining path length is re-sampled using the high majorant. The procedure is illustrated in Figure 8.5.
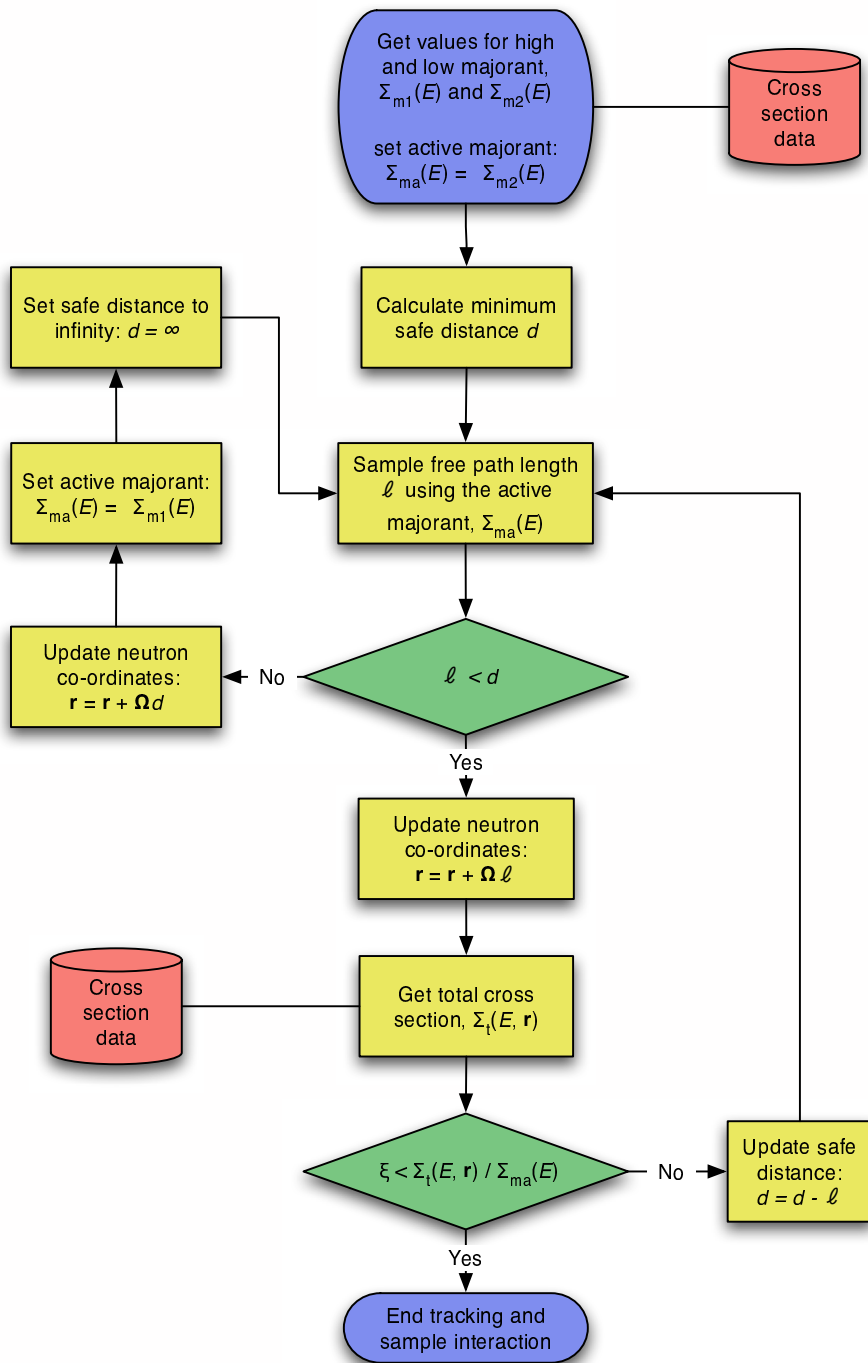
Figure 8.5: The extended delta-tracking algorithm used in PSG.
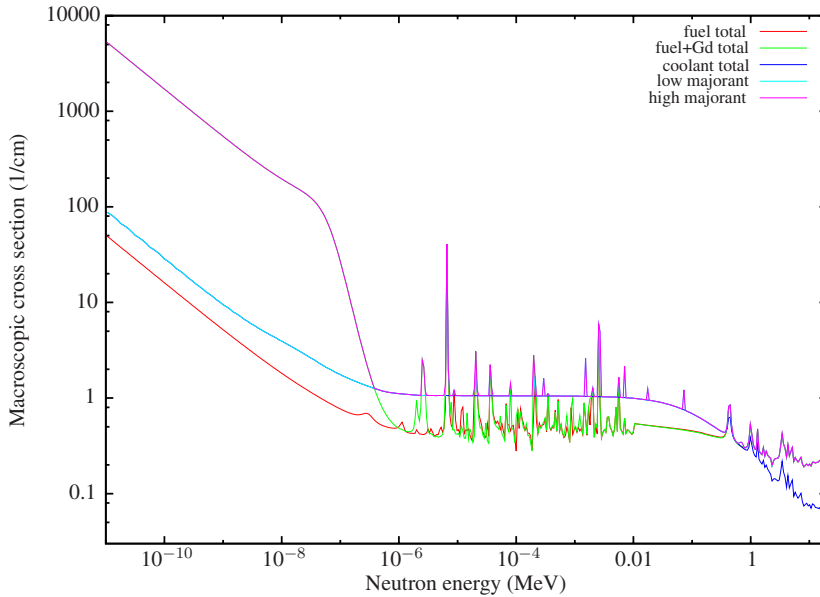
Figure 8.6: The majorant and material total cross sections in a PWR fuel assembly with burnable absorber (ENDF/B-VI.8). The total cross section of cladding is not dominant in any energy region and it is omitted for the sake of clarity.

The optical distance to a cylindrical boundary surface is very simple to calculate. The procedure is not very time-consuming either, especially since the calculation has to be carried out only once, at the beginning of each neutron track. The increase in efficiency, however, can be quite dramatic. The typical virtual collision fraction in a LWR fuel assembly without burnable absorber ranges from 30 to 40%. The introduction of Gd pins can increase this fraction up to 95%, which has a significant impact on efficiency and running time. The fraction can be lowered down to about 50% using the extended delta-tracking algorithm, which reduces the computing time close to the case without burnable absorber. A practical example is given in Section 10.6.1 of Chapter 10.

The high and low majorant cross sections together with material totals in a PWR fuel assembly with burnable absorber are plotted in Figure 8.6. It can be seen how the gadolinium isotopes dominate the high majorant cross section. The difference between the two majorants is several orders of magnitude. The contribution of heavy absorber is omitted in the low majorant and the dominating cross sections are the elastic scattering cross section of hydrogen in water and some discrete resonance peaks of fuel isotopes. These materials are more homogeneously distributed throughout the geometry, which results in a considerably lower virtual collision rate.

8.3.2 Geometry Setup

The use of delta-tracking considerably simplifies the geometry routines. The reason is that the optical distance to the nearest material boundary does not have to be calculated each time the free path length is sampled. It is instead sufficient to determine the material at each tentative collision site. Apart from this difference, the geometry setup in PSG is very similar to any other Monte Carlo neutron transport code.

The geometry consists of homogeneous material cells, defined by combinations of elementary boundary surfaces. These combinations may include the logical union, intersection and complement operators. Using this simple description, it is possible to define almost any reactor geometry using only planar and cylindrical surfaces. Many codes allow the use of macro-objects, such as boxes or prisms, composed of several elementary surfaces. Such a description may considerably simplify the user input, but it may also lead to serious efficiency problems if complicated geometries are built from advanced macro-objects.

The use of delta-tracking simplifies the geometry routines and the treatment of complicated surfaces. It turned out that the most efficient way to set up the geometry in PSG is to use the simplest possible combination of surfaces, even if it contains complicated macro-objects. It was hence decided to omit the union operator altogether, and use only intersections of elementary surfaces and macro-objects, and their complements. The lack of the union operator is compensated for by providing the user with a sufficiently large collection of macro-objects that can be used for defining almost any geometry type encountered in reactor physics calculations.

Since reactor geometries consist of repeated structures, such as assembly- and pin-cell lattices, it is not the most efficient way to define each small geometry unit independently. Infinite repeated structures of similar cells can be described using reflective or periodic boundary conditions. In such a case, each neutron crossing the geometry boundary is either reflected back (reflective boundary) or moved to the opposite boundary surface (periodic boundary). Since the delta-tracking method does not deal with surface crossings, the boundary conditions are implemented by making a transformation in the neutron spatial and angular co-ordinates each time the collision site is sampled outside the geometry[6].

Another type of systematic structure is needed for describing the pin layout in a fuel assembly or the loading pattern of assemblies in the reactor core. This type of geometry is constructed using lattices and sub-universes. Each lattice cell is filled with a sub-universe, which has its own independent geometry description. An example of

---

[6]Because the points of surface crossing are not calculated in PSG, it is not possible to define the so-called *white boundary*, which means that neutrons are isotropically reflected back in the geometry.

such a structure is the pin-cell lattice in a fuel assembly. Each pin type is defined separately and the lattice description links the pin universes to the lattice positions. The fuel assembly can be surrounded by reflective or periodic boundary conditions or it can be included in another lattice, which determines the reactor loading pattern in a full-core calculation.

PSG has three types of systematic structures: square and hexagonal lattices and the circular array, which is needed for describing the cluster-type fuel assemblies of CANDU and RBMK reactors and the core layout of some small research reactors.

8.4 Interactions

The interaction is sampled after the neutron has reached its final collision site. As can be seen in Figure 8.4, the way in which each interaction is processed, depends on the interaction type. Both capture and fission terminate the neutron history and no further steps are required for the incident neutron.

The treatment of fission reactions is very similar to the general description given in Section 5.4.2 of Chapter 5. The emitted fission neutrons make up the source of the preceding neutron cycle. The energy distributions of emitted neutrons are given in the ACE format data as Maxwell (law 7), Watt (law 11) or evaporation spectra (law 9), or as arbitrary tabular distributions (law 4). The "law" numbers refer to the reaction law types in the ENDF data format [13]. The sampling procedures are described in reference [14] and will not be repeated here. The angular distribution of fission neutrons is always isotropic in the L-frame.

The dynamics of elastic scattering follows the procedure described in Section 5.4.3. The target velocity is sampled from a Maxwellian distribution if the target nuclide is free hydrogen or the incident neutron energy is below a certain threshold. The angular distributions are given in the C-frame, as 32 equi-probable cosine bin distributions (law 1) or as arbitrary tabulated functions (law 4).

Inelastic level scattering is treated similarly to the elastic case. The only difference is the non-zero reaction Q-value, that slightly complicates the collision dynamics. Continuum inelastic scattering and (n,xn)-reactions are treated by sampling both the emission energy and the scattering angle from correlated distributions (laws 44, 66 and 67). The energy and momentum are not conserved in individual reactions, but the conservation laws hold on average.

Scattering from bound nuclei replaces the free-gas elastic scattering for some commonly used moderator materials, such as light water, heavy water and graphite. The

bound scattering reaction consists of one or two inelastic reaction channels [87, 88]. The first channel is known as *incoherent inelastic scattering*, and it takes into account the presence of other atoms in the target molecule. The reaction is treated very similar to the continuum inelastic reaction, using correlated tabular energy-angle distributions in the laboratory frame[7].

The second reaction channel is confusingly called *elastic scattering*, as the energy of the neutron does not change in the collision. Such a reaction is related to scattering from various lattice structures, where the target mass is effectively infinite. The bound elastic scattering can have two components: coherent elastic scattering, in which case only certain discrete scattering angles are possible, and incoherent elastic scattering, in which case the distribution is continuous. The elastic angular distributions are given in a tabular format[8].

---

[7]There have been studies on the use of synthetic analytical scattering functions for modelling the incoherent inelastic reaction channel for hydrogenous moderators [89]. Although not crucial for code development, it might be an interesting research topic to include such models in the PSG code as well.

[8]The description of bound atom scattering was not found to be sufficiently detailed in the ACE format documentation [14] and some details of the exact methodology had to be looked up in the MCNP4C source code. These are the only few lines of PSG source code not completely written from scratch.

Chapter 9

Group Constant Generation in Monte Carlo

9.1 Diffusion Coefficient in Monte Carlo

The generation of homogenised group constants for deterministic reactor simulator codes may seem like a natural application for the Monte Carlo method. It is quite surprising, however, that the studies related to the topic are not as numerous as might be expected. One reason is probably the lack of computer resources. The capacities of affordable workstations and computer clusters have only recently become sufficient for the task and code development simply lags behind. The technique has not yet been put into practice, at least on a large scale, and it may take years before Monte Carlo codes are used for group constant generation in a routine manner.

The homogenisation of reaction cross sections is trivial and can be carried out using the standard functionality of any Monte Carlo neutron transport code. The same applies to assembly discontinuity factors. Group-transfer cross sections are not a problem either, but the calculation requires certain special techniques that are usually not included in the standard routines of general-purpose codes.

The real challenge lies in the calculation of diffusion coefficients. All the other group constants can be directly derived from continuous-energy reaction cross sections, but the diffusion coefficient is based on an *approximation*. The parameter is required in diffusion calculations to characterise the rate of neutron leakage over the geometry boundaries, but the exact definition may vary. It is an inevitable fact that the diffusion coefficient plays no role in Monte Carlo calculation and any attempt to calculate this parameter will lead to certain problems.

Fick's law (4.8) suggests that the diffusion coefficient could be calculated as the ratio of neutron current density and flux gradient. This definition, however, is not useful in the Monte Carlo method, simply because the integration of such parameters is not possible in practice. Current integrals can be defined in principle, but the high level of flux symmetry in most practical cases implies that both positive and negative values are scored, which leads to close-to-zero results with excessively large variances.

A better solution is to calculate the diffusion coefficient using the transport cross section, as defined in Eqs. (4.9) and (4.10). This solution, however, is not without problems either. The transport cross section should basically be homogenised using the current spectrum, not the flux spectrum as the weighting function (see Appendix A). Since the integration of the current density is not possible in practice, the only option is to calculate the flux-weighted transport cross section and accept the fact that the results are inconsistent with theory. The flux spectrum is generally softer than the current spectrum, which leads to the an under-estimation of the diffusion coefficient.

9.2 Previous Studies

The procedures used for group constant generation in PSG are discussed in this chapter. Before going into details, some previous studies are introduced. Group constant generation using MCNP was studied at VTT some years ago [90]. A special tallyx-subroutine[1] was written for MCNP4C [14] to simplify the calculation of homogenised group-wise cross sections. The same subroutine was used in an attempt to calculate the diffusion coefficients, but the results were not found to be satisfactory. The project was discontinued before conclusive results had been attained [91].

9.2.1 Group Constant Generation in Existing Monte Carlo Codes

All Monte Carlo neutron transport codes are probably capable of calculating volume- and energy-integrated reaction rates, from which the homogenised reaction cross sections can be derived as described in Section 4.2.1 of Chapter 4. The calculation of assembly discontinuity factors is not a problem either. It is not possible to list all the codes that are capable of generating diffusion coefficients, group-transfer cross sections, effective delayed neutron fractions and other non-standard output parameters, but it is assumed that some of the most widely used codes, such as MCNP [14], KENO [52], TRIPOLI [92] and MVP [82], are not capable of the task. Two significant exceptions are briefly introduced below.

---

[1]The MCNP tallyx-subroutine is subroutine supplied by the user for the modification of the result estimates.

VIM is a continuous-energy Monte Carlo neutron/photon transport code, developed at the Argonne National laboratory [93]. The VIM 4.0 code [94] calculates k_{eff} estimates, macroscopic reaction rates and cross sections integrated over different material regions and energy groups. The optional output includes isotopic reaction rates, microscopic cross sections, integral net currents and various microscopic group-to-group scattering cross sections and average scattering cosines. These parameters are sufficient for deriving the group constants needed for diffusion calculation.

MCU is a continuous-energy Monte Carlo code, developed at the RRC Kurchatov Institute [18]. The code is able to calculate few-group constants, effective delayed neutron fractions and diffusion coefficients using different methods. Delta-tracking is available as an alternative tracking method and the code is capable of burnup calculation. Unfortunately the MCU code was not available at VTT at the time of this study and the methodology description in Ref. [18] does not go into details.

9.2.2   R. C. Gast 1981

The problem of calculating neutron diffusion coefficients using the Monte Carlo method was studied by R. C. Gast in 1981 [21]. The report reviews various deterministic methods and concludes that most of them cannot be used in Monte Carlo calculation. The main reason is that the methods require the spatial integration of flux gradients and current densities, which as discussed above, produces unreasonably large statistical errors in the result estimates.

The only viable option for the Monte Carlo method is the Selengut-Goertzel type diffusion coefficient, which is defined using the transport cross section as in Eqs. (4.9) and (4.10) in Chapter 4. The average scattering cosine multiplier in (4.10) is obtained from the scattering angles recorded from physical interactions. The method was implemented in the RCP01 code, which is still in use today [16].

It is recognised that the appropriate way to homogenise the transport cross section is to use the neutron current density as the weighting function. The RCP01 code uses an empirical correction factor to adjust the final value of the (flux-weighted) diffusion coefficient. Comparison calculations show that the results are sufficiently close to deterministic reference values.

9.2.3   E. L. Redmond II 1997

E. L. Redmond II approached the homogenisation problem in his Ph.D. studies at the Massachusetts Institute of Technology (MIT) in the late 1990s [22]. Extensive mod-

ifications were made to the MCNP4B code for the direct calculation of homogenised group constants. Since the generation of group-wise reaction cross sections is relatively straightforward using the standard version of MCNP, the work was focused on group-transfer cross sections and the Legendre components of differential scattering cross sections[2].

The approach taken in the study was to extend the existing capabilities of MCNP, without disturbing the course of simulation. Two methods were developed for the calculation of group-transfer cross sections. The first method takes advantage of the standard MCNP scattering routines and calculates a Monte Carlo estimate for $\Sigma_{s,g'\to g}$ by simulating scattering events for one or several target nuclei. The second, explicit method, calculates the group-to-group scattering rates by integration from the associated ENDF scattering laws. Similar methods were used for calculating the group-wise fission spectra.

The Monte Carlo approach used for calculating the group-transfer cross sections also produces the PDF distributions of scattering cosines, which are needed for estimating the Legendre scattering components. An alternative direct method was developed as well. The number of energy groups and the Legendre order of scattering cross sections was not restricted. Assembly discontinuity factors are briefly mentioned in connection with methods developed for the simplified calculation of cell-to-cell current estimates, but the topic is not discussed in detail. Kinetic and delayed neutron parameters or leakage models and fundamental mode calculation are not covered.

The calculation methods were validated by running three test problems and the results were found to be satisfactory, despite the inconsistent flux-weighting of the Legendre scattering cross sections.

9.2.4 G. Ilas and F. Rahnema 2003

G. Ilas and F. Rahnema from Georgia Institute of technology have studied the use of a Monte Carlo based nodal diffusion method for criticality analysis of spent LWR fuel storage lattices [23]. The motivation for the study was to combine the accuracy of continuous-energy Monte Carlo calculation and the computational efficiency of the nodal diffusion method. In a fuel storage geometry, sharp flux gradients near the interface between the assembly wall and the surrounding water may lead to difficulties when deterministic transport methods are used for homogenisation. This is not a problem for the Monte Carlo method.

---

[2]The intention was to be able to generate input parameters not only for diffusion codes, but for codes using higher-order P_N methods as well. The spherical harmonics methods are extensively covered in various textbooks [7–9].

The MCNP code was used for calculating homogenised two-group reaction cross sections and flux discontinuity factors. In addition, three methods were developed for the calculation of diffusion coefficients. The lattice cell geometry was divided into two regions, one consisting of the fuel assembly and the other of the surrounding water gap. The two-group cross sections and diffusion coefficients were calculated separately for each region.

The first two methods are based on the Selengut-Goertzel definition of the diffusion coefficient, using the transport cross section. In the first method, both group-wise transport cross sections in the fuel region and the thermal transport cross section in the water region were approximated by the total cross sections. The fast transport cross section in the water was used as a free parameter, which was adjusted to attain the k_{eff} in the diffusion calculation equal to the eigenvalue of the Monte Carlo calculation. The procedure was based on the assumption that the cell-to-cell leakage is mainly dependent on fast neutron streaming.

In the second method, the group-wise transport cross sections were calculated directly, using similar methods to those introduced in Section 9.2.2. The task was accomplished by using a special tallyx-subroutine. The empirical correction factor used by Gast to account for the inconsistency of using flux as the weighting function in the homogenisation was not applied in this study.

The third method was based on the preservation of the multiplication factor by allowing variation in the values of all diffusion coefficients. The task is basically reduced to an optimisation problem involving four free variables, and it was solved using a genetic algorithm. It should be noted that this method differs significantly from all the other methods based on the transport cross section.

The above methods were validated by benchmark calculations. The results of nodal diffusion calculation were compared to results obtained from an MCNP simulation of the full-scale storage rack. It was concluded that all three methods perform well in the test cases.

G. Ilas et al. have also studied few-group cross section generation for high-temperature gas-cooled pebble bed reactors (PBR) [95]. The emphasis was on the analysis methods used for modelling the double-heterogeneous reactor configuration[3]. MCNP calculations were compared to deterministic results and the effects of different assumptions on the results discussed. The Monte Carlo calculations were restricted to multiplication factors, spectral indexes and six-group capture and fission cross sections.

---

[3]The "double-heterogeneous" configuration refers to the random dispersion of the microscopic fuel particles inside the macroscopic pebbles, as well as the random orientation of the pebbles in the reactor core.

9.2.5 M. Tohjoh et al. 2005

M. Tohjoh, M. Watanabe and A. Yamamoto used the continuous-energy Monte Carlo code MVP-BURN [96] for generating group constants for full-core BWR reactor simulator calculations [24]. The standard version of MVP-BURN can be used for the calculation of homogenised reaction cross sections and assembly discontinuity factors. The code is unable to produce diffusion coefficients or group-transfer cross sections, and methods were developed for their calculation without making modifications in the source code.

The method used for calculating diffusion coefficients is very simple, and it is based on the transport cross section. The group-wise total and scattering cross sections were taken from the Monte Carlo calculation and fixed values were used for the average scattering cosine: 0.667 for scattering from hydrogen and 0.35 for all the other reactions.

Group-transfer cross sections were calculated for a three-group structure, consisting of fast, resonance and thermal energy groups. The method is based on neutron balance in the infinite-lattice calculation. If up-scattering is assumed negligible and all reaction cross sections are given by the Monte Carlo calculation, the unknown group-transfer cross sections are easily solved from the set of algebraic group-diffusion equations.

A special feature of the MVP-BURN code system is the capability to perform burnup calculation. This enabled the generation of a full set of group constants for various burnup and thermal hydraulic conditions. The results were successfully validated first by comparing them to reference data produced by a deterministic lattice code, and then by using the generated parameters in three-dimensional full-core nodal diffusion calculation.

9.2.6 S. C. van der Marck et al. 2006

The last study presented here was carried out by S. C. van der Marck, J. C. Kuijper and J. Oppe at the NRG. Homogenised group constants were generated for the full-core analyses of the Petten High Flux Reactor (HFR) in the Netherlands [25]. The motivation for the study was the high level of heterogeneity in the reactor core. The HFR is used for irradiation studies and isotope production. Fissile and high-absorbing material samples are often irradiated in the core, which has a significant impact on the neutronics. The homogenisation of the complicated geometry regions requires detailed modelling and advanced transport methods based on continuous-energy Monte Carlo calculation.

The MCNP code was modified to write a binary output file containing data on all collisions taking place during the transport cycle. This output file is read by a processing code called ELNINJO, which uses the data together with some standard tally output to generate homogenised group constants using the analog collision estimator. The system is able to produce all macroscopic and microscopic reaction cross sections, group-transfer cross sections and flux-weighted transport cross sections. The reason for this approach was that the calculation of all required reaction cross sections in a complicated geometry would be far too time-consuming using the standard track length tallies of MCNP.

The coupled system was validated in two test cases. The generated group constants were used in diffusion calculations and the final results compared to reference data. It was concluded that the method is able to reproduce multiplication factors and flux distributions consistent with deterministic and Monte Carlo calculations. The code system is currently used for the Petten HFR core analyses in a routine manner.

9.3 Result Estimates in PSG

The PSG code calculates automatically various integral parameters, criticality eigenvalues, homogenised group-wise reaction cross sections, group-transfer cross sections, diffusion parameters, assembly discontinuity factors, delayed neutron parameters and some kinetic parameters. The energy group structure is unrestricted, but so far mainly two-group calculations have been studied. The procedures used for the calculation of the default parameters are discussed in the following.

The code output also includes data on simulated physical events, reaction modes, and the number of source neutrons simulated, absorbed and leaked, and so on. User-defined detectors[4] can be set up for the calculation of various integral and spectral reaction rate and cross section estimates in physical or superimposed detector cells and lattices. A superimposed cell refers here to a cell that is used for detector calculation only, and not as a part of the actual geometry.

9.3.1 Eigenvalues

PSG uses by default the k-eigenvalue criticality source method (see Section 5.5.2 of Chapter 5) for the simulation of a self-sustaining chain reaction. The eigenvalue of the simulation is given by the ratio of source size between two successive neutron

---

[4]The commonly used Monte Carlo term "tally" is not used for PSG detectors, since the word translates very poorly in Finnish.

cycles, as defined in Eq. (5.52). When this value is averaged over all active cycles, the result is an analog estimate of the effective multiplication factor, also called the *generation estimate* of k_{eff}.

An implicit *absorption estimate* is also calculated, as the ratio of total neutron production and loss by absorption and leakage. The reaction rates are calculated using the collision estimator, discussed in Section 6.1.2 of Chapter 6. Leakage is scored each time a neutron escapes the system through the outer boundary of the geometry. When the leakage rate is omitted, the result is the absorption estimate of k_{∞}, which is also calculated by default.

PSG has two alternative criticality source methods, both aiming at $k_{\text{eff}} = 1$ by artificially modifying the neutron population during the simulation. In the α-eigenvalue method (see Section 3.2.3 of Chapter 3 and Section 5.5.2 of Chapter 5), the modification is based on time-absorption or -production reactions with an effective reaction cross section α/v. The value of α is iterated to attain criticality. The second method is the B_1 fundamental mode calculation method, discussed more thoroughly in Section 9.5. The method has a certain analogy with the α-eigenvalue calculation in that the neutron population is modified by leakage-absorption or -production reactions. The reaction rate is adjusted by iterating the geometry buckling to yield $k_{\text{eff}} = 1$. Both methods are currently under development and have not been comprehensively tested. The preliminary results have been promising but not completely satisfactory.

9.3.2 Homogenised Cross Section

The homogenisation of reaction cross sections was discussed in Section 4.2.1 of Chapter 4 and the calculation of flux and reaction rate integrals in Monte Carlo described in Chapter 6. Unlike most general-purpose codes, PSG calculates homogenised cross sections directly[5]. Cycle-wise integral reaction rate and flux estimates are calculated from the scores recorded during each cycle. The results are combined according to (4.42), which yields a cycle-wise estimate of the homogenised cross section. When the procedure is carried over all active cycles, the result is a sequence of values that is used for calculating the statistical mean and the associated standard deviation of the parameter.

Diffusion calculations require absorption, fission production and group-transfer (or -removal) cross sections, fission spectra and diffusion coefficients. The calculation of the first two parameters is simple, and carried out as described above. The generation

---

[5]General-purpose codes like MCNP can be used for calculating integral flux and reaction rate tallies in each material region. Homogenised cross sections and the associated statistical errors are calculated by combining these results after the simulation is completed. PSG extends the integration over the entire lattice geometry and combines the results already during the simulation.

of diffusion parameters is the topic of Section 9.3.3. The remaining two terms require some explanation.

The difficulty in the calculation of group-transfer cross sections (4.6) is that the differential scattering cross sections do not exist in the ACE format interaction data. Scattering reactions are described by the *total* scattering cross section (see Eq. (3.11) in Chapter 3) and separate energy-dependent distributions for the scattering angle. Some inelastic reactions also include energy distributions for the emitted neutron(s).

It is hence necessary to take a different approach. PSG calculates the *group-transfer probability*, which can be written as:

$$P_{g' \to g} = \frac{\int_V \int_{E_g}^{E_{g-1}} \int_{E_{g'}}^{E_{g'-1}} \Sigma_{\mathrm{s}}(\mathbf{r}, E' \to E) \phi(\mathbf{r}, E') d^3 r dE dE'}{\int_V \int_{E_{g'}}^{E_{g'-1}} \Sigma_{\mathrm{s}}(\mathbf{r}, E') \phi(\mathbf{r}, E') d^3 r dE'} . \tag{9.1}$$

This probability is easily calculated using an analog Monte Carlo estimator (the fraction of neutrons scattering from group g' to g). The group-transfer cross section is then calculated by multiplying the corresponding group-transfer probability by the homogenised total scattering cross section:

$$\Sigma_{\mathrm{s},g' \to g} = P_{g' \to g} \Sigma_{\mathrm{s},g'} . \tag{9.2}$$

It is easy to see that this definition is consistent with that given in Chapter 4. The denominator in (9.1) is the integral total scattering rate and the numerator the integral group-transfer rate.

The fission neutron emission spectra in the ACE data are given in such a format that direct integration similar to (4.4) becomes complicated. The group-wise fission spectrum χ_g is calculated using an analog Monte Carlo estimator, based on the emission probabilities calculated from the physical fission events.

9.3.3 Diffusion Parameters

Various methods for the calculation of diffusion coefficients were discussed in Sections 9.2.1–9.2.6. The common feature is the preservation of some physical quantity when the group constant data is used for diffusion calculation in the homogenised medium. This principle is very similar to the preservation of the integral reaction rate balance, which is the basis of cross section homogenisation. There is, however, one crucial difference, which has been discussed several times throughout this text. The diffusion coefficient, or the transport-corrected total cross section (transport cross

section) from which it is often derived, have no continuous-energy counterparts in general transport theory. The parameters are, instead, based on an approximation.

Most of the methods discussed above rely on the preservation of the linearly aniso-tropic scattering component, which is characterised by the total scattering cross section and the cosine of the average scattering angle. The procedure necessarily yields inconsistent results in Monte Carlo calculation, since the homogenisation has to be carried out using the flux spectrum as the weighting function. This method is applied in PSG as well[6], but the code mainly relies on a completely different approach.

It was shown in Section 4.1.3 of Chapter 4 that according to diffusion theory, the mean of the square-distance the neutrons migrate in a homogeneous medium is directly related to the diffusion area L^2. Using the result of Eq. (4.24), an analog estimate of the diffusion area in energy group g is given by:

$$L_g^2 = \frac{1}{6}\overline{r_g^2},\tag{9.3}$$

where $\overline{r_g^2}$ is the mean value of all scored square distances that neutrons have made within energy group g. The starting points are the locations where neutrons have entered the group by fission or scattering from another (higher) energy group. The end points are the locations at which the neutrons are lost from the group either by absorption or scattering to another (lower) energy group.

An estimate for the diffusion coefficient in group g can be calculated directly from the previous result, using the definition in Eq. (4.20):

$$D_g = \frac{L_g^2}{\Sigma_{\mathrm{r},g}},\tag{9.4}$$

where $\Sigma_{\mathrm{r},g}$ is the group-removal cross section, calculated as in (4.14). The group-wise diffusion area in (9.3) is calculated as if the neutrons were diffusing through an infinite homogeneous medium. This is obviously not the case in the actual simulation taking place in a heterogeneous geometry, but it is, in fact, exactly what is meant by the homogenisation of the spatial dependence of the medium.

The group-wise diffusion areas and diffusion coefficients can be used for deriving other parameters, consistent with the assumptions made above. The transport cross section is given by:

$$\Sigma_{\mathrm{tr},g} = \frac{1}{3D_g},\tag{9.5}$$

---

[6]PSG actually calculates the flux-weighted Legendre scattering components up to order 3, and it is easy to extend the calculation to higher-order terms as well. The results have not been compared to any reference data, since the main focus has been on the generation of input parameters for diffusion codes. The generation of P_N scattering kernels is an important topic for future work.

the average scattering cosine by:

$$\overline{\mu}_g = \frac{\Sigma_{\mathrm{t}g} - \Sigma_{\mathrm{tr},g}}{\Sigma_{\mathrm{s},g}} \; ,$$ (9.6)

the migration area by:

$$M^2 = \sum_{g=1}^{G} L_g^2$$ (9.7)

and the material buckling by:

$$B_{\mathrm{m}}^2 = \frac{k_\infty - 1}{M^2} \; .$$ (9.8)

The entire methodology is based on the assumption that the diffusion approximation holds to within reasonable accuracy. This is, in fact, the only approximation that needs to be made, which is not the case in the other methods described above. The procedure is simple and straightforward, and it is considered to be the best means to calculate diffusion coefficients using the Monte Carlo method[7].

9.3.4 Kinetic and Delayed Neutron Parameters

The present version of PSG calculates analog and implicit estimates for various kinetic parameters. The reciprocal of mean neutron speed is calculated for each energy group and the full spectrum by integrating (4.2) over the entire geometry. The one-group value is used for calculating implicit estimators for prompt neutron lifetime:

$$l_{\mathrm{p}} = \frac{1}{v\Sigma_{\mathrm{a}}}$$ (9.9)

and neutron generation time:

$$\Lambda = \frac{1}{v\nu\Sigma_{\mathrm{f}}} \; .$$ (9.10)

These definitions are consistent with those given in Section 4.3.1 of Chapter 4. If the geometry is not infinite, neutron leakage is included in the denominator of (9.9).

The analog estimates are based on the physical interpretations of the two parameters. Prompt neutron lifetime l_{p} is defined as the average time between the birth of a neutron in fission and its eventual loss by absorption or escape. Neutron generation time Λ is the average time between neutron emission and the subsequent absorption

---

[7]The fact that different methods yield similar results for the diffusion coefficient may actually be an indication that diffusion theory is applicable in the system. If this is not the case, it is very difficult to say which method yields better results for the final application, since the entire calculation is based on false assumptions.

leading to a new fission. Both estimates are easy to calculate. PSG also calculates the mean delayed neutron emission time and a lifetime estimate that includes delayed neutrons.

It should be noted that the analog lifetime estimate fails in finite geometries, in which neutrons may also be lost by escape. The reason is that the instant of time the neutron leaves the system is not known, simply because the crossing of the outer boundary is not recorded in delta-tracking. Solutions to the problem are being considered.

Delayed neutron fractions can be defined either as physical or effective, as discussed in Section 4.3.2 of Chapter 4. The physical delayed neutron fraction β_0 is simply the fraction of neutrons emitted as delayed. PSG calculates this for each precursor group using a simple analog estimate based on the simulated fission events (see Table 4.1 on page 83 for some isotopic delayed neutron parameters).

The effective delayed neutron fraction β_{eff} is essentially a measure of the importance of delayed neutrons for the fission chain reaction. The definition is an approximation, which takes into account the spatial and energy-dependence of the emitted neutrons. Delayed neutrons are emitted at a relatively low energy and their potential to cause fission may differ significantly from prompt neutrons. It is hence essential to use the effective, instead of the physical fractions in deterministic reactor kinetics calculations.

According to transport theory, the effective delayed neutron fraction is calculated using the adjoint neutron flux as the weighting function (see Eq. (4.71) on page 86). Such a calculation is very complicated to perform using the Monte Carlo method, and practically impossible if continuous-energy interaction data is used. An alternative method for estimating β_{eff} using forward Monte Carlo calculation has been developed at the NRG [97, 98] and this method is implemented in PSG as well.

The basic idea is very simple. The effective delayed neutron fraction can be interpreted, not as the fraction of neutrons emitted as delayed, but rather as the fraction of fission reactions caused by delayed neutrons. Such an estimate is very easy to calculate, but the efficiency is not very good. A potential solution could be to use some non-analog method for delayed neutron emission, similar to the implicit neutron capture discussed in Section 6.4 of Chapter 6. The application of such a method will be studied in the future.

Delayed neutron parameters in the ACE format data are given in 6 or 8 precursor groups. The decay constants in the old six-group representation are different for each isotope, and it is hence important to calculate the effective decay constants for the homogenised data. These values are calculated as averages, weighted by the corresponding effective delayed neutron fractions.

The generation of delayed neutron parameters in Monte Carlo calculation has been studied quite extensively during the last few years [99, 100]. There has also been discussion on the calculation of the effective neutron generation time Λ_{eff}, which according to transport theory, should also be calculated as the adjoint flux-weighted average [101, 102]. This topic will be addressed in the future development of PSG.

9.3.5 Assembly Discontinuity Factors

It was discussed in Section 4.2.2 of Chapter 4 that advanced nodal codes allow the discontinuity of neutron flux over the node boundaries, which enables a more accurate description of the intra-nodal flux shape and the preservation of some important quantities, such as the volume-integrated reaction rates and the surface averaged flux and current over each boundary. The procedure results in the introduction of assembly discontinuity factors, which are calculated for each boundary surface and corner.

Since it is not possible to calculate surface and point fluxes using the collision estimator, the integrals in (4.45) and (4.46) must be approximated by volume-integrated values. The approach taken in PSG is to define surface and corner cells in a thin layer near the outer geometry boundary and write the discontinuity factor for surface (corner) i as:

$$F_{i,g} \approx \frac{\dfrac{1}{V_i} \displaystyle\int_{V_i} \int_{E_g}^{E_{g-1}} \phi(\mathbf{r}, E) d^3 r dE}{\dfrac{1}{V} \displaystyle\int_{V} \int_{E_g}^{E_{g-1}} \phi(\mathbf{r}, E) d^3 r dE} , \qquad (9.11)$$

where V_i is the volume of the microscopic surface (corner) region.

The thickness of the surface layer is a trade-off between the accuracy of the approximation and the efficiency of the estimate. Fuel assemblies are often symmetrical to at least some extent, which can be taken into account in the calculation.

9.4 Normalisation of Results

It was discussed in Chapter 6 that the neutron flux and reaction rate estimates calculated using the Monte Carlo method are more or less arbitrarily normalised and their values depend on the number of simulated neutron histories. The arbitrary normalisation is not an issue in the calculation of group constants, since the values are given by the ratios of two similarly normalised variables. In some cases, however, it is the absolute value of the parameter that is of interest. In such a case, the neutron source rate has to be normalised to some user-given value.

There are three optional normalisations available in the PSG code. The normalisation coefficient c is calculated from a user-defined fission rate, S_f (in fissions/s):

$$c = \frac{S_f}{\int_V \int_0^\infty \Sigma_f(E)\phi(\mathbf{r}, E)d^3rdE}, \qquad (9.12)$$

neutron emission rate, S_n (in neutrons/s):

$$c = \frac{S_n}{\int_V \int_0^\infty \nu\Sigma_f(E)\phi(\mathbf{r}, E)d^3rdE} \qquad (9.13)$$

or total power, P (in W):

$$c = \frac{P}{\int_V \int_0^\infty w\Sigma_f(E)\phi(\mathbf{r}, E)d^3rdE}. \qquad (9.14)$$

The first two normalisations are quite trivial and unambiguous, but the third one requires some interpretation. The coefficient w in (9.14) is the average energy *deposited* in the system per one fission reaction. The definition of this value is not as trivial as it may first seem. The average fission energy *released* was discussed earlier in Chapter 2 and the fission energy of ^{235}U is divided into different components in Table 2.1 on page 38. This energy, however, is not the same thing as the energy converted to heat in the reactor core.

Over 80% of the fission energy is deposited instantly at the fission site as the kinetic energy of the fission fragments. The energy of delayed betas is also deposited directly in the fuel. The deposition of the remaining recoverable energy depends on the system. Neutron and gamma leakage can be very low in a large power reactor core, but not completely ignored. It can be very difficult to estimate the exact amount of energy deposited in a system, especially if the transport calculation is able to track only neutrons. The only thing that is certain is that the 4.3% of total energy carried away by neutrinos can *never* be recovered.

Another problem arises from the time-dependence of the energy release. The delayed betas and gammas are emitted in the radioactive decay of fission product isotopes. When the reactor has been operated at a constant power level for a long time, the level of decay heat has reached an equilibrium, and the values given in Table 2.1 hold. The situation is different at reactor start-up. It takes time for the decay heat power to saturate and before that the total energy release per fission is a few per cent lower.

The maximum recoverable energy, 193.7 MeV, does not include the energy released in non-fission nuclear interactions. Most of the reactions have negative or zero

Q-values, so that no extra energy is released in the system. A significant exception is the (n,γ)-reaction, for which the Q-value ranges from about 4 to 10 MeV. An estimate of the average (n,γ)-energy released per one fission reaction in an infinite critical geometry is determined by the fraction of fission neutrons parasitically absorbed in the system:

$$w_\gamma = \overline{Q}_\gamma (\overline{\nu} - 1) \,, \tag{9.15}$$

where $\overline{Q}_\gamma$ is the average Q-value of the (n,γ)-reactions. Since the average number of emitted fission neutrons ranges from 1 to 6, it is clear that the (n,γ)-heating cannot be completely ignored.

Because of the uncertainties discussed above, it is very difficult to determine the exact amount of energy deposited in the system per one fission reaction. This energy is generally of the order of 200 MeV. Although completely coincidental, this value is confusingly close to the fission Q-value, which includes the energy lost to neutrinos.

The normalisation problem is solved in PSG by determining a user-defined value for the total energy deposited in the system per one ^{235}U fission. The values for the other actinide isotopes are scaled from this according to the ratios of the recoverable fission energies, which are found in the nuclear data libraries. The normalisation of reaction rates is necessary in detector-type calculations. It is also essential for the estimation of isotopic transmutation rates, which are needed in fuel depletion analysis (see Section 4.4 of Chapter 4). As was mentioned before, the capability to perform burnup calculation is one of the long-term plans in PSG development.

9.5   Leakage Models in Monte Carlo Calculation

Neutron leakage models in lattice calculation were discussed in Section 4.2.3 of Chapter 4. Such models were not applied, or even mentioned, in any of the studies introduced in Section 9.2. The use of leakage corrections with the Monte Carlo method is not an extensively covered research topic, although some studies have been carried out over the years [103, 104]. It is not known how many computer codes have been developed that actually use these methods. The only one encountered so far is the Russian MCU, although the exact methodology is not known[8].

The leakage model used in PSG is based on the same calculation routine used for the α-eigenvalue method (see Section 5.5.2 of Chapter 5 for details). The idea is that an additional cross section-like parameter is introduced in the tracking process,

---

[8]The MCU project website [18] mentions that the code has the capability to calculate "neutron transport functionals for infinite uniform heterogeneous lattices with translational symmetry with leakage given by buckling vector". The exact description of the methodology is not available.

and when the reaction occurs, the neutron is either multiplied ($k_{\text{eff}} < 1$) or killed ($k_{\text{eff}} > 1$). The value of the interaction parameter is homogeneous throughout the geometry and depends only on neutron energy. In the α-eigenvalue method, the parameter is given by α/v, where v is the neutron speed, and in the leakage method, by $D_h B_{\text{g}}^2$, where D_h is the diffusion coefficient and B_{g}^2 the geometry buckling. The eigenvalue, either α or B_{g}^2, is iterated to attain $k_{\text{eff}} = 1$.

The relation between neutron speed and energy is trivial. The diffusion coefficient, however, cannot even be defined as a continuous-energy parameter. The solution is to calculate the removal cross section and the diffusion area for each neutron cycle using an internally defined micro-group energy structure (group index h). The diffusion coefficients used for determining the leakage probability in the next cycle are then calculated from these parameters using similar methods to those discussed in Section 9.3.3. The leakage rate calculated in this way depends on neutron energy, although the dependence is not continuous.

It is assumed that this method is equivalent to (or at least close to) the B_1 fundamental mode approximation in transport theory. The verification of the method, however, still requires both theoretical work and comprehensive validation studies. The development of leakage models for PSG is among the most incomplete topics introduced in this study. This description was included mainly for the sake of completeness, since it was considered interesting to apply the method in some of the validation calculations discussed in Chapter 10.

The implementation of Monte Carlo leakage models is considered as one of the high-priority topics in PSG development. One of the problems encountered so far is that the existing models developed for deterministic codes [39] rely heavily on transport theory, and in many cases, on adjoint calculation methods. Such methods are not easily translated to Monte Carlo. On the other hand, the stochastic nature of the calculation process offers capabilities that are completely unavailable to deterministic codes. It is considered preferable in the spirit of Monte Carlo calculation, that the leakage model would be based on some analogy with the natural process, rather than mathematical derivation from transport theory.

A similar approach has been taken in some recent studies related to the calculation of effective delayed neutron fractions (see Section 9.3.4). Instead of relying on a strict mathematical approach involving transport theory and adjoint calculation, the methods are based on the physical interpretation of the problem. It is the author's opinion that this is the right way to develop new Monte Carlo based calculation methods. Complicated mathematical problems often turn out to be surprisingly simple and intuitive, when the flux-centred way of thinking is dropped and the problems are approached from the single neutron's point of view.

Chapter 10

Code Validation

10.1 Comparison Tools

Code validation is necessary for evaluating the reliability of the calculation system. The results are often subject to biases and uncertainties, which have to be taken into account in the applications. Physical deficiencies and programming errors can be identified by comparing the results to some reference data. Such data can be obtained from experimental measurements, or it can be produced by another code, known to give more reliable results. It should be noted that all computer codes use methods that are more or less based on approximations, and there is always some uncertainty in the results. Physical measurements and nuclear interaction data must not be considered flawless either, and the complexity of the problem has to be kept in mind.

This chapter summarises the validation work that has been carried out during PSG development. The majority of the studies consists of comparison calculations, in which LWR group constant data generated by PSG is compared to reference MCNP and CASMO results. The group constants are also tested in a simple reactor simulator calculation. Because of the stochastic nature of the calculation method, it is important to verify the statistical validity of the results. The current version of PSG has no built-in capability to perform any kind of statistical analysis. It is hence essential for code validation to test that the output parameters converge, that the error estimates are applicable and that the results are normally distributed.

The final section in this chapter deals with code performance. The typical running times are compared to other transport calculation codes and the parallel calculation capabilities of PSG are briefly discussed. The reference reactor physics codes used in the validation are introduced in the following.

10.1.1 MCNP

MCNP [14] is a Monte Carlo particle transport code developed at the Los Alamos National Laboratory. The current version of the code, MCNP5, was not available at VTT at the time of this study and the calculations were carried out using code version 4C. The MCNP code is probably the best known and the most widely used transport calculation code based on the Monte Carlo method. The geometry and physics descriptions are very general and the code can be used for a variety of neutron, photon and electron transport problems.

Because of the wide use and the long history of development, MCNP can be considered as one of the most reliable and best validated transport calculation codes. It was therefore seen well-suited as the main reference code for PSG validation. Since both codes use the same ACE format cross section data libraries, the uncertainties originating from evaluated nuclear data is cut to minimum. The MCNP results should not, however, be viewed as the "correct" answers to the problems. The calculations are subject to the same uncertainties, approximations and physical deficiencies as the calculations carried out using any computer code.

Despite its versatility in transport calculation, MCNP also has its limitations. The code has not been designed for lattice calculations in particular and it lacks the capability to generate group constant data directly. The standard version of the code calculates reaction rates integrated over energy and discrete material regions[1]. Since the geometries consist of several materials, group constants averaged over the entire assembly need to be combined from the partial results, as described in Eq. (4.43) in Chapter 4. The problem is that the combination of the statistical error estimates becomes complicated.

To ease some of the burden, a simple tallyx-subroutine was written to perform the integration over the entire geometry. The group constants are then calculated by dividing the integral reaction rates by the integral flux. The error estimates are given by the combination of two partial terms. The common practice in such a case is to use their square sum as the combined estimate [59]. The confidence intervals formed in this way are somewhat conservative and it is hence not reasonable to assess code performance by comparing the statistical error estimates to the directly formed estimates of PSG.

MCNP was used for calculating multiplication factors, prompt neutron lifetimes, group-wise reaction cross sections and assembly discontinuity factors. It was not

---

[1]Although the cell flux tally in MCNP can be defined for a combination of cells, it is always associated with a single material. Reaction rates integrated over multiple cells with different materials need to be calculated separately.

possible to calculate group-transfer cross sections or any diffusion parameters. The calculation of delayed neutron parameters was not possible either, but reference results calculated using a special NRG version of MCNP4C3 [97] were available for the validation.

All PSG-MCNP comparison calculations were run in the k-eigenvalue criticality source mode, or "KCODE" mode in MCNP terminology. The fundamental mode calculation and leakage corrections discussed in Chapters 4 and 9 are not included in MCNP methodology. The probabilistic treatment of unresolved resonances (see Chapter 7) is not yet possible with PSG and the treatment was disabled in the MCNP calculations as well. This deficiency is not considered too severe, as the impact on LWR criticality calculations is usually quite insignificant [63, 105].

10.1.2 CASMO

CASMO is a two-dimensional deterministic assembly burnup code developed by Studsvik Scandpower. The transport calculation is based on the method of characteristics using up to 70 energy groups. The code version used in this study was CASMO-4E [38], which has the capability to produce all the output parameters calculated by PSG in both zero-buckling and fundamental calculation modes.

The micro-group cross section data used in the calculations was based on two evaluated nuclear data files: ENDF/B-VI.8 and JEF-2.2. The corresponding ACE libraries were available for PSG calculations, but despite the same origin of the fundamental data, the uncertainties are expected to be larger than those encountered in the MCNP comparison.

The details of the CASMO-4E transport methods are not particularly well documented. One potential source of discrepancy is that CASMO uses an isotropic scattering model for all reactions, together with some artificial corrections in the transport calculation. It is known that the method may lead to problems in large material regions with highly anisotropic scattering properties, which is probably reflected in the results as well. It is also believed that there are some inconsistencies in the modelling of hexagonal geometries, which may become an issue in VVER-440 lattice calculations.

10.1.3 ARES

ARES [106] is a new reactor simulator code, under development at the Finnish Radiation and Nuclear Safety Authority (STUK). The code performs three-dimensional

175

two-group diffusion calculations based on the so-called Analytic Function Expansion Nodal method (AFEN). The nodal diffusion calculation is coupled to a thermal hydraulics model and the result is a static full-core simulation of the reactor response under different operating conditions. The input parameters are derived from data libraries produced by CASMO, in a format originally developed for the POLCA and SIMULATE reactor simulator codes.

ARES has the capability to model core behaviour throughout the entire operating cycle. The code can be used for various fuel management, core follow and reload design studies. The coupled reactor physics/thermal hydraulics model is able to cope with xenon transients, but the steady-state diffusion model is insufficient for reactor dynamics calculation. The output parameters include axial and radial power distributions, peaking factors, reactivity coefficients, various shutdown and safety margins, integral parameters and variables related to fuel burnup.

10.2   LWR Lattice Calculations

Two-dimensional LWR lattice calculations can be considered as the most important part of PSG validation. The task is divided in two parts. This section presents some results of PSG calculations in comparison with MCNP4C and CASMO-4E results. The following section deals with reactor simulator calculation using group constant data generated by PSG and CASMO-4E.

It was decided early in PSG development to take a systematic approach in code validation and construct a library of standard cases, which could be used for comparing the three codes in a routine manner. The library consists of various fuel assembly types in different geometries and operating conditions. The objective is to cover as wide range of reactor physical conditions as possible. So far the library includes:

– 32 VVER-440 reactor and storage lattices, two fuel assembly types, different fuel enrichments and operating conditions.

– 24 PWR UOX and MOX reactor lattices at full-power conditions with and without boron shim, a varying number of burnable absorber pins and two types of control rods.

– 24 BWR reactor lattices at full-power conditions, three variations of the basic fuel assembly type, varying coolant void conditions.

Of the total 80 comparison cases, three cases are presented here. Some of the main geometry parameters are summarised Table 10.1. The selected example cases have

Table 10.1: The main parameters of the LWR comparison cases.

Parameter	VVER-440	PWR MOX	BWR+Gd
Lattice type	127-pin hex.	17×17 sq.	10×10 sq.
Symmetry	1/12	1/8	1/2
Fuel pitch (cm)	1.230	1.260	1.295
Assembly pitch (cm)	14.70	21.50	15.38
Number of fuel pins	126	269	91
Number of burnable absorber pins	-	-	10
Number of water tubes	1	20	1[a]
Fuel enrichment (wt-% ^{235}U)	3.6	0.025	1.8-3.7[b]
Plutonium content (wt-%)	-	4.8-10.6[c]	-
Cladding material	Zr-Nb alloy	Zircalloy	Zircalloy
Moderator density (g/cm^3)	0.7207	0.7044	0.7396
Moderator boron conc. (ppm)	650	-	-
Moderator void fraction	-	-	0.4

[a] single square water channel covering 9 pin positions

[b] seven types of fuel pins

[c] three types of MOX pins

been used for code validation since the very beginning of the project. Some results have been published before [2, 3], although the differences to the reference calculations have been considerably narrowed down with code development.

The first case is a VVER-440 reactor lattice, which represents a typical uranium-fuelled PWR core from the neutronics point of view. The fuel type has a special significance for the Finnish nuclear industry, since there are two VVER-440 reactors operating at the Loviisa nuclear power plant. The case was included also to show that PSG can handle the geometrically more challenging hexagonal pin lattice.

The second case is a MOX-fuelled PWR lattice. This case is physically more complicated than the first, owing to the high plutonium content in the fuel. The characteristic features include high epithermal resonance peaks of plutonium isotopes, significant thermal neutron absorption and low fraction of delayed neutrons. The neutronics of a MOX fuel in the reactor core closely resembles that of a high-burnup UOX fuel.

The third case is a BWR reactor lattice with burnable absorber. The geometry is more asymmetric compared to the other two cases. It contains seven fuel pin types, including one with burnable absorber (Gd). As was discussed earlier, the use of localised heavy absorbers leads to efficiency problems with the delta-tracking method. This topic is revisited in Section 10.6.1.
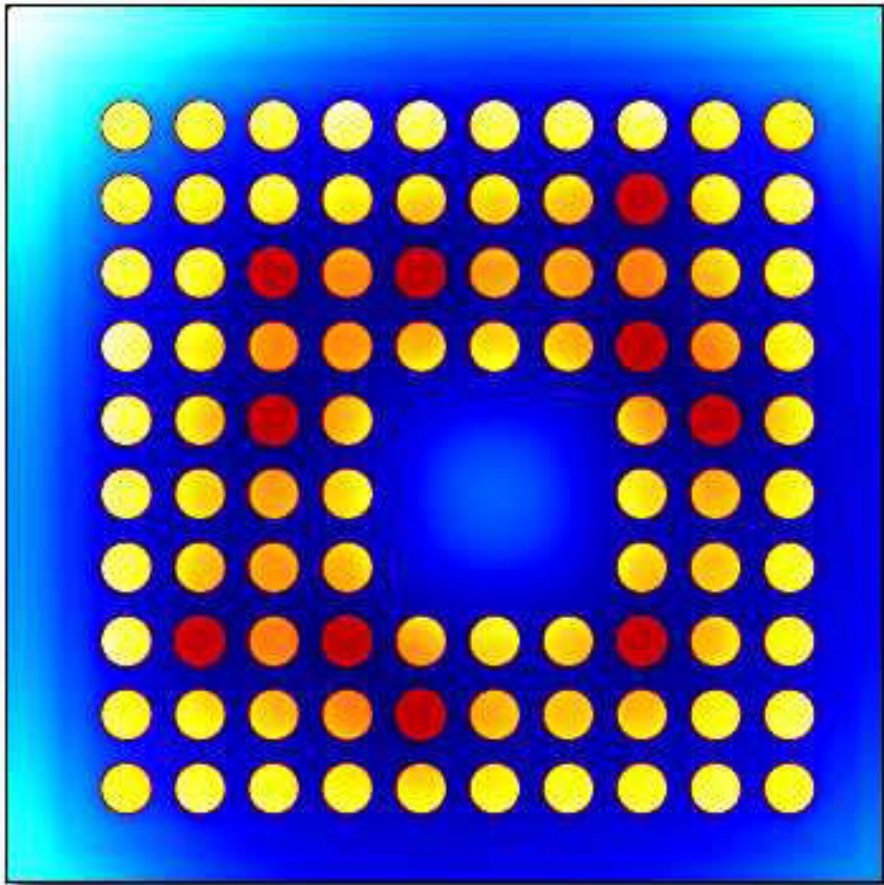
Figure 10.1: Thermal flux ("cold" shades) and fission rate ("hot" shades) distributions in the BWR fuel lattice. Bright and dark colours indicate high and low values, respectively.

The absolute values of the output parameters have no significance in this comparison study and they are hence not discussed in detail. In addition to numerical results, PSG has the capability to produce some graphical output, which can be useful for visualising the neutronics. One example is given in Figure 10.1, which shows the relative spatial distributions of thermal neutron flux and fission rate. The calculation case is the BWR fuel lattice with burnable absorber. Flux peaking in the water regions and its effect on fission rate in the nearby fuel pins is clearly visible. Burnable absorber pins are distinguished from the rest by the low fission rate caused by thermal neutron absorption in the gadolinium isotopes.

10.2.1 Comparison Between MCNP and PSG

Table 10.2 shows selected group-wise reaction cross sections and integral parameters calculated using MCNP and PSG. The same ENDF/B-VI.8 based cross section libraries generated at the Royal Institute of Technology (Sweden) [107] were used by both codes in each case. All calculations were run in the k-eigenvalue criticality source mode using 100 inactive and 500 active cycles of 5,000 source neutrons.

Each value is associated with a relative statistical error, which is given here in units of per cent. It is reminded that MCNP does not produce the group-wise cross sections directly. Instead, these parameters had to be calculated from the group-wise reaction rate and the corresponding group flux, which may result in a slight over-estimation of the combined statistical error.

Table 10.2 shows that the results are generally in a good agreement. The multiplication factors and most of the fast group reaction cross sections calculated by MCNP are within the 95% confidence intervals of PSG results. This is an indication that the differences are not statistically significant. The same calculations were repeated using several cross section libraries at different operating temperatures, and the differences remained similar in all cases.

The differences in the thermal group constants are relatively small as well, but in many cases by an order of magnitude larger than the discrepancies in the fast energy group. There also seems to be a systematic tendency to over-predict the values. This anomaly is one of the most persistent problems in PSG development. It is almost certain that the inconsistency originates from the thermal free-gas treatment (see Section 5.4.3 of Chapter 5) used for low-energy scattering reactions from other isotopes than bound hydrogen. This assumption is backed up by the fact that the differences are even larger when the bound atom scattering treatment is omitted and the free-gas treatment is used for hydrogen as well.

The assembly discontinuity factors are listed in Table 10.3. Because of the symmetry of the assemblies, all the surface and corner values are the same in the first two cases. The BWR lattice is more asymmetric and it has two unique boundary surfaces and three unique corners (the asymmetry can be seen Figure 10.1). It is seen that although the differences between the two codes are small, they are significantly larger compared to the homogenised group constants. One source of discrepancy may lie in the thickness of the surface cells used for calculating the local fluxes. Because of the delta-tracking method used by PSG, the surface layer had to be defined somewhat thicker in order to attain a sufficient number of scores.

The comparison of neutron spectra shows that PSG is able to reproduce the energy distribution calculated by MCNP. Figure 10.2 shows the flux spectra integrated over

179

Table 10.2: Group constants and integral parameters in the LWR lattice calculations. Comparison between MCNP and PSG.

Case	Parameter	MCNP	PSG	Diff. (%)
VVER-440	k_{eff}	1.26685 (0.030)	1.26678 (0.027)	-0.006
	l_{p} (μs)	18.062 (0.079)	18.019 (0.086)	-0.238
	$\Sigma_{\text{t},1}$	0.5275 (0.036)	0.5276 (0.015)	0.026
	$\Sigma_{\text{t},2}$	1.2441 (0.099)	1.2472 (0.024)	0.248
	$\Sigma_{\text{f},1}$	0.0029 (0.058)	0.0029 (0.060)	0.074
	$\Sigma_{\text{f},2}$	0.0605 (0.106)	0.0609 (0.053)	0.659
	$\Sigma_{\text{c},1}$	0.0071 (0.076)	0.0071 (0.073)	-0.014
	$\Sigma_{\text{c},2}$	0.0300 (0.099)	0.0302 (0.031)	0.507
	$\Sigma_{\text{s},1}$	0.5175 (0.036)	0.5176 (0.015)	0.026
	$\Sigma_{\text{s},2}$	1.1537 (0.099)	1.1562 (0.026)	0.219
	$\overline{\nu}_1$	2.5333 (0.071)	2.5335 (0.006)	0.007
	$\overline{\nu}_2$	2.4367 (0.113)	2.4367 (0.000)	-0.000
PWR MOX	k_{eff}	1.17775 (0.036)	1.17805 (0.035)	0.025
	l_{p} (μs)	3.524 (0.105)	3.528 (0.095)	0.104
	$\Sigma_{\text{t},1}$	0.5347 (0.036)	0.5344 (0.016)	-0.049
	$\Sigma_{\text{t},2}$	1.6453 (0.156)	1.6478 (0.037)	0.152
	$\Sigma_{\text{f},1}$	0.0056 (0.058)	0.0056 (0.058)	-0.058
	$\Sigma_{\text{f},2}$	0.2048 (0.163)	0.2053 (0.095)	0.242
	$\Sigma_{\text{c},1}$	0.0124 (0.076)	0.0124 (0.065)	-0.127
	$\Sigma_{\text{c},2}$	0.1514 (0.156)	0.1516 (0.095)	0.179
	$\Sigma_{\text{s},1}$	0.5166 (0.036)	0.5164 (0.016)	-0.047
	$\Sigma_{\text{s},2}$	1.2891 (0.163)	1.2908 (0.050)	0.134
	$\overline{\nu}_1$	2.9035 (0.071)	2.9037 (0.003)	0.005
	$\overline{\nu}_2$	2.8755 (0.170)	2.8755 (0.000)	0.001
BWR+Gd	k_{eff}	1.06779 (0.035)	1.06806 (0.040)	0.025
	l_{p} (μs)	28.236 (0.068)	28.125 (0.080)	-0.394
	$\Sigma_{\text{t},1}$	0.4562 (0.036)	0.4560 (0.014)	-0.042
	$\Sigma_{\text{t},2}$	1.2608 (0.099)	1.2629 (0.025)	0.168
	$\Sigma_{\text{f},1}$	0.0021 (0.067)	0.0021 (0.066)	-0.006
	$\Sigma_{\text{f},2}$	0.0323 (0.099)	0.0325 (0.070)	0.538
	$\Sigma_{\text{c},1}$	0.0052 (0.085)	0.0052 (0.083)	0.113
	$\Sigma_{\text{c},2}$	0.0317 (0.114)	0.0318 (0.076)	0.322
	$\Sigma_{\text{s},1}$	0.4489 (0.036)	0.4487 (0.015)	-0.044
	$\Sigma_{\text{s},2}$	1.1968 (0.099)	1.1986 (0.028)	0.153
	$\overline{\nu}_1$	2.5452 (0.085)	2.5454 (0.007)	0.008
	$\overline{\nu}_2$	2.4367 (0.099)	2.4367 (0.000)	0.000

Table 10.3: Assembly discontinuity factors in the LWR lattice calculations (the super- and subscripts are explained Section 4.2.2 of Chapter 4). Comparison between MCNP and PSG.

Case	Parameter	MCNP	PSG	Diff. (%)
VVER-440	$F_{1,1}^{\text{s}}$	0.9823 (0.153)	1.0097 (0.201)	2.797
	$F_{1,2}^{\text{s}}$	1.2058 (0.337)	1.2447 (0.414)	3.226
	$F_{1,1}^{\text{c}}$	0.9754 (0.661)	1.0023 (1.144)	2.766
	$F_{1,2}^{\text{c}}$	1.2677 (1.382)	1.2747 (1.756)	0.554
PWR MOX	$F_{1,1}^{\text{s}}$	0.9919 (0.163)	1.0048 (0.209)	1.303
	$F_{1,2}^{\text{s}}$	1.2418 (0.718)	1.2329 (0.695)	-0.713
	$F_{1,1}^{\text{c}}$	0.9627 (1.080)	1.0010 (2.073)	3.983
	$F_{1,2}^{\text{c}}$	1.5363 (5.151)	1.5783 (5.163)	2.737
BWR+Gd	$F_{1,1}^{\text{s}}$	0.9182 (0.114)	0.9282 (0.179)	1.094
	$F_{1,2}^{\text{s}}$	1.8897 (0.231)	1.8953 (0.237)	0.293
	$F_{2,1}^{\text{s}}$	0.9675 (0.114)	0.9788 (0.185)	1.175
	$F_{2,2}^{\text{s}}$	1.3150 (0.250)	1.3126 (0.298)	-0.182
	$F_{1,1}^{\text{c}}$	0.8717 (0.711)	0.8782 (1.313)	0.737
	$F_{1,2}^{\text{c}}$	2.6262 (0.913)	2.6821 (1.211)	2.129
	$F_{2,1}^{\text{c}}$	0.9092 (0.701)	0.9261 (1.331)	1.866
	$F_{2,2}^{\text{c}}$	2.0763 (1.032)	2.0751 (1.261)	-0.060
	$F_{3,1}^{\text{c}}$	0.9663 (0.681)	0.9961 (1.217)	3.082
	$F_{3,2}^{\text{c}}$	1.5862 (1.162)	1.6002 (1.484)	0.882

the VVER-440 fuel lattice. The two curves are completely overlapping and any differences are hard to see[2]. A closer analysis in Figure 10.3 shows mostly random variation between the two results, and the same consistency applies to the other two example cases as well. If the thermal free-gas treatment had been used for all isotopes, the differences in the Maxwellian energy peak would have been more clearly visible.

The MCNP-PSG comparisons given here represent quite well the results calculated for the 80 LWR lattices in the validation library. The differences are generally of the same order of magnitude and there are no particular configurations that would stand out by giving more inconsistent results. More cases will be included in the future and new problems may be encountered, but at this point it seems that the PSG code gives fairly consistent results compared to MCNP in these types of calculations.

---

[2]The high peaks in the Maxwellian thermal distribution in Figure 10.2 are due to the $S(\alpha, \beta)$ scattering laws used in the ACE format interaction data, not the result of any physical phenomenon.
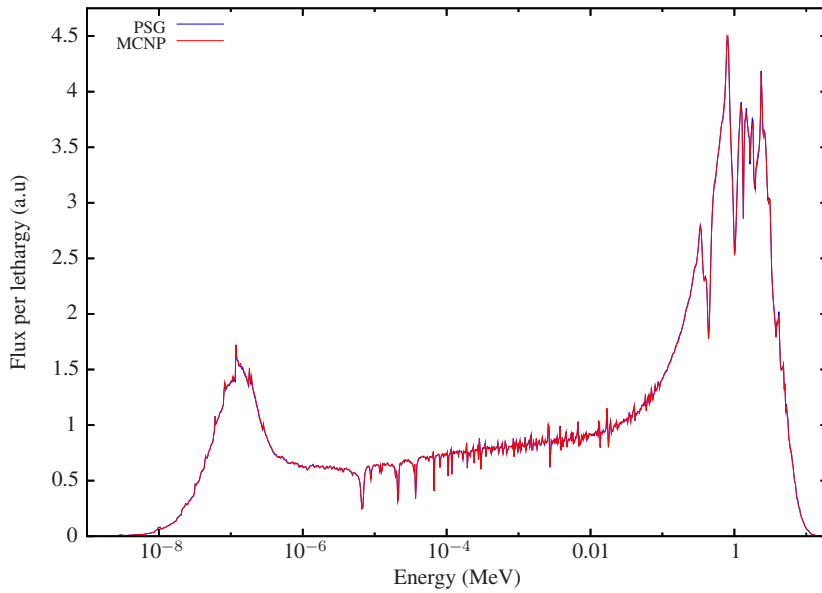
Figure 10.2: Flux spectra (flux per lethargy) integrated over the VVER-440 fuel assembly. The energy spectrum is divided into 1000 equally-spaced lethargy intervals.
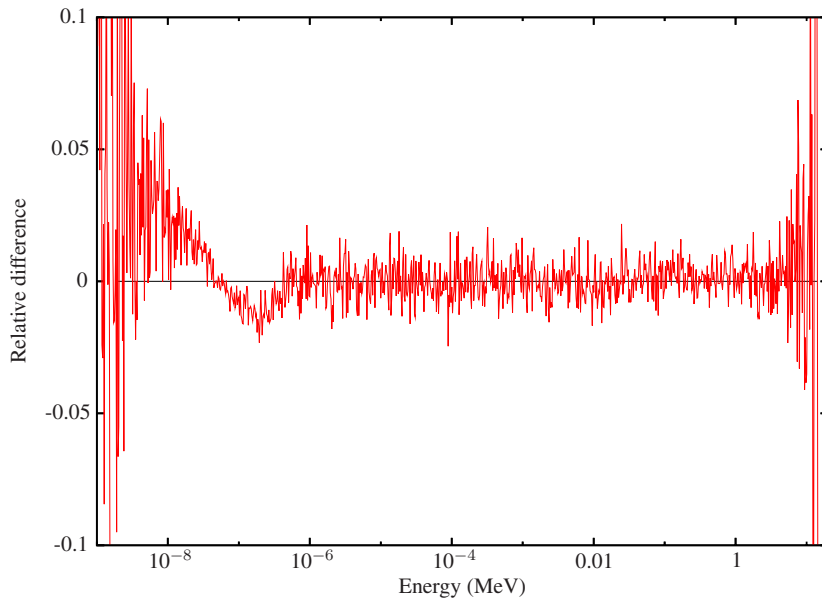
Figure 10.3: Relative differences between the two spectra in Figure 10.2.

10.2.2 Comparison Between CASMO and PSG

The comparison between PSG and CASMO is more problematic than the previous MCNP comparison. Even though the cross section libraries used in the calculations originate from the same evaluation (both ENDF/B-VI.8 and JEF-2.2 based libraries were used), the uncertainties cannot be narrowed down to zero because of the micro-group condensation of the CASMO data. The transport calculation methods are fundamentally different as well, and it is hence important to realise that the two codes are not even expected to yield exactly the same results.

When the results of the two codes are compared, there are three open questions to be kept in mind: 1) Are the observed differences larger than what is to be expected? 2) What are the reasons behind these differences? 3) What is the impact of the differences on the end results, if the group constants are used in a reactor simulator calculation? The last question is the most important one and some answers will be given in Section 10.3.

Since the validation of reaction cross sections and assembly discontinuity factors is easily carried out by a comparison between MCNP and PSG, the main focus here is on the parameters that cannot be calculated using the main reference code. Even though the development of leakage models and fundamental mode calculation in PSG is still under way, it was decided to include both calculation modes in the comparison to show that the leakage correction does have a small impact on of the results.

Zero-buckling Calculations

The calculations in the zero-buckling mode are consistent with the previous comparison between MCNP and PSG. Some of the results are presented in Table 10.4. It can be seen that even though the differences between the two Monte Carlo codes are less than about 0.5%, there are significantly larger differences between CASMO and PSG, even in simple reaction cross sections like Σ_a and $\nu\Sigma_f$. It is therefore not reasonable to expect smaller discrepancies in any other results either. This gives some insight to the first of the three questions above.

The parameters that cannot be validated by comparing to MCNP results are the fast removal cross section $\Sigma_{r,1}$[3], the migration area M^2 and the two diffusion coefficients D_1 and D_2. In each calculation case, the differences in the first two are of the order of a few per cent, which is of the same order of magnitude as the discrepancies in the reaction cross sections.

---

[3]The fast removal cross section in CASMO is defined as $\Sigma_{r,1} = \Sigma_{s,1\to 2} - \frac{\Phi_2}{\Phi_1}\Sigma_{s,2\to 1}$

Table 10.4: *Group constants and diffusion parameters in the LWR lattice calculations. Zero-buckling mode calculation, comparison between CASMO and PSG.*

Case	Parameter	CASMO	PSG	Diff. (%)
VVER-440	k_∞	1.26889	1.26678 (0.027)	-0.166
	$\Sigma_{a,1}$	0.0096	0.0100 (0.058)	4.336
	$\Sigma_{a,2}$	0.0876	0.0910 (0.045)	3.921
	$\nu\Sigma_{f,1}$	0.0070	0.0073 (0.059)	4.111
	$\nu\Sigma_{f,2}$	0.1423	0.1483 (0.053)	4.197
	$\overline{\nu}$	2.4584	2.4585 (0.002)	0.007
	$\Sigma_{r,1}$	0.0145	0.0149 (0.080)	2.404
	M^2	63.350	63.130 (0.082)	-0.347
	D_1 (method 1)	1.4124	1.4659 (0.082)	3.791
	D_2 (method 1)	0.4114	0.4277 (0.115)	3.975
	D_1 (method 2)	1.4124	1.0847 (0.018)	-23.200
	D_2 (method 2)	0.4114	0.3517 (0.029)	-14.500
PWR MOX	k_∞	1.18494	1.17805 (0.035)	-0.581
	$\Sigma_{a,1}$	0.0176	0.0180 (0.052)	2.182
	$\Sigma_{a,2}$	0.3513	0.3570 (0.095)	1.605
	$\nu\Sigma_{f,1}$	0.0161	0.0164 (0.058)	1.455
	$\nu\Sigma_{f,2}$	0.5812	0.5904 (0.095)	1.583
	$\overline{\nu}$	2.8888	2.8893 (0.001)	0.019
	$\Sigma_{r,1}$	0.0102	0.0102 (0.097)	0.634
	M^2	52.550	53.173 (0.092)	1.186
	D_1 (method 1)	1.4376	1.4828 (0.089)	3.146
	D_2 (method 1)	0.3043	0.2857 (0.163)	-6.109
	D_1 (method 2)	1.4376	1.0922 (0.020)	-24.024
	D_2 (method 2)	0.3043	0.2638 (0.053)	-13.303
BWR+Gd	k_∞	1.06882	1.06806 (0.040)	-0.071
	$\Sigma_{a,1}$	0.0072	0.0074 (0.066)	1.881
	$\Sigma_{a,2}$	0.0628	0.0643 (0.059)	2.312
	$\nu\Sigma_{f,1}$	0.0054	0.0054 (0.066)	1.500
	$\nu\Sigma_{f,2}$	0.0773	0.0792 (0.070)	2.451
	$\overline{\nu}$	2.4613	2.4613 (0.002)	-0.003
	$\Sigma_{r,1}$	0.0145	0.0147 (0.073)	0.995
	M^2	83.010	83.977 (0.080)	1.165
	D_1 (method 1)	1.6631	1.7102 (0.083)	2.830
	D_2 (method 1)	0.4107	0.4394 (0.104)	6.994
	D_1 (method 2)	1.6631	1.3026 (0.019)	-21.680
	D_2 (method 2)	0.4107	0.3509 (0.029)	-14.541

Table 10.5: *Group constants and diffusion parameters in the LWR lattice calculations. Fundamental mode calculation, comparison between CASMO and PSG.*

Case	Parameter	CASMO	PSG	Diff. (%)
VVER-440	k_∞	1.26616	1.25939 (0.031)	-0.535
	$\Sigma_{a,1}$	0.0093	0.0097 (0.065)	4.824
	$\Sigma_{a,2}$	0.0875	0.0909 (0.049)	3.826
	$\nu\Sigma_{f,1}$	0.0069	0.0072 (0.067)	4.527
	$\nu\Sigma_{f,2}$	0.1422	0.1480 (0.058)	4.105
	$\overline{\nu}$	2.4604	2.4607 (0.002)	0.013
	$\Sigma_{r,1}$	0.0137	0.0138 (0.097)	0.790
	M^2	66.910	66.802 (0.095)	-0.161
	D_1 (method 1)	1.4276	1.4916 (0.097)	4.488
	D_2 (method 1)	0.4118	0.4281 (0.133)	3.958
	D_1 (method 2)	1.4276	1.0956 (0.020)	-23.254
	D_2 (method 2)	0.4118	0.3523 (0.034)	-14.444
PWR MOX	k_∞	1.18829	1.18054 (0.038)	-0.652
	$\Sigma_{a,1}$	0.0172	0.0176 (0.059)	2.631
	$\Sigma_{a,2}$	0.3513	0.3564 (0.105)	1.443
	$\nu\Sigma_{f,1}$	0.0158	0.0161 (0.064)	1.805
	$\nu\Sigma_{f,2}$	0.5812	0.5896 (0.107)	1.432
	$\overline{\nu}$	2.8891	2.8897 (0.001)	0.019
	$\Sigma_{r,1}$	0.0098	0.0099 (0.107)	0.865
	M^2	54.650	54.737 (0.100)	0.159
	D_1 (method 1)	1.4485	1.4861 (0.099)	2.594
	D_2 (method 1)	0.3043	0.2842 (0.170)	-6.609
	D_1 (method 2)	1.4485	1.1005 (0.023)	-24.026
	D_2 (method 2)	0.3043	0.2643 (0.060)	-13.165
BWR+Gd	k_∞	1.06883	1.06826 (0.041)	-0.053
	$\Sigma_{a,1}$	0.0072	0.0073 (0.067)	1.838
	$\Sigma_{a,2}$	0.0628	0.0642 (0.063)	2.214
	$\nu\Sigma_{f,1}$	0.0053	0.0054 (0.068)	1.632
	$\nu\Sigma_{f,2}$	0.0773	0.0791 (0.073)	2.351
	$\overline{\nu}$	2.4619	2.4618 (0.002)	-0.002
	$\Sigma_{r,1}$	0.0143	0.0144 (0.076)	0.749
	M^2	84.210	84.876 (0.084)	0.791
	D_1 (method 1)	1.6677	1.7106 (0.089)	2.574
	D_2 (method 1)	0.4108	0.4393 (0.110)	6.942
	D_1 (method 2)	1.6677	1.3057 (0.019)	-21.703
	D_2 (method 2)	0.4108	0.3509 (0.030)	-14.583

Diffusion coefficients are calculated by PSG using two fundamentally different methods, both described in Chapter 9. Method 1 refers to the default method, which assumes the conservation of the group-wise diffusion area. The second method is based on the transport cross section, which is inconsistently homogenised using the neutron flux as the weighting function.

There are clearly large differences between the two methods. It was discussed in Section 9.1 of Chapter 9 that the flux-weighting of the transport cross section tends to under-estimate the diffusion coefficient. R. C. Gast used a similar method in his 1981 study with the RCP01 code [21], but the final results were modified using an empirical correction factor to account for the homogenisation inconsistency. It is interesting to notice that the correction factors used by Gast for LWR cases are in the order of 1.3. If similar corrections are applied to the PSG results, the differences between the two methods are considerably narrowed down.

It seems that the first method gives quite reasonable results compared to the reference CASMO calculations. This method is considered preferable in future calculations as well. The differences are, however, generally larger than the discrepancies in the other group constants. This is especially the case for the last two lattices, and the problem needs to be discussed more thoroughly.

At first it must be realised how different the methods used by the two codes actually are. PSG derives the value by calculating the mean square distance between the emission site and the site where the neutron is removed from the energy group by scattering or absorption. CASMO uses the transport cross section, which depends on the total and the scattering cross sections and the average scattering cosine, all tabulated in the micro-group data library.

There are several possible reasons for the observed discrepancies. The value of D_2 is over-estimated compared to CASMO in the VVER-440 and BWR lattices. The neutron spectra in these two cases are well thermalised and scattering from bound hydrogen atoms is particularly important. It is possible that the differences in the treatment of collision kinematics are simply pronounced here. In that case the differences could be emphasised in the BWR lattice, in which there are large water regions where the thermal flux is peaked (see Figure 10.1).

The thermal diffusion coefficient is under-estimated in the PWR MOX lattice. Thermal neutron absorption in the fuel is considerably stronger compared to the other two cases, as is also seen by comparing the absorption cross sections. The high absorption rate eats away the Maxwellian energy peak, shortens the thermal diffusion length and lowers the value of the diffusion coefficient. It is possible that the deterministic calculation method tends to under-estimate the self-shielding effect inside the fuel pins, which could be reflected in the value of the diffusion coefficient as well.

The given explanations are based on mere speculation. It must again be pointed out that, unlike the reaction cross sections and other group constants formed by homogenising the equivalent continuous-energy parameters, the calculation of the diffusion coefficient is based on an approximation. The diffusion approximation is expected to break down near strong absorbers and in material regions with highly anisotropic scattering properties. If the diffusion theory is not applicable, it is only natural that the two different interpretations of the diffusion coefficient become inconsistent as well.

The above discussion raises yet another question: is the calculation of the diffusion parameters reasonable at all in systems where the diffusion theory may not hold? The Monte Carlo estimate of D_g is potentially very accurate, but what happens if the underlying assumptions are incorrect? Unfortunately, there are no answers to these questions, and the only thing that can be done is to be aware of the potential flaws.

There is one more, somewhat disturbing issue that needs be addressed: the transport cross sections calculated by CASMO are actually homogenised using the *flux spectrum* as the weighting function, which contradicts everything discussed above. It seems likely, however, that the values are corrected in some way to yield better results in diffusion calculation[4]. The CASMO code has a long history and the calculation methods have been comprehensively validated in LWR calculations. Therefore, it seems reasonable to view the results as good reference values for this study, regardless of the exact methodology. Although several questions remain unanswered, this discussion clearly shows how complicated the whole concept of a diffusion coefficient really is.

Fundamental Mode Calculations

As has been discussed several times earlier in the text, the basic k-eigenvalue method in an infinite fuel lattice leads to a distorted flux solution if the source and absorption rates are not in balance. This distortion affects the values of the homogenised group constants as well and produces inconsistent results in the final reactor simulator calculation. The leakage correction applied in the fundamental mode calculation enforces neutron balance by adding or removing neutrons from the population, thus mimicking the effects of non-zero leakage currents over the node boundaries.

The simplest B_1-fundamental mode approximation assumes a homogeneous leakage rate over the entire lattice volume. The preliminary methodology developed for

---

[4]It was mentioned earlier that CASMO uses an isotropic scattering model and artificial corrections in the transport calculation. It is likely that the corrections have an impact on the value of the transport cross section and the diffusion coefficient as well.

Monte Carlo calculation was discussed in Section 9.5 of Chapter 9. The results of PSG fundamental mode calculation compared to CASMO results are presented in Table 10.5. All three calculation cases are super-critical in the zero-buckling calculation mode. The leakage correction hence removes the excess neutrons from the population.

A comparison between the results in Tables 10.4 and 10.5 shows that the leakage correction mainly affects the parameters in the fast energy group. The absorption, fission and removal cross sections are lowered by several per cent. The diffusion parameters, on the other hand, show slightly increased values. The effects are quite similar for both CASMO and PSG, but in most cases far less significant than the general differences between the two codes. At this point, it is quite impossible to analyse the results in more detail, and the topic is best left for future studies.

The example results presented here were calculated using ENDF/B-VI.8 based cross section libraries. Similar differences were observed when the calculations were repeated using the JEF-2.2 data.

10.3   PSG Group Constants in Reactor Simulator Calculation

When PSG is used for group constant generation, the main problem is the incapability to perform burnup calculation. This restricts the applicability quite significantly, but does not completely rule out code validation. In an effort to keep the calculation simple, yet realistic, a conceptual initial core of the European Pressurised Reactor (EPR) was chosen as the test case. The core is loaded with three types of fuel assemblies with fresh uranium fuel, enriched up to 3.3% in ^{235}U. Two assembly types are loaded with partial-length burnable absorber pins. Since PSG is not able to calculate equilibrium xenon concentrations, the core is assumed to be in a hot zero power (HZP) condition at an isothermal 600 K temperature.

The lattice calculation was carried out for each assembly type using the three transport codes: CASMO-4E, MCNP4C and PSG. The partial-length burnable absorber pins increase the number of cases from 3 to 5. The EPR control rods are composed of two separate absorber zones containing AIC and boron carbide absorber, which makes the total number of cases 15. PSG group constants were compared directly to MCNP and CASMO results and the data produced by CASMO and PSG used in ARES reactor simulator calculations. The PSG calculation time per case ranges from 6 to 8 minutes when 100 inactive and 500 active cycles of 5,000 neutrons were run, summing up to 110 minutes in overall calculation time.

Table 10.6: Results of ARES calculations using group constant data generated by CASMO-4E and PSG.

Case	Parameter	CASMO	PSG	Diff. (%)
CR withdrawn	Multiplication factor	1.00187	0.99682	0.504
	Radial power peaking	1.3931	1.3835	0.689
	Axial power peaking	1.4667	1.4649	0.123
	Nodal power peaking	2.0448	2.0279	0.826
	Axial offset	-0.1300	-0.1375	-5.769
	Fast-to-thermal flux ratio	5.5732	5.6473	-1.330
CR inserted	Multiplication factor	0.68786	0.67280	2.190
	Radial power peaking	1.6171	1.6180	-0.056
	Axial power peaking	3.2387	3.1950	1.349
	Nodal power peaking	5.2103	5.1409	1.332
	Axial offset	-0.9817	-0.9783	0.346
	Fast-to-thermal flux ratio	9.5892	9.9068	-3.312

The comparison of two-group constants shows very similar results to the three test cases discussed in the previous section. The PSG results are well consistent with the MCNP calculations and differences compared to CASMO are of the order of a few per cent. This is also the case for the diffusion parameters calculated using the default method. The comparison also involved some simple infinite-lattice reactivity coefficients. The moderator boron worth and fuel Doppler-coefficient were evaluated by calculating the change in k_∞, caused by the variation in boron concentration and fuel temperature, respectively. The results are very similar for all three codes.

The HZP calculations were carried out with control rods withdrawn by 94% of the maximum top position. The critical boron concentration was 1215 ppm. The same calculation was repeated with the control rods fully inserted. Some of the integral parameters calculated by ARES are presented in Table 10.6[5]. The axial power profiles at the core centre are plotted in Figure 10.4.

It seems that the results calculated using PSG group constants are well consistent with the reference results, especially for the critical core. This is exactly what was expected, since the differences in the parameters compared to CASMO values are not that significant either. There are larger discrepancies in the integral parameters when the control rods are inserted, but even then the differences are not very significant.

---

[5]The radial power peaking factor is defined as the maximum assembly power divided by core average. Axial and nodal peaking factors are defined similarly. The axial offset is related to the position of the axial power peak with respect to core mid-plane.
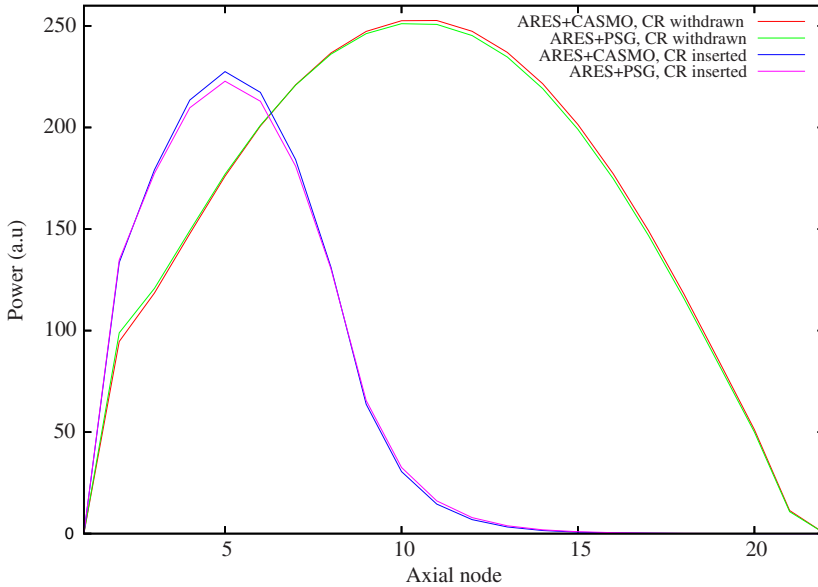
Figure 10.4: Axial power distributions at core centre. Group constants generated using CASMO and PSG.

The ARES code constructs homogeneous intra-nodal flux and linear power distributions at each axial nodal plane. The thermal flux distribution at core mid-plane is plotted in Figure 10.5 as an example. The relative differences between the results calculated using PSG- and CASMO-generated group constants are plotted in Figure 10.6. The maximum differences are just below 5% and similar discrepancies are found at higher and lower axial planes as well. The fast flux and linear power distributions are also in good agreement.

Some uncertainties in the PSG group constant data were taken for a closer analysis. As in the three test cases presented in Section 10.2, there is some significant statistical variation in the assembly discontinuity factors. This could also have an impact on the final results. The critical core ADF values are quite close to unity, which results from the relatively flat local flux distributions inside the assemblies. It turned out that the final results are not very sensitive to small variations in the assembly discontinuity factors, which was shown by forcing all values to unity. The effect on flux distribution was less than two per cent[6].

---

[6]Discrepancies in the assembly discontinuity factors could have a major impact on results if the flux is strongly peaked. Such a condition could result, for example, from the withdrawal of a single control rod cluster, while the other rods remain fully or partially inserted. This is a typical scenario in LWR transient analysis.

Figure 10.5: Thermal neutron flux distribution at core mid-plane. Group constants generated using PSG.

Figure 10.6: Thermal neutron flux distribution at core mid-plane. Relative difference between results calculated using PSG- and CASMO-generated group constants.

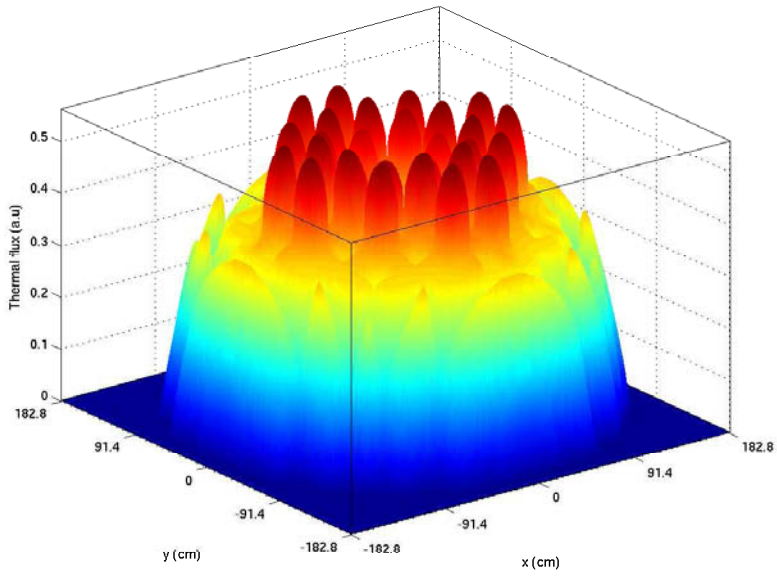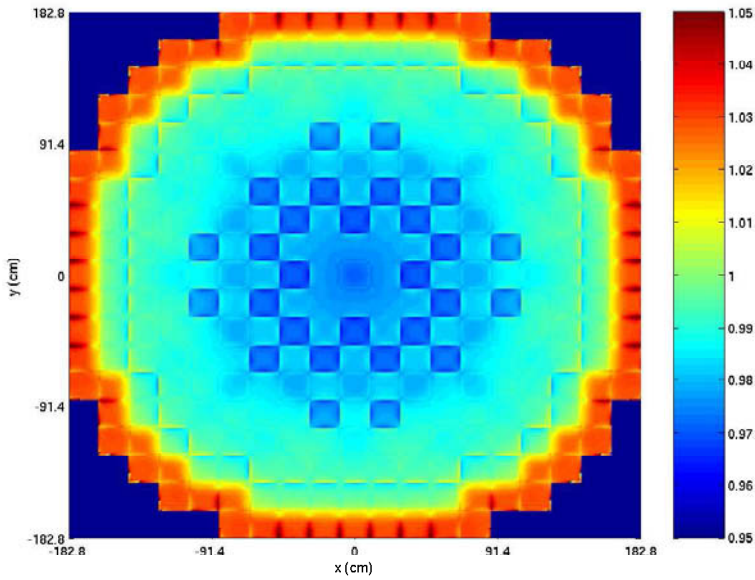Another interesting factor is the diffusion coefficient, which in PSG can be calculated in two fundamentally different ways. The alternative method yields values that are about 22% lower in the fast group and 13% lower in the thermal group, compared to the default method. The diffusion lengths increase considerably, which has a significant impact on the flux distributions. The maximum local differences in the mid-plane thermal flux distribution increase from less than 5% to over 15%. The effective multiplication factor increases from 0.99682 to 1.00031.

The group constant generation was carried out in the zero-buckling calculation mode, without leakage corrections. It was discussed in Section 10.2.2 that the impact of fundamental mode calculation is quite insignificant compared to the general differences between PSG and CASMO. The differences are even less pronounced in the reactor simulator calculation. This may seem a bit unexpected, as the importance of leakage models has been emphasised throughout this text. Even though the effect in this particular core is not very significant, this may not always be the case[7]. The impact of the leakage correction on flux spectrum is perhaps best seen in an assembly burnup calculation. Neutron leakage in the ^{238}U resonance region directly affects the rate of plutonium build-up, which may lead to large discrepancies in the group constants as fuel burnup increases.

This example case demonstrates that the group constant data generated by PSG can be used in a reactor simulator calculation, even though the applications are quite restricted without burnup capability. It should be noted that the ARES simulations were carried out in a zero-power condition, which means that the calculation does not include any actual thermal hydraulics. It is not clear how the thermal hydraulic feedback would affect the observed discrepancies. A well-known fact is, however, that the uncertainties related to the modelling of two-phase flow, nucleate boiling and other fluid phenomena clearly exceed the uncertainties in the neutronics.

10.4   Miscellaneous Results

This section covers some miscellaneous studies that have been carried out along with PSG development. The first case deals with the validation of delayed neutron parameters, omitted in the LWR lattice calculations in Section 10.2. The second case is a computational reactor dosimetry benchmark exercise, in which an experimental reactor configuration was modelled using PSG. The third case presents k_{eff} calculations

---

[7]The leakage correction basically affects both the homogenised group constants and the assembly discontinuity factors, and the overall effect may become quite complicated. Assembly discontinuity factors in CASMO/SIMULATE calculations are actually generated in a zero-buckling lattice calculation. The leakage correction can be implemented by modifying the values during the full-core simulation. A similar model is not available in the ARES code [108].

in various critical assemblies included in the Handbook of International Criticality Safety Benchmark Experiment Project (ICSBEP).

10.4.1 Delayed Neutron Parameters

The standard version of MCNP is incapable of calculating any delayed neutron parameters. A comparison with CASMO-4E results would have been possible, but it was instead decided to present a comparison with results provided by the NRG [109]. The comparison covers the same LWR lattices introduced in Section 10.2. The reference results were calculated using a special NRG version of the MCNP4C3 code [97]. The calculation of delayed neutron parameters in PSG is based on the same methodology (see Section 9.3.4 of Chapter 9). The same ENDF/B-VI based cross section libraries [110] were used by both codes and the results should be well comparable without additional discrepancies originating from the cross section data.

The physical and effective delayed neutron fractions are compared in Tables 10.7 and 10.8. Although the differences between the two codes are relatively large, they are generally within the limits of statistical accuracy. It seems that there are no large systematic discrepancies in the results.

It is immediately seen that the statistical accuracy is quite poor compared to the two-group cross sections, especially in the case of effective delayed neutron fractions. This largely results from the calculation method. The number of neutrons emitted as delayed is very small and only a fraction of those neutrons end up causing fissions. It is this chain of events that is scored for the estimate of β_{eff}. The statistical accuracy is slightly better for MCNP, probably owing to the use of implicit capture, which allows more delayed neutrons to end up causing fissions.

It should be noted that this comparison is the only validation study performed on the delayed neutron parameters at the time of writing. It is therefore quite premature to make any final conclusions about the capabilities of PSG for generating delayed neutron parameters for reactor dynamics calculations.

10.4.2 The VENUS-2 Benchmark

Although the main intended use of PSG is in reactor physics calculations at the fuel assembly level, it is important for code validation that more complicated experimental systems can be modelled as well. This was the main motivation for the VENUS-2 MOX-fuelled reactor dosimetry benchmark calculations. The results discussed here were also presented at the PHYSOR-2006 conference [4].

Table 10.7: Fundamental delayed neutron fractions in the LWR lattice calculation. Comparison between MCNP and PSG.

Case	Parameter	MCNP	PSG	Diff. (%)
VVER-440	β_0	734.70 (0.531)	735.34 (0.026)	0.087
	$\beta_{0,1}$	24.00 (2.917)	23.84 (0.003)	-0.663
	$\beta_{0,2}$	126.40 (1.266)	126.75 (0.010)	0.274
	$\beta_{0,3}$	123.40 (1.297)	123.11 (0.016)	-0.235
	$\beta_{0,4}$	283.80 (0.846)	284.27 (0.026)	0.165
	$\beta_{0,5}$	124.30 (1.287)	125.22 (0.050)	0.738
	$\beta_{0,6}$	52.70 (1.898)	52.16 (0.048)	-1.033
PWR MOX	β_0	403.50 (0.694)	406.30 (0.086)	0.693
	$\beta_{0,1}$	10.20 (4.902)	9.83 (0.041)	-3.610
	$\beta_{0,2}$	79.30 (1.639)	79.10 (0.049)	-0.253
	$\beta_{0,3}$	63.10 (1.743)	62.32 (0.070)	-1.243
	$\beta_{0,4}$	142.40 (1.194)	143.19 (0.096)	0.551
	$\beta_{0,5}$	79.80 (1.629)	82.51 (0.112)	3.395
	$\beta_{0,6}$	28.60 (2.797)	29.36 (0.131)	2.645
BWR+Gd	β_0	742.90 (0.525)	741.40 (0.027)	-0.202
	$\beta_{0,1}$	23.60 (2.966)	23.82 (0.004)	0.935
	$\beta_{0,2}$	126.00 (1.270)	127.09 (0.010)	0.867
	$\beta_{0,3}$	120.70 (1.326)	123.70 (0.016)	2.484
	$\beta_{0,4}$	287.60 (0.834)	286.59 (0.027)	-0.349
	$\beta_{0,5}$	131.80 (1.214)	127.23 (0.051)	-3.466
	$\beta_{0,6}$	53.20 (1.880)	52.96 (0.049)	-0.444

The VENUS facility (Vulcain Experimental NUclear Study) is a pool-type zero-power critical assembly located at the SCK•CEN in Mol, Belgium. The configuration of the VENUS-2 core consists of three types of fuel pins, including a MOX fuel with 2.7 wt-% plutonium content. The fuel is divided into separate regions and surrounded by a water reflector and various radial and axial zones consisting of water and structural materials.

The three-dimensional VENUS-2 MOX-fuelled reactor dosimetry benchmark was initiated in 2004 [111] and the project final report published in 2006 [112]. The experimental measurements at the facility consist of integral parameters, axial and radial fission rate distributions and detector dosimetry data, measured at various positions around the active fuel region.

Table 10.8: Effective delayed neutron fractions in the LWR lattice calculation. Comparison between MCNP and PSG.

Case	Parameter	MCNP	PSG	Diff. (%)
VVER-440	β_{eff}	714.30 (0.672)	727.34 (1.032)	1.826
	$\beta_{\text{eff},1}$	23.20 (3.448)	23.84 (5.863)	2.758
	$\beta_{\text{eff},2}$	125.80 (1.590)	120.93 (2.629)	-3.873
	$\beta_{\text{eff},3}$	118.70 (1.601)	122.33 (2.552)	3.059
	$\beta_{\text{eff},4}$	277.10 (1.083)	279.43 (1.679)	0.840
	$\beta_{\text{eff},5}$	118.40 (1.605)	128.64 (2.477)	8.648
	$\beta_{\text{eff},6}$	51.30 (2.534)	52.17 (4.161)	1.705
PWR MOX	β_{eff}	379.50 (0.870)	381.35 (1.300)	0.487
	$\beta_{\text{eff},1}$	9.60 (5.208)	8.32 (8.691)	-13.331
	$\beta_{\text{eff},2}$	76.30 (1.966)	73.03 (2.960)	-4.289
	$\beta_{\text{eff},3}$	59.60 (2.181)	59.70 (3.678)	0.171
	$\beta_{\text{eff},4}$	134.00 (1.493)	129.41 (2.274)	-3.425
	$\beta_{\text{eff},5}$	72.60 (2.066)	81.03 (2.838)	11.613
	$\beta_{\text{eff},6}$	27.30 (3.297)	29.86 (4.833)	9.367
BWR+Gd	β_{eff}	722.10 (0.720)	726.01 (1.139)	0.541
	$\beta_{\text{eff},1}$	22.60 (3.982)	21.90 (6.393)	-3.077
	$\beta_{\text{eff},2}$	122.30 (1.717)	123.95 (2.636)	1.348
	$\beta_{\text{eff},3}$	117.20 (1.792)	122.90 (2.637)	4.865
	$\beta_{\text{eff},4}$	278.40 (1.149)	278.19 (1.737)	-0.075
	$\beta_{\text{eff},5}$	128.30 (1.715)	122.55 (2.577)	-4.482
	$\beta_{\text{eff},6}$	53.20 (2.632)	56.51 (3.890)	6.230

The PSG calculations were not included in the official benchmark exercise project. The study was carried out independently for the purpose of code validation. The main interest was to see if PSG could handle detector-type calculations, in which reaction rates are integrated over small volumes. This task was expected to cause problems due to the limitations posed by the delta-tracking method.

The details of the calculations are presented in Ref. [4] and hence not repeated here. The main conclusion of the study was that it is possible to obtain statistically converged results, despite the poor efficiency of the collision estimator. The results are fairly consistent with the experimental measurements. Because of the large number of neutron histories run, the overall calculation time became too long for practical detector calculations. The study showed, however, that similar benchmark exercises could be used for code validation in the future.

10.4.3 ICSBEP Criticality Benchmark Calculations

The Handbook of International Criticality Safety Benchmark Experiment Project is a large collection of documented criticality experiments carried out over the past six decades. The data in the handbook is frequently used for validating computer codes and cross section libraries used for reactor physics calculations, especially criticality safety analyses. Such validation is important for determining the biases and uncertainties of the calculation system. These factors must be taken into account in the estimation of conservative criticality safety margins.

This study shows the results of criticality calculations in 10 experimental configurations. The number is not very large, mainly because most of the configurations are complicated in detail and the construction of the geometry models takes considerable time. The included experiments are summarised in Table 10.9. The first 7 cases are fast-spectrum systems made up of bare and reflected uranium and plutonium spheres. The remaining 3 cases are liquid solution systems consisting of different fissile isotopes. All experimental reactor lattice geometries are considerably more complicated and at this time not included in the study.

The PSG results are plotted Figure 10.7. The calculations were repeated using the reference MCNP4C code. Two cross section libraries were used in the calculations, one based on ENDF/B-VI.8 [107] and the other on JEF-2.2 [113] data. It can be seen that all the results are relatively close to the critical value. The two codes give very similar results when the same cross section library is used. It is also seen that the origin of the nuclear interaction data can have a major impact on the results. The cross section library based discrepancies clearly exceed the differences between the two codes. This example is a good remainder of the importance of knowing the biases and uncertainties of the interaction data. The topic has been thoroughly studied over the years and one such study is found in Ref. [65].

10.5   Statistical Considerations

It was discussed in Section 6.3 of Chapter 6 that from the central limit theorem it follows that the results of Monte Carlo calculation are normally distributed random variables. It was also stated that the law of large numbers implies that the associated standard deviations decrease as the number of active neutron cycles increases. The estimates converge towards the "true" result, i.e. the value that would be attained if the simulation was run forever. The advantage of having normally distributed results is that the interpretation of the standard deviations becomes simple, as they can easily be related to the corresponding confidence intervals.

Table 10.9: *The ICSBEP cases included in the study.*

| #	Identification	Description
1	HEU-MET-FAST-001	Bare HEU sphere (Godiva)
2	HEU-MET-FAST-002	Reflected HEU sphere (Topsy)
3	PU-MET-FAST-001	Bare ^{239}Pu sphere (Jezebel)
4	PU-MET-FAST-002	Bare ^{239}Pu + ^{240}Pu sphere (Jezebel)
5	PU-MET-FAST-005	Tungsten-reflected ^{239}Pu sphere
6	PU-MET-FAST-006	Uranium-reflected ^{239}Pu sphere
7	PU-MET-FAST-001	Graphite-reflected plutonium sphere
8	PU-SOL-THERM-004	Water-reflected plutonium nitrate solution
9	HEU-SOL-THERM-001	Uranyl fluoride solution in heavy water
10	U233-SOL-THERM-005	Water-reflected ^{233}U uranyl nitrate solution
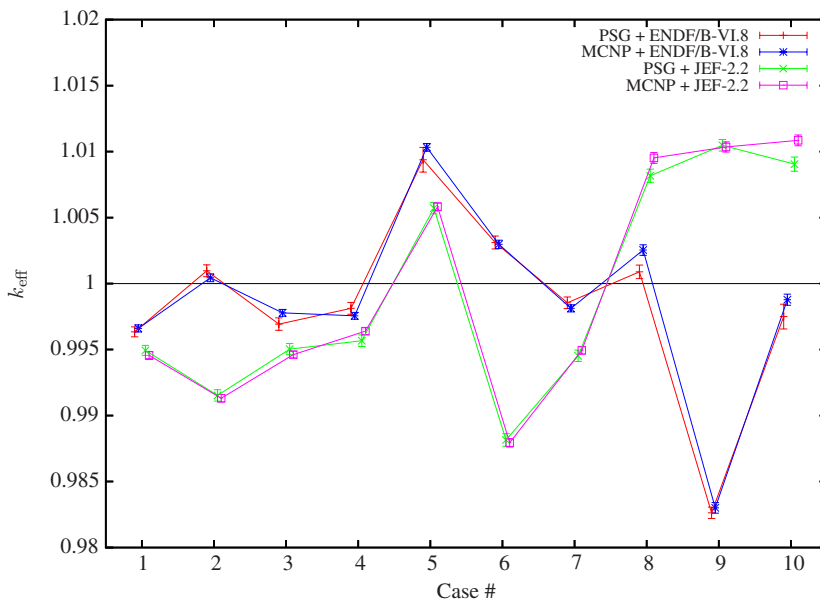
Figure 10.7: *Results of the ICESBP criticality calculations using MCNP and PSG and two different cross section libraries. The error bars show the 1σ-confidence intervals.*

The validity of the two fundamental statistical laws depends on certain assumptions on the sequence of cycle-wise random values used for the result estimates. Statistical methods are often included in Monte Carlo codes to test the validity of the results. PSG does not yet have such capability, but the tests can also be performed afterwards.

10.5.1 Convergence

To test the statistical convergence, one of the LWR lattice cases (VVER-440) was run for 3,000 active cycles and the results plotted after each new 20 cycles were completed. One such plot is presented in Figure 10.8. The parameters shown here are the two available estimates of the effective multiplication factor. The corresponding standard deviations are plotted in Figure 10.9.

It can be seen in the first plot that the result estimates oscillate to some extent before settling to a level close to the final value. The 500 active cycles run in the LWR lattice calculations seem to be sufficient for attaining statistically converged results. The statistical accuracy improves as the number of cycles increases, but since the oscillation of the mean values is not very strong, running the simulation longer does not yield significantly more information on the results. It should be noted, however, that although the two estimates give very consistent results when the number of cycles is around 500, the values depart as more cycles are run. When the 2σ confidence intervals are considered, the differences do not seem that large, but this example still clearly illustrates the stochastic nature of the simulation.

If the result estimates are statistically valid, the standard deviations should be inversely proportional to the square root of the number of active cycles run [12]. This behaviour is remarkably illustrated in Figure 10.9. The solid curves behind the discrete points are functional $\sim 1/\sqrt{N}$ fits made on the set of simulated values. The standard deviations decrease steeply at first, but the curves saturate after a sufficient number of cycles are run. It is easy to see that running the simulation any longer may not be the best means to improve the statistical accuracy. If more accurate results are desired, it may be preferable to increase the number of source neutrons per cycle, or to turn to variance reduction techniques for faster convergence. In many cases, however, better accuracy inevitably implies a considerable increase in calculation time.

10.5.2 Validity of the Central Limit Theorem

The validity of the central limit theorem and the normality of the results were assessed by studying a large sample of results obtained from independent simulations. In the example presented here, the BWR+Gd calculation case was run 5,800 times, yielding
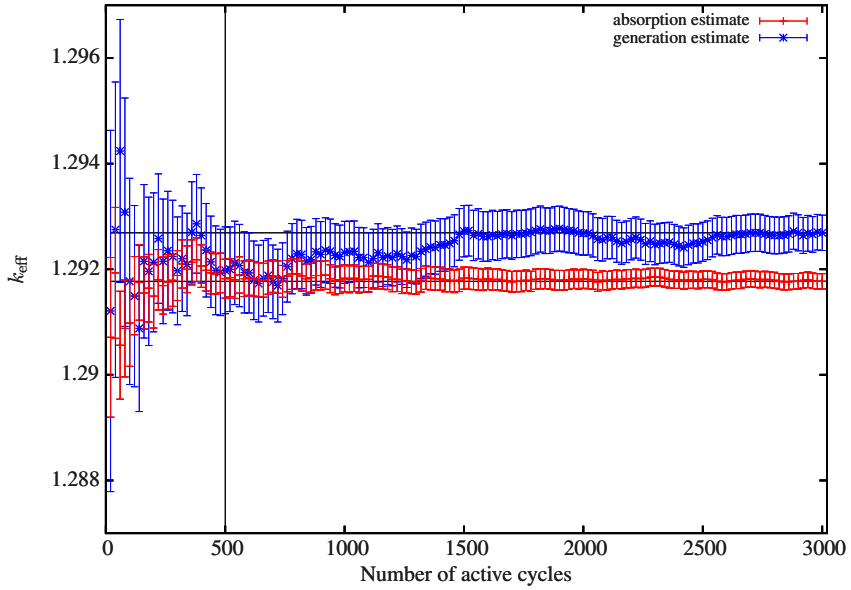
Figure 10.8: Absorption and generation estimates of k_{eff} (1σ-confidence intervals) as function of number of active cycles (VVER-440 calculation case).
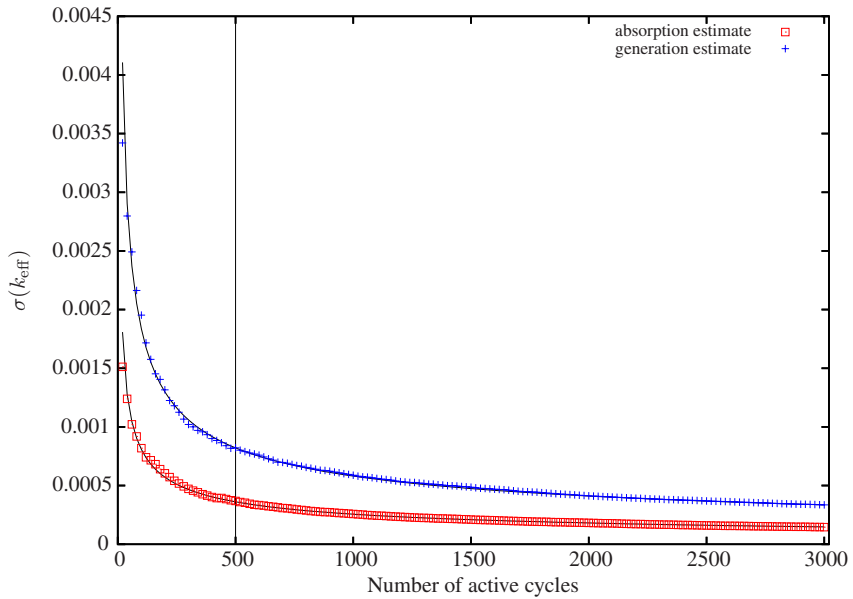
Figure 10.9: Standard deviations of absorption and generation estimates of k_{eff} as function of number of active cycles (VVER-440 calculation case).
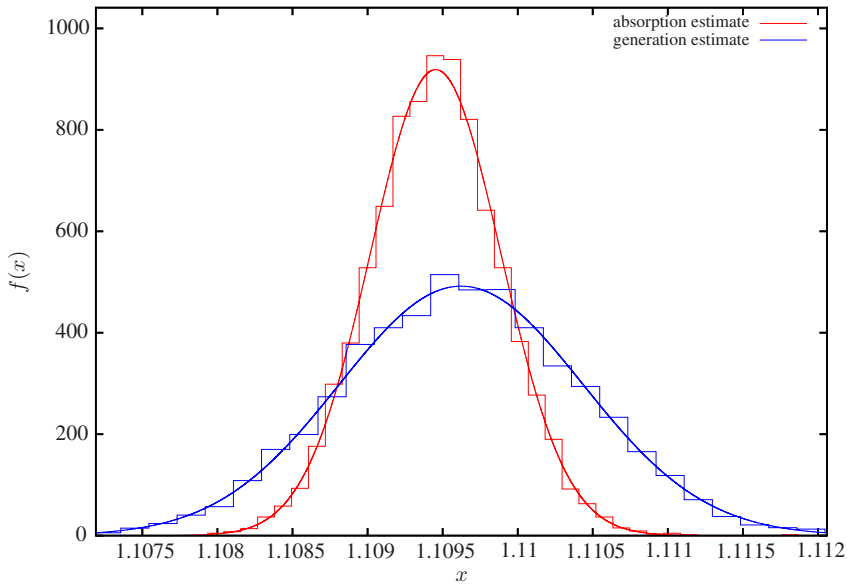
Figure 10.10: Probability distribution functions of two k_{eff} estimates. The histogram distributions are calculated from 5,800 simulated values. The solid curves show the normal distributions corresponding to the sample mean and standard deviation.

an equal number of sample values for each parameter. The values are randomly distributed, and it is relatively easy to construct the corresponding PDFs.

Figure 10.10 shows the distribution functions of two such parameters: the absorption and the generation estimate of k_{eff}. The histogram distributions are calculated by dividing the sample space into 35 bins and counting the number of values falling on each bin. After the appropriate normalisation, it can be seen that the results are well consistent with the solid curves, which give the actual normal distributions with means and standard deviations calculated from the sample values.

Since the graphical representation is not a very practical way to test the normality of a large number of parameters, some numerical methods were applied as well. The first requirement for the statistical error estimates to be reasonable is that the standard deviations are of the correct order of magnitude. The standard deviation calculated from the set of 5,800 estimates of mean value should hence be close to the mean value taken from the 5,800 estimates of standard deviation. Tables 10.10–10.12 show this type of comparison performed on the main parameters of interest. Relative statistical error instead of standard deviation is used as the measure of precision for the sake of convenience. It is seen that ratios of the two quantities are close to unity.

Table 10.10: Statistical analysis of the BWR+Gd case (5,800 sample runs). Multiplication factors, group constants and group-transfer cross sections.

Parameter	Relative errors			Confidence intervals			KS-test	
	$\overline{\sigma(x)/\overline{x}}$	$\sigma(\overline{x})/\overline{\overline{x}}$	Ratio	$< 1\sigma$	$< 2\sigma$	$< 3\sigma$	D	Pass?
k_{eff} (abs)	0.0004	0.0004	1.00	0.684	0.954	0.997	0.20	OK
k_{eff} (gen)	0.0007	0.0007	0.99	0.680	0.954	0.996	0.86	OK
Φ_{tot}	0.0004	0.0004	1.00	0.684	0.955	0.997	0.41	OK
$\Sigma_{\text{c,tot}}$	0.0005	0.0005	0.99	0.683	0.954	0.996	0.82	OK
$\Sigma_{\text{f,tot}}$	0.0006	0.0006	1.01	0.688	0.960	0.997	0.73	OK
$\Sigma_{\text{a,tot}}$	0.0004	0.0004	1.00	0.685	0.955	0.997	0.30	OK
$\Sigma_{\text{s,tot}}$	0.0003	0.0003	0.98	0.678	0.949	0.997	0.21	OK
$\Sigma_{\text{t,tot}}$	0.0003	0.0003	0.98	0.680	0.949	0.997	0.26	OK
$\nu\Sigma_{\text{f,tot}}$	0.0006	0.0006	1.01	0.688	0.959	0.997	0.47	OK
D_{tot}	0.0009	0.0009	1.01	0.687	0.954	0.997	0.71	OK
$\Sigma_{\text{tr,tot}}$	0.0009	0.0009	1.01	0.687	0.954	0.997	0.95	OK
$\overline{\mu}_{\text{tot}}$	0.0005	0.0005	1.01	0.683	0.954	0.998	0.93	OK
Φ_1	0.0005	0.0005	0.99	0.680	0.953	0.996	0.43	OK
$\Sigma_{\text{c,1}}$	0.0009	0.0009	0.99	0.673	0.954	0.996	0.33	OK
$\Sigma_{\text{f,1}}$	0.0007	0.0007	0.99	0.679	0.949	0.997	0.99	OK
$\Sigma_{\text{a,1}}$	0.0007	0.0007	0.99	0.673	0.956	0.997	0.93	OK
$\Sigma_{\text{s,1}}$	0.0001	0.0002	0.98	0.678	0.948	0.996	0.60	OK
$\Sigma_{\text{t,1}}$	0.0001	0.0001	0.98	0.683	0.949	0.997	0.54	OK
$\nu\Sigma_{\text{f,1}}$	0.0007	0.0007	0.99	0.680	0.950	0.998	0.99	OK
D_1	0.0009	0.0009	1.01	0.688	0.952	0.997	0.69	OK
$\Sigma_{\text{tr,1}}$	0.0009	0.0009	1.01	0.687	0.953	0.997	0.44	OK
$\overline{\mu}_1$	0.0006	0.0006	1.01	0.690	0.956	0.998	0.82	OK
Φ_2	0.0007	0.0007	1.00	0.687	0.957	0.997	0.97	OK
$\Sigma_{\text{c,2}}$	0.0007	0.0008	1.00	0.681	0.952	0.997	0.76	OK
$\Sigma_{\text{f,2}}$	0.0007	0.0007	1.01	0.682	0.956	0.998	0.30	OK
$\Sigma_{\text{a,2}}$	0.0006	0.0006	1.00	0.685	0.956	0.997	0.66	OK
$\Sigma_{\text{s,2}}$	0.0003	0.0003	0.99	0.678	0.954	0.996	0.52	OK
$\Sigma_{\text{t,2}}$	0.0003	0.0003	0.99	0.674	0.952	0.996	0.69	OK
$\nu\Sigma_{\text{f,2}}$	0.0007	0.0007	1.01	0.682	0.956	0.998	0.36	OK
D_2	0.0010	0.0010	1.01	0.688	0.956	0.998	0.83	OK
$\Sigma_{\text{tr,2}}$	0.0010	0.0010	1.01	0.685	0.955	0.998	0.83	OK
$\overline{\mu}_2$	0.0016	0.0016	1.00	0.681	0.952	0.998	0.99	OK
$\Sigma_{\text{s,}1\to1}$	0.0001	0.0001	0.98	0.680	0.950	0.996	0.79	OK
$\Sigma_{\text{s,}2\to1}$	0.0104	0.0102	1.02	0.690	0.958	0.998	0.76	OK
$\Sigma_{\text{s,}1\to2}$	0.0005	0.0005	0.99	0.684	0.951	0.997	0.53	OK
$\Sigma_{\text{s,}2\to2}$	0.0003	0.0003	0.99	0.678	0.955	0.996	0.40	OK

Table 10.11: Statistical analysis of the BWR+Gd case (5,800 sample runs). Kinetic and delayed neutron parameters.

Parameter	Relative errors			Confidence intervals			KS-test	
	$\overline{\sigma(x)/\overline{x}}$	$\sigma(\overline{x})/\overline{\overline{x}}$	Ratio	$< 1\sigma$	$< 2\sigma$	$< 3\sigma$	D	Pass?
α	0.0040	0.0040	1.00	0.684	0.953	0.996	0.88	OK
l_p (ana.)	0.0009	0.0009	0.99	0.678	0.953	0.996	0.49	OK
Λ (ana.)	0.0011	0.0012	0.99	0.677	0.954	0.998	0.73	OK
l_p (impl.)	0.0007	0.0007	1.01	0.681	0.959	0.997	0.81	OK
Λ (impl.)	0.0008	0.0008	1.01	0.681	0.957	0.997	0.71	OK
β_eff	0.0107	0.0107	1.00	0.684	0.950	0.997	0.58	OK
$\beta_{\mathrm{eff},1}$	0.0599	0.0597	1.00	0.680	0.956	0.997	0.70	OK
$\beta_{\mathrm{eff},2}$	0.0259	0.0258	1.00	0.694	0.954	0.996	0.82	OK
$\beta_{\mathrm{eff},3}$	0.0262	0.0264	0.99	0.679	0.949	0.998	0.96	OK
$\beta_{\mathrm{eff},4}$	0.0172	0.0173	0.99	0.679	0.953	0.997	0.76	OK
$\beta_{\mathrm{eff},5}$	0.0258	0.0259	1.00	0.686	0.953	0.996	0.89	OK
$\beta_{\mathrm{eff},6}$	0.0399	0.0402	0.99	0.683	0.949	0.995	0.69	OK
β_0	0.0003	0.0003	0.99	0.684	0.947	0.996	0.62	OK
$\beta_{0,1}$	0.0000	0.0000	0.98	0.673	0.951	0.996	0.00	FAIL
$\beta_{0,2}$	0.0001	0.0001	0.99	0.682	0.949	0.998	0.00	FAIL
$\beta_{0,3}$	0.0002	0.0002	0.99	0.684	0.948	0.996	0.01	FAIL
$\beta_{0,4}$	0.0003	0.0003	0.99	0.684	0.947	0.996	0.37	OK
$\beta_{0,5}$	0.0005	0.0005	0.99	0.683	0.948	0.996	0.51	OK
$\beta_{0,6}$	0.0005	0.0005	0.99	0.684	0.948	0.996	0.73	OK
λ	0.0154	0.0156	0.99	0.683	0.951	0.996	0.44	OK
λ_1	0.0003	0.0003	0.98	0.667	0.944	0.990	0.01	FAIL
λ_2	0.0003	0.0003	1.01	0.690	0.954	0.996	0.72	OK
λ_3	0.0002	0.0002	0.99	0.676	0.953	0.995	0.01	FAIL
λ_4	0.0004	0.0004	0.98	0.670	0.950	0.997	0.69	OK
λ_5	0.0007	0.0007	1.01	0.686	0.956	0.997	0.83	OK
λ_6	0.0010	0.0010	1.01	0.688	0.958	0.997	0.40	OK

The second test presented in Tables 10.10–10.12 takes advantage of the confidence intervals of normally distributed random variables (see Section 6.3.1 of Chapter 6). In theory, the 1-, 2- and 3-sigma confidence intervals should hold 68.3, 95.5 and 99.7% of all sample values, respectively. It is very easy to calculate the corresponding fractions from the simulated data and the results show that the confidence intervals hold reasonably well for all parameters. Even this, however, does not yet confirm that the result estimates are normally distributed, since the test yields very little information on the actual shape of the distributions.

Table 10.12: Statistical analysis of the BWR+Gd case (5,800 sample runs). Assembly discontinuity factors.

Parameter	Relative errors			Confidence intervals			KS-test	
	$\sigma(x)/\overline{x}$	$\sigma(\overline{x})/\overline{\overline{x}}$	Ratio	$< 1\sigma$	$< 2\sigma$	$< 3\sigma$	D	Pass?
$F_{1,1}^{\mathrm{s}}$	0.0018	0.0019	0.95	0.662	0.942	0.996	0.94	OK
$F_{2,1}^{\mathrm{s}}$	0.0025	0.0025	0.98	0.671	0.952	0.998	0.98	OK
$F_{3,1}^{\mathrm{s}}$	0.0018	0.0018	0.97	0.669	0.951	0.996	0.93	OK
$F_{4,1}^{\mathrm{s}}$	0.0029	0.0030	0.96	0.657	0.948	0.996	0.52	OK
$F_{1,2}^{\mathrm{s}}$	0.0018	0.0019	0.95	0.657	0.943	0.995	0.44	OK
$F_{2,2}^{\mathrm{s}}$	0.0029	0.0030	0.97	0.667	0.948	0.996	0.73	OK
$F_{3,2}^{\mathrm{s}}$	0.0018	0.0018	0.98	0.677	0.947	0.996	0.60	OK
$F_{4,2}^{\mathrm{s}}$	0.0025	0.0025	0.98	0.672	0.949	0.996	0.57	OK
$F_{1,1}^{\mathrm{c}}$	0.0132	0.0132	1.00	0.679	0.956	0.997	0.98	OK
$F_{2,1}^{\mathrm{c}}$	0.0113	0.0114	0.99	0.678	0.952	0.997	0.71	OK
$F_{3,1}^{\mathrm{c}}$	0.0130	0.0131	0.99	0.680	0.952	0.997	0.07	OK
$F_{4,1}^{\mathrm{c}}$	0.0128	0.0130	0.98	0.676	0.951	0.997	0.71	OK
$F_{1,2}^{\mathrm{c}}$	0.0127	0.0129	0.99	0.674	0.956	0.997	0.84	OK
$F_{2,2}^{\mathrm{c}}$	0.0147	0.0149	0.98	0.672	0.954	0.996	0.98	OK
$F_{3,2}^{\mathrm{c}}$	0.0130	0.0130	1.00	0.688	0.952	0.997	0.34	OK
$F_{4,2}^{\mathrm{c}}$	0.0128	0.0128	1.00	0.693	0.951	0.997	0.50	OK

The third test is known as the Kolmogorov-Smirnov test, which is a commonly used numerical method for evaluating the distributions of unknown samples [60]. The details of the method are not discussed here, but the test basically calculates the difference between a known reference distribution and the unknown distribution formed by the sample values. The test used in this study is included in the standard functions of the GNU Octave mathematical software package [114]. The function yields a single output value, D, that characterises the validity of the hypothesis. The criterion used here is to compare the value of D to the critical value at a 5% confidence level. The critical value for a sample size of 5,800 is 0.018. It can be seen that, apart from a few delayed neutron parameters, all the values in Tables 10.10–10.12 are well above the critical level, which suggests that the results are normally distributed[8].

---

[8]There is a peculiar feature in the β_0- and λ-parameters that failed the Komogorov-Smirnov test. Both parameters are directly dependent on tabulated precursor data, which is different for the two actinide isotopes (^{235}U and ^{238}U, see Table 4.1 on page 83) involved in this calculation case. It is possible that the scores are centred around two tabulated values, which produces a non-Gaussian two-peak probability distribution.

The convergence of the initial fission source was not discussed at all. This topic has been thoroughly studied for decades and it still remains one of the most interesting fundamental problems in Monte Carlo criticality calculation. The number of inactive saturation cycles in the LWR lattice calculations was set to 100. This value is quite large, considering the relatively small dimensions of the geometries and the strong coupling between the fuel pins. It is hence assumed that the source distributions are well converged and that the results are not dependent on the initial guess.

10.6 Code Performance

It was stated already in the introduction of this text that one of the main goals in PSG development is high performance and reduced calculation time. Chapter 8 listed two features in the code design for achieving this goal: the delta-tracking method and the uniform energy grid used for all isotopes in the cross section data. The main reference code, MCNP4C, is not designed for maximum performance and other, significantly faster codes do exist. Since, however, the comparison of code performance is not among the most important aspects in this particular study, it was considered sufficient to compare the running times and parallelisation capabilities of PSG to MCNP. Comparison to CASMO-4E is discussed as well, but it must be realised that the differences in the calculation times mostly originate from the fundamental differences in the transport methods.

10.6.1 Running Time

Table 10.13 shows the calculation times of the three codes in the LWR lattice calculations discussed in Section 10.2. All three codes were run on a 2.6 GHz AMD Opteron PC. The Monte Carlo codes were run with 100 inactive and 500 active cycles of 5,000 neutrons. The BWR+Gd case was repeated with and without the special treatment for localised heavy absorbers included in the modified delta-tracking method used by PSG (see Section 8.3.1 of Chapter 8). The last two columns in the table ("M/P" and "P/C") give the ratios of MCNP to PSG and PSG to CASMO calculation times, respectively.

It is seen that the PSG code is considerably faster compared to MCNP in the three test cases. Generally the factor varies from about 4 to 15 in LWR lattice calculations. The differences are smaller in simple geometries with a high leakage rate. It should be noted that the running time of MCNP is strongly dependent on the number of tallies and that the tallyx-subroutine used for calculating the integral reaction rates may affect the calculation times as well. It is also a well-known fact that MCNP can be

Table 10.13: Comparison of running times (in seconds) in the LWR lattice calculation cases.

Case	MCNP	CASMO	PSG	M/P	P/C
VVER-440	5589	2	461	12.1	230.5
PWR MOX	4662	13	359	13.0	27.6
BWR+Gd (special treatment)	5520	3	572	9.7	190.7
BWR+Gd (simple delta-tracking)	5520	3	737	7.5	245.7

made considerably faster by appropriately optimising the compilation[9]. Such optimisation was not performed for the code version used in this study and it is possible that the comparison gives favourable results for PSG performance.

The differences in the calculation times are even larger between CASMO and PSG, as would have been expected. When group constants are generated for reactor simulator calculations, the process has to be repeated for some hundreds of lattice cases. The overall calculation time using CASMO is of the order of hours. The hypothetical generation time using PSG would hence be of the order of weeks or even months, which is not very practical for routine calculations[10].

Table 10.13 shows how the special heavy absorber treatment affects the PSG calculation time. When the treatment is turned off in the BWR+Gd calculation case, the virtual collision fraction jumps from 58 to 91% and computing time is wasted in the re-sampling of the collision distance. The dramatic increase results from the fact that high-absorbing gadolinium isotopes are allowed to dominate the majorant cross section (see Figure 8.6 on page 153 and the discussion in Section 8.3.1). The virtual collision fraction in the other two cases is of the order of 37%, and the use of the special heavy absorber treatment does not lead to a significant gain in efficiency[11].

The three cross section data formats used internally within PSG were introduced in Section 8.2.2 of Chapter 8. There are two optional methods for generating the master energy grid used for all cross sections. The first method is to generate the grid from scratch, based on user input and the resolution of the original data. The second method is to include all original energy grid points of all cross sections in the new grid. The advantage of the first method is that the grid index needed for interpolating the cross sections between tabulated energy points can be calculated

---

[9]This topic is constantly discussed at the MCNP forum [115].

[10]Group constant generation in the study by M. Tohjoh et al. (see Ref. [24] and Section 9.2.5 of Chapter 9) took 40 days using the MVP-BURN code.

[11]It is possible to label all fuel pins as high-absorbing materials, but various test calculations have shown that such practice does not usually lead to a noticeable reduction in calculation time.

without any iteration. The advantage of the second method is that all the information in the original data format is preserved.

The data formats have been tested in various comparison calculations. It was initially expected that the first method would lead to a considerably shorter calculation time compared to the second one. It has turned out, however, that the differences are usually quite marginal. It was also expected that there would be large differences in the results, if the number of grid points in method 1 is set low. Such differences have not been encountered either, as long as the resolution is still reasonable. The topic requires further studies before making any final conclusions, but at this point it seems that there are no crucial differences between the two methods. In order to avoid any unexpected discrepancies, method number two is clearly preferable.

One of the unanswered questions in this study is the amount efficiency gain from the use of the delta-tracking method. This question is very difficult to answer, since the geometry routines are exclusively based on delta-tracking, and there are other, more significant factors affecting the overall calculation time (such as the uniform energy grid used for the cross sections). The efficiency gain from the simplified geometry routines is balanced by the penalty resulting from the rejection algorithm. Most likely the overall speed-up is very much case-dependent, and in some cases the routines may lead to an increase in calculation time. It is impossible to make any final conclusions at this stage of code development, since there is no reference to compare to.

10.6.2 Parallelisation

All calculations discussed so far were carried out using a single-processor computer. It was mentioned in Chapter 8 that PSG also has the capability to be run in a parallel multi-processor environment. Parallel calculation is a reasonable option when the overall running time seriously restricts the code applicability. With present computer resources, group constant generation using the Monte Carlo method is a good example of such a case.

The linearity of the Monte Carlo method makes it an excellent candidate for parallelisation. Each neutron is simulated independently and there is no reason why the simulation could not be run simultaneously in multiple hosts. The parallelisation in PSG is implemented using the Message Passing Interface (MPI) [83] and a very simple procedure that divides the entire simulation into several parallel sub-tasks. The results are combined at the end of the calculation.

The overall speed-up achieved by parallel calculation was tested by running the LWR lattice calculations in a computer cluster composed of 10 processors. Figure 10.11 shows how the calculation times fall as the number of processors is in-
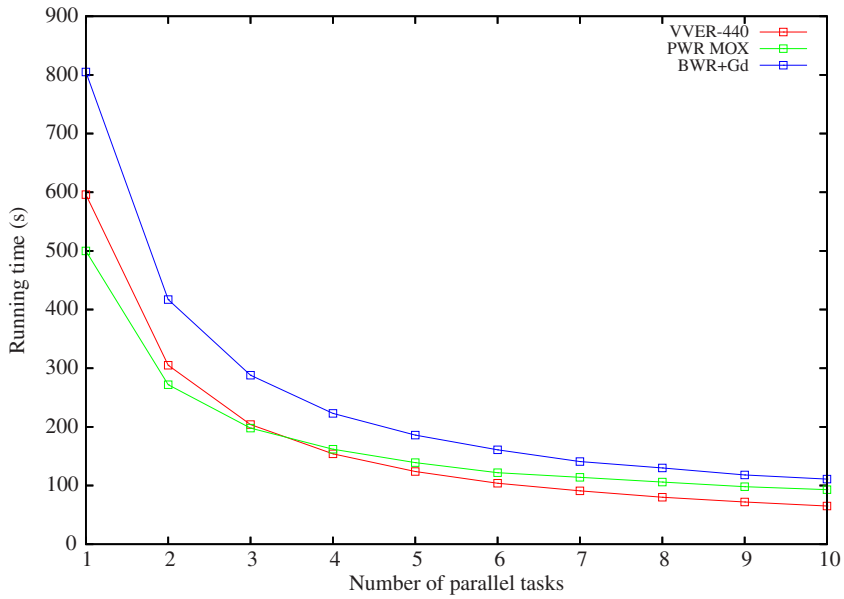
Figure 10.11: Calculation times in the LWR lattice cases as function of number of parallel tasks.
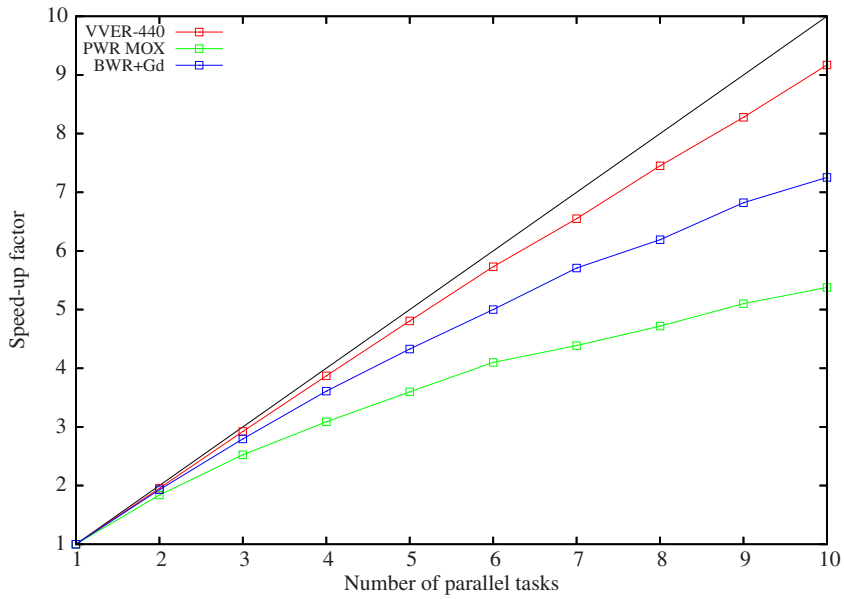

Figure 10.12: Relative running speeds in the LWR lattice cases as function of parallel tasks.

creased. The speed-up factors compared to a single-processor calculation are plotted in Figure 10.12. It is seen that although there are some differences between the three cases, the running time can be significantly cut in each case.

Figure 10.12 shows that the increase in efficiency is almost linear at first, but then saturates as more processors are included. With 10 processors, the speed-up factor in the VVER-440 case is above 9, which is truly remarkable. One reason why the other two cases do not perform as well is that the total number of isotopes in the materials is much larger. The pre-processing of the interaction data is not divided into multiple hosts and the preparation takes more time.

Because of the saturation of the speed-up factor, it is not reasonable to use too many processors for the task. If several processors are available for the calculation, it may instead be advantageous to run multiple cases at the same time. The months or weeks of overall calculation time it takes to generate the full set of group constants may in a large computer cluster be cut to a few days at best, which is not an impossible time span at all.

The same parallelisation tests were repeated using MCNP. The version 4C of the code uses the Parallel Virtual Machine (PVM) [116] for parallelisation, but the differences between the two environments should not be significant in practice. It was shown that MCNP is also able to achieve a significant speed-up in the calculation. The factors are slightly lower compared to PSG, which may result from the implementation of the parallel calculation mode. The parallel tasks in MCNP share information after each neutron cycle. This increases reliability and enables dynamic load sharing, but slows down the calculation to some extent.

In order to confirm that the statistical validity of the results is preserved when the calculation is divided into multiple hosts, the statistical analysis discussed in Section 10.5 was repeated in the parallel calculation mode using 2 and 8 processors. No differences were encountered compared to the one-processor calculation.

Chapter 11

Summary and Conclusions

11.1   Summary

The Monte Carlo method is widely used for solving various neutron transport problems encountered in nuclear reactor physics. The applications are typically related to criticality safety analyses, radiation shielding problems and various detector calculations. Monte Carlo codes are also used for providing reference results for the validation of deterministic transport codes. The common factor in all applications is the need to model the geometry and the interaction physics to within maximum accuracy and detail.

The potential to produce accurate results without major approximations is clearly the most significant advantage of the Monte Carlo method. Neutron interaction data collected in the evaluated nuclear data files can be used in a continuous-energy format, without the micro-group condensation necessary for all deterministic transport methods. This data represents the best available knowledge on neutron interactions with matter. The continuous-energy data format is general and it can be used in any type of application. The simulation is carried out one neutron at a time, which retains a close relation to the underlying physical process. Resonance self-shielding and other collective phenomena are consistently modelled without additional effort.

The Monte Carlo method is a computing-intensive technique, which restricts the applications to some extent. The development of computer capacities and the growing interest in parallel calculation suggest that the importance of Monte Carlo calculation will only increase in the future, especially since the method is particularly well-suited for parallelisation. New applications will probably arise along with code development, but it may take decades before Monte Carlo codes start to compete with deter-

ministic transport methods in coupled full-core analyses. The presently-used reactor simulator codes are typically based on few-group nodal diffusion methods.

An interesting near-future application for the Monte Carlo method is the generation of homogenised group constants for deterministic reactor simulator codes. This task is presently handled by second-generation lattice codes, based on advanced deterministic transport methods. The task is becoming increasingly challenging, along with the development in nuclear technology. Increasing fuel burnup, advanced MOX fuels and next-generation reactor concepts may require the use of more elaborate transport methods, and Monte Carlo calculation seems like a viable choice.

Previous studies related to group constant generation using the Monte Carlo method are not as numerous as might be expected [21–25]. The homogenisation problem is basically reduced to the calculation of the neutron diffusion coefficient, which is the only parameter without any analogy in the continuous-energy Monte Carlo calculation. Another difficulty lies in the generation of effective kinetic and delayed neutron parameters for dynamic calculations. This basically requires adjoint calculation, which is very complicated in Monte Carlo and practically impossible if continuous-energy interaction data is used. There seems to be a growing interest in this topic and several studies have been published quite recently [97–102].

A very fundamental problem in the methodology is that the group constant data is produced in a two-dimensional infinite-lattice calculation, which is inconsistent with physical reality. The traditional solution is to apply some leakage correction, which accounts for the streaming of neutrons over the system boundaries, and compensates for the non-physical boundary conditions. The deterministic theory for leakage models is well developed, but not easily translated in Monte Carlo.

A new Monte Carlo neutron transport code is being developed at VTT Technical Research Centre of Finland. The PSG (Probabilistic Scattering Game) code is specifically designed for reactor physics calculations, particularly at the fuel assembly level. One of the main project goals is the generation of input parameters for deterministic reactor simulator codes. This capability requires certain specialisation, which has been taken into account from the beginning of PSG development.

PSG can be characterised as a three-dimensional continuous-energy neutron transport code. The geometry description is not restricted, but the code is best suited for two-dimensional infinite-lattice calculations. Neutron transport in PSG is based on the delta-tracking method. This limits the range of applications to some extent, since the track length estimate of neutron flux is not available and integral reaction rates are calculated using the less efficient collision estimator. The limitation is not considered severe, however, if the integration is carried over a large geometry volume, which is usually the case in lattice calculations.

Neutron interaction data used by PSG is read from continuous-energy ACE format data libraries. All reaction channels are modelled according to classical collision kinematics and ENDF reaction laws. Cross sections are reconstructed in a uniform energy grid, which is used for all isotopes. This procedure results in a significant speed-up in calculation, with the cost of wasted computer memory.

PSG calculates all input parameters needed in few-group nodal diffusion calculations, including diffusion coefficients using two fundamentally different methods. The primary method relies on the conservation of group-wise diffusion areas. This approach is simple and consistent with diffusion theory. The optional method is based on the transport cross section. The method is inconsistent with deterministic transport theory, since the homogenisation of transport cross section is carried out using the flux spectrum as the weighting function. This is an inevitable problem in the methodology, since the correct homogenisation using the current spectrum is not possible in Monte Carlo calculation.

11.2   Conclusions

At its current stage of development, the PSG code can be considered as a versatile research tool that is best used in parallel with other transport codes. The code is fast and efficient, and it can be run in a multi-processor computing environment. PSG is not ready to be used as a production code in a routine manner, although it has the capability to calculate all the input parameters needed in nodal diffusion calculations. The main restricting factor is the incapability to model fuel depletion and to produce group constants for burned fuel.

PSG has been validated by comparing the group constants to reference results produced by other transport codes. Comparison between MCNP and PSG suggests that there are no serious flaws in the physical models and calculation routines. There seems to be a persistent anomaly in the free-gas model used for thermal neutron scattering, which is also reflected as a systematic discrepancy in the results at the thermal energy region. The differences compared to MCNP results are not that significant, however, when the free-gas model is replaced by bound-atom scattering data used for moderator isotopes. Such data is available for LWR calculations and PSG results are generally well consistent with the reference data. Maximum discrepancies are of the order of 0.5% and for most of the parameters well below that.

The differences between deterministic and Monte Carlo calculations are typically of the order of few per cent in group-wise reaction cross sections and several hundred pcm in the multiplication factor. Similar differences are observed in comparisons between CASMO and PSG. Discrepancies in the diffusion coefficients are often a few

per cent larger, which can be explained by the fundamental differences in the calculation methods, together with the questionable validity of the diffusion approximation.

The simple neutron leakage model developed for PSG has been tested but not systematically validated. Comparison with CASMO fundamental mode calculation shows that the discrepancies are comparable to a similar calculation without the leakage correction. The problem in the validation is, however, that the impact of the correction is of the same order in magnitude as the general differences between the two codes. More studies need to be carried out before making any final conclusions.

Homogenised group constants produced by PSG have been tested in simple reactor simulator calculations using the ARES nodal diffusion code. The test case was a conceptual initial core of the EPR reactor at hot zero-power conditions. The calculation was simple and involved no actual thermal hydraulics, but the results clearly showed that the group constants generated by PSG performed equally well as the reference CASMO data.

Although mainly intended for lattice calculations, PSG has been successfully used for modelling full-core geometries and criticality experiments as well. Since the collision estimate of neutron flux is used for calculating integral reaction rates, the efficiency is quite poor if the integration is carried over a small volume or in a region of low collision density. This problem is typically encountered in detector modelling. The code cannot be considered as a very practical tool for detector calculations, but there is no reason why any problem in reactor physics could not be approached with PSG. More importantly, the capability to model complicated reactor configurations enables the code to be validated against experimental results.

11.3   Where to proceed from here?

It was mentioned in the introduction of this text that PSG is not a complete project and it may take some time before the code can be fully used for its intended tasks. Code development was frozen in June 2006, when the main focus was turned to the writing of this thesis. It is now May 2007, and there are some interesting research projects that have been completed quite recently, but had to be omitted in this text.

VTT and Fortum Nuclear Services are participating in an IAEA Regional Project, established for assessing the local power-peaking problem caused by excessive neutron moderation in the joint region of a VVER-440 control assembly. The project is at its final stage, and a computational benchmark exercise [117] has been initiated based on experimental measurements carried out at the LR-0 test reactor at the NRI Řež plc. in the Czech Republic.

The benchmark calculations were carried out using MCNP4C and successfully repeated with PSG [118]. The calculations consist of axial fission rate distributions in fuel pins adjacent to a central control assembly. What is remarkable in the PSG results is that the efficiency of the collision flux estimator is comparable to the track-length estimate used by MCNP, which was clearly not the case in the VENUS-2 detector calculations [4], discussed in Section 10.4.2 of Chapter 10. The difference is that the reaction rates are calculated in a region of high collision density, which compensates for the small volumes of the detector cells. This, in turn, suggests that the efficiency of the collision estimator is well sufficient for calculating reaction rates in similar configurations, especially inside active fuel pins.

Another on-going study deals with the development of a randomly dispersed particle fuel model for high-temperature gas-cooled reactor calculations [5]. The model takes full advantage of the delta-tracking method, and the capability to track neutrons in the geometry without explicitly dealing with surface crossings. This capability is particularly valuable in the modelling of HTGR fuels, in which the microscopic fuel particles are dispersed throughout the graphite matrix in a completely random manner.

More future plans are summarised in the following. Both long- and short-term goals are discussed. Code development goes hand-in-hand with validation, which currently lags behind.

11.3.1 Refinements in Existing Capabilities

The internal cross section data format used by PSG was introduced in Section 8.2.2 of Chapter 8. The code uses the same energy grid for all reaction cross sections, which leads to a considerable speed-up in the calculation routines. The downside of this approach is that computer memory is wasted for storing redundant data points. Memory size has not become a restricting factor in the calculation cases studied so far. It can be expected, however, that this situation will change with burnup calculation. The number of important actinide and fission product isotopes in irradiated fuel becomes so large, that it may become necessary to develop more memory-efficient methods for handling the cross section data.

The optional user-defined energy grid format in PSG does not include all grid points in the original data. Grid size is fixed and the amount of allocated memory increases linearly with the number of isotopes. It was discussed earlier that there seems to be no large discrepancies between the use of the accurate grid construction and the approximate representation, as long as the resolution is sufficiently high. This option needs to be studied and the existing methods refined.

Another possibility is to use the accurate grid format only for the most important reaction channels, such as elastic scattering, capture and fission. This approach may turn out to be very efficient, especially in LWR calculations, in which over 90% of interactions consist of elastic scattering with hydrogen. The problem with the method is the identification of the important isotopes, which should be carried out automatically before the energy grid is constructed.

The calculation of effective kinetic and delayed neutron parameters is a hot research topic in Monte Carlo calculation. PSG already implements a recently developed method for calculating β_{eff}. The efficiency is not very good compared to the other parameters, and implicit methods for delayed neutron emission have been considered for obtaining better statistics. Such methods would require some fundamental changes in the analog calculation procedure and it might be reasonable to include implicit neutron capture and other non-analog techniques along with the changes. These methods are routinely used in most general-purpose Monte Carlo codes, and the reason why they are not already included in PSG is that the efficiency gain is not considered significant in lattice calculations.

The neutron life and generation time estimates in PSG are based on simple analog and implicit methods, which are not consistent with the adjoint-flux weighted effective parameters derived from transport theory. There have been some recent studies on the calculation of Λ_{eff} [101, 102] using the forward Monte Carlo method, and similar methodology is being planned for PSG as well.

Detector calculation in PSG was only briefly discussed in this text. The code has the capability to calculate various integral and spectral quantities in user-defined detector cells and lattices, which is considered sufficient for most applications. The problem in detector modelling is the poor efficiency of the collision estimator, and the use of the track length estimate has been considered as an option. This would require some modifications to the geometry routines, but the calculation of neutron track lengths inside simple superimposed detector cells should not become a major problem. Similar methodology, or the use of surface flux estimates, could be used for calculating assembly discontinuity factors.

PSG has no capability to assess the convergence or the statistical validity of the result estimates. This topic was discussed in Section 10.5 of Chapter 10, where the statistical analysis was performed afterwards. There were no serious anomalies in the statistics, but it is clear that this type of analysis is not practical for routine calculations. Most of the widely-used Monte Carlo codes use built-in methods for statistical analysis, and similar methodology must be developed for PSG as well.

Another concern related to statistics is the convergence of the initial fission source. This topic was briefly discussed in Section 5.5.2 of Chapter 5. Although source

convergence is probably not a serious problem in assembly-level calculations, it may become an issue in full-core calculations or other applications that may emerge along with PSG development.

11.3.2 Code Development in the Long Term

Two major development projects can be identified in the long term: neutron leakage models and burnup calculation. The current leakage correction based on the homogeneous absorption or production of neutrons is considered insufficient and methodologically questionable, despite the promising results compared to CASMO fundamental mode calculations. More elaborate leakage models have been developed for deterministic codes, but the existing theory is not easily applied in Monte Carlo calculation.

The Monte Carlo method is able to track the movement individual neutrons over the geometry boundaries and it would seem reasonable to base the leakage model on the fact that neutrons may only escape the system by crossing the boundary surfaces. Population control by removing or duplicating neutrons when the boundary conditions are applied seems like a simple and intuitive solution. A Monte Carlo specific leakage model may nevertheless require some considerable theoretical work, including new methods for calculating the diffusion coefficients.

The main challenge in burnup calculation is not in the methodology, but rather in the practical implementation. A reasonable starting point could be the calculation of equilibrium ^{135}Xe concentrations. This task should not become too complicated in a lattice-based geometry. The fission rate distribution is not uniform and each fuel pin must be treated separately. The fuel regions must be divided into several annular sub-regions, to account for the local flux-depression caused by spatial self-shielding effects. The sub-division of the geometry should be handled internally in the code, without additional user effort.

The subroutines developed for the equilibrium xenon calculation could be used as a basis for the actual burnup calculation. This task requires the solution of the Bateman equations (see Section 4.4 of Chapter 4), written separately for each fuel region. The transmutation cross sections of over one hundred actinide and fission product isotopes need to be calculated for each region. The automated collection and handling of such amount of data becomes complicated. As discussed above, it may also require major modifications in the cross section data format.

Monte Carlo burnup calculation is not a new idea and various code systems have been developed for the task (see e.g. Refs. [44, 96, 119, 120]). A new feature planned for PSG is the handling of the Bateman equations after each neutron generation, which

produces a sequence of cycle-wise estimates for the isotope concentrations. The advantage of this approach is the capability to produce statistical error estimates for the isotopic compositions calculated after each depletion step. This procedure may turn out to be too inefficient in practice, but it is certainly worth studying. Error propagation in Monte Carlo burnup calculation is not an extensively covered research topic, although some studies have been carried out [121, 122].

Other future plans include the generation of input parameters for higher-order spherical harmonics (P_N) codes and some special capabilities enabled by the delta-tracking method. Such capabilities include the modelling of axially continuous coolant void distributions inside BWR flow channels and non-uniform radial temperature distributions inside fuel pellets. These type of studies may not be considered important for practical applications, but they could provide interesting results for basic research.

11.3.3 Major Validation Projects

PSG has mainly been validated against MCNP results. This is a natural choice in this early stage of development, since the two Monte Carlo codes share the same cross section library format. Some comparison calculations have been carried out using CASMO and more studies are planned for the near future. The use of only two reference codes is considered somewhat insufficient and more diversity is clearly needed in the validation.

The calculation of diffusion coefficients, group-transfer cross sections and delayed neutron parameters is not possible in most general-purpose Monte Carlo codes. This is quite unfortunate, since reference results provided by deterministic codes are always subject to a greater level of uncertainty. There are probably various special versions of MCNP that could handle the calculation. Chapter 9 listed two other candidates: VIM [94] and MCU [18]. The latter could also be used for the validation of fundamental mode calculation.

The validation cases have mainly consisted of conventional LWR lattices. Although this covers the majority of applications in which the PSG code is likely to be used, it would be interesting to extend the studies to other reactor types as well. There is no reason why the code could not already be used for calculating CANDU, RBMK or fast reactor fuels. The recently developed randomly-dispersed particle fuel model allows some HTGR calculations to be performed using PSG as well.

It is clear that simple code-to-code comparison is not sufficient for assessing the capabilities of PSG in group constant generation. Further, it is not even expected that a Monte Carlo based calculation routine would simply reproduce the results of presently-used deterministic lattice codes. If this was actually the case, there would

be no reason to develop a new, considerably slower calculation method at all. The use of PSG-generated group constants is presently limited by the incapability to perform burnup calculation. The development of such methodology takes time and until then the validation is limited to calculations in which the isotopic compositions are known in advance, similar to the EPR initial core simulation discussed in Section 10.3 of Chapter 10.

The only large-scale experimental reactor configurations modelled using PSG are the VENUS-2 core and the LR-0 power peaking experiment, discussed above. These studies have shown that it is possible to model complicated systems using PSG and that similar benchmark exercises could be used for code validation in the future. The ICSBEP [74, 75] and IRPhEP [76, 77] handbooks could serve as valuable references for future studies.

11.4   Final Comments

The calculation methods used in nuclear reactor analysis are constantly developing. The modelling of core neutronics is only a part of the task, and quite often, the easiest part. There are some major uncertainties in the thermal hydraulics calculation of water-cooled reactors, especially BWRs. These uncertainties may exceed the physical inconsistencies of even the crudest neutronics models. It is hence impossible to say whether the introduction of more elaborate transport methods will actually improve the quality of the final results.

It is nevertheless important to continue developing neutron transport methods, and it is quite certain that this development will eventually become apparent in the reactor-scale calculations as well. Computer capacities are constantly improving and it will be interesting to see if the increasing use of Monte Carlo methods will open up new possibilities in reactor modelling. The presently-used reactor simulator codes have been designed from the beginning to use input data generated by deterministic lattice codes. The development of next-generation lattice codes based on the Monte Carlo method brings new capabilities, and may eventually lead to an entirely new generation of reactor simulator codes as well.

The future plans outlined above and the new challenges emerging from the evolution of reactor technology and neutron transport methods ensure that the work on PSG development is not likely to come to an end, at least in the near future. So far the work has shown some very encouraging results and hopefully this trend will continue in the future.

Bibliography

[1] R. Rhodes. *Dark Sun – The Making of the Hydrogen Bomb*. Simon & Schuster Paperbacks, 1995.

[2] J. Leppänen. *A New assembly-level Monte Carlo neutron transport code for reactor physics calculations*. In *Proc. International Topical Meeting on Mathematics and Computation, Supercomputing, Reactor Physics and Nuclear and Biological Applications, M&C 2005*. Avignon, France, Sept. 12–15 2005.

[3] J. Leppänen. *Diffusion Code Group Constant Generation Using the Monte Carlo Method*. In *Proc. XII Meeting on Reactor Physics Calculations in the Nordic Countries*. Halden, Norway, May 17–18 2005.

[4] J. Leppänen. *Current Status of the PSG Monte Carlo Neutron Transport Code*. In *Proc. PHYSOR-2006 American Nuclear Society's Topical Meeting on Reactor Physics Organized and hosted by the Canadian Nuclear Society*. Vancouver, BC, Canada, Sept. 10–14 2006.

[5] J. Leppänen. *Randomly Dispersed Particle Fuel Model in the PSG Monte Carlo Neutron Transport Code*. In *Proc. Joint International Topical Meeting on Mathematics & Computation and Supercomputing in Nuclear Applications (M&C + SNA 2007)*. Monterey, California, April 15–19 2007.

[6] *OECD/NEA Data Bank Home Page*. URL `www.nea.fr/html/databank/`, reviewed March 2007.

[7] J. J. Duderstadt and L. J. Hamilton. *Nuclear Reactor Analysis*. John Wiley & Sons, Inc., 1976.

[8] G. I. Bell and S. Glasstone. *Nuclear Reactor Theory*. Van Nostrand Reinhold Company, 1970.

[9] J. R. Lamarsh. *Introduction to Nuclear Reactor Theory*. Addison-Wesley Publishing Company, 1972.

[10] W. M. Stacey. *Nuclear Reactor Physics*. John Wiley & Sons, Inc., 2001.

[11] E. E. Lewis and W. F. Miller, Jr. *Computational Methods of Neutron Transport*. John Wiley & Sons, Inc., 1984.

[12] I. Lux and L. Koblinger. *Monte Carlo Particle Transport Methods: Neutron and Photon Calculations*. CRC Press, inc., 1991.

[13] V. McLane, editor. *ENDF-102, Data Formats and Procedures for the Evaluated Nuclear Data File ENDF-6*. BNL-NCS-44945-01/04-Rev. Brookhaven National Laboratory, 2001.

[14] J. F. Briesmeister, editor. *MCNP – A General Monte Carlo N-Particle Transport Code*. LA-13709-M. Los Alamos National Laboratory, 2000.

[15] E. R. Woodcock et al. *Techniques Used in the GEM Code for Monte Carlo Neutronics Calculations in Reactors and Other Systems of Complex Geometry*. In *Proceedings of the Conference on Applications of Computing Methods to Reactor Problems*, ANL-7050. Argonne National Laboratory, 1965.

[16] L. A. Ondis II, L. J. Tyburski and B. S. Moskowitz. *RCP01 – A Monte Carlo program for solving neutron and photon transport problems in three-dimensional geometry with detailed energy description and depletion capability*. B-TM-1638. Bettis Atomic Power Laboratory, 2000.

[17] T. N. Sutton et al. *The Physical Models and Statistical Procedures Used in the RACER Monte Carlo Code*. KAPL-4840. Knolls Atomic Power Laboratory, 1999.

[18] *MCU Code: MCU Project Home Page*. URL mcu.vver.kiae.ru/earea1.html, reviewed March 2007.

[19] Y. Morimoto et al. *Neutronic analysis code for fuel assembly using a vectorized Monte Carlo method*. Nucl. Sci. Eng., **103** (1989) 351–358.

[20] M. J. Armishaw. *An introduction to the Hole Geometry Package as used in MONK and MCBEND*. ANSWERS/MONK/REPORT/003. Serco Assurance.

[21] R. C. Gast. *A Procedure for Obtaining Neutron-Diffusion Coefficients from Neutron-Transport Monte Carlo Calculations*. WAPD-TM–1446. Bettis Atomic Power Laboratory, 1981.

[22] E. L. Redmond II. *Multigroup cross section generation via Monte Carlo methods*. Ph.D. Thesis, Massachusetts Institute of Technology, 1997.

[23] G. Ilas and F. Rahnema. *A Monte Carlo based nodal diffusion model for criticality analysis of spent fuel storage lattices*. Ann. Nucl. Energy, **30** (2003) 1089–1108.

[24] M. Tohjoh, M. Watanabe and A. Yamamoto. *Application of continuous-energy Monte Carlo code as a cross-section generator of BWR core calculations*. Ann. Nucl. Energy, **32** (2005) 857–875.

[25] S. C. van der Marck et al. *Homogenized Group Cross Section by Monte Carlo*. In *Proc. PHYSOR-2006 American Nuclear Society's Topical Meeting on Reactor Physics Organized and hosted by the Canadian Nuclear Society*. Vancouver, BC, Canada, Sept. 10–14 2006.

[26] *IAEA Fast Reactor Database*. URL `www-frdb.iaea.org/index.html`, reviewed March 2007.

[27] G. Youinou et al. *Heterogeneous Assembly for Plutonium Multirecycling in PWRs: The CORAIL Concept*. In *Proc. Global 2001*. Paris, France, Sept. 9–13 2001.

[28] H. Golfier et al. *Plutonium and Minor Actinides Recycling in PWRs With the New APA Concepts*. In *Proc. Global 2001*. Paris, France, Sept. 9–13 2001.

[29] G. Youinou et al. *Plutonium and Americium Multirecycling in European Pressurized Reactor (EPR) Using Slightly Over-Moderated U-235 Enriched MOX Fuel Assemblies*. In *Proc. Global 2003*. New Orleans, Louisiana, Nov. 16–20 2003.

[30] T. A. Aiwo et al. *Assessment of a Heterogeneous PWR Assembly for Plutonium and Minor Actinide Recycle*. Nucl. Technol., **155** (2006) 34–54.

[31] S. K. Kivelä. *Vektorimuuttujan Analyysi*. Otatieto, 1997. (in Finnish).

[32] J. Vanderlinde. *Classical Electromagnetic Theory*. John Wiley & Sons, Inc., 1993.

[33] D. E. Cullen et al. *Static and Dynamic Criticality: Are They Different?* UCRL-TR-201506. Lawrence Livermore National Laboratory, 2003.

[34] J. R. Lamarsh. *Introduction to Nuclear Engineering*. Addison-Wesley Publishing Company, 1983.

[35] G. B. Arfken and H. J. Weber. *Mathematical Methods for Physicists*. Academic Press, 1995.

[36] K. Smith. *Spatial Homogenization Methods for Light Water Reactor Analysis*. Ph.D. Thesis, Massachusetts Institute of Technology, 1980.

[37] K. Koebke. *A New Approach to Homogenization and Group Condensation*. IAEA-TECDOC-231. International Atomic Energy Agency, 1978.

[38] J. Rhodes, K. Smith and M. Edenius. *CASMO-4E Extended Capability CASMO-4 User's Manual*. SSP-01/401. Studsvik Scandpower, 2001 (proprietary).

[39] A. Hébert. *Applied Reactor Physics*. IGE-281. Institut de Génie Nucléaire, École Polytechnique de Montréal, 2005.

[40] P. F. Zweifel. *Reactor Physics*. McGraw-Hill, Inc., 1973.

[41] J. Lewins. *Renaming the generation time the reproduction time*. Ann. Nucl. Energy, **33** (2006) 1071.

[42] C. Moler and C. V. Loan. *Nineteen Dubious Ways to Compute the Exponential of a Matrix*. SIAM Review, **20** (1978) 801–836.

[43] A. G. Croft. *A User's Manual for the ORIGEN2 Computer Code*. ORNL/TM-7175. Oak Ridge National Laboratory, 1980.

[44] D. I. Poston and H. R. Trellue. *User's Manual, Version 2.0 for Monteburns, Version 1.0*. LA-UR-99-4999. Los Alamos National Laboratory, 1999.

[45] L. Devroye. *Non-Uniform Random Variate Generation*. Springer-Verlag, 1986.

[46] W. A. Coleman. *Mathematical Verification of a Certain Monte Carlo Sampling Technique and Applications of the Technique to Radiation Transport Problems*. Nucl. Sci. Eng., **32** (1968) 76–81.

[47] L. L. Carter et al. *Monte Carlo Sampling with Continuously Varying Cross Sections Along Flight Paths*. Nucl. Sci. Eng., **48** (1972) 403–411.

[48] F. B. Brown and W. R. Martin. *Direct Sampling of Monte Carlo Flight Paths in Media With Continuously Varying Cross Sections*. LA-UR-02-6430. Los Alamos National Laboratory, 2002.

[49] D. E. Cullen. *Sampling the Number of Neutrons Emitted per Fission*. UCRL-TR-222526. Lawrence Livermore National Laboratory, 2006.

[50] P. Laininen. *Sovellettu todennäköisyyslasku*. Teknillinen korkeakoulu, Systeemianalyysin laboratorio, 1997. (in Finnish).

[51] Y. Ronen. *CRC Handbook of Nuclear Reactor Calculations*. CRC Press, inc., 1986.

[52] D. F. Hollenbach et al. *KENO-VI: A General Quadratic Version of the KENO Program*. ORNL/NUREG/CSD-2/V2/R6. Oak Ridge National Laboratory, 1998.

[53] F. Brown et al. *MCNP Calculations for the OECD/NEA Source Convergence Benchmarks for Criticality Safety Analysis*. LA-UR-01-5181. Los Alamos National Laboratory, 2001.

[54] J. Ueki and F. B. Brown. *Stationarity and Source Convergence in Monte Carlo Criticality Calculation*. LA-UR-02-6228. Los Alamos National Laboratory, 2002.

[55] T. Yamamoto, T. Nakamura and Y. Miyoshi. *Fission Source Convergence of Monte Carlo Criticality Calculations in Weakly Coupled Fissile Arrays*. J. Nucl. Sci. Technol., **37** (2000) 41–52.

[56] *The NEA Expert Group on Source Convergence in Criticality-Safety Analysis*. URL www.nea.fr/html/science/wpncs/convergence/, Reviewed March 2007.

[57] R. N. Blomquist et al. *Source Convergence in Criticality Safety Analyses, Phase I: Results for Four Test Problems*. NEA No. 5431. OECD/NEA, 2006.

[58] F. B. Brown. *On the Use of Shannon Entropy of the Fission Distribution for Assessing Convergence of Monte Carlo Criticality Calculations*. In *Proc. PHYSOR-2006 American Nuclear Society's Topical Meeting on Reactor Physics Organized and hosted by the Canadian Nuclear Society*. Vancouver, BC, Canada, Sept. 10–14 2006.

[59] G. Knoll. *Radiation Detection and Measurement*. John Wiley & Sons, Inc., 3rd edition, 2000.

[60] V. K. Rohatgi and A. K. Saleh. *An introduction to Probability and Statistics*. John Wiley & Sons, Inc., 2001.

[61] J-D. Kim and C-S. Gil. *Validation of ENDF/B-VI.2, JEF-2.2 and JENDL-3.2 Through MCNP Analysis of BWR-simulated Critical Experiments*. Ann. Nucl. Energy, **24** (1997) 197–204.

[62] O. P. Joneja et al. *Validation of an MCNP4B whole-reactor model for LWR-PROTEUS using ENDF/B-V, ENDF/B-VI and JEF-2.2 cross-section libraries*. Ann. Nucl. Energy, **28** (2001) 701–713.

[63] W. Bernnat et al. *Validation of Nuclear Data Libraries for Reactor Safety and Design Calculations*. J. Nucl. Sci. Technol., **Supp. 2** (2002) 884–887.

[64] H. Takano et al. *Validation of JENDL-3.3 by Criticality Benchmark Testing*. J. Nucl. Sci. Technol., **Supp. 2** (2002) 847–851.

[65] J. Leppänen. *Systematic Comparison of Evaluated Nuclear Data Files*. Lic.Sc. thesis, Department of Engineering Physics and Mathematics, Helsinki University of Technology, 2004.

[66] R. E. MacFarlane and D. W. Muir. *The NJOY Nuclear Data Processing System*. LA-12740-M. Los Alamos National Laboratory, 1994.

[67] A. Borella et al. *High Resolution Cross Section Measurements at GELINA in Support of ADS and P&T*. In *Proceedings of the International Workshop on P&T and ADS Development 2003*. SCK·CEN Club House, Belgium, October 2003.

[68] N. Colonna and the n_TOF Collaboration. *Neutron cross-section measurements at the n_TOF facility at CERN*. Nucl. Instr. and Meth. B, **213** (2004) 49–54.

[69] K. H. Guber et al. *Neutron Cross Section Measurements at the Spallation Neutron Source*. J. Nucl. Sci. Technol., **Supp. 2** (2002) 638–641.

[70] V. McLane. *EXFOR Systems Manual Nuclear Reactions Data Exchange Format*. BNL-NCS-63330-04/01. Brookhaven National Laboratory, 2001.

[71] V. G. Pronyaev and O. Schwerer, editors. *Nuclear Reaction Data Centres Network*. INDC(NDS)-401, Rev. 4. IAEA Nuclear Data Committee, 2003.

[72] *NEA Data Bank Nuclear Data Services: Bibliographic Information*. URL `www.nea.fr/html/dbdata/data/bibliographic.htm`, reviewed March 2007.

[73] F. H. Fröhner. *Evaluation and Analysis of Nuclear Resonance Data*. JEFF Report 18. OECD/NEA, 2000.

[74] *International Criticality Safety Benchmark Evaluation Project (ICSBEP)*. URL `icsbep.inel.gov/`, reviewed March 2007.

[75] NEA Nuclear Science Committee. *International Handbook of Evaluated Criticality Safety Benchmark Experiments*. NEA/NSC/DOC(95)03/I-VII. OECD/NEA, 2003.

[76] *International Reactor Physics Experiment Evaluation Project (IRPhEP)*. URL `nuclear.inel.gov/irphep/`, reviewed March 2007.

[77] NEA Nuclear Science Committee. *International Handbook of Evaluated Reactor Physics Experiments*. NEA/NSC/DOC(2006)I. OECD/NEA, 2006.

[78] *Cross Section Evaluation Working Group*. URL `www.nndc.bnl.gov/csewg`, reviewed March 2007.

[79] *NEA Data Bank Nuclear Data Services: JEF/EFF Project*. URL `www.nea.fr/html/dbdata/projects/nds_jef.htm`, reviewed March 2007.

[80] *Japanese Evaluated Nuclear Data Library*. URL `wwwndc.tokai-sc.jaea.go.jp/jendl/jendl.html`, reviewed March 2007.

[81] C. Nordborg et al. *International Co-operation in Nuclear Data Evaluation*. J. Nucl. Sci. Technol., **Supp. 2** (2002) 1449–1453.

[82] S. Matsuda, editor. *MVP/GMVP II: General Purpose Monte Carlo Codes for Neutron and Photon Transport Calculations based on Continuous Energy and Multigroup Methods*. JAERI 1348. Japan Atomic Energy Research Institute, 2005.

[83] *The Message Passing Interface (MPI) Standard*. URL `www-unix.mcs.anl.gov/mpi/`, reviewed March 2006.

[84] S. C. van der Marck et al. *New Temperature Interpolation in MCNP*. In *Proc. International Topical Meeting on Mathematics and Computation, Supercomputing, Reactor Physics and Nuclear and Biological Applications, M&C 2005*. Avignon, France, Sept. 12–15 2005.

[85] *MCNP5 Home Page*. URL `mcnp-green.lanl.gov/index.html`, reviewed March 2007.

[86] F. Brown. *Monte Carlo Advances & Challenges*. In *The 2005 Frederic Joliot / Otto Hahn Summer School*. Karlsruhe, Germany, 24 August – 2 September 2005. (lecture notes).

[87] R. E. MacFarlane. *New Thermal Neutron Scattering Files for ENDF/B-VI Release 2*. LA-12639-MS (ENDF 356). Los Alamos National Laboratory, 1994.

[88] D. E. Cullen et al. *Thermal Scattering Law Data: Implementation and Testing using the Monte Carlo neutron transport codes COG, MCNP and TART*. UCRL-ID-153656. Lawrence Livermore National Laboratory, 2003.

[89] V. H. Gillette et al. *Thermal neutron cross sections for moderator materials: comparison of a synthetic scattering function and NJOY results*. Ann. Nucl. Energy, **26** (1999) 1167–1181.

[90] A. Tanskanen. *Untitled project report*. VTT Energy, 2001. (Unfinished, in Finnish).

[91] A. Tanskanen. Private communications, August 11 2006.

[92] J. P. Both. *User Manual for version 4.3 of the TRIPOLI-4 Monte Carlo method particle transport computer code*. CEA-R-6044. CEA/Saclay, 2003.

[93] R. N. Blomquist. *Status of the VIM Monte Carlo Neutron/Photon Transport Code*. ANL/RAE/CP-106063. Argonne National Laboratory, 2002.

[94] R. N. Blomquist. *VIM Monte Carlo Neutron/Photon Transport Code User's Guide Version 4.0*. Argonne National Laboratory, 2000.

[95] G. Ilas et al. *On the few-group cross-section generation methodology for PBR analysis*. Ann. Nucl. Energy, **33** (2006) 1058–1070.

[96] K. Okumura et al. *Validation of a continuous-energy Monte Carlo burn-up code MVP-BURN and its application to analysis of post irradiation experiment*. J. Nucl. Sci. Technol., **37** (2000) 128–138.

[97] R. K. Meulekamp and S. C. van der Marck. *Calculating the Effective Delayed Neutron Fraction with Monte Carlo*. Nucl. Sci. Eng., **152** (2006) 142–138.

[98] S. C. van der Marck et al. *Benchmark results for delayed neutron data*. In *Proc. International Conference on Nuclear Data for Science and Technology*. Santa Fe, New Mexico, USA, September 26 – October 1 2004.

[99] J. Vollaire et al. *Determination of β_{eff} using MCNP-4C2 and application to the CROCUS and PROTEUS reactors*. In *Proc. PHYSOR-2006 American Nuclear Society's Topical Meeting on Reactor Physics Organized and hosted by the Canadian Nuclear Society*. Vancouver, BC, Canada, Sept. 10–14 2006.

[100] Y. Nauchi and T. Kameyama. *Estimation of 6 Groups of Effective Delayed Neutron Fraction Based on Continuous Energy Monte Carlo Method*. In *Proc. PHYSOR-2006 American Nuclear Society's Topical Meeting on Reactor Physics Organized and hosted by the Canadian Nuclear Society*. Vancouver, BC, Canada, Sept. 10–14 2006.

[101] B. Verboomen, W. Haeck and P. Baeten. *Monte Carlo calculation of the effective neutron generation time*. Ann. Nucl. Energy, **33** (2006) 911–916.

[102] Y. Nauchi and T. Kameyama. *Proposal of Direct Calculation of Kinetic Parameters β_{eff} and Λ Based on Continuous Energy Monte Carlo Method*. J. Nucl. Sci. Technol., **42** (2005) 503–514.

226

[103] E. M. Gelbard and R. Lell. *Monte Carlo Treatment of Fundamental-Mode Neutron Leakage in the Presence of Voids*. Nucl. Sci. Eng., **63** (1977) 9–23.

[104] L. V. Maiorov. *Calculating Neutron-flux Functionals by the Monte Carlo Method in Breeder Systems With Leakage Specified by a Geometric Parameter*. Atomnaya Énergiya, **58** (1985) 93–96. (translated from Russian).

[105] R. C. Little and R. E. MacFarlane. *ENDF/B-VI Neutron Library for MCNP With Probability Tables*. XCI-RN(U)98-041, LA-UR-98-5718. Los Alamos National Laboratory, 1998.

[106] R. Mattila. *Three-Dimensional Analytic Function Expansion Nodal Model*. YE-PD-9/2002. VTT Energy, 2002.

[107] *ZZ-MCB-ENDF/B6.8, MCB Continuous-Energy Neutron Cross Section Libraries for Temperatures from 300 to 1800 K*. OECD/NEA Data Bank Package ID: NEA-1669/03.

[108] R. Mattila / STUK. Private communications, November 10 2006.

[109] S. C. van der Marck / NRG. Private communications, April 8–13 2005.

[110] J. S. Hendricks et al. *ENDF/B-VI Data for MCNP*. LA-1289. Los Alamos National Laboratory, 1999.

[111] C. Y. Han et al. *VENUS-2 MOX-fuelled Reactor Dosimetry Calculations, Benchmark Specification*. NEA/NSC/DOC(2004)6. OECD/NEA, 2004.

[112] N. Messaoudi and B.-C. Na. *VENUS-2 MOX-fuelled Reactor Dosimetry Calculations, Final Report*. NEA/NSC/DOC(2005)22. OECD/NEA, 2004.

[113] *ZZ-MCB-JEF2.2, MCB Continuous-Energy Neutron Cross Section Libraries for Temperatures from 300 to 1800 K*. OECD/NEA Data Bank Package ID: NEA-1667/01.

[114] *GNU Octave Home Page*. URL `www.octave.org`, reviewed July 2006.

[115] *MCNP Forum for Users*. URL `mcnp-green.lanl.gov/forum.html`, reviewed August 2006.

[116] *PVM: Parallel Virtual Machine*. URL `www.csm.ornl.gov/pvm/`, reviewed August 2006.

[117] R. Jošek, E. Novák and. V. Rypar. *WWER-440 Local Power Peaking Experiment: Benchmark Geometry and Material Specification*. UJV Z 1651. NRI, 2006.

[118] J. Leppänen. *VVER-440 Local Power Peaking Experiment Benchmark*. VTT-R-02688-07. VTT Technical Research Centre of Finland, 2007.

[119] J. Cetnar, J. Wallenius and W. Gudowski. *MCB: A continuous energy Monte Carlo Burnup simulation code*. In *Actinide and Fission Product Partitioning and Transmutation*, EUR 18898 EN. OECD/NEA, 1999.

[120] A. Ranta-aho. *Burnup calculations for an EPR-type assembly – Comparison of CASMO-4E and ABURN*. In *Proc. XIII Meeting on Reactor Physics Calculations in the Nordic Countries*. Västerås, Sweden, March 29–30 2007.

[121] T. Takeda, N. Hirokawa and T. Noda. *Estimation of Error Propagation in Monte-Carlo Burnup Calculations*. J. Nucl. Sci. Technol., **36** (1999) 738–745.

[122] M. Tohjoh et al. *Effect of error propagation of nuclide number densities on Monte Carlo burnup-up calculations*. Ann. Nucl. Energy, **33** (2006) 1424–1436.

Appendix A

Derivation of Fick's Law

Fick's law (4.8) states that the neutron current density is proportional to the gradient of the scalar flux:

$$\mathbf{J}_g(\mathbf{r}, t) = -D_g(\mathbf{r})\nabla\phi(\mathbf{r}, t)\,, \tag{A.1}$$

where the energy-dependence of the parameters is condensed into discrete groups. The diffusion coefficient is written using the transport-corrected total cross (or simply transport cross section):

$$D_g(\mathbf{r}) = \frac{1}{3\Sigma_{\text{tr},g}(\mathbf{r})}\,. \tag{A.2}$$

This proportionality and the formulation of the transport cross section are derived in the following. Similar derivations are found in various textbooks [7, 8, 40][1].

Linearly Anisotropic Flux Approximation

One of the major approximations in diffusion theory is that the flux is only weakly dependent on the angular variables. This dependence can be written by linearising the angular flux:

$$\psi(\mathbf{r}, \hat{\mathbf{\Omega}}, E, t) \approx A(\mathbf{r}, E, t) + \hat{\mathbf{\Omega}} \cdot \mathbf{B}(\mathbf{r}, E, t)\,. \tag{A.3}$$

The assumption that the flux is only linearly anisotropic is equivalent to the P_1 approximation in the spherical harmonics method if the energy-dependence is condensed into a single group [7]. The first of the unknown functions, $A(\mathbf{r}, E, t)$, can be

---

[1]Diffusion theory is derived in most textbooks using the one-speed approximation, and the results are later generalised to the multi-group diffusion theory. The approach taken here is slightly different, although the final conclusions are the same.

resolved using the definition of the scalar flux (3.12):

$$\phi(\mathbf{r}, E, t) = \int_{4\pi} \psi(\mathbf{r}, \hat{\mathbf{\Omega}}, E, t) d\hat{\mathbf{\Omega}} = \int_{4\pi} \left[A(\mathbf{r}, E, t) + \hat{\mathbf{\Omega}} \cdot \mathbf{B}(\mathbf{r}, E, t) \right] d\hat{\mathbf{\Omega}}$$

$$= A(\mathbf{r}, E, t) \int_{4\pi} d\hat{\mathbf{\Omega}} + \mathbf{B}(\mathbf{r}, E, t) \cdot \int_{4\pi} \hat{\mathbf{\Omega}} d\hat{\mathbf{\Omega}} = 4\pi A(\mathbf{r}, E, t) \,.$$

(A.4)

Equations (3.17) and (3.18) defining the neutron current density yield for the second unknown function:

$$\mathbf{J}(\mathbf{r}, E, t) = \int_{4\pi} \mathbf{j}(\mathbf{r}, \hat{\mathbf{\Omega}}, E, t) d\hat{\mathbf{\Omega}} = \int_{4\pi} \hat{\mathbf{\Omega}} \psi(\mathbf{r}, \hat{\mathbf{\Omega}}, E, t) d\hat{\mathbf{\Omega}}$$

$$= \int_{4\pi} \left[\hat{\mathbf{\Omega}} A(\mathbf{r}, E, t) + \hat{\mathbf{\Omega}} \hat{\mathbf{\Omega}} \cdot \mathbf{B}(\mathbf{r}, E, t) \right] d\hat{\mathbf{\Omega}}$$

(A.5)

$$= A(\mathbf{r}, E, t) \int_{4\pi} \hat{\mathbf{\Omega}} d\hat{\mathbf{\Omega}} + \frac{4\pi}{3} \mathbf{B}(\mathbf{r}, E, t) = \frac{4\pi}{3} \mathbf{B}(\mathbf{r}, E, t) \,.$$

The integration above takes advantage of two well-known identities:

$$\int_{4\pi} d\hat{\mathbf{\Omega}} = 4\pi$$

(A.6)

and

$$\int_{4\pi} \hat{\mathbf{\Omega}} d\hat{\mathbf{\Omega}} = 0 \,.$$

(A.7)

The integrals in (A.4) are trivial. The difficult part is to understand the integration of the second term enclosed in brackets in Eq. (A.5). The integration is best understood by first writing all vectors in component form. When the variable dependence of $\mathbf{B}$ is omitted for clarity, the integration is written as:

$$\int_{4\pi} \hat{\mathbf{\Omega}} \hat{\mathbf{\Omega}} \cdot \mathbf{B} d\hat{\mathbf{\Omega}} = \int_{4\pi} \left[(\Omega_x + \Omega_y + \Omega_z)(\Omega_x B_x + \Omega_y B_y + \Omega_z B_z) \right] d\hat{\mathbf{\Omega}}$$

$$= \int_{4\pi} \left[(\Omega_x \Omega_y + \Omega_x \Omega_z) B_x + (\Omega_y \Omega_x + \Omega_y \Omega_z) B_y + (\Omega_z \Omega_x + \Omega_z \Omega_y) B_z \right] d\hat{\mathbf{\Omega}}$$

$$+ \int_{4\pi} \left[\Omega_x^2 B_x + \Omega_y^2 B_y + \Omega_z^2 B_z \right] d\hat{\mathbf{\Omega}} \,.$$

(A.8)

Since B_x, B_y and B_z have no angular dependence, the integration essentially consists of two types of terms. It is relatively easy to show that:

$$\int_{4\pi} \Omega_x^2 d\hat{\mathbf{\Omega}} = \int_{4\pi} \Omega_y^2 d\hat{\mathbf{\Omega}} = \int_{4\pi} \Omega_z^2 d\hat{\mathbf{\Omega}} = \frac{4\pi}{3}$$

(A.9)

A.2

and
$$\int_{4\pi} \Omega_x \Omega_y d\hat{\mathbf{\Omega}} = \int_{4\pi} \Omega_x \Omega_z d\hat{\mathbf{\Omega}} = \int_{4\pi} \Omega_y \Omega_z d\hat{\mathbf{\Omega}} = 0 \,. \tag{A.10}$$

The integration of terms Ω_z^2 and $\Omega_x \Omega_z$ is demonstrated in the following and the other terms are treated in a similar manner.

First, a co-ordinate transformation is made into the spherical system. The Cartesian components of $\hat{\mathbf{\Omega}}$ are written as in (3.5):
$$\begin{aligned} \Omega_x &= \sin\eta\cos\vartheta \\ \Omega_y &= \sin\eta\sin\vartheta \\ \Omega_z &= \cos\eta \end{aligned} \tag{A.11}$$

and
$$d\hat{\mathbf{\Omega}} = \cos\eta\sin\eta \, d\eta d\vartheta \,. \tag{A.12}$$

The integration of Ω_z^2 is hence written as:
$$\int_{4\pi} \Omega_z^2 d\hat{\mathbf{\Omega}} = \int_0^\pi \int_0^{2\pi} \cos^2\eta\sin\eta \, d\eta d\vartheta = \int_0^\pi \int_0^{2\pi} (1 - \sin^2\eta)\sin\eta \, d\eta d\vartheta$$

$$= 2\pi \int_0^\pi (\sin\eta - \sin^3\eta) d\eta = 2\pi \left[\int_0^\pi \sin\eta \, d\eta - \int_0^\pi \sin^3\eta \, d\eta \right] =$$

$$= 2\pi \left(2 - \frac{4}{3} \right) = \frac{4\pi}{3} \tag{A.13}$$

and the integration of $\Omega_x \Omega_z$ as:
$$\int_{4\pi} \Omega_x \Omega_z d\hat{\mathbf{\Omega}} = \int_0^\pi \int_0^{2\pi} \sin^2\eta\cos\eta\cos\vartheta \, d\eta d\vartheta$$

$$= \int_0^\pi \int_0^{2\pi} (1 - \cos^2\eta)\cos\eta\cos\vartheta \, d\eta d\vartheta \tag{A.14}$$

$$= \int_0^\pi (\cos\eta - \cos^3\eta) d\eta \int_0^{2\pi} \cos\vartheta \, d\vartheta = 0 \,.$$

The substitution of (A.9) and (A.10) into (A.8) yields:
$$\int_{4\pi} \hat{\mathbf{\Omega}}\hat{\mathbf{\Omega}} \cdot \mathbf{B} d\hat{\mathbf{\Omega}} = \frac{4\pi}{3} B_x + \frac{4\pi}{3} B_y + \frac{4\pi}{3} B_z = \frac{4\pi}{3} \mathbf{B} \,, \tag{A.15}$$

which is consistent with the result of (A.5). The linearly anisotropic angular flux can finally be written using the scalar flux and the current density by combining the results of (A.4) and (A.5) to (A.3):
$$\psi(\mathbf{r}, \hat{\mathbf{\Omega}}, E, t) \approx \frac{1}{4\pi} \left[\phi(\mathbf{r}, E, t) + 3\hat{\mathbf{\Omega}} \cdot \mathbf{J}(\mathbf{r}, E, t) \right] \,. \tag{A.16}$$

A.3

First-moment Equation

The starting point for the derivation of group-diffusion theory is the time-dependent transport equation (3.20), which is written here without the external source term:

$$\frac{1}{v}\frac{\partial}{\partial t}\psi(\mathbf{r},\hat{\mathbf{\Omega}},E,t) + \hat{\mathbf{\Omega}}\cdot\nabla\psi(\mathbf{r},\hat{\mathbf{\Omega}},E,t) + \Sigma_t(\mathbf{r},E)\psi(\mathbf{r},\hat{\mathbf{\Omega}},E,t)$$

$$= \int_{4\pi}\int_0^\infty \Sigma_s(\mathbf{r},\hat{\mathbf{\Omega}}'\to\hat{\mathbf{\Omega}},E'\to E)\psi(\mathbf{r},\hat{\mathbf{\Omega}}',E',t)d\hat{\mathbf{\Omega}}'dE' \qquad \text{(A.17)}$$

$$+\frac{1}{4\pi}\int_0^\infty \chi(E)\nu\Sigma_f(\mathbf{r},E')\phi(\mathbf{r},E',t)dE'\,.$$

When this is multiplied by the angular variable $\hat{\mathbf{\Omega}}$ and integrated over the full space-angle, the result is an equation known as the *first-moment equation*[2]. The integration of each term is carried out in the following.

From the definition of the angular current density (3.17) it follows that the integration of the time-derivative term yields:

$$\int_{4\pi}\hat{\mathbf{\Omega}}\left[\frac{1}{v}\frac{\partial}{\partial t}\psi(\mathbf{r},\hat{\mathbf{\Omega}},E,t)\right]d\hat{\mathbf{\Omega}} = \frac{1}{v}\frac{\partial}{\partial t}\int_{4\pi}\hat{\mathbf{\Omega}}\psi(\mathbf{r},\hat{\mathbf{\Omega}},E,t)d\hat{\mathbf{\Omega}}$$

$$= \frac{1}{v}\frac{\partial}{\partial t}\int_{4\pi}\mathbf{j}(\mathbf{r},\hat{\mathbf{\Omega}},E,t)d\hat{\mathbf{\Omega}} = \frac{1}{v}\frac{\partial}{\partial t}\mathbf{J}(\mathbf{r},E,t)\,. \qquad \text{(A.18)}$$

The integration of the removal term is carried out similarly:

$$\int_{4\pi}\hat{\mathbf{\Omega}}\left[\Sigma_t(\mathbf{r},E)\psi(\mathbf{r},\hat{\mathbf{\Omega}},E,t)\right]d\hat{\mathbf{\Omega}} = \Sigma_t(\mathbf{r},E)\int_{4\pi}\hat{\mathbf{\Omega}}\psi(\mathbf{r},\hat{\mathbf{\Omega}},E,t)d\hat{\mathbf{\Omega}}$$

$$= \Sigma_t(\mathbf{r},E)\int_{4\pi}\mathbf{j}(\mathbf{r},\hat{\mathbf{\Omega}},E,t)d\hat{\mathbf{\Omega}} = \Sigma_t(\mathbf{r},E)\mathbf{J}(\mathbf{r},E,t)\,. \qquad \text{(A.19)}$$

The second approximation made here is that fission reactions are assumed isotropic in the L-frame, in which case the integration over the fission source term vanishes:

$$\int_{4\pi}\hat{\mathbf{\Omega}}\left[\frac{1}{4\pi}\int_0^\infty \chi(E)\nu\Sigma_f(\mathbf{r},E')\phi(\mathbf{r},E',t)dE'\right]d\hat{\mathbf{\Omega}}$$

$$= \frac{1}{4\pi}\int_0^\infty \chi(E)\nu\Sigma_f(\mathbf{r},E')\phi(\mathbf{r},E',t)dE'\int_{4\pi}\hat{\mathbf{\Omega}}d\hat{\mathbf{\Omega}} = 0\,. \qquad \text{(A.20)}$$

---

[2]The neutron continuity equation (3.30) is correspondingly called the *zero-moment equation*.

The scattering source yields:

$$\int_{4\pi} \hat{\boldsymbol{\Omega}} \left[\int_{4\pi} \int_0^\infty \Sigma_s(\mathbf{r}, \hat{\boldsymbol{\Omega}}' \to \hat{\boldsymbol{\Omega}}, E' \to E)\psi(\mathbf{r}, \hat{\boldsymbol{\Omega}}', E', t)d\hat{\boldsymbol{\Omega}}'dE' \right] d\hat{\boldsymbol{\Omega}}$$

$$= \int_{4\pi} \int_0^\infty \left[\int_{4\pi} \hat{\boldsymbol{\Omega}}\Sigma_s(\mathbf{r}, \hat{\boldsymbol{\Omega}}' \to \hat{\boldsymbol{\Omega}}, E' \to E)d\hat{\boldsymbol{\Omega}} \right] \psi(\mathbf{r}, \hat{\boldsymbol{\Omega}}', E', t)d\hat{\boldsymbol{\Omega}}'dE'.$$

$$\text{(A.21)}$$

Since $\hat{\boldsymbol{\Omega}}' \cdot \hat{\boldsymbol{\Omega}}' = 1$, $(\hat{\boldsymbol{\Omega}}' \cdot \hat{\boldsymbol{\Omega}}')\hat{\boldsymbol{\Omega}} = \hat{\boldsymbol{\Omega}}'(\hat{\boldsymbol{\Omega}}' \cdot \hat{\boldsymbol{\Omega}})$ and $\hat{\boldsymbol{\Omega}}' \cdot \hat{\boldsymbol{\Omega}} = \mu$, the integration can be simplified to:

$$\int_{4\pi} \int_0^\infty \left[\int_{4\pi} (\hat{\boldsymbol{\Omega}}' \cdot \hat{\boldsymbol{\Omega}}')\hat{\boldsymbol{\Omega}}\Sigma_s(\mathbf{r}, \hat{\boldsymbol{\Omega}}' \to \hat{\boldsymbol{\Omega}}, E' \to E)d\hat{\boldsymbol{\Omega}} \right] \psi(\mathbf{r}, \hat{\boldsymbol{\Omega}}', E', t)d\hat{\boldsymbol{\Omega}}'dE$$

$$= \int_{4\pi} \int_0^\infty \left[\int_{4\pi} \hat{\boldsymbol{\Omega}}' \cdot \hat{\boldsymbol{\Omega}}\Sigma_s(\mathbf{r}, \hat{\boldsymbol{\Omega}}' \to \hat{\boldsymbol{\Omega}}, E' \to E)d\hat{\boldsymbol{\Omega}} \right] \hat{\boldsymbol{\Omega}}'\psi(\mathbf{r}, \hat{\boldsymbol{\Omega}}', E', t)d\hat{\boldsymbol{\Omega}}'dE$$

$$= \int_0^\infty \left[\int_{-1}^1 \mu\Sigma_s(\mathbf{r}, \mu, E' \to E)d\mu \right] \left[\int_{4\pi} \hat{\boldsymbol{\Omega}}'\psi(\mathbf{r}, \hat{\boldsymbol{\Omega}}', E', t)d\hat{\boldsymbol{\Omega}}' \right] dE'$$

$$= \int_0^\infty \Sigma_{s1}(\mathbf{r}, E' \to E)\mathbf{J}(\mathbf{r}, E', t)dE'.$$

$$\text{(A.22)}$$

The second identity results from the fact that the double-differential scattering cross section depends only on the angle between directions $\hat{\boldsymbol{\Omega}}$ and $\hat{\boldsymbol{\Omega}}'$ and not on the absolute values of the variables. The dependence is written using the scattering cosine μ, as in (3.9). The s1 scattering cross section:

$$\Sigma_{s1}(\mathbf{r}, E' \to E) = \int_{-1}^1 \mu\Sigma_s(\mathbf{r}, \mu, E' \to E)d\mu \qquad \text{(A.23)}$$

is the linearly anisotropic component of the differential scattering cross section.

By using the linearly anisotropic form (A.16) for the angular flux, the integration of the streaming term can be written as:

$$\int_{4\pi} \hat{\boldsymbol{\Omega}} \left[(\hat{\boldsymbol{\Omega}} \cdot \nabla)\psi(\mathbf{r}, \hat{\boldsymbol{\Omega}}, E, t) \right] d\hat{\boldsymbol{\Omega}} = \int_{4\pi} \hat{\boldsymbol{\Omega}}\hat{\boldsymbol{\Omega}} \cdot \nabla\psi(\mathbf{r}, \hat{\boldsymbol{\Omega}}, E, t)d\hat{\boldsymbol{\Omega}}$$

$$\approx \frac{1}{4\pi} \int_{4\pi} \hat{\boldsymbol{\Omega}}\hat{\boldsymbol{\Omega}} \cdot \nabla \left[\phi(\mathbf{r}, E, t) + 3\hat{\boldsymbol{\Omega}} \cdot \mathbf{J}(\mathbf{r}, E, t) \right] d\hat{\boldsymbol{\Omega}} \qquad \text{(A.24)}$$

$$= \frac{1}{4\pi} \int_{4\pi} \hat{\boldsymbol{\Omega}}\hat{\boldsymbol{\Omega}} \cdot \nabla\phi(\mathbf{r}, E, t)d\hat{\boldsymbol{\Omega}} + \frac{3}{4\pi}\nabla \cdot \mathbf{J}(\mathbf{r}, E, t) \int_{4\pi} \hat{\boldsymbol{\Omega}}\hat{\boldsymbol{\Omega}}\hat{\boldsymbol{\Omega}}d\hat{\boldsymbol{\Omega}}.$$

The integration in the first part yields:

$$\frac{1}{4\pi} \int_{4\pi} \hat{\boldsymbol{\Omega}}\hat{\boldsymbol{\Omega}} \cdot \nabla\phi(\mathbf{r}, E, t)d\hat{\boldsymbol{\Omega}} = \frac{1}{3}\nabla\phi(\mathbf{r}, E, t)\,, \tag{A.25}$$

which can be shown by a similar calculation as in (A.8)–(A.15). The integration of the second part is more laborious. It can be shown, however, that

$$\int_{4\pi} \Omega_x^l \Omega_y^m \Omega_z^n d\hat{\boldsymbol{\Omega}} = 0\,, \tag{A.26}$$

if l, m or n is an odd integer [7]. It is relatively easy to see that when the tensor product $\hat{\boldsymbol{\Omega}}\hat{\boldsymbol{\Omega}}$ is written out using the Cartesian components, each term contains at least one variable with an odd exponential, and the entire term vanishes.

When the results of (A.18)–(A.25) are collected, the first-moment equation can be written as:

$$\frac{1}{v}\frac{\partial}{\partial t}\mathbf{J}(\mathbf{r}, E, t) + \frac{1}{3}\nabla\phi(\mathbf{r}, E, t) + \Sigma_t(\mathbf{r}, E)\mathbf{J}(\mathbf{r}, E, t)$$

$$= \int_0^\infty \Sigma_{s1}(\mathbf{r}, E' \to E)\mathbf{J}(\mathbf{r}, E', t)dE'\,. \tag{A.27}$$

The third approximation to be made is that the time-rate of change of the neutron current density is small compared to the flux gradient. The time-derivative term in (A.27) can then be dropped.

Energy-group Condensation

It is easily seen that because the anisotropic scattering source is integrated over the energy variable, there is still no simple relation between the flux gradient and the current density. The fourth and final approximation is that the anisotropic contribution to energy transfer is neglected. This is a poor approximation with continuous energy-dependence, but it is considered reasonable in few-group diffusion calculation. The scattering term in (A.27) is then reduced to:

$$\int_0^\infty \Sigma_{s1}(\mathbf{r}, E' \to E)\mathbf{J}(\mathbf{r}, E', t)dE' \approx \int_0^\infty \Sigma_{s1}(\mathbf{r}, E)\delta(E' \to E)\mathbf{J}(\mathbf{r}, E', t)dE'$$

$$= \Sigma_{s1}(\mathbf{r}, E)\int_0^\infty \delta(E' \to E)\mathbf{J}(\mathbf{r}, E', t)dE' = \Sigma_{s1}(\mathbf{r}, E)\mathbf{J}(\mathbf{r}, E, t)\,. \tag{A.28}$$

The s1 scattering cross section is often written using the total scattering cross section and the cosine of the average scattering angle:

$$\Sigma_{\text{s1}}(\mathbf{r}, E) = \overline{\mu}(E)\Sigma_{\text{s}}(\mathbf{r}, E)\,, \tag{A.29}$$

where

$$\overline{\mu}(E) = \frac{\displaystyle\int_{-1}^{1} \mu\Sigma_{\text{s}}(\mathbf{r}, \mu, E)d\mu}{\displaystyle\int_{-1}^{1} \Sigma_{\text{s}}(\mathbf{r}, \mu, E)d\mu}\,. \tag{A.30}$$

The final step of the process is the condensation of the energy variable. The substitution of (A.28) and (A.29) into (A.27) and integration over energy group g yields:

$$\frac{1}{3}\int_{E_g}^{E_{g-1}} \nabla\phi(\mathbf{r}, E, t)dE + \int_{E_g}^{E_{g-1}} \Sigma_{\text{t}}(\mathbf{r}, E)\mathbf{J}(\mathbf{r}, E, t)dE$$

$$= \int_{E_g}^{E_{g-1}} \overline{\mu}(E)\Sigma_{\text{s}}(\mathbf{r}, E)\mathbf{J}(\mathbf{r}, E, t)dE\,, \tag{A.31}$$

which results in:

$$\frac{1}{3}\nabla\Phi_g(\mathbf{r}, t) + \Sigma_{\text{t},g}(\mathbf{r})\mathbf{J}_g(\mathbf{r}, t) = \overline{\mu}_g\Sigma_{\text{s},g}(\mathbf{r})\mathbf{J}_g(\mathbf{r}, t) \tag{A.32}$$

or

$$\frac{1}{3}\nabla\Phi_g(\mathbf{r}, t) + \Sigma_{\text{tr},g}(\mathbf{r})\mathbf{J}_g(\mathbf{r}, t) = 0\,, \tag{A.33}$$

where the transport cross section is defined as:

$$\Sigma_{\text{tr},g}(\mathbf{r}) = \Sigma_{\text{t},g}(\mathbf{r}) - \overline{\mu}_g\Sigma_{\text{s},g}(\mathbf{r})\,. \tag{A.34}$$

There is now a simple relation between the group current density and the gradient of the group flux:

$$\mathbf{J}_g(\mathbf{r}, t) = -\frac{\nabla\Phi_g(\mathbf{r}, t)}{3\Sigma_{\text{tr},g}(\mathbf{r})}\,, \tag{A.35}$$

which is equivalent to Fick's law (A.1) if the diffusion coefficient is defined as[3]:

$$D_g(\mathbf{r}) = \frac{1}{3\Sigma_{\text{tr},g}(\mathbf{r})}\,. \tag{A.36}$$

---

[3]The diffusion coefficient can be defined in several ways, depending on the exact methodology. The definition based on the transport cross section is known as the *Selengut-Goertzel* type scalar diffusion coefficient.

It is important to realise that it is not reasonable to define the diffusion coefficient as a continuous-energy parameter. The homogenisation must be performed on the transport cross section, using the current density, not the neutron flux as the weighting function. It is often the case that such calculation is not possible in practice. The current spectrum is harder than the flux spectrum, and the use of neutron flux for the homogenisation generally results in the under-estimation of the diffusion coefficient.

It should also be noted that the average scattering cosine $\overline{\mu}_g$ is not quite equivalent to the average value taken over all scattering reactions. The integrals in (A.30) are non-trivial when the angular dependence of the reaction is complicated. In the simplest case of free-atom elastic potential scattering, however, the reaction is isotropic in the centre-of-mass frame and the average scattering cosine is given by [7]:

$$\overline{\mu} = \frac{2}{3A}, \tag{A.37}$$

where A is the atomic weight ratio, i.e. the target isotope mass divided by the mass of the neutron.

Author(s)
Leppänen, Jaakko

Title

Development of a New Monte Carlo Reactor Physics Code

Abstract

Monte Carlo neutron transport codes are widely used in various reactor physics applications, traditionally related to criticality safety analyses, radiation shielding problems, detector modelling and validation of deterministic transport codes. The main advantage of the method is the capability to model geometry and interaction physics without major approximations. The disadvantage is that the modelling of complicated systems is very computing-intensive, which restricts the applications to some extent. The importance of Monte Carlo calculation is likely to increase in the future, along with the development in computer capacities and parallel calculation.

An interesting near-future application for the Monte Carlo method is the generation of input parameters for deterministic reactor simulator codes. These codes are used in coupled LWR full-core analyses and typically based on few-group nodal diffusion methods. The input data consists of homogenised few-group constants, presently generated using deterministic lattice transport codes. The task is becoming increasingly challenging, along with the development in nuclear technology. Calculations involving high-burnup fuels, advanced MOX technology and next-generation reactor systems are likely to cause problems in the future, if code development cannot keep up with the applications. A potential solution is the use of Monte Carlo based lattice transport codes, which brings all the advantages of the calculation method.

So far there has been only a handful of studies on group constant generation using the Monte Carlo method, although the interest has clearly increased during the past few years. The homogenisation of reaction cross sections is simple and straightforward, and it can be carried out using any Monte Carlo code. Some of the parameters, however, require the use of special techniques that are usually not available in general-purpose codes. The main problem is the calculation of neutron diffusion coefficients, which have no continuous-energy counterparts in the Monte Carlo calculation.

This study is focused on the development of an entirely new Monte Carlo neutron transport code, specifically intended for reactor physics calculations at the fuel assembly level. The PSG code is developed at VTT Technical Research Centre of Finland and one of the main applications is the generation of homogenised group constants for deterministic reactor simulator codes. The theoretical background on general transport theory, nodal diffusion calculation and the Monte Carlo method are discussed. The basic methodology used in the PSG code is introduced and previous studies related to the topic are briefly reviewed. PSG is validated by comparison to reference results produced byMCNP4C and CASMO-4E in infinite two-dimensional LWR lattice calculations. Group constants generated by PSG are used in ARES reactor simulator calculations and the results compared to reference calculations using CASMO-4E data.

Tekijä(t)
Leppänen, Jaakko

Nimeke

Uuden Monte Carlo -reaktorifysiikkakoodin kehittäminen

Tiivistelmä

Monte Carlo -neutronitransportkoodeja käytetään laajasti monissa reaktorifysiikkasovelluksissa, kuten kriittisyysturvallisuus-analyyseissä, säteilysuojelulaskuissa, detektorimallinnuksessa ja determinististen transportkoodien kelpoistamisessa. Menetelmän tärkeimpinä etuina voidaan pitää geometrian ja neutronivuorovaikutusten tarkkaa kuvaamista ilman merkittäviä approksimaatioita. Haittapuolena on laskennan hitaus, erityisesti monimutkaisia geometrioita mallinnettaessa, mikä myös jossain määrin rajoittaa menetelmän sovelluskohteita. Monte Carlo -laskennan merkitys tulee todennäköisesti kasvamaan tulevaisuudessa tietokoneiden laskentatehon ja rinnakkaislaskennan kehityksen myötä.

Kevytvesireaktoreiden latussuunnittelu- ja turvallisuusanalyyseissä käytetään nykyisin deterministisiä reaktorisimulaattori-koodeja, joiden kytketyt neutroniikka-termohydrauliikkamallit pohjautuvat tyypillisesti nodaalidiffuusioteoreettisiin menetelmiin. Nodaalikoodien syöttöparametrit koostuvat homogenisoiduista moniryhmävakioista, jotka tuotetaan deterministisillä nippupalamaohjelmilla. Näiden ohjelmien soveltuvuus saattaa tulla kyseenalaiseksi ydintekniikan kehityksen myötä. Kasvava palama, kehittyneet sekaoksidipolttoaineet sekä uuden sukupolven ydinteknologia tulevat todennäköisesti aiheuttamaan ongelmia, erityisesti geometrian mallinnuksessa, mikäli laskentaan käytetyt ohjelmistot eivät kykene pysymään kehityksessä mukana. Eräs mielenkiintoinen lähitulevaisuuden sovelluskohde Monte Carlo -laskennalle onkin juuri homogenisoitujen ryhmävakioiden tuottaminen deterministisille reaktorisimulaattorikoodeille.

Monte Carlo -menetelmän soveltuvuutta ryhmävakioiden tuottamiseen on tutkittu yllättävän vähän, joskin kiinnostus aiheeseen on selvästi lisääntynyt kymmenen viime vuoden aikana. Homogenisoitujen ryhmävaikutusalojen laskeminen on suoraviivaista, ja se on mahdollista useimmilla Monte Carlo -neutroniikkakoodeilla. Tiettyjen parametrien laskemiseen tarvitaan kuitenkin erikoismenetelmiä, joita ei yleiskäyttöön tarkoitettujen koodien valikoimista yleensä löydy. Selvästi suurin haaste on diffuusiovakioiden laskeminen, mikä vaatii fysiikan tarkkaan mallintamiseen perustuvan Monte Carlo -laskennan ja approksimaatioon pohjautuvan diffuusioteorian yhdistämistä.

Tässä työssä käsitellään kokonaan uuden Monte Carlo -neutronitransportkoodin kehitystä. VTT:ssä kehitetty PSG-koodi on tarkoitettu reaktorifysiikkalaskuihin, erityisesti polttoaineniputasolla. PSG:n yksi tärkeimmistä sovelluskohteista on moniryhmävakioiden tuottaminen deterministisille reaktorisimulaattorikoodeille. Työssä selvitetään neutronien transport-teorian, nodaalidiffuusiomenetelmien sekä Monte Carlo -laskennan teoreettista taustaa. PSG-koodin käyttämät laskenta-rutiinit esitellään pääpiirteittäin, ja muita aiheeseen liittyviä tutkimuksia käydään läpi. Koodin kelpoistamiseksi kevytvesi-reaktorihiloille laskettuja tuloksia verrataan MCNP4C- ja CASMO-4E -ohjelmilla laskettuihin tuloksiin. PSG:n tuottamia ryhmävakioita käytetään ARES-reaktorisimulaattorilaskujen syöttöparametreina, ja tuloksia verrataan laskuihin, joissa moniryhmävakiot on tuotettu CASMO-4E -ohjelmalla.

Avainnimeke ja ISSN	Projektinumero
VTT Publications 1235-0621 (nid.) 1455-0849 (URL: http://www.vtt.fi/publications/index.jsp)	

Julkaisuaika	Kieli	Sivuja
Toukokuu 2007	Englanti, suom.kiel. tiiv.	228 s. + liitt. 8 s.

Avainsanat	Julkaisija
reactor physics, Monte Carlo method, neutron transport codes, PSG code, deterministic reactor simulator codes, homogenisation, homogenised group constants, nodal diffusion method, LWR lattice calculations	VTT PL 1000, 02044 VTT Puh. 020 722 4404 Faksi 020 722 4374

Nuclear reactor analysis involves the modelling of core neutronics, thermal hydraulics and the mechanical behaviour of nuclear fuel. Neutronics calculations are based on transport theory, which can be approached from either a deterministic or a stochastic point of view. Stochastic Monte Carlo methods are commonly used in calculations requiring the detailed modelling of geometry and interaction physics. Examples of such applications include criticality safety analyses, detector modelling and the validation of deterministic transport codes. The applicability of Monte Carlo codes is restricted by the available computing capacity, and new applications are anticipated to emerge along with computer development.

This study introduces a new Monte Carlo reactor physics code, developed at the VTT Technical Research Centre of Finland between 2004 and 2006. The PSG code is specifically intended for calculations at the fuel assembly level. The new code takes full advantage of modern computer resources and extends the calculation method beyond the traditional applications of general-purpose Monte Carlo codes. One of the new applications is the generation of input parameters for deterministic reactor simulator calculations.

Jaakko Leppänen